

Investigating the role of age, sex, and Alzheimer's disease pathology on neurochemical and neuroanatomical trajectories throughout the rat lifespan

Caitlin Fowler, BSc
Department of Biological and Biomedical Engineering
McGill University
Montréal, QC, Canada

March 2022

A thesis submitted to McGill University in partial fulfillment of the requirements for the degree of Doctor of Philosophy

© Caitlin Fowler, 2022

TABLE OF CONTENTS

ABSTRACT	7
RÉSUMÉ	9
LIST OF ABBREVIATIONS	12
ACKNOWLEDGEMENTS	13
CONTRIBUTION TO ORIGINAL KNOWLEDGE	16
CHAPTER 1: INTRODUCTION	20
CHAPTER 2: BACKGROUND	24
2.1. Alzheimer’s disease	24
2.1.1 Disease hallmarks	24
2.1.2 The amyloid cascade hypothesis	25
2.1.3 Current AD biomarkers	26
2.1.4 Age: a major player in sporadic but not familial AD	28
2.1.5 Limitations of existing biomarkers	30
2.2. Animal models as investigative tools for aging and AD research	32
2.2.1 Genetic basis of rodent models and the benefits of rats over mice	32
2.2.2 The Fischer 344 rat as a model of aging	33
2.2.3 The TgF344-AD rat model: a major advancement for preclinical AD research	33
2.3 Fundamentals of neuroimaging techniques for preclinical biomarker development	35
2.3.1 Fundamentals of nuclear magnetic resonance for MRI and MRS acquisition	35
2.3.2 Specifics of MR image acquisition	38
2.3.3 MR image processing and quantification	39
2.3.4 Specifics of MR spectra acquisition	41
2.3.5 Quantification of the MRS signal	42
2.3.6 Interpretation of the neurochemical profile	43
2.4 Implementation of MRI and MRS in aging and AD research: findings and gaps in knowledge	47
2.4.1 Application of structural MRI to study the aging brain	47
2.4.2 Application of single-voxel MRS to study aging	49
2.4.3 Detection and monitoring of AD using MRI and MRS	50
2.4.4 MR-detectable sex differences in aging and AD	54
2.5 Statistical analysis methods	57
2.5.1 Univariate analysis tools for longitudinal data	57
2.6 Chapter 2 Figures	59

Figure 2.6.1 The pathological evolution of Alzheimer’s disease	59
Figure 2.6.2 The amyloid cascade hypothesis	60
Figure 2.6.3 Temporal model of AD biomarkers	61
Figure 2.6.4 Coils comprising an MR machine	62
Figure 2.6.5 Recovery of longitudinal magnetization following a 90° radiofrequency pulse	63
Figure 2.6.6 T1, T2, and T2* relaxation	64
Figure 2.6.7 Two-Level model build pipeline	65
Figure 2.6.8 Example of a neurochemical spectra obtained at 7T and basis functions used for quantification.	66
CHAPTER 3: LONGITUDINAL QUANTIFICATION OF METABOLITES AND MACROMOLECULES REVEALS AGE- AND SEX-RELATED CHANGES IN THE HEALTHY FISCHER 344 RAT BRAIN	67
3.1 Preface	67
3.2 Manuscript Information	68
3.3 Abstract	69
3.4 Introduction	69
3.5 Materials and Methods	71
3.5.1 Animals	71
3.5.2 1H-MRS data acquisition - metabolites	71
3.5.3 1H-MRS data acquisition (macromolecules) and parameterization	72
3.5.4 Generation of metabolite and macromolecule basis spectra	73
3.5.5 Data processing and quantification	73
3.5.6 Application of correction factors for absolute quantification	74
3.5.7 Exclusion criteria	74
3.5.8 Statistical analysis	75
3.6 Results	75
3.6.1 Quantification using an expanded neurochemical profile	75
3.6.2 Metabolite and macromolecule concentrations are altered with age	76
3.6.3 Male and female Fischer rats exhibit differences in brain tissue chemistry	77
3.7 Discussion	77
3.7.1 Comparison with Previous Studies	77
3.7.2 Change in metabolite concentrations associated with healthy aging	78
3.7.3 Characterization of changes in individual macromolecule resonances with age	82
3.7.4 Presence of sex-specific effects in Fisher rat hippocampus	83
3.7.5 Limitations	84
3.8 Conclusion	86
3.9 Chapter 3 Figures	86
Figure 3.9.1	87

Figure 3.9.2 Age-dependent change in metabolite concentrations in the hippocampus of Fischer rats.	88
Figure 3.9.3 Age-dependent change in brain metabolite ratios in Fischer rats	89
Figure 3.9.4 Age-dependent change in macromolecules in Fischer rats	89
Figure 3.9.5 Differences in hippocampal metabolite concentrations exist between male and female Fischer rats	90
Figure 3.9.6 Differences in brain metabolite ratios exist between male and female F344 rats.	91
Figure 3.9.7 Differences in brain macromolecules exist between male and female F344 rats	91
3.10 Chapter 3 Tables	92
Table 3.10.1 Change in neurochemical concentrations with age and sex in Fischer rats	93
3.11 Supplementary Methods	93
3.11.1 Quality Control	93
3.11.2 Processing of macromolecule spectra	94
3.11.3 Parameterization of the macromolecule spectrum	94
3.11.4 Determination of Water and Metabolite Relaxation Constants for Absolute Quantification	95
3.11.5 Retrospective Power Analysis	97
3.11.6 Age- and sex-dependent neurochemical changes over 3 vs 4 timepoints	97
3.12 Supplementary Figures	99
Supplementary Figure 3.12.1 Parameterization of the metabolite-nulled spectrum	99
3.13 Supplementary Table Captions	100
Supplementary Table 3.13.1. SubjectInfo	100
Supplementary Table 3.13.2. BasisSetSimulation	100
Supplementary Table 3.13.3. Correction Factors	100
Supplementary Table 3.13.4. CRLB	100
Supplementary Table 3.13.5. SNR_LW	100
Supplementary Table 3.13.6. Conc.Summary.Age	100
Supplementary Table 3.13.7. Conc.Summary.Sex	100
Supplementary Table 3.13.8. AgeEffect	100
Supplementary Table 3.13.9. SexEffect	101
3.14 Supplementary References	101
3.15 Chapter 3 References	102
CHAPTER 4: LONGITUDINAL CHARACTERIZATION OF NEUROANATOMICAL CHANGES IN THE FISCHER 344 RAT BRAIN DURING NORMAL AGING AND BETWEEN SEXES	108
4.1 Preface	108
4.2 Manuscript Information	109

4.3 Abstract	110
4.4 Introduction	110
4.5 Methods	112
4.5.1 Animals and study design	112
4.5.2 MRI data acquisition	113
4.5.3 MRI pre-processing and registration pipelines	113
4.5.4 Regional volume estimation	115
4.5.5 Statistical Analysis	115
4.6 Results	116
4.6.1 Absolute volumes increase with age and are larger in male Fischer rats	116
4.6.2 Brain-size-corrected volumes show heterogeneous change with age and occur in regions implicated in motor control, learning, and memory	117
4.6.3 The influence of sex on neuroanatomy is strongest in grey matter structures	118
4.6.4 Whole-brain voxel-wise and volumetric analyses provide complementary results	119
4.7 Discussion	120
4.8 Conclusion	126
4.9 Chapter 4 Tables	127
Table 4.9.1 Linear mixed effects model summary for selected brain-size-corrected volumes, listed in alphabetical order.	127
4.10 Chapter 4 Figures	127
Figure 4.10.1 Absolute volumes summed across tissue type increase with age and are larger in males, while brain-size corrected volumes reveal different age and sex-dependent trends across tissue types	128
Figure 4.10.2 Visualization of age and sex effects, along with their interaction, on brain size-corrected brain volumes (LME results) in healthy aging Fischer rats, overlaid on the average anatomy background.	129
Figure 4.10.3 Prominent age and sex-dependent changes in brain-size-corrected volumes are present throughout the brain in both grey and white matter regions, suggesting a multitude of physiological functions are affected by aging	130
Figure 4.10.4 Statistical maps demonstrating local brain size-corrected volume differences due to age, sex, and their interaction in healthy aging Fischer rats, overlaid on the average anatomy background	131
4.11 Supplementary Methods	132
4.11.1 Age- and sex-dependent change in brain-size-corrected volumes over three time points as compared to four time points	132
4.11.2 Detailed description of the quality control process	132
4.12 Supplementary Table Captions	133
Supplementary Table 4.12.1. Subject Data	133
Supplementary Table 4.12.2. Comparison between models containing a linear versus quadratic age term using Akaike information criterion (AIC)	133

Supplementary Table 4.12.3. Linear mixed effects model results for 73 absolute volumes derived from integrated absolute Jacobians	133
Supplementary Table 4.12.4. Absolute volumes of 73 brain regions in mm ³ , split by timepoint and sex	134
Supplementary Table 4.12.5. Linear mixed effects model results for 73 brain-size-corrected volumes derived from integrated relative Jacobians	134
Supplementary Table 4.12.6. Linear mixed effects model results for 73 unique brain-size-corrected volumes derived from integrated relative Jacobians, ranked by adjusted p-value within each model term	134
Supplementary Table 4.12.7. Linear mixed effects model results for brain-size-corrected volumes analyzed over 3 time points as compared to four	134
4.13 Supplementary Figures	136
Supplementary Figure 4.13.1 Workflow illustrating the steps involved in preprocessing anatomical MR images.	136
Supplementary Figures 4.13.2 to 4.13.9: Longitudinal trajectory of brain volumes with age and split by sex, for 71 unique brain regions in the aging Fischer rat	136
Supplementary Figures 4.13.10 and 4.13.11: A side by side comparison between whole-brain voxel-wise changes and regional changes as a result of age, sex, and their interaction, overlaid on the average anatomy background	146
4.14 References	149
CHAPTER 5: NEUROCHEMICAL AND COGNITIVE CHANGES PRECEDE STRUCTURAL ABNORMALITIES IN THE TGF344-AD RAT MODEL	157
5.1 Preface	157
5.2 Manuscript Information	158
5.3 Abstract	159
5.4 Introduction	159
5.5 Materials and Methods	161
5.5.1 Animal care and study design	161
5.5.2 MRI data acquisition and regional volume estimation	162
5.5.3 1H-MRS data acquisition and quantification	163
5.5.4 Behavioural phenotyping via the Barnes Maze test	164
5.5.5 Immunofluorescence experiments and stereology	164
5.5.6 Statistical analysis	165
5.5.7 Data Availability	166
5.6 Results	166
5.6.1 TgF344-AD rats display altered local brain volume, primarily in grey matter structures	166
5.6.2 The TgF344-AD model recapitulates neurochemical features of human AD	167
5.6.3 The TgF344-AD rat model displays cognitive impairment by 4-months of age	168

5.6.4 No genotype-dependent differences detected in microglia and neuronal cell counts	169
5.7 Discussion	170
5.8 Chapter 5 Figures	176
Figure 5.8.1: Genotype-dependent differences in local brain volume with age	176
Figure 5.8.2: Trajectory of neurochemical changes with age in TgF344-AD and WT rats	176
Figure 5.8.3: Barnes Maze probe trial data reveal cognitive impairment as early as 4-months of age	176
Figure 5.8.4. Despite extensive amyloid pathology at 18 months, neuronal and microglial cell counts do not differ significantly between Tg344-AD and wildtype rats	177
5.9 Supplementary Methods	182
5.9.1 Sample Size Calculations and Group Sizes	182
5.9.2 MRI methods	182
5.9.3 MRS methods	184
5.9.3.1 Basis Set	184
5.9.3.2 Quality Control	184
5.9.4 Barnes Maze Testing	185
5.9.5 Immunofluorescence experiments	187
5.9.5.1 Perfusion	187
5.9.5.2 Sectioning	187
5.9.5.3 Application of primary and secondary antibodies and detection solutions	187
5.9.5.4 Imaging and Stereology	188
5.9.6 Statistical Analysis	188
5.9.6.1 Base Packages in R	188
5.9.6.2 Linear model comparison	188
5.9.6.3 Final linear models	189
5.10 Supplemental Table Captions	189
Supplementary Table 5.10.1. Summary of subject demographic data at each timepoint, split by modality and sex	189
Supplementary Table 5.10.2: LME_MRI: Akaike's information criterion (AIC) analysis and linear model summary for 120 brain volumes	189
Supplementary Table 5.10.3: MRI_volume_summary_mm3	190
Supplementary Table 5.10.4: LME_MRS: CRLB values, Akaike's information criterion (AIC) analysis, and linear model summary for 27 neurochemicals	190
Supplementary Table 5.10.5: MRS_conc_summary_mMol	191
Supplementary Table 5.10.6: Barnes_stats	191
Supplementary Table 5.10.7: Barnes_data_summary	191
Supplementary Table 5.10.8: Histology_LME: LME results for microglial and neuronal cell counts	191

Supplementary Table 5.10.9: Correlations_18months: Correlations between microglial and neuronal burden, metabolite concentrations, brain volumes, and behavioural metrics	192
5.11 Supplemental Figures	192
Supplementary Figures 5.11.1 and 5.11.2. Visualization of the longitudinal volume trajectories of all brain structures that display a significant age by genotype interaction	192
Supplementary Figures 5.11.3 and 5.11.4. Visualization of the longitudinal volume trajectories of all brain structures that display a significant age by genotype by sex interaction, prior to FDR correction	192
Supplementary Figure 5.11.5. Longitudinal trajectory of neurochemicals in TgF344-AD and wildtype rats, with some split by sex	193
5.12 Chapter 5 Supplementary References	199
5.13 Chapter 5 References	200
CHAPTER 6: DISCUSSION AND CONCLUSIONS	207
6.1 Summary of results and main conclusions	208
6.2 Limitations	212
6.3 Future directions	213
6.3.1 Identifying multivariate features of aging and AD	213
6.3.2 Developing a more comprehensive translational research platform	215
6.3.3 Delving into molecular mechanisms and histological underpinnings of aging and AD pathology	218
6.3.4 Examination of early preclinical stage to identify earliest disease features and targets for preventative treatment	221
COMPLETE BIBLIOGRAPHY	223

ABSTRACT

Alzheimer's disease (AD) is a progressive and irreversible neurodegenerative disorder that accounts for 60-80% of the 50 million dementia cases worldwide. The most widely accepted risk factor for developing AD is age. The distinction between aging and AD is particularly crucial during the early stages of disease progression since this is when intervention is most likely to be effective. However, there is a lack of biological markers capable of identifying early-stage AD, limiting opportunities for diagnosis and treatment. Comprehensive characterization of aging and disease processes in relevant animal models represents one promising avenue towards developing options for diagnosis and treatment. In particular, longitudinal preclinical studies that employ techniques with high translational potential to clinical studies, such as non-invasive neuroimaging techniques, would enable identification of homologous biomarkers across species.

The content of this thesis describes the application of whole-brain MRI and localized MRS to investigate age- and sex-related changes in neurochemistry and neuroanatomy in a commonly used rat model of aging (the Fischer 344 rat), and the subsequent integration of these techniques with behavioural testing in a transgenic rat model developed on a Fischer 344 background to distinguish the effects of aging versus Alzheimer's disease pathology on neuroimaging and cognitive markers. **Chapters 1 and 2** provide a general introduction and background information on the current state of knowledge regarding the impact of age and AD pathology on brain structure and tissue chemistry, as well as the neuroimaging and statistical methods used to investigate these neurobiological changes. **Chapter 3** presents a published study examining age- and sex-related changes in hippocampal biochemistry in the Fischer 344 rat. Age was associated with prominent differences in metabolites implicated in anaerobic energy metabolism, antioxidant defenses, and neuroprotection, as well as numerous macromolecule changes. **Chapter 4** builds upon the previous study of highly localized effects of aging by examining whole-brain volumetric changes associated with age and sex, again in the Fischer 344 rat. This publication identifies age- and sex-related volume changes in regions such as the cortex, hippocampus, cingulum, caudoputamen, and nucleus accumbens, which are implicated in memory and motor control circuits frequently affected by aging and neurodegenerative disease. **Chapter 5** incorporates the techniques and knowledge developed in earlier chapters by applying the same neuroimaging techniques in combination with behavioural testing in a transgenic model of Alzheimer's disease developed on a Fischer 344 background, the

TgF344-AD rat. The TgF344-AD model demonstrated impaired spatial reference memory by 4 months of age, followed by neurochemical abnormalities by 10 months and major structural changes by 16 months, many of which were similar to findings in human Alzheimer's disease subjects. A mild influence of sex was also seen on neuroimaging and cognitive markers. Finally, **Chapter 6** provides a discussion and summary of the relevance of these findings. Altogether, this thesis describes the application of highly translatable neuroimaging techniques to identify multiple neurobiological features influenced by age-, sex-, and pathology throughout the lifespan of two relevant rat models. This thesis therefore provides support for the use of MRI and MRS in rodent models *in vivo* to develop markers of pathological change which may be used to improve age- and disease-related outcomes in humans.

RÉSUMÉ

La maladie d'Alzheimer (MA) est une maladie neurodégénérative progressive et irréversible qui représente 60-80 % des 50 millions de cas de démence dans le monde. Le facteur de risque primaire pour la MA est l'âge. La distinction entre le vieillissement et la MA est particulièrement cruciale aux premiers stades de la maladie, car c'est à ce moment-là qu'une intervention a le plus de chances d'être efficace. Cependant, on manque de marqueurs biologiques capables d'identifier les premiers stades de la MA, limitant les possibilités de diagnostic et de traitement. La caractérisation complète du vieillissement et des processus pathologiques dans des modèles animaux pertinents représente une voie prometteuse vers le développement d'options de diagnostic et de traitement. En particulier, les études précliniques longitudinales qui utilisent des techniques à fort potentiel de transfert vers les études cliniques, telles que les techniques de neuroimagerie non invasif, permettraient d'identifier des biomarqueurs homologues entre les espèces.

Cette thèse décrit l'application de l'imagerie par résonance magnétique (IRM) du cerveau entier et de la spectroscopie par résonance magnétique (SRM) localisée pour étudier les changements neurochimiques et neuroanatomiques liés à l'âge et au sexe dans le rat Fischer 344, et l'intégration ultérieure de ces techniques avec des tests comportementaux dans un modèle de rat transgénique développé sur un fond de Fischer 344 pour distinguer les effets du vieillissement par rapport à la pathologie de la MA sur la neuroimagerie et les marqueurs cognitifs. Les **chapitres 1 et 2** fournissent une introduction générale et des informations sur l'état des connaissances concernant l'impact de l'âge et de la pathologie de la MA sur la structure du cerveau et la chimie des tissus, ainsi que sur les méthodes de neuroimagerie et de statistique utilisées pour étudier ces changements neurobiologiques. Le **chapitre 3** présente une étude publiée qui examine les changements liés à l'âge et au sexe dans la biochimie de l'hippocampe chez le rat Fischer 344. L'âge a été associé à des différences importantes dans les métabolites impliqués dans le métabolisme énergétique anaérobie, les défenses antioxydantes et la neuroprotection, ainsi qu'à de nombreuses modifications des macromolécules. Le **chapitre 4** s'appuie sur l'étude précédente des effets très localisés du vieillissement en examinant les changements volumétriques du cerveau entier associés à l'âge et au sexe, toujours chez le rat Fischer 344. Cette publication identifie les changements de volume liés à l'âge et au sexe dans des régions telles que le cortex, l'hippocampe, le cingulum, le caudoputamen et le noyau accumbens, qui sont impliquées dans les circuits de mémoire et de

contrôle moteur fréquemment affectés par le vieillissement et les maladies neurodégénératives. Le **chapitre 5** intègre les techniques et les connaissances développées dans les chapitres précédents en appliquant les mêmes techniques de neuroimagerie en combinaison avec des tests comportementaux dans un modèle transgénique de la MA. Le rat TgF344-AD a montré une altération de la mémoire de référence spatiale à l'âge de 4 mois, suivie d'anomalies neurochimiques à l'âge de 10 mois et de changements structurels majeurs à l'âge de 16 mois. Une légère influence du sexe a également été observée sur la neuroimagerie et les marqueurs cognitifs. Enfin, le **chapitre 6** présente une discussion et un résumé de la pertinence de ces résultats. Cette thèse décrit l'application de techniques de neuro-imagerie transférables pour identifier des caractéristiques neurobiologiques influencées par l'âge, le sexe et la pathologie dans deux modèles de rats pertinents. Cette thèse soutient donc l'utilisation de l'IRM et de la SRM dans des modèles de rongeurs *in vivo* pour développer des marqueurs de changement pathologique qui peuvent être utilisés pour améliorer les résultats liés à l'âge et à la maladie chez les humains.

LIST OF ABBREVIATIONS

A β = amyloid beta; Ala = alanine; APP = amyloid precursor protein; ApoE = apolipoprotein E; Asp = aspartate; CSF = cerebrospinal fluid; Cr = creatine; GABA = gamma amino butyric acid; FDG = fluorodeoxyglucose; Glc = glucose; Gln = glutamine; Glu = glutamate; GM = grey matter; GPC = glycerophosphocholine; GSH = glutathione; ICV = intracranial volume; Ins = myo-inositol; Lac = lactate; NAA = N-acetylaspartylaspartate; NAAG = N-acetylaspartylglutamate; MAPT = microtubule associated protein tau; MM = macromolecule; MRI = magnetic resonance imaging; MRS = magnetic resonance spectroscopy; PCh = phosphocholine; PCr = phosphocreatine; PE = phosphoethanolamine; PET = positron emission tomography; PS = presenilin; p-tau = phosphorylated tau; t-tau = total tau; Tau = taurine; TBV = total brain volume; tCho = total choline; tCr = total creatine; Tg = transgenic; WM = white matter; WT = wildtype; 11C-PK11195 = (11)C-(R)-[1-(2-chlorophenyl)-N-methyl-N-(1-methyl-propyl)-3-isoquinolinecarboxamide]; [¹⁸F]ASEM = 4-(6-fluorodibenzo[b,d]thiophen-3-yl)-1,4-diazabicyclo[3.2.2]nonane 5,5-dioxide (JHU82132); [¹⁸F]DPA-714 = N,N-Diethyl-2-(2-(4-(2-[¹⁸F] fluoroethoxy) phenyl)-5,7-dimethylpyrazolo [1,5-a] pyrimidin-3-yl) acetamide;

ACKNOWLEDGEMENTS

The last five years have been a significant period of growth and development for me, both as a scientist and as a person, and I have many people to thank for helping me along the way. First and foremost, I would not be where I am today without the incredible guidance of my supervisor and mentor, Dr. Jamie Near. From the moment in our initial zoom call when we started talking about hockey instead of science, I knew working with Jamie was going to be a grad school experience unlike most. He fosters such a welcoming, open, and supportive lab environment, while also pushing his students to ask questions, consider new approaches, and develop translatable skills. Jamie's passion for science and personal scientific curiosity helped fuel my own excitement about research and my desire to always keep learning. In fact, it was Jamie's supportive mentoring style and his enthusiasm during our many conversations about new ideas and experiments that made me want to continue on to a PhD. Jamie, I am incredibly grateful to have had the privilege of working with you. I admire your eagerness, your collaborative nature, your honest and genuine approach to academia, and your desire to make sure all of your students are taken care of. I have learned so much from you over the course of this degree and I sincerely thank you.

I would next like to thank a number of people who spent time training, advising, supporting, and guiding me throughout my time as a grad student. Dr. Mallar Chakravarty, thank you for agreeing to be my co-supervisor in the final year of my thesis and for always being open to discussing ideas and ways in which my experiments could be improved. I also appreciate all of the time you put into editing my various posters and manuscripts: they were made clearer and more concise as a result of your suggestions. Dr. Axel Mathieu, thank you for teaching me the ways of the MR scanner and for helping me get permission (as a lowly master's student at the time) to operate it on my own, without which I would not have been able to complete the ridiculous number of scans needed for this thesis. Dr. Gabriel Devenyi (i.e. "big Gabe"), the completion of this thesis would literally not have been possible without you. You provided incredible guidance on study design, statistical methods, effects visualization, coding, problem-solving and troubleshooting of everything from the coffee machine to my poorly written code, and so much more. I sincerely appreciate your willingness to help and your patience with me. I would also like to thank Drs. Georgios Mitsis and Christine Tardif for serving on my advisory committee; thank you for sharing your incredible expertise and for ensuring my thesis was always addressing relevant and important questions. Dr. Tardif, I particularly want to acknowledge that you have been quite the role model for me throughout my PhD as one of the few female scientists I have had the pleasure of learning from, in addition to simply being a genuinely skilled, confident, and enthusiastic researcher. I admire your eagerness to address important scientific questions, your dedication to use the best methods and to do things right, and your ability to provide feedback in an honest but supportive manner. I am very grateful to have benefitted from your guidance. Finally, I would like to thank Pina Sorrini, the BBME Student Officer. Pina, the extent to which you care for every single student in the BBME department is incredible, and you do so with enthusiasm, patience, and a real sense of family. Thank you for everything.

Additionally, this research would not have been possible without support from groups that have funded my work over the past several years, including Healthy Brains for Healthy Lives, the department of Biological and Biomedical Engineering, and the Faculty of Medicine.

This thesis represents not only a large volume of work, but a substantial amount of time, during which the friendship, camaraderie, and support of my colleagues and friends kept me going. To all of the members of the Near Lab, past and present, thank you for making work so much fun, and on the days when it wasn't fun, thank you for keeping me going. The same goes to so many members of the CoBrA lab. I appreciated the ease with which you all welcomed me into your offices and treated me like one of your own. In particular, Dan Madularu, you made me feel so welcome during my first interview at Douglas and you are a major reason I joined Jamie's lab. You were always keen to chat, troubleshoot behavioural testing and MR stuff, throw around a frisbee, and of course, drive me to and from Ottawa! I can't imagine my grad student experience without you and I'm so grateful that we've stayed in touch. Chathu Kumaragamage, your obvious passion for your research instantly got my attention, and your patience explaining everything about MRS during my interview made me know I would be welcomed and supported in the Near Lab. Katrina Cruickshank, thank you for always being willing to check out my newest colour scheme, for troubleshooting behavioural testing with me, and for helping me see the humour in our ever-growing list of challenges we overcame during our time in grad school. Dana Goerzen, from childhood pals to labmates, I am so pleased I got to watch you grow into the incredible scientist you are today, while also getting to benefit from your serious skills in image processing. It has been so much fun getting to work with you and I can't wait to see what you do next. Masoumeh Dehghani, thank you for teaching me about pulse sequences and for putting up with all of my questions about modelling and Matlab. Elvisha Dhamala, Steven Zhang, Kristi Drudik, Kristin Ellerbeck, Augustine Pham, Brendan Kadota, Peter Truong, and Sneha Senthil, thank you for creating an entertaining and encouraging work environment. Alex Nuun, you coming through those doors in the Douglas every morning on your way to pick me up for our morning coffee always made my day. I absolutely locked eyes with way too many strangers coming through there in my anticipation for your arrival. Thank you for the bike commutes, gym sessions, office and messenger chats, and your genuine goofiness and friendship. Elisa Guma and Lani Cupo, I would not have finished this thesis without your constant willingness to help me with all things MRI, stats, and behaviour, and our venting/troubleshooting sessions over coffee. You are both such smart, inspiring, and wonderful humans. Jurgen Germann, thank you for the lunchtime running sessions, even though you thoroughly beat me every single time, and for teaching me that hand-grinding coffee beans is the only way to go. Finally, Mike Yitayew and Michelle Tran, I wish we had gotten to spend more of our more recent grad school time together in person because you two always kept me grounded and as happy as a sleep-deprived grad student could be. I am so grateful to have met you both.

Almost last but certainly not least, thank you to my family for forever supporting me throughout this entire process. Especially thanks to my mum for reminding me in third year of undergrad that I might want to start thinking about what I would do after graduation, and to my

sister, Emma, for sending me poster templates and memes, and for ice cream and coffee dates. Living with you during grad school was wonderful.

Finally, thank you Kaylee Sparks, for sticking with me through all of this and for enduring endless Greyhound trips followed by two years of sharing a workspace. Your love, support, and silliness got me through the hardest parts of this degree. I am so grateful to have had you by my side.

CONTRIBUTION TO ORIGINAL KNOWLEDGE

Chapter 3

- Prior to this publication, longitudinal characterization of neurochemical change with age had not been performed in the Fischer 344 rat, despite this strain being both a commonly used model for studying aging and for the development of transgenic rat models, (including the TgF344-AD rat model of Alzheimer's disease)
- Prior to this publication, longitudinal quantification of individual macromolecule resonances with age had not been reported at the preclinical or clinical level
- Proper handling of macromolecule resonances improves quantification accuracy of metabolites, suggesting our results may be more accurate and/or reproducible than those generated without sufficient handling of the macromolecular signal
- Given our use of an expanded neurochemical profile, this manuscript provides the most extensive assessment of change in brain tissue chemistry with age in a rodent model to date
- Prior to this publication, characterizing the influence of sex on neurochemistry over the lifespan had not been performed in any rat model of aging (only in C57BL6 mice)
- This manuscript provides support for the use of MRS to detect brain neurochemical abnormalities with age *in vivo*, providing insight into the many biochemical processes affected by aging that could be used as aging biomarkers and/or targeted by interventions to improve age-related disease outcomes in humans

Chapter 4

- Prior to this publication, longitudinal exploration of age-related change in neuroanatomy had not been performed in a mixed-sex cohort of Fischer 344 rats. This manuscript examines age-related change at both the voxel-wise and regional level in 120 brain volumes
- Prior to this publication, characterizing the influence of sex on neuroanatomy over the lifespan had not been performed in any rat model of aging
- The findings in this manuscript demonstrate that while there are several distinctions between neuroanatomical change with age in the Fischer 344 rat compared to humans, there are many more similarities
- This manuscript provides support for the use of MRI to detect volumetric change with age as well as the use of rodent aging studies for developing homologous biomarkers across species

Chapter 5

- While the TgF344-AD rat model has been examined extensively since its emergence in 2013, we are the first to examine disease-dependent changes in neuroanatomy and the full neurochemical profile

- Ours is also the earliest assessment of cognitive function in this model and we detected impairment in spatial reference memory at an earlier stage than previously reported
- Given our multimodal and longitudinal approach, we were able to capture the chronological appearance and progression of multiple features of disease pathophysiology, providing insight into the many processes comprising disease progression
- The additional examination of sex effects in this model contributes to our overall understanding of the interaction between sex and pathology on several highly translatable potential markers of disease progression (brain tissue chemistry and volume)
- The findings in this manuscript demonstrate that the TgF344-AD model recapitulates major features of human AD and contribute to its validation as a highly relevant model for preclinical AD research
- The neuroimaging techniques employed here are highly translatable to the study of other transgenic models of disease as well as to human clinical studies

In summary, **Chapters 3 and 4** provide novel baseline information on neurochemical and neuroanatomical change with age and sex in the Fischer 344 rat, upon which future research on age-related pathologies or interventions can build. This is particularly true for researchers using the TgF344-AD rat model which was developed on a Fischer 344 background. **Chapter 5** builds on this knowledge with the characterization of neuroimaging and cognitive markers of disease progression in the TgF344-AD rat relative to wildtype littermates. This is the first study to document the chronological order of appearance and longitudinal progression of cognitive, neurochemical, and neuroanatomical abnormalities in this model. Finally, it is important to note that the neuroimaging techniques employed throughout the three manuscripts are highly translatable to the study of other transgenic models of disease, as well as to human clinical studies. This thesis therefore provides support for the use of MRI and MRS for detecting structural and biochemical abnormalities which may be used to develop biomarkers or therapies for the improvement of age- and disease-related outcomes in humans.

CONTRIBUTION OF AUTHORS

The original work in this thesis spans **Chapters 3, 4, and 5**. For each manuscript, I led the experimental design, data collection, analysis, visualization of results, and interpretation under the incredible guidance and supervision of Dr. Jamie Near, and with considerable input from co-supervisor, Dr. M. Mallar Chakravarty, in the final year of my degree. In particular, it was my decision to intentionally examine the influence of sex in our studies, and to perform the methods development required to incorporate macromolecules into the neurochemical basis set used in **Chapters 3 and 5**. It was also my decision to include behavioural testing and immunofluorescence analyses in **Chapter 5**; I was responsible for identifying and piloting an appropriate cognitive testing paradigm, deciding which tissue markers to stain for and analyze, and supervising the students who optimized the staining and stereology protocols. While I wrote the first draft of each manuscript and incorporated edits from co-authors and peer reviewers, each study features a number of co-authors whose contributions (listed below) were integral to the completion of the work.

Chapter 3: Caitlin F. Fowler, Dan Madularu, Masoumeh Dehghani, Gabriel A. Devenyi, Jamie Near. Longitudinal quantification of metabolites and macromolecules reveals age- and sex-related changes in the healthy Fischer 344 rat brain. *Neurobiology of Aging*, 101:109-122, 2021.

- Dan Madularu: performed approximately half of the *in vivo* scanning and provided guidance on data analysis
- Masoumeh Dehghani: responsible for pulse sequence development and implementation for detection of macromolecules
- Gabriel A. Devenyi: supported statistical analyses and guided data visualization
- Jamie Near: supported pulse sequence implementation and supervised the study
- All authors: provided critical or conceptual support and provided suggestions for the manuscript

Chapter 4: Caitlin F. Fowler, Dana Goerzen, Dan Madularu, Gabriel A. Devenyi, M. Mallar Chakravarty, Jamie Near. Longitudinal characterization of neuroanatomical changes in the Fischer 344 rat brain during normal aging and between sexes. In Press at *Neurobiology of Aging*, available online October 16, 2021. <https://doi.org/10.1016/j.neurobiolaging.2021.10.003>

- Dana Goerzen (co-first author): performed MRI preprocessing, registration, and analysis, and contributed to the methods section of this manuscript
- Dan Madularu: performed approximately half of the *in vivo* scanning and provided guidance on data analysis
- Gabriel A. Devenyi: provided support on MRI preprocessing, registration, and analysis, and guided statistical analyses
- M. Mallar Chakravarty: provided guidance on interpretation and presentation of results, and offered suggestions on the contents of the manuscript

- Jamie Near: Supervised the study and provided guidance on conceptualization and interpretation of results. He also significantly contributed to manuscript editing
- All authors: provided critical or conceptual support and provided suggestions for the manuscript

Other related co-authored publications: Dana Goerzen, **Caitlin F. Fowler**, Gabriel A Devenyi, Jurgen Germann, Dan Madularu, M. Mallar Chakravarty, Jamie Near. An MRI-derived neuroanatomical atlas of the Fischer 344 rat brain. 10:1-13, 2020. *Nature Scientific Reports*.

Chapter 5: Caitlin F. Fowler, Dana Goerzen, Gabriel A. Devenyi, Dan Madularu, Katrina Cruickshank, Augustine Vinh-Phuc Pham, Kristin Ellerbeck, Kristi Drudik, Naguib Mechawar, Maria Antonietta Davoli, M. Mallar Chakravarty, Jamie Near. Neurochemical and cognitive changes precede structural abnormalities in the TgF344-AD rat model. Submitted to *Brain communications*, November 2, 2021.

- Dana Goerzen: performed MRI preprocessing, registration, and analysis
- Gabriel A. Devenyi: provided expertise and guidance on statistical analyses, data visualization, and interpretation of results
- Dan Madularu: provided guidance on project design and technical support for behavioural tests
- Katrina Cruickshank: responsible for optimizing immunofluorescence and stereology protocols
- Augustine Vinh-Phuc Pham: performed immunofluorescence experiments and stereology
- Kristin Ellerbeck: performed immunofluorescence and stereology
- Kristi Drudik: responsible for establishing initial perfusion and immunofluorescence protocols
- Naguib Mechawar: provided expertise, laboratory access, and materials for immunofluorescence experiments
- Maria Antonietta Davoli: provided guidance and support for immunofluorescence experiments
- M. Mallar Chakravarty: supported statistical analysis and editing of the manuscript
- Jamie Near: provided guidance on study conceptualization, data analysis and interpretation, and editing the manuscript. He also obtained funding for and supervised this study
- All authors: provided critical or conceptual support and provided suggestions for the manuscript

CHAPTER 1: INTRODUCTION

Alzheimer's disease (AD) is a progressive neurodegenerative disorder that poses an enormous challenge to healthcare systems worldwide. It is the most common cause of dementia, a form of memory loss and impaired thinking that interferes with daily life. Dementia and Alzheimer's disease are not a normal part of aging, but they do primarily affect the elderly population (Jack et al. 2007). As a result of the aging global population, there are currently 50 million people with dementia worldwide—a number that is expected to reach 152 million by 2050—and of these, AD cases comprise 60 to 80% (Patterson 2018). These numbers are particularly distressing when there continues to be a lack of effective therapies to even modify disease progression, let alone cure it. In the last twenty years, only four drugs have been approved for AD patients, and they do not modify disease progression; they simply treat some of the symptoms. Efforts to understand and characterize AD have existed since the first case study by Dr. Alois Alzheimer in 1906. So why, after 115 years of research, are we still unable to accurately diagnose and treat this increasingly common disease?

One reason is that diagnosis is complicated by the close association between AD and age. It is still unclear if AD is a form of accelerated aging or if phenocopy to AD is a result of completely separate processes and some causative factor. We do know that aging is the primary risk factor for AD, with a spike in the incidence rate after the age of 60 (Kawas et al. 2000). Many of the cellular and molecular mechanisms that are altered during aging such as mitochondrial bioenergetics, antioxidant capacity, and the inflammatory response are also dysfunctional in AD (Farooqui and Farooqui 2009). It is equally, if not more, challenging to disentangle the effects of aging versus AD using cognitive impairment as a marker of disease progression because many aspects of cognition affected by AD, such as executive function and episodic memory, also decline during healthy aging (Herrup 2010; Fjell et al. 2014). Finally, even accumulation of amyloid protein is frequently found in approximately one-third of cognitively normal, otherwise healthy, elderly people (Morris et al. 2010). Improving our understanding of the processes and features characterizing normal aging are necessary to understanding and identifying pathological aging trajectories such as AD.

A second, closely related, reason is the difficulty in identifying appropriate biological markers, or biomarkers, of disease progression, thus limiting our ability to detect AD at early stages.

Aspects of Alzheimer's disease pathology can occur up to decades before onset of cognitive symptoms (Jack et al. 2010; Jack et al. 2013; Bateman et al. 2012), which could provide a critical opportunity for therapeutic intervention. Recent advances in neuroimaging now allow for *in vivo* detection of Alzheimer's disease hallmarks, including amyloid- β ($A\beta$) plaques, neurofibrillary tangles (NFTs) composed of hyperphosphorylated tau, and neurodegeneration, which manifests as atrophy, neuronal loss, and gliosis (Jack et al. 2010). However, despite the existence of various imaging and fluid biomarkers of these hallmarks (Leuzy et al. 2018; Tarawneh 2020), the results of clinical trials using these biomarkers have been underwhelming. Two major reasons for the lack of success are likely that interventions are not targeting the right disease processes, or they are not being administered at the right time (Sperling et al. 2011), both of which are a result of inadequate disease biomarkers. Additionally, AD presentation and progression can occur differently in men and women, further muddying disease recognition and appropriate treatment (Mazure and Swendsen 2016). Therefore, there is a need to better characterize aspects of disease progression and to expand the list of current disease biomarkers, with the aim of identifying markers that are altered early in disease progression, reflect features other than just major hallmarks, and can detect sex-related differences, if they are present.

Two tools may prove particularly useful for biomarker development: animal models, which can be designed to express specific pathological features and studied under tightly controlled conditions; and magnetic resonance (MR) techniques, which provide a unique window into a variety of processes taking place in the brain. The Fischer 344 rat and the TgF344-AD rat are particularly important models in the context of studying aging and AD. The Fischer rat is the most commonly used model in aging research (Gallagher et al. 2011) and is also frequently used as a background strain for the generation of transgenic models. One such transgenic model is the TgF344-AD rat (Cohen et al. 2013), a model of Alzheimer's disease developed on a Fischer 344 background that spontaneously develops tau pathology as an apparent result of progressive $A\beta$ accumulation, similar to how the process happens in humans (Jack et al. 2010; Selkoe and Hardy 2016). Not only does the TgF344 AD-model represent a significant advancement for preclinical AD research, but the numerous advantages of studying rats over mice—they are physiological and genetically closer to humans, display a richer behavioural phenotype, and have larger brains (Ellenbroek and Youn 2016)—make the TgF344-AD rat a particularly salient option for preclinical biomarker development.

Neuroimaging techniques such as MR imaging (MRI) and spectroscopy (MRS) represent powerful options for the development of biomarkers of aging and AD. MRI and MRS enable non-invasive, longitudinal assays of brain structure and tissue chemistry and the techniques themselves are highly translatable between preclinical and clinical studies (Gao and Barker 2014; Frisoni et al. 2010; Mueller et al. 2006). MRI detects structural abnormalities which are one of the last pathological features to appear before overt cognitive impairment, so MRI-detectable change in volume is considered a mid- to late-stage disease marker (Jack et al. 2013; Bateman et al. 2012). MRS can quantify up to 27 individual metabolites and macromolecules, providing a detailed survey of brain tissue biochemistry (Fowler et al. 2020; Ross and Sachdev 2004). Quantification of this many neurochemicals allows for the identification of numerous forms of metabolic dysfunction that may occur at various stages throughout both aging and AD progression (Camandola and Mattson 2017). MRI and MRS have been used to study aging and AD in humans and rodents, but longitudinal studies in relevant models such as the Fischer 344 and TgF344-AD rats are still lacking. There is therefore insufficient knowledge regarding the understanding and evolution of the neurobiological changes that occur during aging and AD, as well as few homologous biomarkers across species, limiting our ability to improve age- and disease-related outcomes.

To summarize, a major challenge to the swift advancement of options for AD diagnosis and treatment has been a lack of biomarkers that can distinguish the effects of normal aging from those manifesting due to pathology, specifically at an early stage of the disease. The issue can thus be thought of in two parts: first, we must accurately characterize and understand the baseline processes underlying normal aging; and second, we need a more comprehensive understanding of the earliest processes occurring in AD and what the longitudinal trajectories of their identifying markers look like. Only once these issues have been addressed will researchers be able to distinguish early-stage AD from aging, expand the list of therapeutic targets, and identify the most effective time for intervention.

Specific Objectives of the Thesis: The overarching goal of this thesis is to investigate the effects of age and sex on brain volume and tissue chemistry, and to differentiate these effects from those initiated by the presence of Alzheimer's disease pathology. These investigations were performed in a commonly used model of aging, the Fischer 344 rat, and subsequently in a transgenic rat model of AD developed on a Fischer 344 background, the TgF344-AD rat. Additionally, we assessed

disease-dependent change in cognitive function throughout the lifespan in order to determine the chronological order in which dysfunction occurs in cognition, neuroanatomy, and neurochemistry in the TgF344-AD model. This comprehensive investigation allowed us to specifically address the following questions:

1. How do age and sex affect hippocampal tissue chemistry throughout the adult rat lifespan?
2. How do age and sex influence brain volume trajectories throughout the adult rat lifespan?
3. Does the TgF344-AD rat model recapitulate major cognitive, neurochemical, and neuroanatomical features of human Alzheimer's disease and in what chronological order do these pathological changes appear?
4. How does sex influence the pathological features of AD in the TgF344-AD rat model?

This thesis comprises an introduction (**Chapter 1**), a comprehensive background section (**Chapter 2**), three separate chapters which address the above research questions (**Chapters 3, 4, 5**), and a discussion section (**Chapter 6**) that integrates and contextualizes the relevance of the knowledge generated in the three previous chapters. The background section introduces the reader to relevant aging and AD literature, including details on rodent models and existing AD biomarkers, and highlights the current gaps in knowledge addressed in this thesis. It also covers fundamentals of the neuroimaging and statistical techniques applied throughout the thesis.

CHAPTER 2: BACKGROUND

2.1. Alzheimer's disease

2.1.1 Disease hallmarks

Alzheimer's disease (AD) is a progressive and irreversible neurodegenerative disorder responsible for between 60 and 80% of all dementia cases worldwide (Patterson 2018). AD presents as gradual dysfunction in memory, thinking, and behaviour. This encompasses difficulty with language, remembering people's names and faces, planning and decision-making, and understanding spatial relations, to changes in mood, personality, and emotional regulation. On a molecular level, AD is a disorder marked by the misfolding and aggregation of two specific proteins. The disease is characterized by neuritic plaques composed of aggregated amyloid- β protein ($A\beta$) and neurofibrillary tangles (NFTs) composed of hyperphosphorylated tau protein. The presence of both proteinopathies in post-mortem tissue is still required for pathological diagnosis (Jack et al. 2010; DeTure and Dickson 2019).

$A\beta$ is a small peptide generated by the cleavage of an aptly-named single-transmembrane protein called amyloid precursor protein (APP) that is expressed in both neural and non-neural cells alike. APP is cleaved by β -site APP-cleaving enzyme (BACE) and the catalytic component of γ -secretase known as Presenilin-1 (PS1), or its homologue, Presenilin-2 (PS2), generating $A\beta$ peptides of 38, 40, or 42 amino acids long, depending on the cleavage site of γ -secretase. Being the most hydrophobic of the peptides generated, $A\beta_{42}$ has the highest propensity to form oligomers and aggregate. $A\beta$ oligomers themselves can cause neuronal injury, but depending on the level of oligomerization and aggregation, $A\beta$ proteins can also form extracellular plaques ranging from "diffuse" to "dense-core" plaques, with dense-core plaques being the most neurotoxic (Haass and Selkoe 2007; Selkoe 2011). Dense-core plaques are also frequently referred to as "neuritic" plaques because dystrophic neurites occur within and around these amyloid deposits (Selkoe 2001).

While $A\beta$ plaques are extracellular protein aggregates, neurofibrillary tangles (NFTs) exist in the intracellular space, specifically within neurons. NFTs are aggregates of paired helical filaments (PHFs) composed of hyperphosphorylated tau protein. Tau is a protein that binds to and stabilizes microtubules (MTs), which are key structural and functional elements in axons that support neurite differentiation and growth, as well as axonal transport (Barbier et al. 2019; Hanes

et al. 2009). The binding of tau to MTs is regulated by the activities of several tau kinases and phosphatases which regulate the state of tau phosphorylation (Iqbal et al. 2005). In the event of hyperphosphorylation, as is the case in AD, tau dissociates from MTs, causing MT instability and depolymerization leading to cytoskeletal disruption, particularly regarding axonal transport of organelles and vesicles containing proteins and neurotransmitters (De-Paula et al. 2012). Tau then aggregates within the intracellular space of neurons, forming NFTs which cause neuronal and synaptic dysfunction (Selkoe 2001; Haass and Selkoe 2007).

The accumulation of amyloid and tau pathology occurs in distinct spatiotemporal patterns (**Figure 2.6.1**). A β accumulation initially occurs in regions that have neuronal populations with high energy demands, such as limbic and association cortices, and can begin to accumulate 10-20 years before symptom onset (Ossenkoppele and Hansson 2018). This is known as Stage A, according to initial staging of amyloid deposits by Braak et al (Braak and Braak 1997). A β pathology then spreads to the entire neocortex, allocortex, and the brainstem (Stage B), before eventually reaching the cerebellum (Stage C) (Hempel et al. 2021; Selkoe and Hardy 2016; Braak and Braak 1997). However, the distribution pattern and density of amyloid deposits has traditionally been seen as less informative and less capable of differentiating between neuropathological stages, whereas NFTs exhibit a more characteristic distribution pattern originally described by Braak et al. in the early 90s. Abnormal tau protein is detectable first in the transentorhinal (temporal lobe) and entorhinal regions (stages I-II), with some authors postulating that hyperphosphorylated tau first accumulates in the locus coeruleus and basal forebrain (Giorgi et al. 2019; Braak et al. 2006). NFTs then spread to the limbic allocortex (including the hippocampus) and adjoining neocortex (stages III-IV), and then in the isocortex, including the secondary and primary fields (stages V-VI) (Braak and Braak 1995; Braak and Braak 1991).

2.1.2 The amyloid cascade hypothesis

The process by which these pathological features result in dementia was proposed 30 years ago and coined “the amyloid cascade.” It is a formal hypothesis of disease progression in which accumulation of A β triggers a series of downstream events that ultimately result in the neurodegeneration and cognitive decline associated with AD (Selkoe 1991; Hardy and Allsop 1991) (**Figure 2.6.2**). It has been shown that changes in A β metabolism (rate of production, ratio of A β ₄₂ to A β ₄₀, and degradation/clearance) have direct neurotoxic effects on surrounding neurons while

simultaneously promoting the formation of A β oligomers and plaques (Hampel et al. 2021). Numerous studies have indicated that A β accumulation can occur up to decades prior to the onset of cognitive symptoms (Jack et al. 2013; Hampel et al. 2021; Bateman et al. 2012). The amyloid cascade proposes that as A β concentration (oligomers or plaques) increases, progressive and permanent changes in synaptic structure and function occur: synaptic spine loss, neuritic dystrophy, and impairments in long-term potentiation takes place, in combination with local inflammatory responses (microglial and astrocytic activation), altered neuronal ionic homeostasis (primarily calcium) and oxidative injury due to A β - and calcium-induced increased production of free radicals (Goodman and Mattson 1994; Haass and Selkoe 2007). A β -induced changes to kinase and phosphatase activity resulting in tau hyperphosphorylation, oligomerization, and formation of NFTs, leading to disruptions in axonal transport and neuronal function. Finally, the cascade culminates in widespread synaptic and neuronal dysfunction and cell death, leading to progressive dementia (Selkoe 1991). Given the progressive nature with which these pathological features manifest and/or accumulate, AD is considered a biological-clinical continuum that spans preclinical (pathology exist but the individual is asymptomatic), mild cognitive impairment (MCI: more pathology, some cognitive complaints), and dementia stages (Hampel et al. 2021). It is the major biological components of this cascade—amyloid, tau, and neurodegeneration—that have become the focus for biomarker development.

2.1.3 Current AD biomarkers

Since 1984, a conclusive AD diagnosis has required the presence of two features: a clinical phenotype of progressive dementia, comprised of impaired function in multiple cognitive domains (primarily episodic memory) to the point of interference with daily functioning; and specific neuropathological changes, including both intraneuronal neurofibrillary tangles and extracellular neuritic plaques, which are typically accompanied by synaptic loss and/or neurodegeneration (McKhann et al. 1984; Jack et al. 2018; McKhann et al. 2011). Since neuropathological examinations can only be performed after death, “probable AD” diagnoses can be made based on clinical presentation combined with the *in vivo* detection of AD hallmarks via neuroimaging (positron emission tomography, PET, or MRI) or fluid (blood and CSF) sampling techniques (Dubois et al. 2010; McKhann et al. 2011). However, given that cognitive dysfunction is one of the last features of AD to appear after up to decades of underlying brain pathological changes at the

cellular and molecular level (Jack et al. 2013; Bateman et al. 2012), it is not useful as a marker of early stages of the disease. Instead, biological (as opposed to symptom-based) criteria using neuroimaging and fluid biomarkers have been developed for staging across the entire disease spectrum (Jack et al. 2018; Jack et al. 2016). Importantly, this approach theoretically allows for identification of AD neuropathological change during preclinical stages when people are asymptomatic in an attempt to better identify individuals at risk of progressing to clinical AD dementia and the time at which preventative treatment might be most effective (Sperling et al. 2011; Dubois et al. 2010; McKhann et al. 2011; Jack et al. 2018).

The most recent framework for AD biomarkers includes three general groups of biomarkers: 1) amyloid (A), reflected by increased cortical amyloid PET ligand binding or low CSF A β ₄₂, which correlate with fibrillar A β deposits in post-mortem brain tissue (Tapiola et al. 2009; Ikonomic et al. 2008); 2) fibrillar tau (T), reflected by elevated CSF phosphorylated tau (P-tau) and increased cortical tau PET ligand binding, both of which correlate with NFT burden in brain tissue at autopsy (Buerger et al. 2006; Schöll et al. 2016); and 3) neurodegeneration or neuronal injury (N), indicated by increased CSF total tau (T-tau), hypometabolism detected by fluorodeoxyglucose 18F (FDG) PET, and specific patterns of MRI-detectable brain atrophy involving the medial temporal lobes, paralimbic, and temporoparietal cortices (Jack et al. 2018). However, of the biomarkers for neurodegeneration, MRI-detectable atrophy within medial temporal regions, including the hippocampus and entorhinal cortex, is the most established and validated, and is also the biomarker most closely associated with conversion from MCI to AD dementia (Leuzy et al. 2018; Frisoni et al. 2010; Jack et al. 2010). It is also now possible to detect brain-specific proteins in blood, with plasma tau, neurofilament light protein, and A β showing promise as candidate blood biomarkers (Nakamura et al. 2018; Dage et al. 2016; Mattsson et al. 2017). Plasma phospho-tau₂₁₇ (tau phosphorylated at threonine 217) in particular has similar accuracy to established CSF- and PET-based measures, and has been shown to be elevated in *PS1* mutation carriers as early as 20 years prior to symptom onset, supporting its application in early detection (Palmqvist et al. 2020). Blood draws are considerably easier than lumbar punctures for CSF and therefore a blood-based biomarker would have significant advantages. Additionally, abnormally high blood homocysteine, low plasma levels of the obesity-related hormone leptin, have recently been identified as risk factors for AD pathogenesis (Weiner et al. 2017). However, additional work is required to further optimize these assays, validate findings in diverse populations, and examine their role in clinical care, so they are

not currently as widely used as neuroimaging or CSF biomarkers. Based on both the amyloid cascade and experimental evidence, it is generally accepted that there is a temporal order to the appearance of abnormalities in AD biomarkers, although the manifestation and progression of each is heavily subject-dependent (**Figure 2.6.3**). CSF A β_{42} and amyloid PET binding are altered first, followed by CSF tau and FDG PET, then MRI-detectable atrophy. The last stage is characterized by the appearance of clinical symptoms where individuals progress from mild cognitive impairment (MCI) to AD dementia (Jack et al. 2013; Masters et al. 2015; Weiner et al. 2017).

It is important at this point to note that the generation of A β itself is not purely pathological but normally occurs as part of regular cellular metabolism (Selkoe 2001). Prior to oligomerization, A β monomers may even have neuroprotective effects (Giuffrida et al. 2009). Similarly, under normal conditions, tau is highly soluble and binds to neuronal MTs rather than forming aggregates. So what causes the shift towards pathological protein aggregation in AD?

2.1.4 Age: a major player in sporadic but not familial AD

An initiating factor in AD pathogenesis is relatively clear for the approximately 1 to 5% of cases that fall under the category of familial AD (FAD). This form of AD is inherited in an autosomal dominant manner and is characterized by early symptom onset between 40 and 65 years of age (average age ~ 45 years), which is why it is also often referred to as “early onset” AD (Selkoe 2001; DeTure and Dickson 2019). The early age of onset is a result of mutations in genes involved in A β production, specifically *APP*, *PS1*, and *PS2*. Mutations in *PS1* and *PS2* genes alter the proteolytic process of APP such that the A β_{42} variant of A β is produced more frequently than A β peptides of other lengths, while mutations in the A β region of the *APP* gene increase the propensity of the A β peptide to oligomerize and aggregate (Haass and Selkoe 2007). It is this gradual increase in the steady-state levels of A β that is thought to initiate the amyloid cascade leading to downstream accumulation of tau, neurodegeneration, and manifestation of cognitive impairment. Conversely, despite tau being a pathological protein in AD, mutations in genes regulating the production of tau do not appear to cause familial AD. The microtubule-associated protein tau (*MAPT*) gene is one such example: mutations in *MAPT* are associated with frontotemporal dementia, which is a disorder characterized by widespread NFT formation but not amyloid deposits (Masters et al. 2015). The ability for APP and presenilin mutations to cause downstream tau pathology but not vice versa

supports the view that A β accumulation is an early pathological event upstream of tau phosphorylation and tangle formation.

For the 95% of AD cases that are considered “sporadic” or late-onset (80-90 years of age), the initiating factors are unknown (Masters et al. 2015; Mawuenyega et al. 2010). Some researchers believe the majority of AD cases will eventually prove to have a genetic determinant of some kind (Selkoe 2011), while others suggest that AD is likely the consequence of multiple interacting pathologies (Villeneuve et al. 2015). The most prevalent genetic risk factor for sporadic cases is inheritance of one or two alleles of the ϵ 4 allele of ApolipoproteinE (ApoE), which increases A β oligomerization and reduces A β clearance from the brain, predisposing people to AD in over 40% of cases (Selkoe and Hardy 2016; Kline 2012). Recently, new genetic risk factors were identified, primarily affecting three main processes that contribute to aspects of A β homeostasis: cholesterol metabolism, inflammation/the brain’s innate immune system, and endosomal vesicle recycling, supporting the concept that A β accumulation may be the consequence of an earlier, initiating event (Jones et al. 2010; Lambert et al. 2013; Selkoe and Hardy 2016). There are also modifiable risk factors for AD that have been identified, including midlife hypertension, midlife obesity, physical inactivity, depression, smoking, and low educational attainment (Masters et al. 2015).

Of all of the non-genetic risk factors, age plays the largest role. Aging is a multifactorial physiological process characterized by gradually reduced biological function at the molecular, cellular, and histological level: our ability to learn and form memories deteriorates, our motor functions are reduced, the structural complexity of our brain cells decreases, and our homeostatic mechanisms fail, all of which increase vulnerability to age-related diseases and death (Herrup 2010; Hou et al. 2019; Azam et al. 2021). Age is the primary risk factor for neurodegenerative diseases such as AD, with an estimated prevalence of AD between 10 and 30% in people over 65 years of age (Masters et al. 2015). Understanding the aging process may therefore facilitate our understanding of and development of treatments for age-associated diseases such as AD. Given the commonality of neurodegenerative disease in the elderly population, AD is often argued to be a natural consequence of aging and that all people over 90 years of age will show some level of preclinical, prodromal, or clinical AD. However, post-mortem studies indicate that the prevalence of AD increases with age but then tapers off after 98 years of age (Masters et al. 2015). This information provides us with two possible interpretations: 1) AD is a natural consequence of the aging process but some individuals are resilient to disease development and/or progression due to

a variety of factors that provide adequate protection; or 2) AD is not simply a form of accelerated aging but rather, follows a pathological trajectory that is eventually distinct from the aging process. In either case, at some undetected point in time, the processes that underlie the normal aging process become pathogenic. It is this need for early distinction from the aging process that we run into the limitations presented by the current AD biomarkers.

2.1.5 Limitations of existing biomarkers

Despite the extent to which the current AD biomarkers have revolutionized how we understand and currently identify AD, there are still numerous caveats that support the need for additional biomarkers to complement those in the current biomarker model (Jack et al. 2013). First and most importantly, the etiology of AD remains to be elucidated. While A β accumulation is clearly an early event, several studies point to A β being necessary but not sufficient to cause progression to AD dementia (Villeneuve et al. 2015). For example, up to one third of cognitively normal individuals have significant A β burden in the absence of neurotoxicity in post-mortem brain tissue (Nelson et al. 2009; Herrup 2010), and there is a lack of coherence between amyloid burden and cognitive impairment (Doig et al. 2017). Additionally, promising drugs have been developed that successfully bind to and remove A β from the brain (primarily monoclonal antibodies such as solanezumab), or reduce amyloid production by inhibiting gamma- and beta-secretase (such as semagacestat and avagacestat), but these therapies did not significantly improve cognitive symptoms in clinical trials (De-Paula et al. 2012; Doody et al. 2014; Volloch and Rits 2018; Maia and Sousa 2019; Sperling et al. 2011), suggesting factors other than A β accumulation are at play. It is important to note that monoclonal antibody, aducanumab, was recently approved by the US Food and Drug Administration, despite insufficient evidence of cognitive improvement, and with the added high risk (~40%) of developing brain swelling (Knopman et al. 2021; Mullard 2021; Tampi et al. 2021), indicating that the scientific community is still in search of safe treatment that effectively slows cognitive decline. Finally, there is significant variability between individuals regarding disease manifestation and rate of progression, suggesting contribution from additional environmental, genetic, and epigenetic factors, as well as comorbidities, to vulnerability or resilience to AD (Bocancea et al. 2021; Villeneuve et al. 2015; Mattson and Magnus 2006). As such, it is likely that there are pathological events occurring “upstream” of A β that play an important, possibly larger, role in AD pathogenesis.

Second, several biomarkers used for diagnosis and monitoring of disease progression are not specific to AD (Jack et al. 2018; Nelson et al. 2009). CSF T-tau increases in neurodegenerative conditions without tau pathology and is therefore reflective of general as opposed to AD-specific neuronal damage (Masters et al. 2015). MRI-detectable atrophy indicating neurodegeneration is also not specific to AD; atrophy occurs in Parkinson's disease, dementia with Lewy bodies, synucleinopathies, and numerous other disorders (Nelson et al. 2009; Grothe et al. 2014). Finally, NFTs are found in frontotemporal dementias, some prion diseases, and other brain diseases, in addition to in AD (Nelson et al. 2009). Not only are many of these markers not specific to AD, but several of them have been identified in cognitively normal individuals (amyloid deposition (Morris et al. 2010; Bateman et al. 2012), NFTs (Braak and Del Tredici 2011)), and/or throughout the aging process (atrophy (Fjell and Walhovd 2010)), increased CSF tau (Nakai et al. 2021)) further complicating definitive diagnosis.

Finally, given the obvious complexity of AD and lack of success in targeting the amyloid accumulation process, it is likely that any effective intervention will be a combination therapy targeting multiple disease pathways. As such, the list of potential target mechanisms and their respective biomarkers needs to be expanded. For example, investigators have proposed alternative models of the disease process including early dysfunction in neuronal cell cycle control (Yang et al. 2003; Kruman et al. 2004), progressive oxidative damage (Zhu et al. 2006), reduced calcium homeostasis (Bezprozvanny and Mattson 2008; Green and LaFerla 2008), neuroinflammation (Ferreira et al. 2014; Heneka and O'Banion 2007; Krstic and Knuesel 2013), and loss of mitochondrial function (Swerdlow et al. 2014), all of which also become dysfunctional with age, further implicating the aging process with AD (Hou et al. 2019; Santiago et al. 2017; Franceschi et al. 2018). The implication of mitochondrial dysfunction with disease etiology and progression is a particularly convincing hypothesis that nicely incorporates other AD-associated phenomena, including increased oxidative stress and inflammation, all processes that yield several candidate biomarkers (Swerdlow et al. 2014). However, none of these processes have been pursued as potential biomarker options or disease-modifying targets.

In summary, it is clear that our understanding of and biological markers for the pathophysiological events comprising AD is incomplete, particularly at the earliest stages of the disease. We must also improve our understanding of the processes that occur as part of aging and how they tie aging to neurodegeneration. These gaps in knowledge limit our ability to accurately

distinguish early AD from aging and unnecessarily restricts the list of potential therapeutic targets.

2.2. Animal models as investigative tools for aging and AD research

2.2.1 Genetic basis of rodent models and the benefits of rats over mice

To address these important gaps in knowledge, we turn to preclinical research in animal models, specifically rodents. Mice (*Mus musculus*) and rats (*Rattus norvegicus*) are the most widely used models in biomedical research because they are genetically similar to humans, available in many standard or knock-in and knock-out strains, relatively easy to handle and inexpensive to house, and their genetics are extremely well-characterized (Lanz et al. 2020; Mitchell et al. 2015). Additionally, unlike human clinical studies, environmental and genetic influence can be tightly controlled, resulting in less variable data. Finally, an added benefit of using rodent models is their shorter lifespan compared to humans (approximately 20-26 months (Chesky and Rockstein 1976)), which greatly facilitates longitudinal studies, providing more power to detect neurobiological changes. All of these factors result in rodent studies being particularly well-suited for the creation of pre-clinical platforms for the development of biomarkers and evaluation of novel therapeutics.

Historically, mice have been used more than rats due to greater availability of genetic engineering tools developed in and designed for mice (Ellenbroek and Youn 2016). However, with the recent development of tools for altering the rat genome, other factors become more important when choosing between mice and rats to answer specific scientific questions, such as physiological, anatomical, biochemical, and pharmacological differences. For neuroscience research in particular, while mice have the benefits of being smaller and easier to house, and more readily available genetic modification techniques exist for them, rats may be preferred over mice for several reasons. First, rats have larger brains, which results in better spatial resolution for non-invasive magnetic resonance (MR) techniques such as structural MR imaging, (MRI) functional MRI (fMRI), and MR spectroscopy (MRS), which are frequently used in preclinical neuroscience research. Second, rats are genetically more similar to humans than mice regarding CNS metabolism and circuitry, meaning they are better models for studying basic brain function and metabolism, as well as human brain diseases (Lanz et al. 2020). In fact, there are several mouse models of AD that do not develop pathology to the same extent as their rat equivalents (TTg2576 mouse vs Tg6590 rat), despite expressing the same genetic mutations (Ellenbroek and Youn 2016). Finally, rats are significantly

more social than mice, are easier to handle, generally require less training, and exhibit more complex behaviour (Lanz et al. 2020; Gallagher et al. 2011). These factors make rats the preferred model for a variety of cognitive tests to characterize brain function, which is particularly important for studies on aging and neurodegeneration because the major clinical symptom is often cognitive dysfunction. The studies discussed in this thesis take advantage of all of these benefits by employing the Fischer 344 rat and the TgF344-AD rat to study aging and AD, respectively.

2.2.2 The Fischer 344 rat as a model of aging

The Fischer 344 rat is an inbred strain that has been provided by the National Institute on Aging (NIA) since its inception in 1974 and is considered the most commonly used rat model for aging research (Gallagher et al. 2011). Several studies on the longevity of this strain have been conducted, with an average lifespan of approximately 24 months (Chesky and Rockstein 1976; Masoro 1980). This relatively short lifespan, and thus short timeframe over which cohorts can be bred, aged, and studied, is one of the reasons they are used so frequently in aging research. Additionally, the inbred nature of the Fischer strain, as opposed to outbred strains like the Wistar rat, ensures a minimum of genetic variability (Gallagher et al. 2011). While the lack of genetic diversity can also be considered a downside as it does not completely replicate the diversity inherent to the process of human aging (or disease), it remains important to study inbred strains such as the Fischer rat because of their frequent use as background strains for transgenic models of disease (e.g. TgF344-AD model of AD (Cohen et al. 2013), HIV-1 model of HIV infection (Vigorito et al. 2015), Rag1-knockout immunodeficient rat (Ménoret et al. 2013)). As such, characterizing strain-specific effects of aging in the Fischer rat will provide a baseline with which to compare aging research in other strains to determine if findings from one genetic/biological background can be generalized to another, while also permitting a deeper understanding of the effects that occur when aging and transgene insertion are compounded, as is the case with transgenic models.

2.2.3 The TgF344-AD rat model: a major advancement for preclinical AD research

Early-stage disease characterization in transgenic animal models of AD represents one promising avenue towards the development of new biomarkers and intervention approaches at a clinical level. While transgenic models of AD have existed since the mid 1990s, rodent models that

fully recapitulate the neuropathological features of human AD have been lacking (for reviews, see (Do Carmo and Cuello 2013; Shineman et al. 2011)). The identification of mutations in *APP*, *PS1*, and *PS2* genes in human FAD have led to the generation of numerous AD rodent models via insertion of human transgenes into the mouse or rat genome. These A β overproducing rodents are considered “gold standard” models of FAD, but the majority do not display robust tauopathy or neuronal loss—two major hallmarks of AD—unless additional human transgenes are expressed that are not associated with FAD. One example is the 3xTg-AD rat (Oddo et al. 2003), a triple transgenic model harbouring *PS1*_{M146V}, *APP*_{Swe}, and *tau*_{P301L} mutations which replicates most major features AD with the exception of hippocampal neuronal loss (Nakai et al. 2021), but requires the expression of a tau mutation which is not associated with human FAD to do so. Another rat model that has become more commonly used as of late is the McGill-R-Thy1-APP rat; this is the only model capable of producing extensive amyloid pathology with a single transgene, but it fails to develop tau pathology (Leon et al. 2010). Rodent models of sporadic AD exist and neuropathology develops as a result of expressing variants of genes known to be strong genetic risk factors, such as *APOE* and *TREM2* (“triggering receptor expressed on myeloid cells” which mediates inflammatory responses (Foidl and Humpel 2020)). However, neither of these models of sporadic develops tau pathology or widespread neuronal loss (Nakai et al. 2021).

As such, the generation of the TgF344-AD rat, a model of Alzheimer’s disease developed on a Fischer 344 background (Cohen et al. 2013), represents a major advancement for preclinical AD research. This model displays progressive A β deposition, tauopathy including NFTs, gliosis, neuronal loss, and cognitive impairment, despite only expressing mutant human *APP* (*APP*_{Swe}, KM670/671NL) and *PS1* (Δ E9) genes (Morrone et al. 2020; Chaney et al. 2021; Cohen et al. 2013; Berkowitz et al. 2018). As such, this rat recapitulates the major neuropathological features of AD via the same genetic modifications as in human FAD. Interestingly, the insertion of the same transgenes in a mouse do not result in the same extensive pathology. Tg-*APP*_{Swe}/*PS1* Δ E9 mice show progressive amyloid pathology, cognitive deficits, and some tau pathology (Jankowsky et al. 2001; Liu et al. 2008), but they do not display NFTs or frank neuronal loss, and they display fewer soluble oligomeric A β species than the TgF344-AD rat (Do Carmo and Cuello 2013). It is theorized that the reason tau pathology forms in the TgF34-AD rat but not the comparable mouse model is that rats, like humans, have six isoforms of the tau protein, whereas mice only have 3 (Liu and Götz 2013). All six isoforms are affected by abnormal post-translational modifications in AD, and

hyperphosphorylation of these tau isoforms is a major driver of tangle formation, supporting the presence of NFTs in rats but not in mice (Hanes et al. 2009). Therefore, in addition to the recapitulation of other major AD hallmarks, the TgF344-AD rat is unique in its ability to develop extensive tau pathology and NFTs without insertion of a human tau transgene, making it a particularly salient option for preclinical biomarker development.

2.3 Fundamentals of neuroimaging techniques for preclinical biomarker development

Neuroimaging techniques such as MRI and MRS represent a powerful means of detecting and monitoring neurobiological changes *in vivo* at the preclinical and clinical level. Structural MRI is used to obtain a detailed three-dimensional anatomical picture of the brain's soft tissue and is frequently used in a quantitative manner to determine if there are volume changes reflecting underlying neuronal atrophy or hypertrophy (Bobinski et al. 2000). MRI scans are composed of tens of thousands of voxels whose signals come from protons in water and represent the bulk properties of the tissues being imaged. MRS is a method used to detect and quantify a wide range of neurochemicals in living brain tissue, providing key information about brain metabolism and function (Gao and Barker 2014). MRS spectra are obtained from a single, larger voxel within the brain, and are typically composed of signals from protons on multiple brain metabolites. Variants of MRS do exist for mapping of neurochemicals throughout the whole brain (i.e. MR spectroscopic imaging), and for observation of other (non-proton) nuclei, but these methods are beyond the scope of this thesis). Each metabolite is identified by one or more spectral peaks, each with a characteristic chemical shift and signal multiplicity (peak-splitting pattern). Both methods can be applied repeatedly with no side effects, facilitating longitudinal studies of brain structure and biochemistry. MRI and MRS protocols can be performed using the same scanner and equipment and are guided by the same basic principles of nuclear magnetic resonance (NMR), though with a few method-specific differences.

2.3.1 Fundamentals of nuclear magnetic resonance for MRI and MRS acquisition

The MR scanner consists of several sets of coils that generate and receive the MR signal, including magnet coils, three gradient coils, shim coils, and radiofrequency coils (**Figure 2.6.4**).

The magnet coils are used to generate a strong, constant magnetic field (B_0), measured in Tesla (T), which interacts with protons in the subject's tissue (Plewes and Kucharczyk 2012). Gradient coils representing the x, y, and z directions generate their own magnetic field and are superimposed on top of B_0 in such a way that the main magnetic field strength varies along the direction of the gradient field. The magnitude and direction of field strength variation are used to localize the MR signal (Elmaoğlu and Çelik 2011). Shim coils are used to correct for subject-dependent susceptibility effects on the main magnetic field; “shimming” is the process of adjusting the current in the shim coils to make the magnetic field as homogeneous as possible, which is critical for obtaining good spectral resolution and image quality. Finally, radiofrequency (RF) coils exist within the main MR system that generate their own magnetic field (B_1) and are used to both transmit RF energy into and receive RF signal back from the tissue of interest (Currie et al. 2013). For neuroimaging, separate RF transmitter and receiver coils are often used to simultaneously maximize the transmit RF field uniformity/coverage and the receive sensitivity to signals emitted from brain tissue. The majority of MR techniques measure signals from protons in hydrogen nuclei (^1H), which are present in the highest concentration in human tissue relative to other nuclei such as deuterium, sodium, or phosphorus (Plewes and Kucharczyk 2012).

MRI and MRS are based on the fundamentals of NMR which is the study of the magnetic properties and energies of nuclei, specifically the stimulated absorption and emission of electromagnetic radiation (de Graaf R.A., 2007). NMR itself is based on the concept of nuclear spin. A charged particle (such as a proton) spinning around its axis creates an electric current which generates a small magnetic field, also known as a magnetic moment, which has both an amplitude and direction. The magnetic moments of protons in tissue are typically randomly oriented, and thus the spins cancel each other out, resulting in a net magnetic moment (M_0) of zero. However, when an external magnetic field (B_0) is applied, two phenomena occur: the magnetic moments align either with (parallel) or against B_0 (antiparallel), and they experience a torque (rotational force) that causes the spins to rotate or “precess” about the magnetic field, similar to the movement of a spinning top (de Graaf 2018). The rate of precession (number of precessions per second, ω_0 , also known as the Larmor frequency) is proportional to the strength of B_0 and is determined by the Larmor equation: $\omega_0 = \gamma B_0$, where γ is the specific gyromagnetic ratio of the nucleus (hydrogen is 42.6 MHz/T) and B_0 is the strength of the magnetic field (Currie et al. 2013). Upon exposure to B_0 , more magnetic moments will align parallel to B_0 , as it is the lower, and thus preferred, energy state, resulting in an

M_0 parallel to B_0 . The sum of the magnetic moments of an ensemble of nuclei is called the magnetization, or M_0 , and in equilibrium it is oriented parallel to the applied magnetic field (along the z-axis). In order to detect an NMR signal, the magnetization vector must be perturbed by applying an additional magnetic field (B_1) in the form of a short duration radiofrequency pulse oriented perpendicular to the B_0 field (Elmaoğlu and Çelik 2011) (**Figure 2.6.5**).

The energy from the RF pulse is transferred to the protons themselves, causing some of the protons to move into the higher energy state (antiparallel to B_0), reducing longitudinal magnetization. At the same time, protons become synchronized and begin to precess in phase (instead of with random phases). As a result, the net magnetization vector tips away from B_0 into the transverse (xy) plane, generating transverse magnetization (Currie et al. 2013; de Graaf 2007). Energy transfer can only occur if the RF pulse has the same frequency as the precessional frequency of the protons, and thus RF pulses are set to the Larmor frequency. Additionally, the RF pulse can be set to tip M_0 away from B_0 at any desired angle, though the most common are 90° excitation into the transverse plane or inversion into the -z axis by a 180° pulse. Following the radiofrequency pulse some components of the magnetization are tipped into the transverse (x-y) plane. Once the RF pulse is turned off, the protons go through a process known as relaxation as they release the energy from the RF pulse. They begin to fall out of phase with each other, resulting in reduced transverse magnetization (T2 relaxation), while also returning to the lower energy state parallel to B_0 , which increases longitudinal magnetization (T1) back to its original value (Plewes and Kucharczyk 2012). These two processes occur simultaneously and independently: T1 relaxation is the process in which protons exchange energy with their surroundings (known as the lattice) to return to their lower energy state, and is also referred to as spin-lattice relaxation; T2 relaxation is the process in which phase coherence decreases due to exchange of energy between proton spins resulting in slowly fluctuating magnetic field variations (inhomogeneity) in tissue, and is therefore also known as spin-spin relaxation (Currie et al. 2013; Elmaoğlu and Çelik 2011). T2* (T2 star) relaxation is a related process that also describes the process by which transverse magnetization decreases, but it is a result of the combined effect of T2 relaxation and dephasing as a result of B_0 inhomogeneity.

As a result of T1, T2, and T2* relaxation, the magnetic moment moves from the transverse plane back to the longitudinal plane, following a spiraling path with constantly changing magnitude and direction. This process generates an electrical signal known as a free induction decay (FID) in

a receiver coil placed in the transverse plane (Gruber et al. 2018). The FID has the greatest magnitude immediately after the RF pulse is switched off and then decreases with time as relaxation occurs (**Figure 2.6.6**). The frequency of the FID is constant, and thus the signal takes the form of a sine wave (or a superposition of sine waves) with decreasing amplitude at a rate described by T_2^* . 180° refocusing pulses are used to compensate for the rate of signal decay; the pulse rephases the magnetic moments of the protons, resulting in a temporary gain in signal intensity at time echo time (TE) termed the spin echo (SE) (Currie et al. 2013). A pulse sequence with multiple 180° refocusing pulses results in a chain of spin echoes, each of lower intensity than the first as a result of T_2 relaxation effects. The curve connecting the spin echo amplitudes is the T_2 curve, whereas the T_2^* curve is generated when refocusing pulses are not used and thus signal decay is very fast (Plewes and Kucharczyk 2012). Pulse sequences are typically designed to take advantage of the inherently different relaxation rates within different tissues (grey matter, white matter, CSF, blood) and/or different neurochemicals in order to increase signal contrast (Plewes and Kucharczyk 2012).

In the case of both MRI and MRS experiments, the NMR (also called MR) signal originates from the entirety of the magnetized tissue, so in order to form MR images or spectra, it is necessary to localize and spatially encode the signal. These two steps are where the acquisition methods differ between MRI and MRS, so each will be discussed separately.

2.3.2 Specifics of MR image acquisition

Localization of signal acquisition for MR images is performed via slice selection. Slice selection is achieved by using a frequency selective RF pulse containing a specific range of frequency components (defined by a bandwidth) in combination with a magnetic field gradient of a chosen strength (to define the slice thickness) (Currie et al. 2013). This results in selective excitation of protons within a specific slab in space and leaves spins outside of this range unaffected. Spatial encoding for MRI is performed via a combination of frequency- and phase-encoding, both of which take advantage of gradient coils within the bore of the scanner. Gradient coils generate magnetic field gradients that alter the overall magnitude of the B_0 field in such a way that the intensity of the magnetic field becomes a linear function of position. To obtain three-dimensional spatial information, gradients are applied in the x, y, and z directions. Application of a new gradient magnetic field (phase-encoding gradient) in the y-direction is performed immediately after the excitatory RF pulse to make some protons precess faster than others depending on their position

within the gradient, resulting in spin phases that vary linearly over the phase-encode direction. A frequency-encoding gradient is applied after and perpendicular (x-direction) to the phase-encoding gradient, which causes the protons to rotate at different frequencies depending on their position within the gradient (Elmaoğlu and Çelik 2011; Plewes and Kucharczyk 2012). Therefore, provided the strength of the magnetic field is known, the position of an NMR signal can be determined simply by measuring its frequency and phase. This two-dimensional information is stored in a raw data matrix called “k-space” or “Fourier space”(Currie et al. 2013). The MR signal data stored in k-space can be converted to an MR image by applying the Fourier transform along each spatial dimension. The Fourier transform is a mathematical technique that decomposes a signal in the time domain (the FID) into a sum of sine waves of different frequencies, phases, and amplitudes in the frequency domain. The end result is a gray-scale MR image with various structures and/or tissues distinguished by differences in image contrast.

2.3.3 MR image processing and quantification

Small animal MRI is a unique method for detecting and monitoring altered brain structure *in vivo*. Its non-invasive nature and high tissue contrast have resulted in extensive use for studying normal development, aging, and numerous disease states. In particular, the development of several widely used preprocessing and analysis pipelines (Friedel et al. 2014; Tustison et al. 2014; Jenkinson et al. 2012), has facilitated quantification of longitudinal neuroanatomical change, with demonstrated success in preclinical studies (Rollins et al. 2019; Kong et al. 2018) and with equal applicability to human MRI data. Structural image analysis can be performed in several different ways (for a detailed review, see (Lerch et al. 2017)), two of which—deformation-based morphometry and volumetric analysis—will be discussed below.

Deformation-based morphometry (DBM) is an approach that examines macroscopic neuroanatomical change, that is, quantifies sizes and shapes across multiple voxels as opposed to within voxels (microscopic), and boasts the advantage of not requiring segmentation of a priori regions of interest (Gaser et al. 2001; Ashburner et al. 1998). This technique deforms each brain scan until it matches either a study average or a common space, and then uses the amount and direction of deformation (deformation field or vector) required to fit each scan to the average or template brain image to determine the amount of volume change at each voxel (Mietchen and Gaser 2009). DBM can be performed using cross-sectional data to detect group differences, or

longitudinal data to detect temporal variations in brain morphology. The process underlying the generation of deformation fields is image registration, which is the transformation that maps one image into the space or coordinate system of another. Image registration happens in multiple steps. In this thesis, image registration was performed using a least squares fit function (LSQ), of which there are two types: LSQ6 and LSQ12, denoting 6 and 12 degrees of freedom, respectively. First, linear rigid registration, LSQ6, is performed, which involves three translations and three rotations (hence 6 degrees of freedom). Second, an affine (or linear) LSQ12 fit is performed, which includes the translations and rotations from LSQ6 as well as scaling in the x, y, and z direction and shearing over the xy, xz, and yz planes. Finally, non-linear registration is performed which involves non-uniform deformation of an input image to the target (Friedel et al. 2014; Ashburner et al. 1998). Once all images are in the same stereotaxic space, differences between the input and template images can be determined on a voxel-to-voxel level by examining the deformation fields required to achieve the transformations. It is these deformations that can be used to calculate volume changes by way of the Jacobian determinant, which specifies the volume of the unit-cube, or voxel, after the deformation (Chung et al. 2001; Lepore et al. 2006).

For longitudinal data, there are a few additional steps that are required to obtain meaningful volume measurements. The two-level-model-build pipeline (Friedel et al. 2014) (**Figure 2.6.7**) is an incredibly useful tool for co-registration of images from a longitudinal dataset, where each subject has multiple images. First, a subject-specific average is generated by interactive group-wise registration that aligns all images from a given subject to each other (from time point 1, 2, etc). This permits meaningful statistical comparison across all timepoints for a given subject. Then all subject-specific averages are registered together using the same iterative group-wise registration process to create a population average (Friedel et al. 2014). This process creates deformation fields for each subject at each timepoint, which can be used to estimate the Jacobian determinant at each voxel. Two sets of Jacobian determinations are generated by the co-registration process: the absolute Jacobian, composed of the sum of the linear and non-linear mappings, reflects the global changes in voxel volume; and the relative jacobian, which is composed solely of the non-linear transformations, reflects local or relative changes in voxel volume (Chung et al. 2001; Chung et al. 2003).

Volumetric analysis focuses on examining specific regions or structures of interest defined by segmentation, which can be performed manually or using automatic segmentation algorithms.

Manual segmentation is an extremely labour-intensive process that requires highly trained anatomists to manually define regions of interest in each slice of a brain scan based on anatomical priors (Despotović et al. 2015). The volume of a region is then estimated based on the number of voxels within the region and the scan resolution. Given the length of time required to manually segment brain regions, this method is not particularly scalable to large studies, and it is also prone to errors. As a result, manual segmentation is more frequently used in small studies or to develop brain atlases (Goerzen et al. 2020; Dorr et al. 2008) that are then used in automatic segmentation algorithms (Chakravarty et al. 2013; Lerch et al. 2017).

Automatic segmentation algorithms aim to segment brain scans into distinct, non-overlapping regions, often making use of a manually segmented atlas. A combination of linear and non-linear image registration and/or tissue classification based on image features is performed to align an image with the atlas. Once registration is complete, segmentation of the atlas can be transferred to the target image via label propagation, multi-atlas methods, or probabilistic techniques (Despotović et al. 2015). For a review on these atlas-based segmentation techniques, please see (Cabezas et al. 2011). In this thesis, label propagation was used and regional volumes were calculated by multiplying the Jacobian determinant with the voxel volume at each voxel, resulting in absolute and brain-size-corrected volumes generated from the absolute and relative Jacobians, respectively (Lerch et al. 2017).

2.3.4 Specifics of MR spectra acquisition

In single-voxel MRS, spatial localization is used to remove unwanted signals from outside the ROI (such as extracranial lipids) and to achieve more meaningful spectra, as different tissue types can have unique metabolic profiles (Juchem and Rothman 2014). There are multiple pulse sequences for volume selection but the Point Resolved Spectroscopy sequence was applied in this thesis and will therefore be discussed here. The PRESS sequence is a double spin-echo sequence consisting of three slice-selective RF pulses (90° , 180° , 180°) in three orthogonal planes which isolates the signal to the intersection of the three planes (the voxel) (de Graaf 2007).

In contrast to an MR image wherein the frequency of signal varies as a function of position, in an MR spectra the frequency of the signal varies only as a function of chemical shift. This frequency shift is a result of the chemical environment surrounding the proton emitting the signal, meaning that nuclei within the same molecule can absorb energy at different resonant frequencies

depending on what other nuclei are around them (Juchem and Rothman 2014; Dona et al. 2016). The phenomenon is caused by shielding of nuclei from B_0 by surrounding electrons, thus reducing the magnetic field experienced by the nucleus. The effective magnetic field (B) experienced by a nucleus is expressed as $B=B_0(1-\sigma)$, where σ is the shielding coefficient, measured in parts per million (ppm). The resulting resonant frequency, accounting for the chemical shift, is given by $\omega_0=\gamma B_0(1-\sigma)$. For example, the CH₃ and CH₂ protons in lactate experience different magnetic fields due to differing chemical environments, and thus CH₃ and CH₂ show up as separate peaks, despite the signals coming from the same nuclei, i.e. hydrogen. The separation of these signals provides direct information regarding the chemical environment of nuclei, thus aiding in the identification of compounds. Additionally, the integrated resonance area (under the peaks) are directly proportional to the concentration of each set of nuclei (i.e. CH₃ contains 3 hydrogens, CH₂ contains 2 hydrogens), making NMR a quantitative technique (Juchem and Rothman 2014).

J coupling (also known as spin-spin coupling or scalar coupling) is another phenomenon that provides additional information as to the identity of a specific molecule. J coupling describes a phenomenon whereby the spin of one nucleus affects the spin of another nucleus through their chemical bonds, and thus “sharing” of electrons (Juchem and Rothman 2014; de Graaf 2018). It is J coupling that results in the splitting of peaks into doublets, triplets, etc., depending on how many J-coupled spins a nucleus is interacting with. For a detailed description on peak splitting, please see (de Graaf 2018).

As a result of chemical shift and J-coupling, combined with the fact that the MRS signal comes from up to 27 metabolites and macromolecules (Mlynárik et al. 2008; Fowler et al. 2020), the resulting FID signal is composed of layers upon layers of signals, each with their own frequency and amplitude. This is where the Fourier Transform is again applied, resulting in conversion of the FID signal into the frequency domain, known as an NMR spectrum. In this form, each neurochemical can be identified based on its unique frequency (ppm) and splitting pattern.

2.3.5 Quantification of the MRS signal

Quantification of the complex NMR signal is challenging for a number of reasons, but particularly because of the overlapping resonances and complex splitting patterns of the many metabolites underlying the signal (**Figure 2.6.8**). One of the most commonly used algorithms for spectral fitting is LCModel (Linear Combination of Model spectra) developed by Provencher et al.

(Provencher 1993; Provencher 2001). LCModel, as the name implies, fits the NMR signal using a linear combination of metabolite basis function, whereby the weighting or scaling of each metabolite's basis function reflects its concentration. This method requires advanced prior knowledge about the chemical shift and splitting patterns of expected metabolites (Govindaraju et al. 2000; Behar and Ogino 1991). The information is then incorporated into the spectral fitting process in the form of simulated basis functions (i.e. Lorentzian or Gaussian curves), with chemical shifts and peak splitting patterns specific to each metabolite, simulated using the study's pulse sequence parameters (Near et al. 2020). Recently, basis sets have been developed and implemented to handle the underlying macromolecule signal, both to improve metabolite quantification and to quantify the macromolecule resonances themselves (Považan et al. 2018; Lee and Kim 2017; Lopez-Kolkovsky et al. 2016; Snoussi et al. 2015). Quantification can be performed relative to a major peak in the spectrum (typically total creatine) or in absolute units wherein concentrations are referenced to the water peak obtained in a separate scan. Total creatine has been shown to change with age, sex, and in some pathologies (Fowler et al. 2020; Duarte et al. 2012; Haga et al. 2009; Zhang et al. 2009), so referencing to water is more common (Near et al. 2020). For details on the complexities of spectral quantification, including preprocessing, please see the following expert consensus papers (Near et al. 2020; Lanz et al. 2020; Kreis et al. 2020).

Currently, up to 21 individual metabolites and 7 macromolecules are quantifiable in the rodent brain at high magnetic fields ($\geq 7T$) (Fowler et al. 2020; Mlynárik et al. 2008; Duarte et al. 2012). Metabolites visible in the 1H MRS spectra include total choline (tCho: sum of glycerophosphocholine, GPC, and phosphocholine, PCh), N-acetylaspartate (NAA), myo-inositol (Ins), total creatine (tCr: sum of creatine, Cr, and phosphocreatine, PCr), glutamine (Gln), glutamate (Glu), lactate (Lac), taurine (Tau), glutathione (GSH), and gamma-amino butyric acid (GABA). Several of the most commonly quantified metabolites will be discussed briefly below, as well as in the context of aging and AD in **section 2.3.7**.

2.3.6 Interpretation of the neurochemical profile

N-acetylaspartate (NAA): NAA is a nervous-system specific metabolite synthesized from L-aspartate and acetyl-coenzyme A (acetyl CoA) in neurons, and is present in the brain in concentrations of 10mM or higher, making it extremely prominent in the NMR signal. Since NAA is synthesized exclusively in neuronal mitochondria, and thus is localized in neurons, axons, and

dendrites, NAA has traditionally been used as a marker of neuronal density (Gao and Barker 2014; Moffett et al. 2007). More recently, NAA has also been proposed as a marker of neuronal dysfunction, specifically neuronal mitochondrial dysfunction, rather than reflecting just neuronal loss, due to the discovery that the synthesis of NAA from aspartate and acetyl CoA by brain mitochondria is energy-dependent (stimulated by ADP) and is regulated by aspartate synthesis in mitochondria (Clark 1998; de Graaf 2018; Moffett et al. 2014). A role for NAA in the maintenance of myelin, particularly during development, is also likely: within oligodendroglia in the developing brain, hydrolysis products of NAA are used for fatty acid and sterol synthesis which are the building blocks for myelin lipid synthesis (Moffett et al. 2007; Clark 1998; McKenna et al. 2012). Finally, NAA also serves as a precursor for the most concentrated neuroactive peptide in the human brain, N-acetylaspartylglutamate (NAAG) (Moffett et al. 2014). In summary, NAA is a highly reliable marker of neuronal health that may also reflect several different metabolic processes, so interpretation in the context of other metabolic changes is important for a full understanding of what alterations in NAA may indicate.

Total Creatine (tCr): tCr consists of a sum of creatine (Cr) and phosphocreatine (PCr), both of which (in combination with ATP) play an important role in tissue energy metabolism (de Graaf 2018). Through the actions of creatine kinase (CK), an N-phosphoryl group from phosphocreatine can be reversibly transferred to ADP to generate ATP, creating Cr in the process. This process is particularly crucial in neurons due to their high and readily changing energy demands, and a number of reports emphasize the importance of maintaining the CK/PCr/Cr system for normal brain function due to the role of PCr and CK as an energy buffer and as an energy shuttle from mitochondria to energy utilizing sites (Andres et al. 2008; Béard and Braissant 2010; de Graaf 2018). tCr is frequently used as an internal reference, but this should be done with caution as a number of studies have indicated changes with age, sex, and some pathologies (Fowler et al. 2020; Haga et al. 2009). PCr and Cr resonances can occasionally be separated at 7T and above but are frequently reported together due to high correlation (representing high spectral overlap) between the two during fitting (de Graaf 2018; Marjańska et al. 2019).

Total Choline (tCho): after NAA and tCr, the most prominent resonance in proton MRS spectra from brain tissue arises from protons within cytosolic choline-containing compounds, phosphocholine (PCh) and glycerophosphocholine (GPC). Given the difficulty in separating the two resonances, they are often reported as a sum (de Graaf 2018). Choline-containing compounds

such as GPC and PCh are thought to reflect membrane turnover due to their involvement in phospholipid synthesis and degradation pathways as breakdown products of phosphatidylcholine (Graff-Radford and Kantarci 2013). As such tCho is proposed as a metabolic marker of cell density and membrane integrity. However, given the downstream effects of cell membrane breakdown and thus loss of homeostasis, increased tCho may also reflect myelin breakdown, inflammation, gliosis, and neurodegeneration (Hammen and Kuzniecky 2012; Klein 2000).

Myo-inositol (Ins): Ins is a simple sugar alcohol with estimated brain tissue concentrations of approximately 6mM (Best et al. 2014). The exact function of Ins is not known but many roles for it have been suggested. Ins is primarily localized in glial cells and has traditionally been considered as a marker of glial cell proliferation and/or activation (Brand et al. 1993; Harris et al. 2015), though a few studies have disputed this (Murray et al. 2014; Pardon et al. 2016). It was recently proposed as a surrogate marker of neuroinflammation in AD (Kantarci and Goldberg 2016), and has also demonstrated a very strong relationship with A β plaque pathology, leading others to suggest its use as a proxy for A β burden (Murray et al. 2014; Voevodskaya et al. 2019), and even as a risk marker of preclinical AD when combined in a ratio with NAA (Waragai et al. 2017; Godbolt et al. 2006; Kantarci et al. 2002; Kantarci and Goldberg 2016). Ins is also an organic osmolyte in CNS tissue, whereby Ins efflux from neurons and glia (particularly astrocytes) takes place via a volume-sensitive organic osmolyte channel (Harris et al. 2015). This channel regulates efflux of osmolytes such as Ins and Taurine (Tau) as a response to cell swelling and osmotic stress (Best et al. 2014), and as such, intracellular Ins concentrations increase as a response to extracellular hypertonicity (Lee et al. 1994). Some intracellular Ins acts as a precursor for second messengers (mainly phosphatidylinositol, PI, and inositol phosphates, InsP, (Gonzalez-Uarquin et al. 2020)) formed by the phosphoinositol cycle, which is involved in cellular regulation and signal transduction, particularly insulin and lipid signalling and glucose metabolism (Ross and Sachdev 2004; Gao and Barker 2014; Bevilacqua and Bizzarri 2018). For example, Ins interacts directly with insulin target tissues and has been shown to induce insulin sensitivity (Chhetri 2019). Finally, Ins has been shown to promote antioxidant effects (Jiang et al. 2009; Hoffman-Kuczynski and Reo 2004), though this requires further investigation.

Glutamate (Glu) and Glutamine (Gln): Glu is a nonessential amino acid with multiple metabolic roles and is the most abundant amino acid in the brain (Ross and Sachdev 2004). It is the major excitatory neurotransmitter in mammalian brain; a precursor for the major inhibitory

neurotransmitter, GABA; and also contributes to the synthesis of small molecules such as GSH. Glu is typically present in the brain at concentrations between 6-12.5 mM and appears in all cell types, with the largest pool within glutamatergic neurons (de Graaf 2018). Glu is also part of the Glu-Gln neurotransmitter cycle: in glutamatergic neurons, glutamate acts as an excitatory neurotransmitter and is released into the synaptic cleft. Glu interacts with post-synaptic receptors and is then taken up by astroglia, where it is synthesized into the amino acid Gln by Gln synthetase. Gln is then transported back to the glutamatergic neuron whereby it is converted back to Glu by glutaminase (de Graaf 2018). A similar pathway exists between GABAergic neurons and astroglia, where Gln is transported from astroglia to the GABAergic neuron, converted into Glu for use in the tricarboxylic acid cycle (TCA) and/or converted to GABA for inhibitory neurotransmission before re-uptake back into the astroglia. It has been proposed that MRS-detectable Glu primarily reflects the concentration of Glu within the intracellular compartment (Gao and Barker 2014), and as such, Gln may be a more accurate measure of Glu-Gln cycling (Ross and Sachdev 2004). Despite being present in both neurons and astroglia, Gln is primarily localized in astroglia, and appears at a concentration of 2-4 mM. Glu and Gln are typically only distinguishable at field strengths of 7T and above and so are frequently reported as a sum, referred to as Glx (Gao and Barker 2014).

Macromolecules (MM): proton spectra obtained at higher magnetic fields and/or using sequences with short echo times (TE) display significant contributions from high molecular weight molecules known as macromolecules (MM) (de Graaf 2018). Due to the strong contribution of MM to the overall signal, proper handling is important to achieve accurate metabolite measurements and improve reproducibility (Hofmann et al. 2002). Approximately 10 MM resonances can be identified in most proton spectra. Behar and colleagues identified that individual resonances represent signals from methyl and methylene resonances of cytosolic protein amino acids, such as leucine, isoleucine, valine, threonine, alanine, etc., though exact attribution of amino acids to peaks has not been possible (Behar and Ogino 1993; Behar et al. 1994). It has been proposed that increased MM content may reflect increased free fatty acids or higher visibility of cytosolic proteins after cell death (Saunders et al. 1997). However, given the complexity of attributing cellular or molecular change to specific MM peaks, changes in the MM signal may be more useful as an overall biomarker of health or pathology rather than being indicative of a particular mechanism.

In summary, given the amount of biochemical information that can be obtained from a single, non-invasive scan, MRS is a particularly useful tool for the study of aging and

neurodegenerative disorders where comprehensive and longitudinal characterization of brain tissue chemistry could be used to develop diagnosis or therapeutic efficacy criteria at the preclinical or clinical level. MRS may complement MRI for these applications given that MRI-detectable volume changes typically occur in older populations and/or in mid-to-late stages of AD, whereas MRS may inform on a multitude of processes affected by aging or neurodegeneration at varying points throughout the lifespan.

2.4 Implementation of MRI and MRS in aging and AD research: findings and gaps in knowledge

2.4.1 Application of structural MRI to study the aging brain

Thanks to its excellent safety profile, non-invasive nature, excellent soft tissue contrast, and widespread availability, MRI has been used extensively to study aging in humans. A recent review of 56 studies of brain volume indicated both grey matter and white matter volume decline with age, particularly in frontal regions, though white matter volume may decrease at a slower rate (MacDonald and Pike 2021). In particular, volume loss in the hippocampus, amygdala, caudate, putamen and cerebellum have been identified, with more moderate effects in the globus pallidus and thalamus (Raz and Rodrigue 2006; Raz et al. 2005). Overall brain size is generally stable from the 20s through the mid-50s, and then slowly declines with increasing age as a result of loss of axonal fibers and neuronal shrinkage (Sowell et al. 2004; Scahill et al. 2003). Cortical thinning is also observed in most regions of the brain but with slightly higher rates in the frontal lobes (Sowell et al. 2004; Raz and Rodrigue 2006). In addition, increases in ventricular size and CSF volume are one of the most notable features that change with age, particularly in the lateral ventricles (MacDonald and Pike 2021; Raz and Rodrigue 2006; Pfefferbaum et al. 2013). Other reviews support most of these findings (Fjell and Walhovd 2010; Walhovd et al. 2005).

Due to a variety of challenges, the majority of aging studies in humans are cross-sectional group comparisons or cross-sectional continuous study designs which frequently suffer from cohort effects and do not allow for examination of non-linear volume changes with age, a phenomenon that has been observed in aging rodents (Kong et al. 2018) and in humans (Pfefferbaum et al. 2013; Tullo et al. 2019). Additionally, and with a few exceptions (Tullo et al. 2019; Raz and Rodrigue 2006), most human studies do not examine subcortical structures, limiting our understanding of

smaller-scale changes in brain structure with age. This may be partly because of lower spatial resolution that is attainable on preclinical scanners, which typically operate at 1.5 to 3T. Preclinical aging studies in rodents can adequately address these limitations.

Interestingly, despite the non-invasive nature of MRI facilitating longitudinal studies, few preclinical studies have been performed that take advantage of a longitudinal paradigm and those that have were all performed in mice (Reichel et al. 2017; Maheswaran et al. 2009; von Kienlin et al. 2005; Oberg et al. 2008), which are genetically less similar to humans than rats (Ellenbroek and Youn 2016). Additionally, the vast majority of studies examining longitudinal neuroanatomical change have done so during development or adulthood (Spring et al. 2010; Sumiyoshi et al. 2017; Casas et al. 2018; Qiu et al. 2018), disregarding the aging brain. Of the studies examining the aging rodent brain, several findings were generally consistent, both relative to each other and to human aging studies: hippocampal volume decreased (Driscoll et al. 2006; Maheswaran et al. 2009; Hamezah et al. 2017; Reichel et al. 2017), ventricles increased (von Kienlin et al. 2005; Oberg et al. 2008; Maheswaran et al. 2009; Hamezah et al. 2017), the medial prefrontal cortex, caudoputamen, and thalamus decreased, and the corpus callosum, corticospinal tract, and fornix system increased (Maheswaran et al. 2009). One finding that was contrary to human studies but was consistently reported in rodents was an overall increase in absolute brain volume with age (Gaser et al. 2012; Maheswaran et al. 2009; von Kienlin et al. 2005; Oberg et al. 2008). This finding, as well as a report of increased dentate gyrus volume with age (Alexander et al. 2020), require further investigation. Finally, two additional limitations to these studies are the limited number of brain regions examined—despite high spatial resolution facilitating the delineation of more structures—and the exclusive use of a single sex, with the exception of the study by Oberg et al. (Oberg et al. 2008).

Gap in knowledge #1: Significant work has been done to study the aging process in humans using MRI, but longitudinal studies are lacking due to the long timeframe over which the studies must be conducted. In a preclinical setting, while these longitudinal paradigms are feasible, the majority of studies have been conducted during development or adulthood, disregarding the aging brain, or aging studies have been conducted but in a cross-sectional manner. To our knowledge, a longitudinal examination of neuroanatomical change with age has not been performed in any aging rat cohort. In particular, the field is lacking aging studies that examine many brain regions across the brain and are performed in both sexes.

2.4.2 Application of single-voxel MRS to study aging

In comparison to examination of the whole brain via structural MRI, single-voxel MRS provides a more localized look at changes taking place in the brain as a result of aging or AD. Just as structural MRI allows for measurement of numerous brain structures, MRS can quantify many different neurochemicals, providing a comprehensive survey of tissue biochemistry at a point in time, or longitudinally, within an isolated area of the brain. When MRS is applied in humans, typically only the major resonances, such as NAA, tCho, tCr, and sometimes Ins, are quantified due to low scanner strength (1.5 to 3T) and thus low spectral resolution. Comprehensive reviews of age-related brain metabolite changes in the human brain show that NAA tends to decrease, while tCho and tCr tend to increase, but there are many studies within these reviews that indicate no change in these metabolites (Haga et al. 2009; Cleeland et al. 2019). Studies that examined Ins reported an increase with age (Cleeland et al. 2019; Ross et al. 2006). These changes, which have also been observed at higher field strengths (7T) are generally thought to reflect reduced neuronal viability (NAA), increased cell membrane turnover (tCho), altered energy metabolism (tCr), and increased gliosis, osmotic stress, or altered cell signalling (Marjańska et al. 2017), all phenomenon shown to be altered during the aging process (Camandola and Mattson 2017; Mattson and Magnus 2006; Mattson and Arumugam 2018).

Preclinical systems mainly operate at 7 to 9.4T with scanners going as high as 17.2T, providing significantly better spectral resolution which allows for identification of up to 21 metabolites. Several authors have characterized neurochemical change with age in mice and rats, though with inconsistencies between studies. In one of the only longitudinal MRS studies of aging in rodents, Duarte et al. identified reductions in many hippocampal metabolites, including GABA, Glu, Asp, (involved in neurotransmission), Glc, Lac, tCr (involved in energy metabolism), ascorbate (Asc, anti-oxidant), phosphoethanolamine (PE), and NAA, along with increased tCho (latter three involved in membrane metabolism) in male and female C57BL/6 mice from 3 to 24 months (Duarte et al. 2014). In a cross-sectional examination of hippocampal metabolism, 22 month-old male Fischer rats demonstrated decreased ascorbate, aspartate, phosphoethanolamine, and increased total choline relative to 2-months old rats, similar to the above study, but additional increases in Glc, Gln, Ins, and NAAG were also reported (Harris et al. 2014). Cross-sectional studies using high-resolution magic angle spinning nuclear magnetic resonance support increased Ins and Lac in older rats (male and female Sprague-Dawley rats, 1 to 24 months old) (Zhang et al.

2009), as well as reduced Asp and NAA (male Long Evans rats, 4 to 30 months old) (Paban et al. 2010), but opposing effects were also reported, such as reduced tCho (Paban et al. 2010). Finally, in contrast to the majority of the aforementioned studies, in a cross-sectional analysis of female Fischer 344 x Brown Norway hybrid (FBNF1) rats between 3 and 24 months, Driscoll et al. identified stable concentrations of NAA, tCho, and tCr with age (Driscoll et al. 2006). While many of the neurochemical changes identified in these studies reflect known age-related changes in neurotransmission (e.g. Glu, GABA), energy metabolism (Glc, Lac, tCr), cell membrane turnover (tCho, PE), and oxidative stress (Asc) (Camandola and Mattson 2017), there are also significant inconsistencies that would be best addressed by a longitudinal study that examines neurochemical change in both sexes, in brain regions relevant to age-related disorders, and using techniques that appropriately account for the macromolecule signal.

At higher fields, the contribution from underlying macromolecules (MM) is larger, which requires proper handling for accurate metabolite quantification (Hofmann et al. 2002), but also provides an opportunity to quantify the MM resonances themselves and gain more insight into the biochemical status of the brain tissue during aging. Only two reports exist that discuss individual MM changes with age, and they are both in aging human populations, whereby increases in MM resonances at 1.7, 2.0, and 3.9 ppm were reported (Hofmann et al. 2001; Marjańska et al. 2017). MMs have been successfully quantified in the rat brain but not in the context of aging (Lopez-Kolkovsky et al. 2016; Lee and Kim 2017; Cudalbu et al. 2012).

Gap in knowledge #2: Despite MRS facilitating longitudinal studies, many preclinical studies are still performed cross-sectionally. As such, longitudinal investigations of neurochemical change with age in the rat brain have not yet been performed. Additionally, changes in individual MMs with age have not been documented in either humans or rodents, particularly not in conjunction with the rest of the neurochemical profile.

2.4.3 Detection and monitoring of AD using MRI and MRS

MR-detectable volume loss indicating neurodegeneration in specific brain regions is already an accepted biomarker for Alzheimer's disease and can be used to support a clinical diagnosis of AD (Pini et al. 2016; McKhann et al. 2011). Volumetric measurement of the hippocampus and entorhinal cortex specifically are currently the best-established biomarkers for Alzheimer's disease (Teipel et al. 2013; Leuzy et al. 2018; Frisoni et al. 2010; Pini et al. 2016). While decreased medial

temporal lobe (MTL) volume loss is also a feature of aging, the extent of the decrease is larger in MCI and AD patients (Leuzy et al. 2018; Kantarci and Jack 2003). Compared to normal aging, individuals with MCI demonstrate accelerated atrophy in whole brain volume, temporal gray matter, and orbitofrontal and temporal association cortices (including the hippocampus), as well as further ventricular atrophy (Driscoll et al. 2009). Additionally, annualized rates of hippocampus volume loss correlate with progression of clinical diagnoses from MCI and AD dementia (Jack et al. 2000), and structural brain changes have also been shown to accurately reflect Braak stages of NFT deposition (Frisoni et al. 2010). Finally, it is important to note that histopathological analyses confirm that MR-detectable volume loss is representative of tissue atrophy as a result of microstructural changes (dendritic and axonal loss), neuronal loss, or reduction in size, though the exact cellular cause of atrophy may differ by region (Frisoni et al. 2010; Bobinski et al. 2000).

Studies in transgenic models generally reflect the MTL atrophy found in human AD but with some exceptions. The 3xTg and APP/PS1 models appear to recapitulate the hippocampal atrophy reported in humans (APP/PS1:(Lau et al. 2008; Oberg et al. 2008)), along with reductions in the cortex, cerebellum, and olfactory bulbs (3xTg: (Güell-Bosch et al. 2020)), as well as decreased fornix, fimbria, and entorhinal cortex volumes (3xTg: (Kong et al. 2018)). The McGill-R-Thy-1-APP rat also demonstrates hippocampal atrophy, specifically between 9 and 16 months of age (Parent et al. 2017). However, there are also conflicting reports: for example, the TgCRND8 model demonstrates reduced hippocampal volume as early as 9 weeks prior to significant amyloid deposition, but the volume stabilized by 12 weeks (Allemang-Grand et al. 2015), while APP/J20 mice actually demonstrated hypertrophy in hippocampus and dentate gyrus volumes (Badhwar et al. 2013), and the TgF344-AD rat did not show any hippocampal atrophy by 18 months, but did have reduced volume in the Raphe nuclei, mesencephalic reticular formation, and cerebral peduncle (Anckaerts et al. 2019). Further complicating the preclinical AD literature, only some authors noted increased ventricular volume in transgenic rats relative to WT controls (Oberg et al. 2008), while others reported a decrease (Kong et al. 2018; Lau et al. 2008). Many of these transgenic models differ in terms of background strain, number and type of mutations, and even species, which likely contributes to the inconsistencies reported here. In order to obtain results that are closer to those reported in humans, studies may need to focus on rat models as opposed to mouse models. Rate of disease progression is significantly slower in the TgF344-AD rat or the McGill-R-Thy1-APP rat as compared to the aforementioned mouse models, which more closely mimics disease progression in

humans. This may be partly a result of the closer genetic relationship between rats and humans than that of mice and humans. Additionally, the larger brain size in rats may provide better spatial resolution and thus more accurate quantification of brain structural volumes. However, it is important to note that neurodegeneration-related atrophy is one of the last features to appear before the onset of cognitive symptoms (Jack et al. 2013; Gordon et al. 2018), significantly reducing its potential for detecting disease early into disease progression.

This is where MRS in combination with MRI may prove particularly useful. MRS is one of the most extensively studied MR techniques for AD diagnosis (Kantarci and Jack 2003); simply the ratio of NAA/Ins has been shown to distinguish clinical confirmed AD patients from healthy individuals with a sensitivity of 83% and a specificity of 98% (Shonk et al. 1995). Other than the NAA/Ins ratio, the most commonly quantified metabolites are NAA, tCho, and tCr, which are the easiest to distinguish on an MR spectrum, and occasionally Ins. There appears to be a temporal order in which these major metabolites become disrupted, one that may both support and complement structural MRI findings. Several studies using cross-sectional sampling schemes have demonstrated elevated Ins early on in disease progression, suggesting some level of gliosis or neuroinflammation, and then decreased NAA—thought to reflect neuronal viability—in more advanced cases of AD when a cognitive diagnosis of dementia was made (Kantarci et al. 2000; Pfefferbaum et al. 1999; Murray et al. 2014), potentially aligning with findings of MRI-detectable neurodegeneration towards the later stages of the disease. tCho has also been shown to be increased in elderly populations and in patients with MCI and AD (Marjańska et al. 2019), as has tCr (Pfefferbaum et al. 1999), suggesting these two markers may be altered somewhere in the middle of Ins and NAA.

Preclinical studies in transgenic rodent models generally replicate these findings while providing additional metabolic insight as a result of higher spectral resolution. Similar to findings in human AD studies, increased Ins followed by decreased NAA were reported by authors studying the 3xTg mouse (Choi et al. 2014), the Tg2576 mouse (Marjanska et al. 2005), and the APP_{swE}/PS1_{M146L} mouse (Oberg et al. 2008), while others reported altered Ins but no change in NAA (Forster et al. 2013; Güell-Bosch et al. 2020), or decreased NAA in the absence of altered Ins (Dedeoglu et al. 2004; Chaney et al. 2018; Kuhla et al. 2017). Some authors have also reported increased tCho (Chaney et al. 2018), decreased Glu (Marjanska et al. 2005; Oberg et al. 2008; Forster et al. 2013), increased tCr (Forster et al. 2013), decreased GSH (Dedeoglu et al. 2004), and

both increased (Dedeoglu et al. 2004) and decreased Tau (Güell-Bosch et al. 2020) at a variety of ages in transgenic mouse models, indicating widespread biochemical disruption throughout disease progression. Findings in rat models of AD are more sparse and less consistent. Chaney et al. reported only decreased hippocampal NAA by 18 months in the TgF344-AD rat but no other significant metabolic changes (Chaney et al. 2021). Nilsen et al. demonstrated lower Glu, GABA, NAA, and tCho along with increased Ins and Tau by 9 months in the McGill-R-Thy1-APP rat, but then only Tau was increased at 12 months (Nilsen et al. 2012). Much of the inconsistencies between studies can be attributed to the differences between transgenic models, which are generated using a plethora of different mutations and background strains, and thus present with variations and differing rates of progression of underlying neuropathology (for reviews see (Do Carmo and Cuello 2013; Drummond and Wisniewski 2017)). For example, it has been shown that Tau rather than Ins tends to increase with age in mouse models only harbouring an APP mutation (Dedeoglu et al. 2004; Marjanska et al. 2005), whereas Ins increases in mice with both APP and PS1 mutations (Güell-Bosch et al. 2020; Choi et al. 2014; Oberg et al. 2008), suggesting some effect of PS1 mutations on organic osmolytes. This specific example aside, not all rodent models recapitulate the full spectrum of neuropathological features, and thus cannot be expected to mimic the neurochemical profile of an individual with AD. In addition, several of these studies were only conducted in one sex, leading to potentially biased results. Despite these limitations, when performed in an appropriate rodent model, in both sexes, and in a longitudinal fashion, MRS provides a comprehensive analysis of biochemical changes taking place in the brain, and given the non-invasive nature of the technique, can establish a temporal order to these metabolic processes.

Gap in knowledge #3: Longitudinal characterization of neurochemistry and neuroanatomy in rodent models that recapitulate the full spectrum of AD neuropathology are lacking. The TgF344-AD rat model meets this requirement but changes in brain structure and the full neurochemical profile have yet to be documented. Additionally, these features have not been examined in conjunction with cognitive testing, limiting the understanding of when AD features manifest relative to one another in this model.

In summary, despite all of the previous work using MR techniques to study aging and AD, there are still major gaps in knowledge hindering the proper understanding, diagnosis, and management of pathological aging trajectories. Preclinical studies in rodents using MRI and MRS facilitate longitudinal assessments of brain structure and tissue chemistry, yet longitudinal

paradigms studying change with age and AD are still lacking. Longitudinal examination combined with the additional biochemical information and higher spatial resolution available at higher magnetic fields used in preclinical studies could be used to identify and better understand processes that become dysfunctional with age or AD, as well as to further distinguish aging from AD. Finally, an important component to developing an accurate understanding of age- and AD-related changes in neuroanatomy and neurochemistry is the intentional examination of the influence of sex, a factor that a majority of researchers have previously failed to take into account.

2.4.4 MR-detectable sex differences in aging and AD

While age is the primary risk factor for AD, female sex is the second, with women (particularly post-menopausal women) accounting for two out of three AD patients over the age of 60 (Rahman et al. 2019). In addition, age of onset, manifestation, and rate of progression of AD-related features can differ between men and women (Rahman et al. 2019; Barnes et al. 2005). For example, neurodegeneration and cognitive decline in particular occur more rapidly for women once a diagnosis is suspected (Podcasy and Epperson 2016; Barnes et al. 2005). Additionally, a study by Buckley et al. indicated greater tangle burden in women than in men with comparable A β levels, suggesting an earlier onset of AD pathophysiology (Buckley et al. 2018). There has therefore been emphasis placed on identifying sex-specific differences in disease etiology, manifestation, and progression in an effort to develop strategies for prevention, detection, and management of AD that appropriately address the influence of sex. Further, given the interaction between age and sex in conferring risk for AD, examining the influence of sex during the aging process is just as critical as doing so in individuals along the AD continuum. The effect of sex on neuroanatomy and neurochemistry during both aging and AD will be briefly discussed below, though it should be noted that MR studies on these topics are limited.

Brain volume loss as a result of age differs between men and women, with men generally showing greater age-related changes. Women experience more substantial hippocampal loss and increases in the parietal lobe with age, whereas age-related whole-brain volume loss and increases in the frontal and temporo-parietal lobes occur in men (Coffey et al. 1998; Cowell et al. 1994; Murphy et al. 1996). However, more recent reports have indicated that hippocampal and entorhinal cortex loss occurs more drastically in men (Armstrong et al. 2019; Driscoll et al. 2009), so the sex-related effects of age on hippocampal volume may require further investigation. Grey and white

matter loss occurs in men and women but both appear to decline more quickly in men (Cosgrove et al. 2007; Pfefferbaum et al. 2013; Armstrong et al. 2019). Age-related change in CSF volume also appears to differ by sex, whereby ventricular hypertrophy was more pronounced in men, particularly in the lateral ventricles (Pfefferbaum et al. 2013; Sullivan et al. 2004; Gur et al. 1991). Finally, there are very few reports on the interaction between age and sex on subcortical volumes other than the hippocampus, but the ones that do exist indicate similar rates of atrophy between men and women in volumes such as the thalamus and caudate (Sullivan et al. 2004; Choi et al. 2020).

Interestingly, while there are numerous reports indicating that women are disproportionately affected by AD in terms of both disease prevalence and severity, few studies have actually examined the effect of sex on neuroanatomical change during AD. In the few publications that address this topic, it has been shown that women with AD experience more overall brain atrophy than men (Filon et al. 2016), and even women in preclinical stages of AD show more severe frontal grey and white matter atrophy than men (Mosconi et al. 2017). Additionally, a significant interaction between sex and CSF-A β ₄₂ on longitudinal hippocampal atrophy was identified by Koran et al., indicating faster atrophy in women than men despite less pathology (Koran et al. 2017). Faster hippocampal atrophy in women with AD was also confirmed by another study (Ardekani et al. 2016).

Regarding preclinical literature on these topics, while studies exist examining the influence of sex on neuroanatomical change during normal development or adolescence (Qiu et al. 2018; Spring et al. 2010; Sumiyoshi et al. 2017), there is a complete lack of similar studies in aging rodent populations. It goes without saying that this is a major gap in knowledge that needs to be addressed in order to better understand sex-specific effects of AD on brain anatomy.

Similarly, there is a relative dearth of information regarding sex differences in neuroanatomy in transgenic rodent models. Of the preclinical MRI studies mentioned in **section 2.4.3**, five of eight included both male and female mice but only three intentionally examined the influence of sex on neuroanatomical volume. Lau et al. did not detect any effect of sex on voxel-wise measures of volume in APP/PS1 mice (Lau et al. 2008), and no sex-dependent difference in hippocampal volumes were present in the McGill-R-Thy1-APP model (Parent et al. 2017). However, Kong et al. did report positive age by sex interactions for several regions in the 3xTg mouse brain, including the 3rd ventricle, hippocampus, and caudal entorhinal cortex, and negative

age by sex interactions in the fimbria amygdalo-hippocampal region (Kong et al. 2018), suggesting that the presence of tau pathology may be required for sex effects on neuroanatomy to occur. Given that sex differences exist in other aspects of AD pathophysiology in transgenic models, such as A β deposition (Carroll et al. 2010) and cognitive function (Berkowitz et al. 2018; Saré et al. 2020), it is highly likely that sex modifies the effect of AD pathology on rodent brain anatomy in at least some transgenic models but additional research is required to confirm this theory.

Regarding the influence of sex on the neurochemical profile with age and during AD, there are only a few publications at both the clinical and preclinical levels that explore this topic using magnetic resonance spectroscopy. In aging C57BL/6 mice, striatal Tau was shown to be considerably lower in female mice than their male counterparts, and was hypothesized to be due to estrogen receptors being involved in taurine uptake (Duarte et al. 2014). There were additional sex-dependent effects on tCr, ascorbate, Glc, Lac, Ala, PE, and Asp, but the trajectories in male versus female mice were not shown or described further. Another study demonstrated a more substantial decrease in hippocampal GABA with age in female C57BL/6 mice than in male mice (Roy et al. 2018). In humans, Glu concentration in the anterior cingulate cortex has been shown to be lower in men but to decrease with age more quickly in women (Hädel et al. 2013). Finally, in a study by Marjanska et al. in a healthy aging cohort, Gln differed between sexes when ages and regions were pooled but not otherwise (Marjańska et al. 2017).

In individuals with AD and in transgenic models, there are similarly few reports. An MRS study by Watanabe et al. in a cohort of healthy controls, MCI and AD patients, there were no significant metabolite differences between men and women (Watanabe et al. 2010), while another report noted lower NAA in male AD patients relative to male controls, but no difference in female patients versus female controls (Colla et al. 2003). The few MRS studies in transgenic models of AD indicate some sex-specificity in the neurochemical profile. Hippocampal GABA was shown to have a different temporal pattern of change between male and female Tg2576 mice (Roy et al. 2018) and a study by van Duijn et al. demonstrated faster age-related decline of NAA and Tau in female APP/PS1 mice versus males. A cross-sectional study by Nilsen et al., indicated male-specific decreases in Glu, NAA, and tCho in the McGill-R-Thy1-APP rat model relative to WT controls, while female McGill-R-Thy1-APP rats were shown to have higher NAA and Ins than their transgenic male counterparts. There is obviously little consistency between these studies, both

within and between species, prompting further investigation into the compound effect of sex and pathology on the neurochemical profile.

Gap in knowledge #4: The influence of sex on neurochemistry and neuroanatomy during aging remains a sorely understudied topic, particularly at the preclinical level, and is important for understanding the influence of sex in the presence of pathology. Subsequently, the interaction of age, genotype, and sex on neuroanatomy and neurochemistry have not been explored in the TgF344-AD rat.

2.5 Statistical analysis methods

2.5.1 Univariate analysis tools for longitudinal data

As mentioned throughout this thesis, neuroimaging methods lend themselves to longitudinal study designs, with individuals being tested at multiple time points. These longitudinal paradigms provide comprehensive and complex biological data, offering crucial insight into the temporal dynamics of biological processes. Additionally, compared to a cross-sectional approach, repeated measures designs offer superior statistical power by reducing the confounding effect of between-subject variability (Thompson et al. 2011). With this added complexity comes the need for more sophisticated statistical approaches to properly model and interpret the data.

The use of linear mixed-effects (LME) models is becoming increasingly common for analysis of longitudinal biological data and is by far the best available option. LME models use linear regression to describe the trajectory of a response variable over time in a given population, whereby the trajectory is expressed as a linear combination of independent variables (Bernal-Rusiel et al. 2013; Bates et al. 2015). They extend traditional linear models by combining fixed and random effects as predictor variables. Fixed effects are typically the variables of interest or grouping factors (e.g. genotype, sex, treatment) which are expected to have an effect on the response variable, while random effects are other grouping factors for which you are trying to control (e.g. litter, subject) but are not part of the study's primary hypotheses. Choosing which predictor variables and interactions to include should be done in a way that it reflects a specific *a priori* hypothesis (Harrison et al. 2018). Optimal model selection can also be performed via tools such as Akaike Information Criterion (AIC), which provides a goodness-of-fit score that reflects a balance between simplicity (fewer variables) and adequate modeling of variance (Akaike et al. 1973; Burnham and

Anderson 2004). For example, one of the linear models employed in **Chapter 5** predicts neuroanatomical volume using a model that includes a quadratic age term interacting with genotype, sex as a categorical variable, and a random effect of subject. This model examines how neuroanatomical trajectories change over time in response to genotype while controlling for the influence of sex and allowing subjects to have their own intercept.

Inclusion of random effects allows for explicit modelling of non-independence in the data that comes from repeated sampling in the same subject or natural hierarchical clustering that results from the study design itself (litter-specific effects, for example) (Harrison et al. 2018; Fitzmaurice and Ravichandran 2008). Modelling of the random effects structure improves estimation of the fixed effects and reduces the probability of false positives and false negatives (Harrison et al. 2018). LMEs permit the incorporation of random intercepts, which allows subject means to vary but assumes all subjects have a common slope for a given fixed effect, as well as random intercepts combined with random slopes, which allows the subject means and slopes to vary (Harrison et al. 2018; Pinheiro and Bates 2000). However, it should be noted that random effects models require quite a lot of data in order for the random intercept term to be accurately estimated, limiting their applicability in smaller datasets. Additionally, LMEs offer the distinct advantage of being compatible with unbalanced data which frequently occur in longitudinal paradigms due to subject non-compliance or lack of availability (clinical studies) or attrition (preclinical studies) (Pinheiro and Bates 2000). Other statistical methods frequently require exclusion of subjects if they do not complete all time points in the study, which results in biased estimates (Fitzmaurice and Ravichandran 2008).

Commonly used alternatives to LMEs include repeated measures analysis of variance, and cross-sectional general linear model-based analysis of summary measures (such as percent or absolute difference) (Garcia and Marder 2017). However, these two approaches are not optimal for longitudinal data as they do not appropriately model the covariance structure of repeated measurements, cannot handle missing data (which is a common feature of longitudinal studies), and cannot take advantage of the information that exists in the intra-subject variance (Bernal-Rusiel et al. 2013; Garcia and Marder 2017). As such, for longitudinal neuroimaging studies such as those performed in this thesis, LME models that include predictors of interest while controlling for other categorical variables and random effects offer the best practical and theoretical approach, providing adequate statistical power and meaningful interpretation.

2.6 Chapter 2 Figures

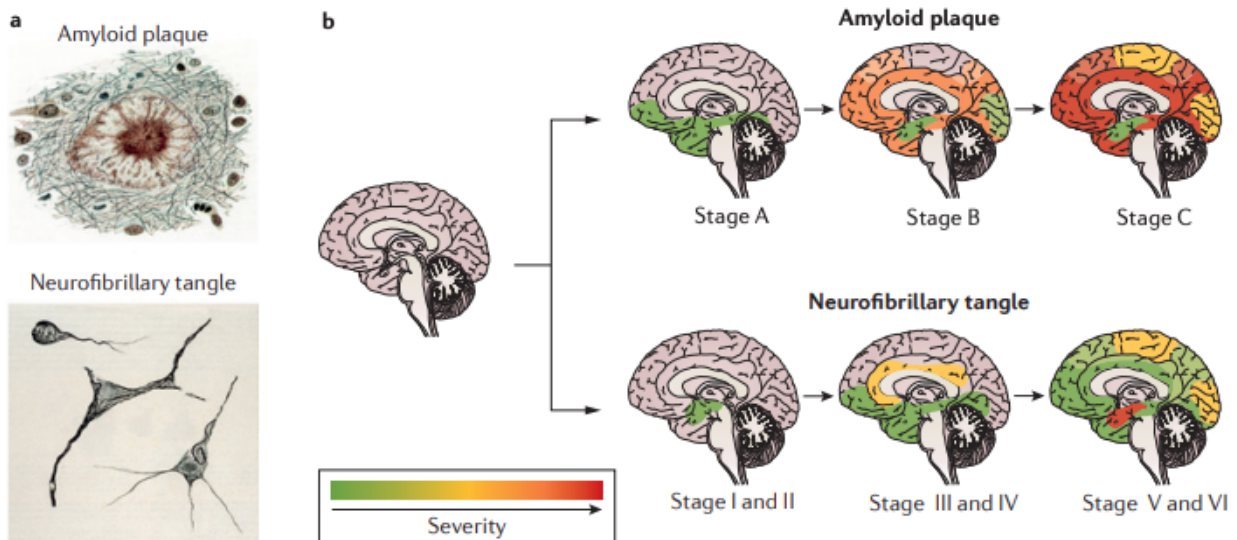


Figure 2.6.1 The pathological evolution of Alzheimer's disease

(A) Amyloid plaques and neurofibrillary tangles spread through the brain as the disease progresses. (B) Spatial distribution of neuropathological features occurs according to Braak Stages A-C and Stages I-VI for amyloid and tau deposition respectively. **Top row.** Amyloid deposition typically precedes that of tau and occurs first in the frontal and temporal lobes, hippocampus, and limbic system. **Bottom row.** Neurofibrillary tangles and neuritic degeneration start in the medial temporal lobes and hippocampus and eventually spread to other areas of the neocortex. Figure and caption adapted with permission from Springer Nature, *Nature Reviews Molecular Cell Biology*, "Alzheimer's disease" by (Masters et al. 2015).

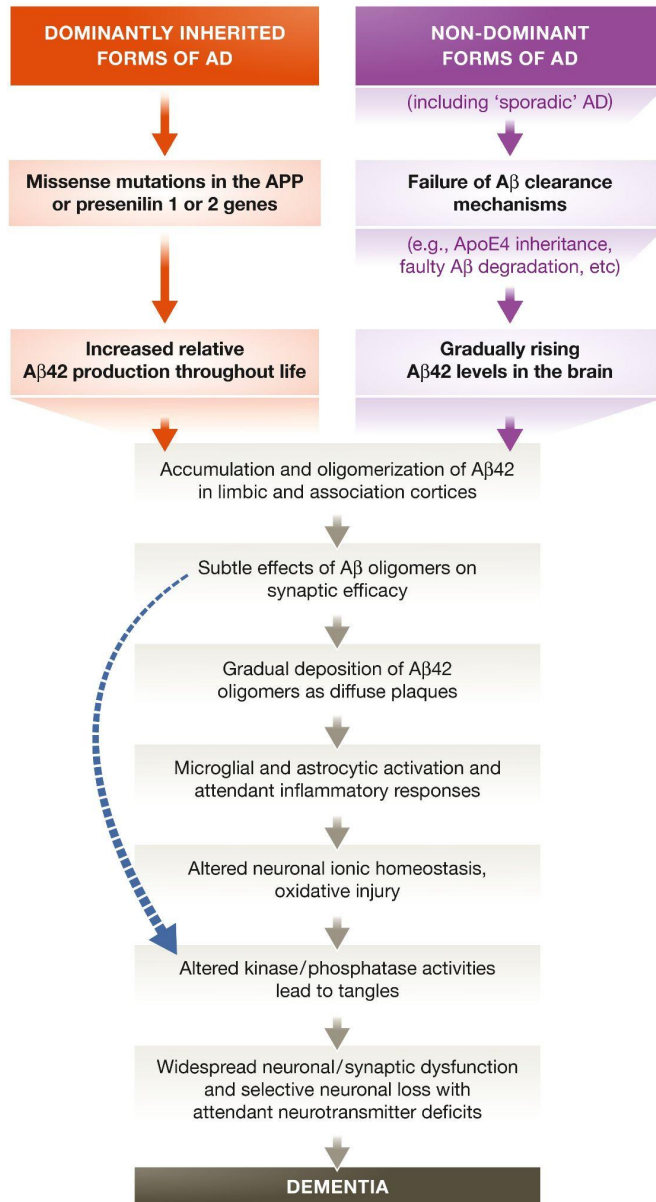


Figure 2.6.2 The amyloid cascade hypothesis

The sequence of major pathological events resulting in Alzheimer’s disease dementia proposed by the amyloid cascade hypothesis. The curved blue arrow indicates that Aβ oligomers may directly injure the synapses and neurites of brain neurons, in addition to activating microglia and astrocytes. Unmodified figure and caption used with permission from EMBO Press, *EMBO Molecular Medicine*, “The amyloid hypothesis of Alzheimer’s disease at 25 years” by (Selkoe and Hardy 2016).

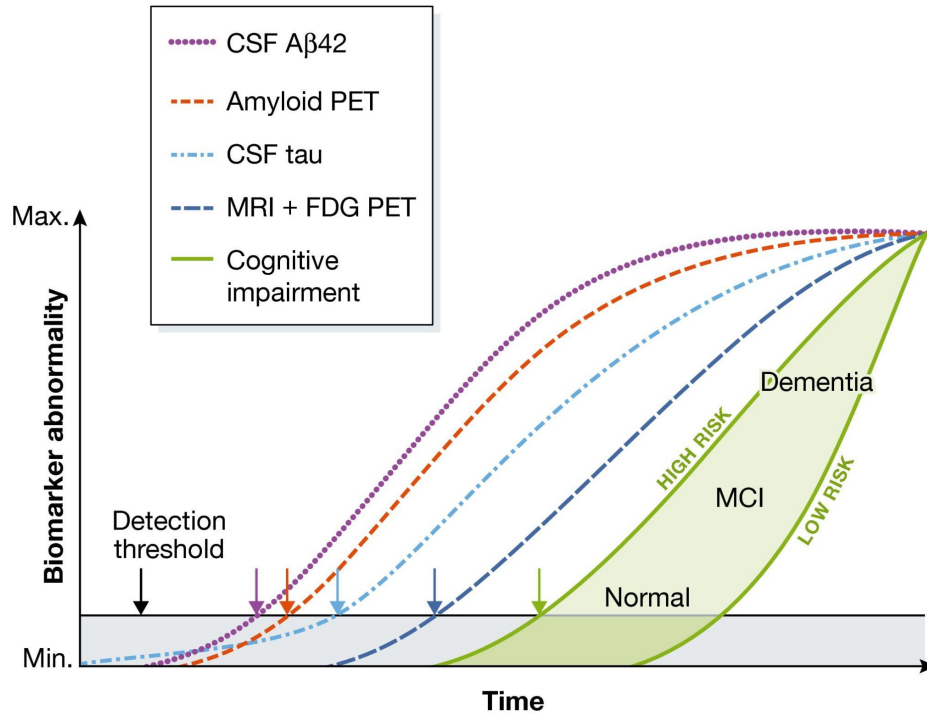


Figure 2.6.3 Temporal model of AD biomarkers

A hypothetical model of the temporal ordering of main Alzheimer’s disease biomarkers. The threshold for the first detection of biomarkers associated with pathophysiological changes is denoted by the black horizontal line. The gray area denotes the zone in which abnormal pathophysiological changes lie below this biomarker detection threshold. In this model, the occurrence of tau pathology can precede A β deposition in time, but only early on at a sub-threshold level. A β deposition occurs independently and rises above the biomarker detection threshold (purple and red arrows) prior to the manifestation of abnormalities in CSF tau (blue arrows; thought to be induced by A β deposition), MRI and FDG-PET (dark blue arrow), and cognitive function (green arrow). Cognitive impairment is shown as a range that depends on the individual’s risk profile. Figure and caption adapted with permission from EMBO Press, *EMBO Molecular Medicine*, “The amyloid hypothesis of Alzheimer’s disease at 25 years” by (Selkoe and Hardy 2016).

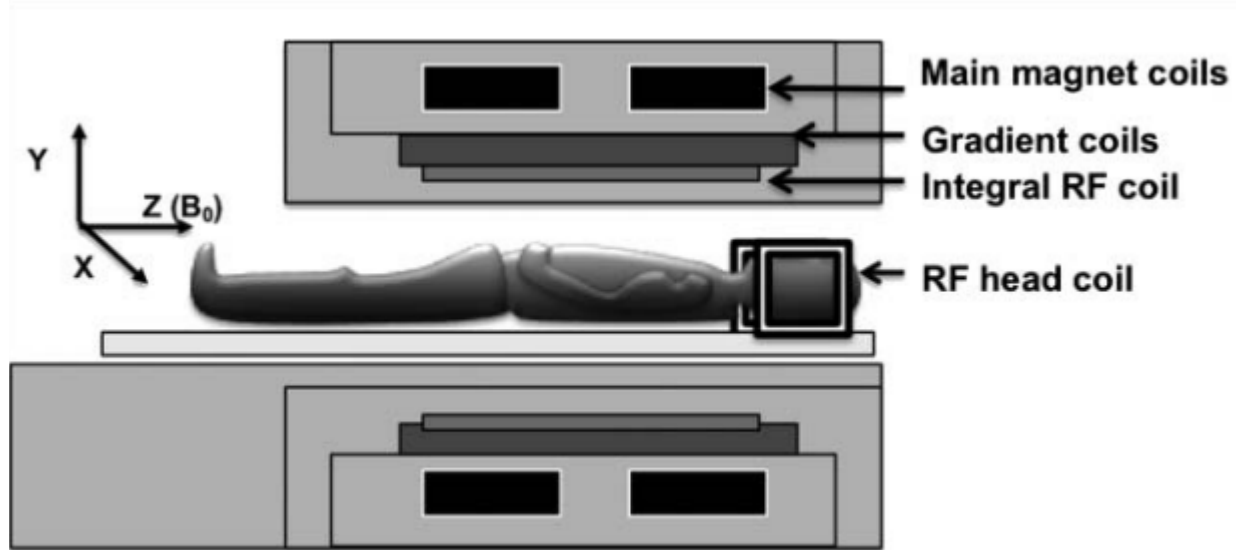


Figure 2.6.4 Coils comprising an MR machine

Schematic demonstrating the relative positions of the different magnet coils comprising the MR machine. The subject is positioned within the bore of the machine and is surrounded by coils that lie concentric to each other and in the following order: main magnet coils, gradient coils, and radiofrequency (RF) coils. For neuroimaging, an additional RF coil is placed around the subject's head to improve signal to noise ratio. Figure and caption adapted with permission from BMJ Publishing Group Limited, *Postgraduate Medical Journal*, "Understanding MRI: basic MR physics for physicians" by (Currie et al. 2013).

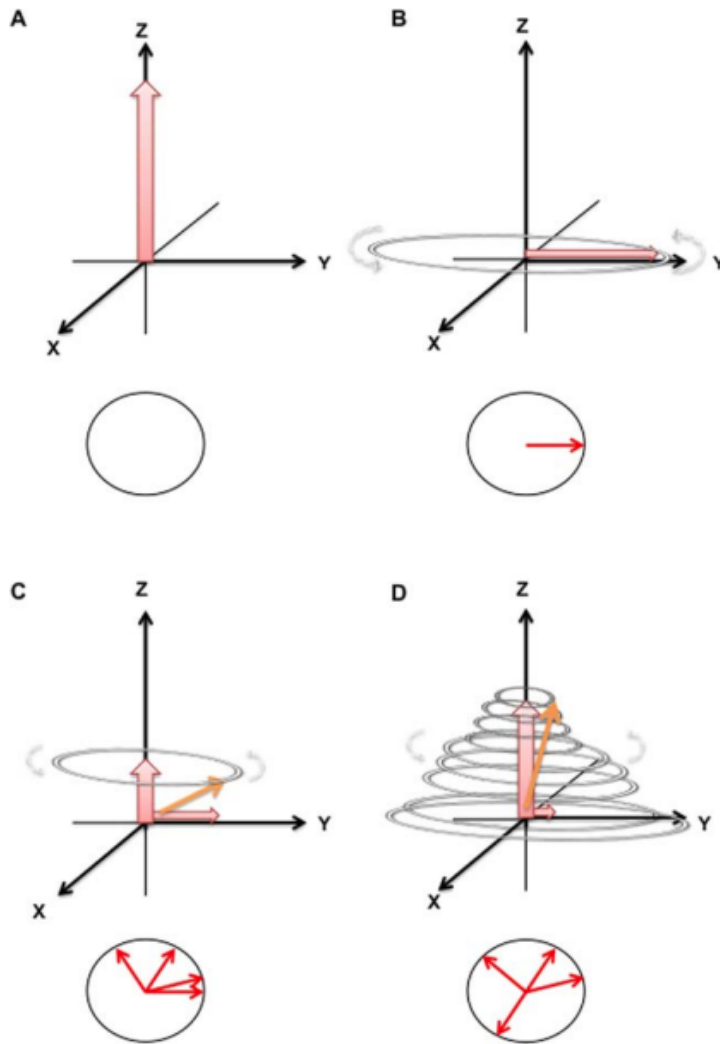


Figure 2.6.5 Recovery of longitudinal magnetization following a 90° radiofrequency pulse

(A) Protons aligned with B_0 produce a sum vector with longitudinal magnetization. (B) When an RF pulse is switched on, longitudinal magnetization decreases and transverse magnetization propagates. Alternatively, it can be said that the sum magnetization ‘tilts’ to the side. An RF pulse that abolishes longitudinal magnetization to zero while inducing transverse magnetization is called a 90° (saturation) pulse as the sum magnetization vector is seen to tilt or flip 90° . Immediately following an RF pulse, protons precess in phase in the transverse plane, depicted by a single vector (arrow) in the lower circle. (C) After the 90° RF pulse, protons fall out of phase (now multiple vectors in the lower circle), transverse magnetization decreases, and longitudinal magnetization begins to recover. During this process, the whole system continues precessing and so the sum vectors takes a spiraling motion. (D) Recovery of longitudinal magnetization is called T1 relaxation and loss of transverse magnetization is called T2 relaxation. Figure and caption adapted with permission from BMJ Publishing Group Limited, *Postgraduate Medical Journal*, “Understanding MRI: basic MR physics for physicians” by (Currie et al. 2013).

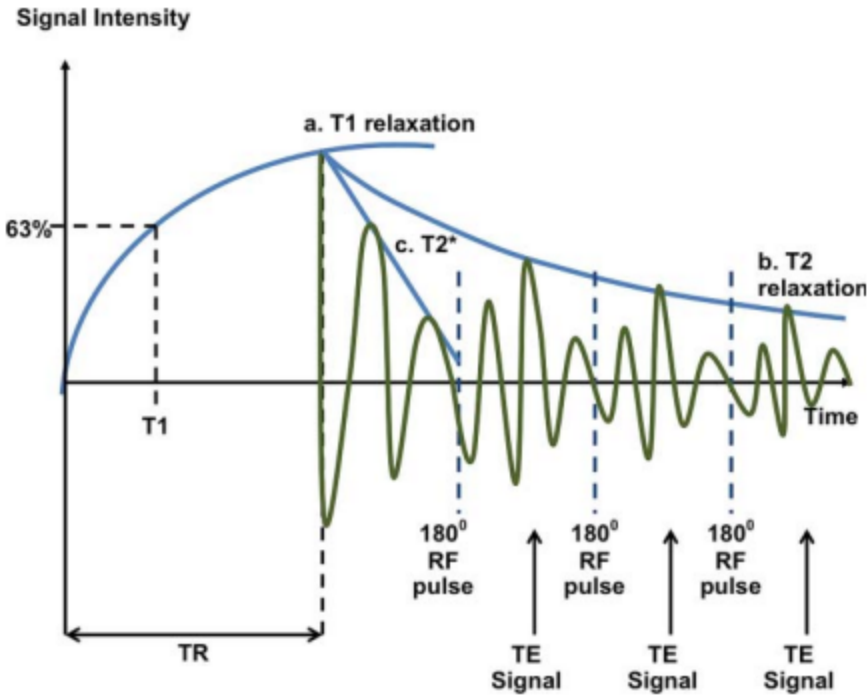


Figure 2.6.6 T1, T2, and T2* relaxation

(A) T1 curve: plotting the recovery of longitudinal magnetization over time following the switching off of a radiofrequency (RF) pulse results in a T1 curve. **(B)** T2 curve: A 180° refocusing pulse acts to ‘combat’ the effects of external magnetic field inhomogeneity by rephasing the protons. This results in a temporary gain in signal intensity at time echo time (TE) termed spin echo. A sequence of 180° pulse results in a chain of spin echoes. Each subsequent echo will be of lower intensity due to T2 effects. A curve connecting the spin echo intensities is the T2 curve. **(C)** T2* curve: this curve results when 180° refocusing pulses are not used. The signal decays much faster due to T2* effects. TR, repetition time. Unmodified figure and caption used with permission from BMJ Publishing Group Limited, *Postgraduate Medical Journal*, “Understanding MRI: basic MR physics for physicians” by (Currie et al. 2013).

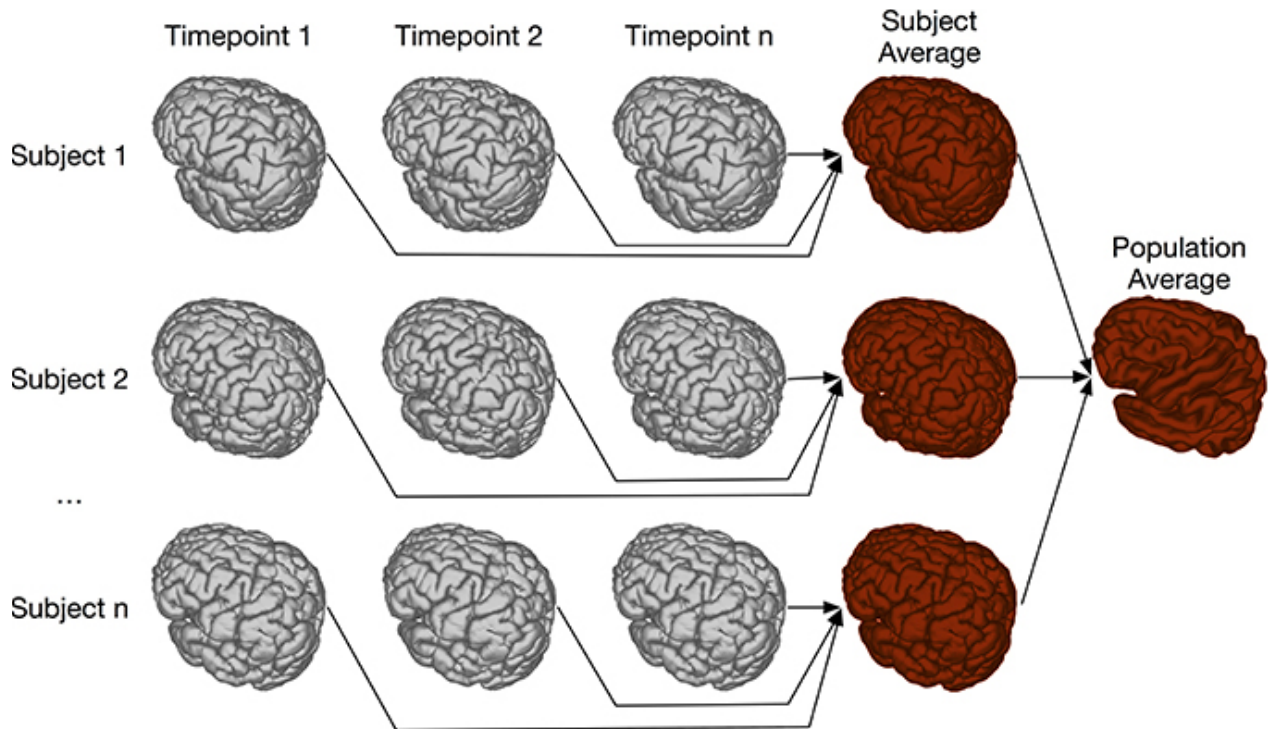


Figure 2.6.7 Two-Level model build pipeline

Schematic of the two-level registration paradigm that creates both subject and population averages. All scans per subject are registered to create a subject-specific average. All subject averages are then registered to create a population average for the whole study. Figure used with permission from *Frontiers in Neuroinformatics*, “Pydipper: a flexible toolkit for constructing novel registration pipelines” by (Friedel et al. 2014).

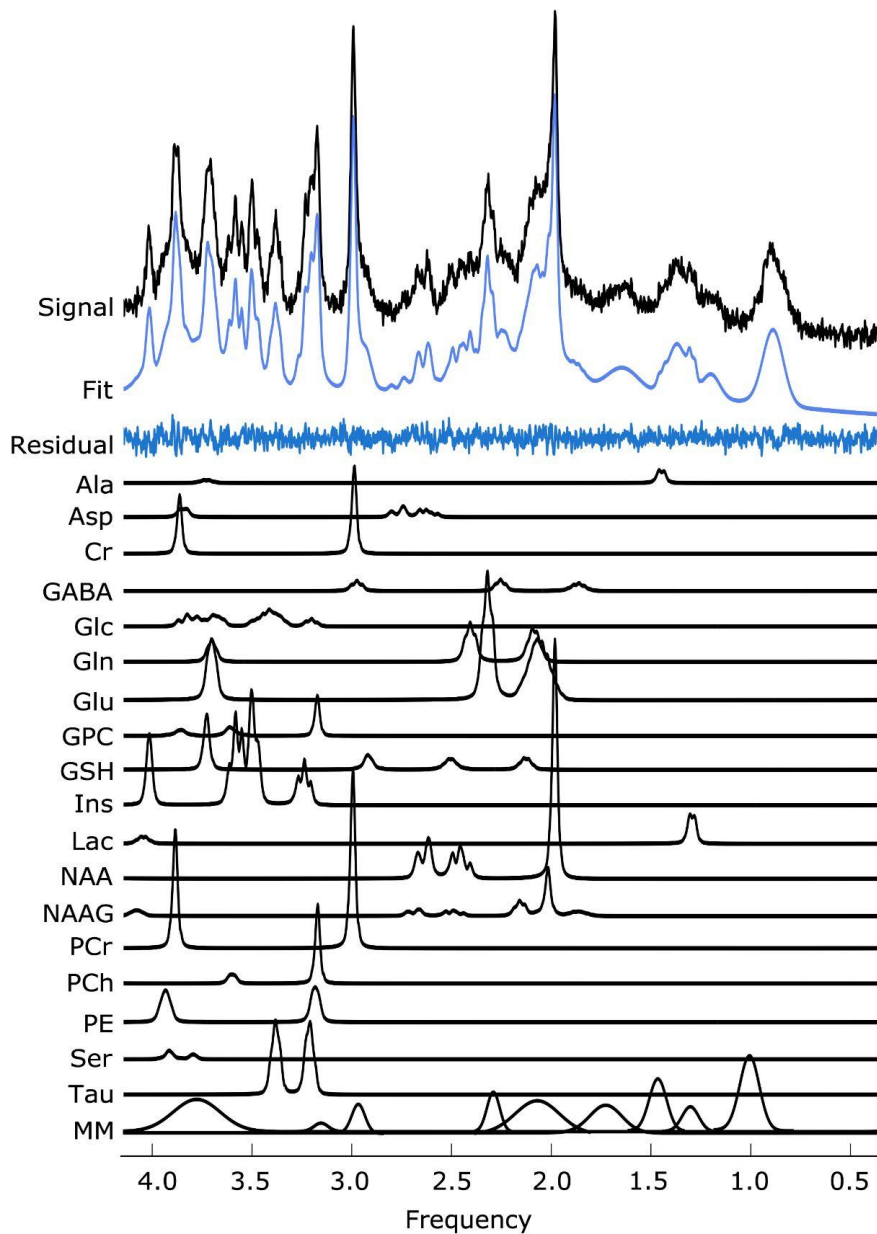


Figure 2.6.8 Example of a neurochemical spectra obtained at 7T and basis functions used for quantification.

The MR signal can be deconstructed into a series of basis functions which are fit via linear combination to determine the concentration of each neurochemical. The original signal is shown in black (7.8 Hz water linewidth), with the fit and residual shown in blue. The basis functions of all neurochemicals are shown below, whereby each neurochemical has a unique chemical shift (frequency, ppm) and peak splitting pattern used to identify it. Original figure created by the author, Caitlin Fowler.

CHAPTER 3: LONGITUDINAL QUANTIFICATION OF METABOLITES AND MACROMOLECULES REVEALS AGE- AND SEX-RELATED CHANGES IN THE HEALTHY FISCHER 344 RAT BRAIN

3.1 Preface

The work presented in **Chapter 3** represents the first longitudinal characterization of age-related neurochemical change in the Fischer 344 rat, despite this strain being frequently used for studying aging and for development of transgenic rat models of disease. This gap in knowledge was identified when planning the TgF344-AD rat publication and we noted baseline changes in the background strain of this model, the Fischer 344 rat, had not yet been documented. We chose to also develop methods for quantification of individual macromolecule resonances, as proper modelling of these signals improves metabolite quantification and can provide more information on biochemical abnormalities than if the standard metabolite profile were used.

To characterize longitudinal changes in the neurochemical profile of the Fischer 344 rat, magnetic resonance spectroscopy scans were performed on a 7T preclinical Bruker system at 4, 10, 16, and 20 months, with spectra acquired from the dorsal hippocampus. Male and female rats were used to explore the influence of sex on brain neurochemistry. The quantification of macromolecules required the development and implementation of an inversion recovery pulse sequence to acquire a metabolite-nulled spectrum, and then parameterization of the signal to identify and characterize 9 individual macromolecule peaks. Basis functions for these peaks were simulated and incorporated into the traditional neurochemical profile such that 18 metabolite peaks and 9 macromolecule peaks were quantified in each rat at each time point.

This study addresses the question of how age and sex influence hippocampal tissue chemistry throughout the life span. The benefits of answering this question are two-fold. First, abnormalities in the neurochemical profile provide incredible insight into the neurobiological processes associated with normal aging, and we anticipate that many of these findings can be translated to human aging populations. Second, these findings provide a baseline for studies performed in transgenic models of disease, in which the effects of age and pathology are compounded. These two outcomes will contribute to better identification of age-related diseases, a critical step towards providing better care for our aging population.

Longitudinal Quantification of Metabolites and Macromolecules Reveals Age- and Sex-Related Changes in the Healthy Fischer 344 Rat Brain

Caitlin F. Fowler^{a,b,*}, Dan Madularu^{b,c,d}, Masoumeh Dehghani^{b,d}, Gabriel A. Devenyi^{b,d}, Jamie Near^{a,b,d}

^a Department of Biological and Biomedical Engineering, McGill University, Montreal, Canada.

^b Centre d'Imagerie Cérébrale, Douglas Mental Health University Institute, Montreal, Canada.

^c Center for Translational NeuroImaging, Northeastern University, Boston, MA, USA

^d Department of Psychiatry, McGill University, Montreal, Canada.

Published: <https://doi.org/10.1016/j.neurobiolaging.2020.12.012>

3.2 Manuscript Information

Funding Sources: This research was supported by the Canadian Institutes of Health Research (PJT-148751) and the Fonds de la Recherche en Santé du Québec (Chercheur boursiers # 0000035275). C.F.F. is supported in part by funding provided by McGill University's Faculty of Medicine Internal Studentship.

Acknowledgements: Sincere thanks are extended to Dana Goerzen and Katrina Cruickshank for their help in editing this manuscript.

Disclosure statement: The authors disclose no conflicts of interest.

3.3 Abstract

Normal aging is associated with numerous biological changes including altered brain metabolism and tissue chemistry. *In vivo* characterization of the neurochemical profile during aging is possible using magnetic resonance spectroscopy, a powerful non-invasive technique capable of quantifying brain metabolites involved in physiological processes that become impaired with age. A prominent macromolecular signal underlies those of brain metabolites and is particularly visible at high fields; parameterization of this signal into components improves quantification and expands the number of biomarkers comprising the neurochemical profile. The present study reports, for the first time, the simultaneous absolute quantification of brain metabolites and individual macromolecules in aging male and female Fischer 344 rats, measured longitudinally using proton magnetic resonance spectroscopy at 7T. We identified age- and sex-related changes in neurochemistry, with prominent differences in metabolites implicated in anaerobic energy metabolism, antioxidant defenses, and neuroprotection, as well as numerous macromolecule changes. These findings contribute to our understanding of the neurobiological processes associated with healthy aging, critical for the proper identification and management of pathological aging trajectories.

3.4 Introduction

Aging is associated with impairments in numerous physiological pathways including antioxidant production, inflammatory response, and cerebral glucose metabolism, with further exacerbation seen in neurodegenerative disorders (Miccheli et al., 2003; Ravera et al., 2019; Yin et al., 2016). The medial temporal lobe, particularly the hippocampus, has a well-documented role in learning and memory consolidation, and is particularly vulnerable to the aging process and neurodegenerative disease (Bettio et al., 2017; Schuff et al., 1999; Van Hoesen et al., 1991). Improving our understanding of the neurobiological processes associated with healthy aging within the hippocampus may aid diagnosis, monitoring, and treatment of age-related neurological diseases such as dementia.

Proton magnetic resonance spectroscopy (^1H -MRS) is a non-invasive technique that provides unique insight into brain metabolism *in vivo*, permitting longitudinal examination of the neurochemical profile. These neurochemicals can serve as biomarkers of specific cellular and

molecular mechanisms, in the context of both health and pathology (Ross and Sachdev, 2004). For example, N-acetylaspartate (NAA) and myo-Inositol (Ins) are thought to reflect altered neuronal viability and gliosis, respectively, and have been reported to change over the course of normal aging (Cleeland et al., 2019; Haga et al., 2009; Harris et al., 2014), as well as in Alzheimer's disease (Marjańska et al., 2019; Nilsen et al., 2014). MRS has been used to characterize altered tissue chemistry in normal brain development and aging, disease, and therapeutic intervention in mice (Choi et al., 2014; Duarte et al., 2014; Marjańska et al., 2014), rats (Harris et al., 2014; Paban et al., 2010; Zhang et al., 2009), and humans (Emir et al., 2011; Murray et al., 2014), reflecting changes in underlying physiology and supporting its use as a translational tool in neuroscience research.

Quantification of at least 18 neurochemicals in the rodent brain is feasible with *in vivo* ^1H MRS at 7T and above, providing a wide array of potential biomarkers of specific cellular and molecular changes (Duarte et al., 2014; Harris et al., 2014; Mlynárik et al., 2006; Pfeuffer et al., 1999). Molecular changes observed with MRS may reflect altered energy metabolism, inflammation, or antioxidant capacity, processes which are affected by aging (Febo and Foster, 2016; McKenna et al., 2012). In addition to brain metabolites, broad macromolecule (MM) resonances are also detected with ^1H MRS, and have been shown to change with age, brain region, and pathological conditions (Behar et al., 1994; Hofmann et al., 2001; Seeger et al., 2003). The MM peaks have previously been assigned to cytosolic proteins and mobile lipids (Behar and Ogino, 1993), and contribute strongly to the overall signal (Cudalbu et al., 2012; Považan et al., 2018).

Historically, the vast majority of MRS studies have focused exclusively on quantification of metabolite levels, while relatively few have sought to selectively measure the MM contribution. Generally, this has been achieved via inversion recovery (IR) experiments to suppress the metabolite signals. The resulting metabolite-suppressed spectrum is then used as a basis to quantify the overall MM contribution in a standard MRS analysis. However, this approach does not allow for quantification of the individual MM components (Craveiro et al., 2014; Cudalbu et al., 2012).

Alternatively, parameterization of the IR-derived MM signal into components has emerged as a viable option for quantifying individual MMs; this process has been successfully applied to MRS and MRSI data obtained in humans from 1.5T and 7T (Otazo et al., 2006; Považan et al., 2018; Seeger et al., 2003), and in rats at 9.4T and 17.2T (Lee and Kim, 2017; Lopez-Kolkovsky et al., 2016). Age-related change in MM concentration has been investigated in humans, but either the MM signal was quantified as a single entity (Marjańska et al., 2018), or individual MMs were

quantified, but not longitudinally (Hofmann et al., 2001). To our knowledge, no preclinical studies have characterized longitudinal changes in individual MMs with age. Thus, the goal of this study was to assess longitudinal changes in both metabolites and individual macromolecules in the hippocampus of Fischer 344 rats to provide new insight into cellular mechanisms and biomarkers associated with healthy aging.

3.5 Materials and Methods

3.5.1 Animals

Homozygous Fischer 344/NHsd wildtype (WT) male and female rats (henceforth referred to as Fischer) were obtained from Envigo Laboratories (Madison, WI, United States; order code: 010) and bred within the Animal Care Facility at the Douglas Hospital Research Centre. Rats were weaned on postnatal day 21 and housed in pairs on a 12 hour light-dark cycle with *ad libitum* access to food and water. All animal procedures and experiments were performed in accordance with the guidelines of the McGill University Animal Care Committee and the Douglas Hospital Research Centre Animal Care Committee.

Neurochemical profiles were measured longitudinally, with scans at 4-, 10-, 16-, and 20-months of age, covering the majority of the adult rat lifespan. A total of 30 rats were included in the study. 12 of 30 rats were scanned at only the 4- and 10-month timepoints due to being part of a separate treatment study thereafter. Additionally, 2 females died prior to the 16-month time point and 5 males died prior to the 20-month time point, all of natural causes, and one scan at 10-months was discarded due to low SNR. As such, the final number of scans for the four time points were 30 (15 males, 15 females), 29 (14 males, 15 females), 16 (7 males, 9 females), and 11 (3 males, 8 females), respectively (**see Supplementary Table 3.13.1**). The imbalance in the number of subjects scanned per time point was accounted for in the statistical analysis by applying a mixed effects linear model.

3.5.2 ¹H-MRS data acquisition - metabolites

MRS data were acquired at the Douglas Centre d'Imagerie Cérébrale using a 7 Tesla Bruker Biospec 70/30 scanner (Bruker, Billerica, MA, United States) with an 86 mm volumetric birdcage coil for transmission and a four-channel surface array coil for signal reception (Bruker). The level

of anesthesia (1-4% isoflurane in oxygen gas) was adjusted to maintain a breathing rate between 50-70 breaths per minute throughout the procedure and warm air (37 °C) was blown into the bore of the scanner to maintain a constant body temperature (SA Instruments, Inc., monitoring system, Stony Brook, NY, United States).

Coronal and sagittal T₂-weighted MR images were acquired using a Rapid Acquisition with Relaxation Enhancement (RARE) sequence (TR = 2049 ms, TE = 10.8 ms, RARE factor = 6, effective echo time = 32.4 ms, FOV = 32 x 22.5 mm, matrix size = 256 x 180, resolution = 125 μm non-isotropic, 1m26s70ms acquisition time) to guide placement of a region of interest for localized magnetic resonance spectroscopy in the right lateral dorsal hippocampus (~31 μL volume, see **Figure 3.9.1**). Voxel positioning was based on anatomic landmarks. Automated localized shimming was performed using the FASTMAP method (Gruetter, 1993) (ParaVision 5.1, Bruker). Specifically, 1st and 2nd order shims were first optimized on a 5x5x5 mm³ voxel, followed by 1st order-only shimming on a smaller, local 3.5x3.5x3.5 mm³ voxel (average water linewidth 9.92 ± 1.03 Hz), both surrounding the region of interest. *In vivo* ¹H-MRS scans were then acquired from a 2.5x3.5x3.5 mm³ voxel using the PRESS sequence (Point Resolved Spectroscopy) with a total acquisition time of 13m0s0ms (TR = 3000 ms, TE = 11.12 ms, 2048 acquisition data points, spectral width = 4006 Hz) in combination with outer volume suppression. 256 averages were acquired with VAPOR water suppression (Tkac̆ et al., 1999) and 8 averages were acquired without water suppression for eddy current correction and as a reference for absolute metabolite quantification, described in the **Supplementary Methods 3.11.4**.

3.5.3 ¹H-MRS data acquisition (macromolecules) and parameterization

“Metabolite-nulled” spectra were acquired in eight Fischer rats at 10-months of age using PRESS localization (TR = 3000 ms, TE = 11.12 ms, 512 averages, 2048 acquisition data points, spectral width = 4006 Hz) preceded by an IR module consisting of a 4th order hyperbolic secant adiabatic full passage (AFP) inversion pulse (pulse duration = 1.0 ms, bandwidth = 6982.0 Hz, inversion time = 800 ms), for a total acquisition time of 25m48s0ms. The eight macromolecule spectra were aligned, summed, and scaled in FID-A (Simpson et al., 2017) to generate an average metabolite-nulled spectrum for parameterization. For details on spectral processing in FID-A, see **Supplementary Methods 3.11.2**. Due to variability in longitudinal relaxation times of metabolites, a single inversion time is unlikely to produce a macromolecule spectrum wherein all metabolites

are completely suppressed (Cudalbu et al., 2012). To identify the residual metabolite peaks in our MM spectrum, two additional MM scans were obtained with the same inversion time (TI=800 ms) and scan parameters as above, but with a long TE (40 ms). Minor residual peaks of NAA (2.00 ppm, inverted; 2.69 ppm), tCr (3.93 ppm), Glu (2.36 ppm), Gln (2.53 ppm), and Tau (3.41 ppm, inverted) were visible and accounted for during the parameterization process.

Iterative parameterization of the MM spectrum was performed in jMRUI using the AMARES fitting tool (Naressi et al., 2001; Stefan et al., 2009; Vanhamme et al., 1997). For full details on the MM parameterization methods, see **Supplementary Methods 3.11.2**.

3.5.4 Generation of metabolite and macromolecule basis spectra

The FID-A Simulation toolbox (github.com/CIC-methods/FID-A, version 1.0, (Simpson et al., 2017) in MATLAB (R2012a, The MathWorks, Inc., Natick, Massachusetts, United States) was used to simulate all metabolite and macromolecule basis functions for LCMoDel analysis. Simulations took into account the exact PRESS refocusing pulse waveforms that were used experimentally (Mao et al., 1988), as well as the actual TE and TR, and metabolite spin systems were based on previously published chemical shifts and J-coupling constants (Govindaraju et al., 2000). Metabolites were simulated with Lorentzian lineshapes and linewidths of 2 Hz. Macromolecules were simulated using Gaussian lineshapes, with linewidths and frequencies based on jMRUI AMARES output (see **Supplementary Table 3.13.2** for MM basis set simulation parameters). The neurochemical basis set consisted of 18 simulated metabolite resonances and 9 macromolecule basis functions: alanine (Ala), aspartate (Asp), creatine (Cr), γ -aminobutyrate (GABA), glucose (Glc), glutamine (Gln), glutamate (Glu), glycerophosphocholine (GPC), glutathione (GSH), lactate (Lac), myo-Inositol (Ins), N-acetylaspartate (NAA), N-acetylaspartylglutamate (NAAG), phosphocholine (PCh), phosphocreatine (PCr), phosphoethanolamine (PE), serine (Ser), taurine (Tau), MM_{0.89}, MM_{1.20}, MM_{1.39}, MM_{1.66}, MM_{2.02}, MM_{2.26}, MM_{2.97}, MM_{3.18}, and MM_{3.84}.

3.5.5 Data processing and quantification

Spectral preprocessing was performed in FID-A, and consisted of removal of motion corrupted scans and spectral registration to correct frequency and phase drift errors (Simpson et al.,

2017). Spectra were analyzed using the linear combination analysis method LCModel (version 6.3, Stephen Provencher Inc, Oakville, Ontario, Canada) using simulated basis functions as described above. Soft constraints on concentration ratios were specified for individual MM resonances, based on AMARES amplitudes (see **Supplementary Table 3.13.2**). Fitting was performed over the spectral range of 0.2 to 4.2 ppm. The unsuppressed water signal measured from the same volume of interest was used as a reference signal for absolute quantification.

For each scan, the matrix of correlation coefficients between the metabolite concentrations was extracted from LCModel's detailed output. If the average correlation between a pair was less than -0.3, we chose to also report those metabolites as a sum (Provencher, 2019, 1993). Therefore, we included the following sums in our neurochemical profile: GPC+PCh (total Choline, tCho), Cr+PCr (total creatine, tCr), and Tau+Glc. We also report summed NAA+NAAG (tNAA) and Glu+Gln (Glx) and the ratios of PCr to Cr, Glu to Gln, Asp to Glu, and NAA to Ins.

3.5.6 Application of correction factors for absolute quantification

For absolute quantification of metabolites and macromolecules, we applied a quantification formula as described in **Supplementary Methods 3.11.4, Supplementary Equation 2**. The formula accounted for T1 and T2 relaxation constants of water and measured neurochemicals, and assumed an NMR-visible water concentration of 43300 mM based on the fact that our voxel contained mostly grey matter, (Ernst et al., 1993). The values of each term in the quantification formula are listed in **Supplementary Table 3.13.3**. All neurochemical concentrations are reported in mmol/L.

3.5.7 Exclusion criteria

The Cramer-Rao lower bound (CRLB) provided by LCModel was used as a measure of reliability of neurochemical quantification on a per-metabolite basis. We employed a strict cut-off of 30% CRLB averaged across all scans, which resulted in the removal of GABA, Serine, and MM_{3.18} from our analysis. See **Supplementary Table 3.13.4** for details on metabolite CRLB across the four time points. These exclusion criteria are based on recommendations by Kreis et al., wherein excluding individual samples with high CRLB is inadvisable as it biases the mean estimated concentrations of cohort data (Kreis, 2016).

3.5.8 Statistical analysis

Metabolites were analyzed using linear mixed effects modeling in R (version 3.6.3, tidyverse_1.3.0, lme4_1.1-21, lmerTest_3.1-0) with the fixed effect variables defined by age and sex, and rat ID as a random effect. AIC comparison showed that six neurochemicals (Glc, Gln, Glu, Tau+Glc, Asp/Glu, and Glu/Gln) were best modelled with age expressed as a second order natural spline as opposed to a linear term; this higher order age term examines both linear and curvilinear change with age. Our study was underpowered to assess the presence of an age by sex interaction so we tested for a main effect of sex by collapsing across the 4 time points. The fixed effect of water linewidth (water.lw), estimated from the water unsuppressed data using FID-A, was included to control for the effect of linewidth on metabolite concentration estimates (Bartha, 2007). A weighting factor of the inverse absolute CRLB for each metabolite (metabolite.sdab) was included to account for differences in fitting reliability between samples, and allowed us to include all observations with CRLB <999. All continuous variables were z-scored so that coefficients (betas, or effect sizes) for each fixed effect would be standardized. As such, the standard betas indicate how many standard deviations metabolite concentration has changed per standard deviation increase in the predictor variable (age or sex). The full linear model is shown below.

$$lmer(\text{metabolite}) \sim \text{age} + \text{sex} + \text{water.lw} + (1|\text{subject}), \text{weights} = \frac{1}{\text{metabolite.sdab}}$$

(1)

Due to the number of comparisons, we used the False Discovery Rate method (Benjamini and Hochberg, 1995) to control the family-wise type I error rate at 5% for the main effects of age and sex. Both p- and q- (FDR-corrected) values are presented in **Table 3.10.1**. A fixed effect was considered significant when $q < 0.05$. Finally, observed power analysis was performed for each metabolite using the CRAN package, SIMR (R version 3.6.3, simr_1.0.5, (Green and MacLeod, 2016) to ensure our results from a relatively small sample size were generalizable to a larger population. See **Supplementary Methods 3.11.5** for details, and **Supplementary Tables 3.13.8 and 3.13.9**, for power analysis results for age and sex, respectively.

3.6 Results

3.6.1 Quantification using an expanded neurochemical profile

A representative NMR spectra from a female rat brain at 16-months shows the excellent spectral quality consistently obtained in this study (**Figure 3.9.1**). All linewidths were well under the 0.1 ppm (30.3 Hz at 7T) full-width half-max (FWHM) considered essential for in vivo ¹H MRS spectra (Forster 2012). See **Supplementary Table 3.13.5** for details on spectral linewidth and SNR.

Figure 3.9.1 also shows the 18 metabolite and nine macromolecule basis functions used by LCModel to fit each spectrum. With the exclusion of high-CRLB metabolites GABA, Ser, and MM_{3.18}, the following compounds comprised the neurochemical profile used to evaluate changes with age and differences between sexes: Ala, Asp, Cr, PCr, Glc, Gln, Glu, GSH, Ins, Lac, NAA, NAAG, PE, Tau, tCho (GPC+PCh), tCr (Cr+PCr), Glx (Glu+Gln), tNAA (NAA+NAAG), Tau+Glc, Glu/Gln, PCr/Cr, NAA/Ins, Asp/Glu, MM_{0.89}, MM_{1.20}, MM_{1.39}, MM_{1.66}, MM_{2.02}, MM_{2.26}, MM_{2.97}, MM_{3.18}, and MM_{3.84}. All 31 neurochemicals were quantified with high reliability: 20/31 and 30/31 neurochemicals displayed average CRLBs of < 10% and < 20%, respectively, with only Alanine, at 21.5%, displaying a CRLB greater than 20%. See **Supplementary Table 3.13.4** for details on metabolite CRLB.

All metabolite concentrations were well within ranges previously reported in the rat brain by numerous authors whose quantification methods incorporated MMs (Harris et al., 2014; Lopez-Kolkovsky et al., 2016; Pfeuffer et al., 1999). As individual MMs have not yet been quantified in rodent brain, we compared our macromolecule concentrations to those cited in a study by Snoussi et al, wherein MMs in healthy adults were quantified in the range of 5-20 mmol/kg, which is in good agreement with our findings (Snoussi et al., 2015).

3.6.2 Metabolite and macromolecule concentrations are altered with age

The levels of 15 of 31 neurochemicals changed significantly with age in Fischer rats (**Table 3.10.1**), after FDR correction at 5%. Change in concentration of metabolites, metabolite ratios, and macromolecules with age are shown in **Figures 3.9.2, 3.9.3, and 3.9.4**, respectively. We observed significant linear reductions in concentration with age for GSH ($\beta = -0.335$), Glu/Gln ($\beta = -1.363$), and NAA/Ins ($\beta = -0.254$), as well as a negative curvilinear relation with age for Asp/Glu ($\beta = -1.491$). Concentration increased linearly with age for Glc ($\beta = 1.872$), Lac ($\beta = 0.355$), Ins ($\beta = 0.363$), NAAG ($\beta = 0.329$), MM_{0.89} ($\beta = 0.331$), MM_{1.20} ($\beta = 0.380$), MM_{1.66} ($\beta = 0.357$), MM_{2.02} ($\beta = 0.423$), and MM_{3.84} ($\beta = 0.290$), and a positive curvilinear relationship was seen for Glu/Gln

($\beta = 1.023$). Absolute concentrations and % change, along with linear model results, are shown in **Supplementary Tables 3.13.6 and 3.13.7**, respectively.

3.6.3 Male and female Fischer rats exhibit differences in brain tissue chemistry

9 of 31 neurochemicals showed significant differences between male and female Fischer rats after FDR correction at 5% (**Table 3.10.1**). Differences in concentration of metabolites, metabolite ratios, and macromolecules between sexes are shown in **Figures 3.9.5, 3.9.6, and 3.9.7**, respectively. The concentration of PCr was significantly increased in females relative to males ($\beta=0.817$), as was tCr ($\beta=0.652$), the ratio of PCr/Cr ($\beta=0.659$), MM_{1.39} ($\beta=0.592$), MM_{2.02} ($\beta=0.593$) and MM_{2.97} ($\beta=0.792$). Glc ($\beta=-0.953$), Tau+Glc ($\beta=-0.915$), and MM_{1.20} ($\beta=-0.654$), were decreased in females relative to males. Absolute concentrations of each metabolite collapsed across timepoints and split by sex, as well as linear model results, are shown in **Supplementary Tables 3.13.6 and 3.13.7**, respectively.

3.7 Discussion

The present study reports, for the first time, the simultaneous absolute quantification of metabolites and individual macromolecules in the aging rat brain, measured longitudinally using high field ¹H-MRS. The addition of modelled macromolecule resonances to the standard array of metabolites measured by ¹H-MRS not only expands the number of potential biomarkers available for detecting pathological changes in brain tissue metabolism, but also improves metabolite quantification (Hofmann et al., 2002). Using this expanded basis set of 31 neurochemicals, we identified age- and sex-related changes in tissue chemistry in the hippocampus, a brain region with a well-documented role in age-related cognitive decline (Bettio et al., 2017; Morrison et al., 2000; Schuff et al., 1999).

3.7.1 Comparison with Previous Studies

Reproducibility of metabolite quantification and consistency between studies depends on proper handling of the MM signal. For example, Hofmann et al. reported that inclusion of an MM spectra as a basis function for quantification resulted in considerably lower concentrations for

metabolites such as Gln, Glu, and PE, with differences of 0.6 to 1.5 mmol/kg, while also reducing the estimated error margin for all major metabolites (Hofmann et al., 2002). Methodological differences in handling of the MM signal may therefore play a large role in the differences between studies regarding reports of metabolite changes with age and sex or gender (Hofmann et al., 2001) and may explain some of the discrepancies between our study and those published previously.

Previous attempts at modelling MM components in proton MRS spectra have been made. In 2003, Seeger et al. first proposed parameterizing a metabolite-nulled spectrum for inclusion into the quantification basis set (Seeger et al., 2003); they adequately modelled the MM contribution in human brain spectra acquired at 1.5T using only four broad MM components, based on resonances identified by Behar in 1994 (Behar et al., 1994). As MM contributions become more resolved at higher field strengths, additional components and more strict fitting constraints are needed to prevent overestimation of overlapping metabolite concentrations (Cudalbu et al., 2012; Pfeuffer et al., 1999; Považan et al., 2018).

In recently published human MRSI data at 7T, Povazan et al. employed direct spectral fitting of nine individual MMs, while Snoussi et al. used the sum of 19 Gaussian lineshapes to fit MM spectra acquired using single-voxel MRS at 3 and 7T (Považan et al., 2018; Snoussi et al., 2015). In rat brain at 9.4T, authors Lee and Kim proposed parameterization of the MM baseline using 25 components directly from short echo time spectra (Lee and Kim, 2017), while Lopez-Kolkovsky et al. used 32 resonances to parameterize MM rat brain spectra acquired at 17.2T (Lopez-Kolkovsky et al., 2016).

In the rat brain at 7T, nine to ten distinct MM resonances are visible, similar to those identified in the human brain at 7T (Považan et al., 2018; Snoussi et al., 2015). Although preclinical studies are attractive due to the expanded metabolic profile available at high fields and the large number of available disease models, little work has been done regarding preclinical quantification of both metabolites and MMs with age and between sexes.

3.7.2 Change in metabolite concentrations associated with healthy aging

We chose to study the hippocampus based on the established relationship between cognitive decline and decreased hippocampal structural integrity, both in aging and in neurodegenerative disease (Bettio et al., 2017; Van Hoesen et al., 1991). Age-related cognitive deficits are associated with impaired cerebral glucose metabolism and energy balance, with further exacerbation seen in

neurodegenerative disorders (Miccheli et al., 2003; Mosconi, 2013; Ravera et al., 2019; Yin et al., 2016). Specifically, aging induces a shift from aerobic to anaerobic energy metabolism, resulting in increased oxidant production, decreased tricarboxylic acid cycle (TCA) activity, and compromised electron transport and oxidative phosphorylation (Dong and Brewer, 2019; Miccheli et al., 2003; Yin et al., 2016). MRS reflects these changes, as many of the compounds comprising the NMR-visible chemical profile are involved in energy metabolism.

Here, we report prominent age-related alterations in metabolites implicated in anaerobic energy metabolism, antioxidant capacity, and neuroprotection, as well as numerous macromolecule changes. Previous clinical and preclinical MRS studies of age-related changes have produced mixed findings, particularly for the more commonly reported metabolites such as NAA, tCho, and tCr. Some of the differences between studies may be attributed to reporting metabolite ratios instead of absolute concentrations, different handling of the underlying MM signal, or the study of single sex cohorts (for reviews, see (Cleeland et al., 2019; Febo and Foster, 2016; Haga et al., 2009).

We detected linear increases in Ins ($\beta=0.363$), Gln ($\beta = 1.040$), Glc ($\beta=0.324$), Lac ($\beta=0.355$), and NAAG ($\beta=0.329$) with age, as well as a positive curvilinear relationship between age and Glu/Gln ($\beta = 1.023$). Linear decrease in concentration with age was seen for GSH ($\beta=-0.335$), Glu/Gln ($\beta = 1.363$), and NAA/Ins ($\beta = -0.254$), as well as a negative curvilinear relationship between age and Asp/Glu ($\beta = -1.491$). Age-related increases in Ins and Gln, and decreased GSH, are in good agreement with previous studies (Emir et al., 2011; Gruber et al., 2008; Harris et al., 2014; Paban et al., 2010; Zhang et al., 2009), while reports of altered Glc, Lac, and NAAG have been more mixed (Dong and Brewer, 2019; Duarte et al., 2014; Harris et al., 2014; Marjańska et al., 2017; Miccheli et al., 2003; Paban et al., 2010). Despite differences between studies, the neurochemical changes that we report are consistent with the known occurrence of Glc hypometabolism and mitochondrial dysfunction with age, resulting in a shift towards anaerobic energy metabolism, decreased antioxidant capacity, and an increased inflammatory response (Camandola and Mattson, 2017; Godbout and Johnson, 2009; Miccheli et al., 2003; Yin et al., 2016).

Glutamine - Synthesized primarily in astrocytes from synaptic Glu, Gln is an important intermediate in energy metabolism via the TCA cycle and malate-aspartate shuttle (Best et al., 2014; McKenna et al., 2012). Increased Gln with age, often accompanied by decreased Glu, has been proposed to reflect a relative increase in the astrocyte population with age (David et al., 1997),

and/or increased citric acid cycle flux (Boumezbeur et al., 2010). Additionally, ¹³C-MRS studies have demonstrated that changes in the Glu-Gln cycle track closely with the rate of glutamatergic neuronal activity, as well as astrocytic glycolysis, such that uptake of Glu increases glycolysis-generated ATP (furthering Glu uptake, and thus Gln synthesis), and lactate (Best et al., 2014; Sibson et al., n.d.). Given our findings of Gln increasing linearly with age, linear and curvilinear relationships for Glu/Gln, increased lactate, glucose, and myo-inositol, and trending changes in Glu and PCr/Cr, all of which will be discussed below, we conclude that altered Gln and Glu/Gln are likely reflecting many interconnected metabolic processes affected by age. It should be noted that Gln and Glu were best fit using a second order age term, so a trend towards curvilinearity was also shown for both individual metabolites.

Myo-Inositol - Ins is found at high concentrations in astrocytes, which, along with microglia, have been reported to display a more reactive phenotype with age (David et al., 1997). It has been proposed that increased Ins levels reflect an elevated inflammatory profile, possibly partly in response to increased oxidative damage with age (Best et al., 2014; Godbout and Johnson, 2009). As Ins is derived from D-Glucose-6-phosphate (D-G6P) – the first intermediate formed during glucose catabolism via glycolysis (Bevilacqua and Bizzarri, 2018; Zhang et al., 2009) – it also plays an important role as a metabolic precursor to the phosphoinositol (PI) cycle, which is involved in signal transduction and cellular regulation, and whose activity has been reported to decrease with age (Akintola and van Heemst, 2015; Frazier et al., 2020). As such, our finding of increased Ins in aged rats could be associated with a number of cell processes affecting neuronal survival and function, including increased glial cell reactivity and decreased PI cycle activity.

Glucose - Glc hypometabolism and mitochondrial dysfunction resulting in decreased energy production are known features of aging that are often further exacerbated in neurodegenerative disorders (Camandola and Mattson, 2017; Frazier et al., 2020; Miccheli et al., 2003; Mosconi, 2013; Yin et al., 2016). Given the expected reduction in Glc utilization with age, our finding of increased Glc is unsurprising, and in agreement with a cross-sectional study performed in male Fisher rats (Harris et al., 2014). While Glc was best fit by a second order age term, only the linear increase with age, as opposed to the curvilinear relationship with age, was deemed significant by the model.

Lactate - Lac is an essential intermediate of Glc metabolism. The glycolytic pathway produces two pyruvate molecules, which then participate in either a) aerobic metabolism via

oxidation of pyruvate to acetyl-CoA for entry into the TCA cycle and oxidative phosphorylation, or b) anaerobic metabolism via reduction of pyruvate to Lac. With age, the pool of nicotinamide adenine dinucleotide (NAD and NAD⁺) available for oxidative reactions decreases and Glc metabolism shifts from aerobic to anaerobic (Camandola and Mattson, 2017; Dong and Brewer, 2019; Yin et al., 2016). This shift results in less pyruvate being routed towards the TCA cycle, and more towards reduction into Lac via lactate dehydrogenase (LDH), particularly because LDH activity increases with age as a result of oxidative stress (Dong and Brewer, 2019; Ravera et al., 2019). Increased pyruvate reduction to Lac ensures the cytoplasmic pool of NAD⁺ is being regenerated, which is necessary for maintaining a high glycolytic rate to produce ATP (Camandola and Mattson, 2017; McKenna et al., 2012). As such, our finding of increased Lac fits well with known age-related metabolic changes, as well as our finding of increased Glc and decreased GSH, the latter of which will be discussed below.

Glutathione - GSH is an important endogenous antioxidant involved in reducing reactive oxygen species and preventing cellular damage. Production of GSH is coupled with that of ascorbate, another CNS antioxidant, wherein both compounds are reduced by NADP⁺ as part of the pentose phosphate pathway (Camandola and Mattson, 2017; McKenna et al., 2012). Reduced oxidative capacity and impaired mitochondrial respiration is consistent with age-related deficits in antioxidant capacity and therefore the decrease in GSH that we see with age (Emir et al., 2011; McKenna et al., 2012). This finding fits with that of increased Lac - likely through increased LDH activity triggered by oxidative stress - as an attempt to compensate for impaired mitochondrial energy metabolism. Lastly, increased oxidative damage and stress with reduced antioxidant capacity can trigger glial cell reactivity, which may be reflected by the increased Ins in our aged rats (Godbout and Johnson, 2009).

N-acetylaspartylglutamate - NAAG is the most abundant neurotransmitter in the CNS, is derived from NAA and Glu, and, like its precursors, is primarily localized in neurons (Benarroch, 2008). It acts as a neuromodulatory agent to down-regulate neurotransmitter release via metabotropic Glu receptors, as well as to provide protection to neurons exposed to high Glc conditions (Benarroch, 2008; Berent-Spillson et al., 2004). Given our finding of increased Glc, as well as this paper's description of generally detrimental age-related processes in the brain, the role of NAAG as a compensatory neuroprotective agent and its subsequent increase with age is a reasonable inference.

Other frequently reported metabolites such as tCr and NAA do not change significantly with age in the Fischer rat brain, though PCr and PCr/Cr trend towards a decrease ($q=0.056$). A decrease in PCr/Cr has been reported by others (Duarte et al., 2014; Harris et al., 2014; Miccheli et al., 2003) and is proposed to reflect increased PCr to Cr conversion, and thus phosphate donation, in an attempt to maintain cellular ATP supply (Best et al., 2014; McKenna et al., 2012); this is consistent with our findings suggesting energy impairment in aerobic metabolism pathways. Additionally, the process of regenerating PCr from Cr is reported to be hindered in the presence of reactive oxygen species, which fits well with our finding of reduced GSH, and thus reduced antioxidant capacity and depletion of the PCr pool (Béard and Braissant, 2010). These results also support the argument that care should be taken when reporting metabolite ratios to total creatine (Duarte et al., 2012; Haga et al., 2009; Zhang et al., 2009). NAA has previously been reported to either decrease or remain unchanged in older populations relative to young (Duarte et al., 2014; Hädel et al., 2013; Harris et al., 2014; Marjańska et al., 2017; Miccheli et al., 2003; Zahr et al., 2013), so our finding of unchanged NAA is consistent with at least some of the reports.

Finally, additional trending changes with age include Glu (both linear and curvilinear relationships), and Asp, as well as a significant curvilinear relationship with age for Asp/Glu. Since Asp and Glu feed into the TCA cycle, changes in these metabolites are typically interpreted as altered TCA cycle activity and impaired mitochondrial bioenergetics (Benarroch, 2008; Dong and Brewer, 2019; Yin et al., 2016). An additional time point may have furthered the trending decreases with age that report here.

3.7.3 Characterization of changes in individual macromolecule resonances with age

We report increased MM signal in five of the nine MMs that were quantified. Increased MM signal with age in humans has previously been described wherein the greatest MM differences associated with age occurred for the 1.7 and 2.0 ppm MM resonances, and a notable increase was observed at 3.9 ppm (Hofmann et al., 2001; Marjańska et al., 2018). This is in agreement with our results, wherein the largest increase occurred in MM_{2.02} ($\beta=0.423$), followed by MM_{1.20} ($\beta=0.380$), MM_{1.66} ($\beta=0.357$), MM_{0.89} ($\beta=0.331$), and MM_{3.84} ($\beta=0.290$). Due to the fact that the broad peaks are likely representative of overlapping multiplets from various amino acids within different proteins, the exact composition of each MM resonance is not known, making it challenging to determine the origin of increased MM signal with age (Behar et al., 1994; Behar and Ogino, 1993;

Marjańska et al., 2018; Považan et al., 2018). That said, it has been proposed that increased MM signal at 0.9 and 1.3 ppm reflect increased free fatty acids, while the increase at 2.0 ppm is thought to be due to higher visibility of cytosolic proteins after cell death (Saunders et al., 1997). Due to its complexity, it is not possible to determine which proteins within the MM signal are changing with age. As such, the global pattern of MM peaks changes may be more useful as an overall biomarker of health or pathology as opposed to being indicative of a particular mechanism.

3.7.4 Presence of sex-specific effects in Fisher rat hippocampus

To date, very little work has been done on the characterization of sex differences in the neurochemical profile with age, despite age-related neurodegenerative (and other) disorders such as Alzheimer's disease differing in prevalence and symptom presentation between sexes (Komoroski et al., 1999; Mazure and Swendsen, 2016; Wickens et al., 2018). In a longitudinal study of C57BL6 mice, sex differences were identified for many metabolites, including ones for which we also report effects of sex (e.g. Glc and tCr), though the direction of these differences was not noted by the authors (Duarte et al., 2014). In humans, Hadel et al. described higher hippocampal total creatine in females (significant in our data) and lower glutamate in males (Hädel et al., 2013). We also found significant differences between sexes for NAA/Ins and PCr/Cr, which, to our knowledge, have yet to be reported in aging literature.

Several of the main effects of sex in our study come from the individual MM resonances at 1.20, 1.39, 2.02, and 2.97 ppm, wherein all but MM_{1.20} were increased in females relative to males. To our knowledge, only a single study by Hofmann et al. has attempted to elucidate sex-specific patterns in the MM signal and they reported no differences between genders in humans (Hofmann et al., 2001). However, given that the study by Hoffmann et al was conducted at 1.5T, it is likely that the MM peaks were simply not well-resolved enough to detect differences due to sex, and that at higher field strengths sex-specific patterns might emerge.

Regarding the origin of the neurochemical differences between males and females that we report, the current methodological approach does not provide adequate information to define the underlying mechanism(s). However, at the neuroendocrine level, the main difference between the sexes after puberty is the diverging concentration of gonadal hormones estrogen and testosterone. This distinction becomes particularly important during the aging process; estrogens (estradiol, estrone, and estrinol) are available to receptors in male brains throughout their lifespan via

aromatization of testosterone, whereas they are unavailable in the brains of post-menopausal women not using estrogen replacement (Gillies and McArthur, 2010; Rasgon et al., 2001). Most relevant to our work, an elegant study in Sprague-Dawley rats demonstrated that by 16-months all female rats were classified as perimenopausal (i.e. reduced estrogen regulation), and that this perimenopausal stage was associated with altered hippocampal gene expression profiles with roles in insulin signalling, glucose metabolism and mitochondrial function, inflammation, and redox balance (Yin et al., 2015). These metabolic changes might be quantifiable by testing for an age by sex interaction, which we were not powered to perform.

Overall, additional work is required to understand sex differences in the neurochemical profile, and future studies should continue to consider both sexes, separately and together, particularly in the context of pathology and treatment. In particular, a reproduction of the detailed gene expression analysis study by Yin et al. in conjunction with MRS data acquisition throughout the male and female lifespan would be extremely informative.

3.7.5 Limitations

There are several limitations of this study that need to be considered. First, the lower number of subjects at our last two timepoints does reduce our overall power. To ensure we were adequately powered for generalization to a larger population, we ran a simulated post-hoc power analysis and present all results, along with their calculated power, for the reader to interpret. We also examined sex effects collapsed across all time points rather than examining age by sex interactions, for which we were underpowered. We recommend that future studies be designed to assess age by sex interactions as they are likely more informative than examining a main effect of sex.

Second, we chose to use water as a reference without correcting for a possible decrease in brain tissue water content with age (Chang et al., 1996; Duarte et al., 2014), which may have resulted in an overestimation of metabolite concentrations towards the later time point. However, given available literature values and the age of the animals in our study, water content would likely have decreased by only a small amount, or approximately 3-5%. As shown in **Supplementary Table 3.13.6**, the significant age-related changes that we report are accompanied by percent differences ranging from -12% to 48.9% between timepoints 4 and 1, with the smallest percent difference at -5.5%. This is with the exception of metabolites modelled using a second order age

term, for which percent difference is not as meaningful a metric for describing change as the effect sizes quoted in the main text. It should also be noted that a change in water content would drive increases with age similarly across all metabolites, while we report both age-related increases and decreases in metabolite concentrations. As such, we are confident that variation in water content is not the dominant driving factor behind the age-related metabolic changes that we observe. Additionally, it was important that we use water referencing as opposed to creatine referencing because altered creatine has been reported with age and disease state, and between brain regions, muddying the waters for interpretation (Jansen et al., 2006; Pfefferbaum et al., n.d.). Our own data supports this decision; total creatine trends towards a decrease with age ($p=0.094$), and is significantly altered between male and female rats. For these reasons we chose to report metabolite concentrations referenced to water as opposed to creatine.

An additional well-known limitation to MRS studies is the possibility of altered relaxation effects with age which may affect metabolite quantification. The measurement of relaxation constants for each neurochemical, including water, is an extremely time-consuming process and therefore not frequently performed, particularly as it is influenced by field strength, age, and brain region (Kreis et al., 2005; Marjańska et al., 2018). Due to a lack of literature values for relaxation constants for either water or neurochemicals, specifically in the rat brain, at ages relevant to our study, correcting for age-associated differences in T1 or T2 was not possible, and therefore we cannot rule out the possibility that this may have affected the observed metabolite changes.

However, in an attempt to minimize the impact of relaxation effects with age on our concentrations, we used a long relaxation time ($TR=3s$) and short echo time ($TE=11\text{ ms}$). Given a TE of 11ms, if the water T2 decreased by 10% in older rats (from 49.13 ms to 44.19 ms), it would decrease water signal intensity by 2.7%, resulting in metabolite concentration estimates that appear 2.7% higher. In the case of a 10% increase or decrease in water T1 in older rats - reports of altered water T1 values with age have been more mixed (Hagiwara et al., 2020; Kupeli et al., 2020; Watanabe et al., 2013) - this would result in a 3.1% change in the apparent metabolite concentration. The magnitude of possible relaxation effects on apparent metabolite concentration is smaller than the percent differences that we report in this study. Additionally, since metabolites such as NAA, Cr, and choline have shorter T1s and longer T2s than that of water (Marjańska et al., 2017; Otazo et al., 2006), the effect of changing metabolite relaxation rates on the metabolite estimates would be even smaller. It is clear that a study measuring T1 and T2 of water and major metabolites at

several ages throughout the rodent lifespan would be of great benefit to the MRS community, and a means towards better standardizing the work in this field.

While we did not measure the age-specific relaxation constants for all neurochemicals, we did measure T1 and T2 relaxation of water in a separate cohort of 10-month Fischer rats to account for relaxation effects specific to our rat strain, acquisition parameters, and region of interest. We also corrected for non-age associated relaxation effects in metabolites and macromolecules by applying correction factors derived from relaxation constants in the literature (see **Supplementary Table 3.13.3**).

Finally, in comparison to the use of a single-component MM spectrum, the parameterization process of a MM spectrum is lengthy and may be subject to overfitting during the quantification process if soft constraints are not properly implemented. The complexity of the process can be a deterrent for researchers looking to include individual MMs in their basis set. As such, we have included extensive methods and supplementary material describing our process, in the hopes that other authors will find it helpful for their own studies.

3.8 Conclusion

The present study reports, for the first time, the simultaneous absolute quantification of metabolites and individual macromolecules in the aging Fischer rat brain, measured longitudinally using high field ^1H -MRS. The addition of modelled macromolecule resonances to the standard array of metabolites measured by ^1H -MRS not only improves metabolite quantification, but also expands the number of potential biomarkers available for detecting pathological changes in brain tissue metabolism. Using this expanded basis set of 31 neurochemicals we identified age- and sex-related changes in tissue chemistry in the hippocampus. The most prominent differences were in metabolites implicated in anaerobic energy metabolism, antioxidant defenses, and neuroprotection, as well as numerous macromolecule changes.

3.9 Chapter 3 Figures

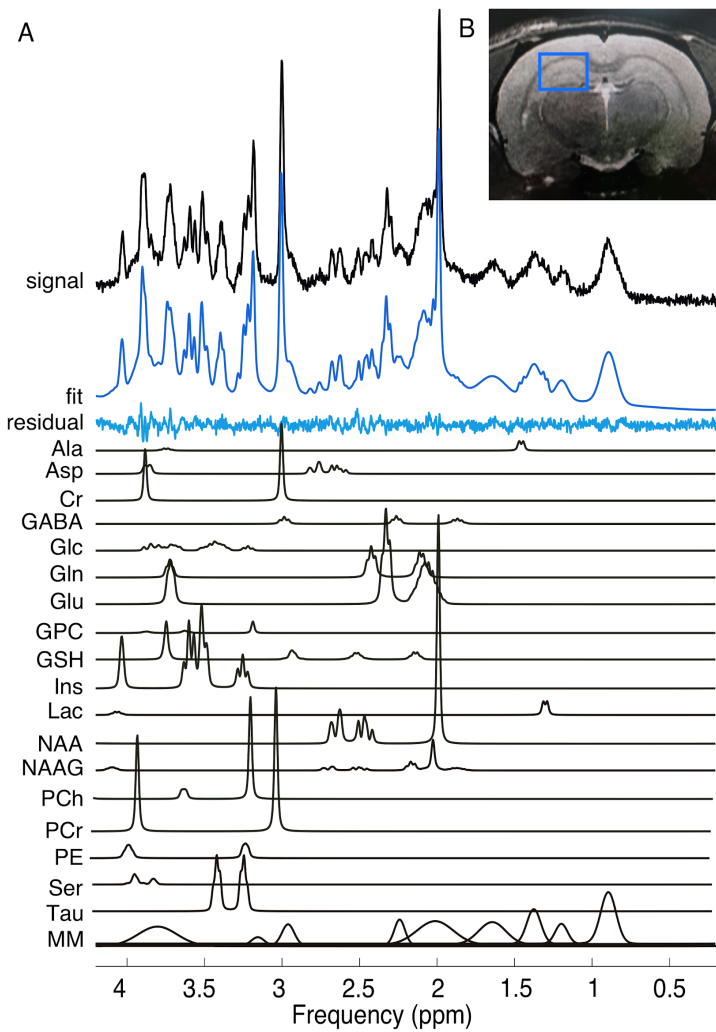


Figure 3.9.1

A. Localized ^1H -MRS spectra from the hippocampus of a 16-month old female rat acquired using a PRESS pulse sequence at 7T. The spectrum was processed using the FID-A toolkit which includes removal of bad averages, frequency drift correction, and zero-order phasing using the creatine peak. Metabolites included in the basis set are shown and assigned as follows: Alanine (Ala), Aspartate (Asp), Creatine (Cr), Gamma-aminobutyric acid (GABA), Glucose (Glc), Glutamine (Gln), Glutamate (Glu), Glycerophosphocholine (GPC), Glutathione (GSH), Myo-inositol (Ins); Lactate (Lac), N-acetylaspartate (NAA), N-acetylaspartyl glutamate (NAAG), Phosphocholine (PCh), Phosphocreatine (PCr), Phosphoethanolamine (PE), Serine (Ser), Taurine (Tau), Macromolecule (MM). **B.** A representative RARE image shows placement of the volume of interest for spectroscopy.

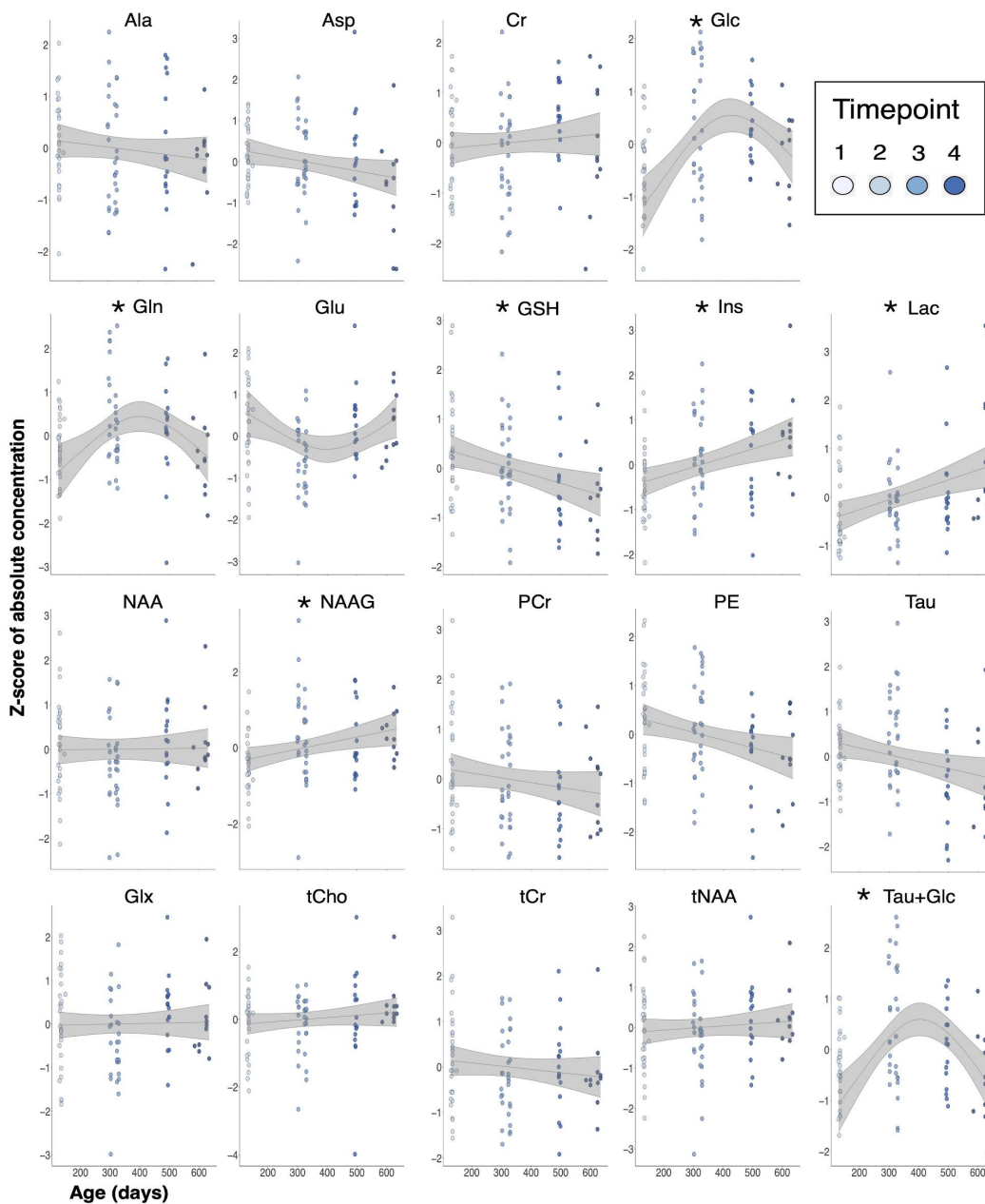


Figure 3.9.2 Age-dependent change in metabolite concentrations in the hippocampus of Fischer rats.

^1H -MRS spectra were acquired longitudinally in rats aged 4-, 10-, 16-, and 20-months old, and an effect of age was determined using linear mixed effects modelling with FDR correction. Each rat is depicted by an individual data point. The line of best fit and 95% confidence interval (shaded) is shown and represents the linear model used to fit the data. Significant effects of age were seen for Glucose (Glc), Glutathione (GSH), myo-Inositol (Ins), Lactate (Lac), and N-acetylaspartylglutamate (NAAG). * indicates significant effects of age at $q < 0.05$.

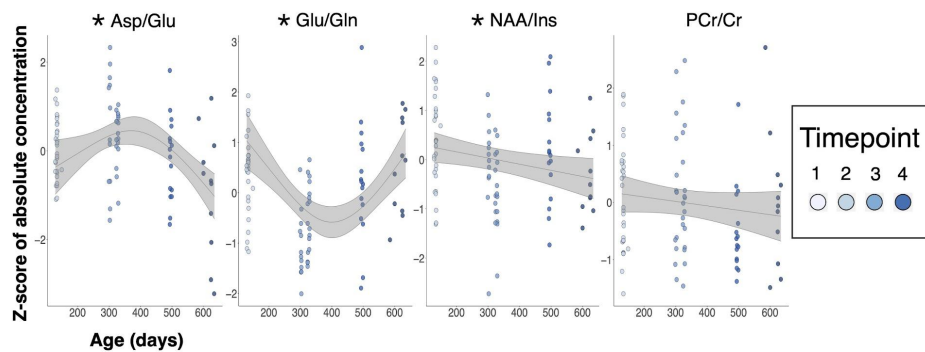


Figure 3.9.3 Age-dependent change in brain metabolite ratios in Fischer rats

¹H-MRS spectra were acquired longitudinally in rats aged 4-, 10-, 16-, and 20-months old, and an effect of age was determined using linear mixed effects modelling with FDR correction. Each rat is depicted by an individual data point. The line of best fit and 95% confidence interval (shaded) are and represent the linear model used to fit the data. Significant effects of age were seen for the ratio of N-acetylaspartate to myo-inositol (NAA/Ins). * indicates significant effects of age at $q < 0.05$.

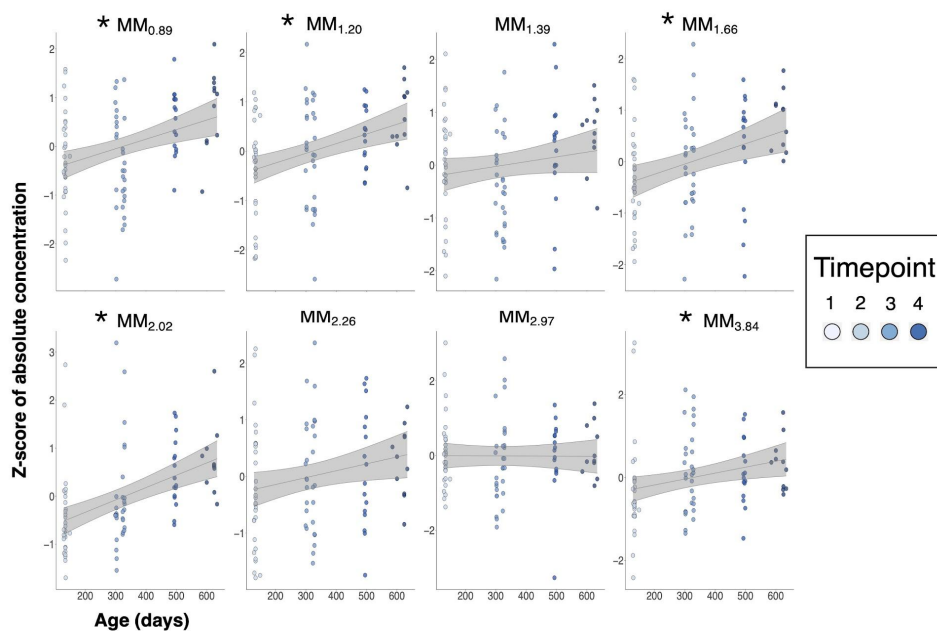


Figure 3.9.4 Age-dependent change in macromolecules in Fischer rats

¹H-MRS spectra were acquired longitudinally in rats aged 4-, 10-, 16-, and 20-months old, and an effect of age was determined using linear mixed effects modelling with FDR correction. Each rat is depicted by an individual data point. The line of best fit and 95% confidence interval (shaded) are shown and represent the linear model used to fit the data. Significant effects of age were seen for MM_{0.89}, MM_{1.20}, MM_{1.66}, MM_{2.02}, and MM_{3.84}. * indicates significant effects of age at $q < 0.05$.

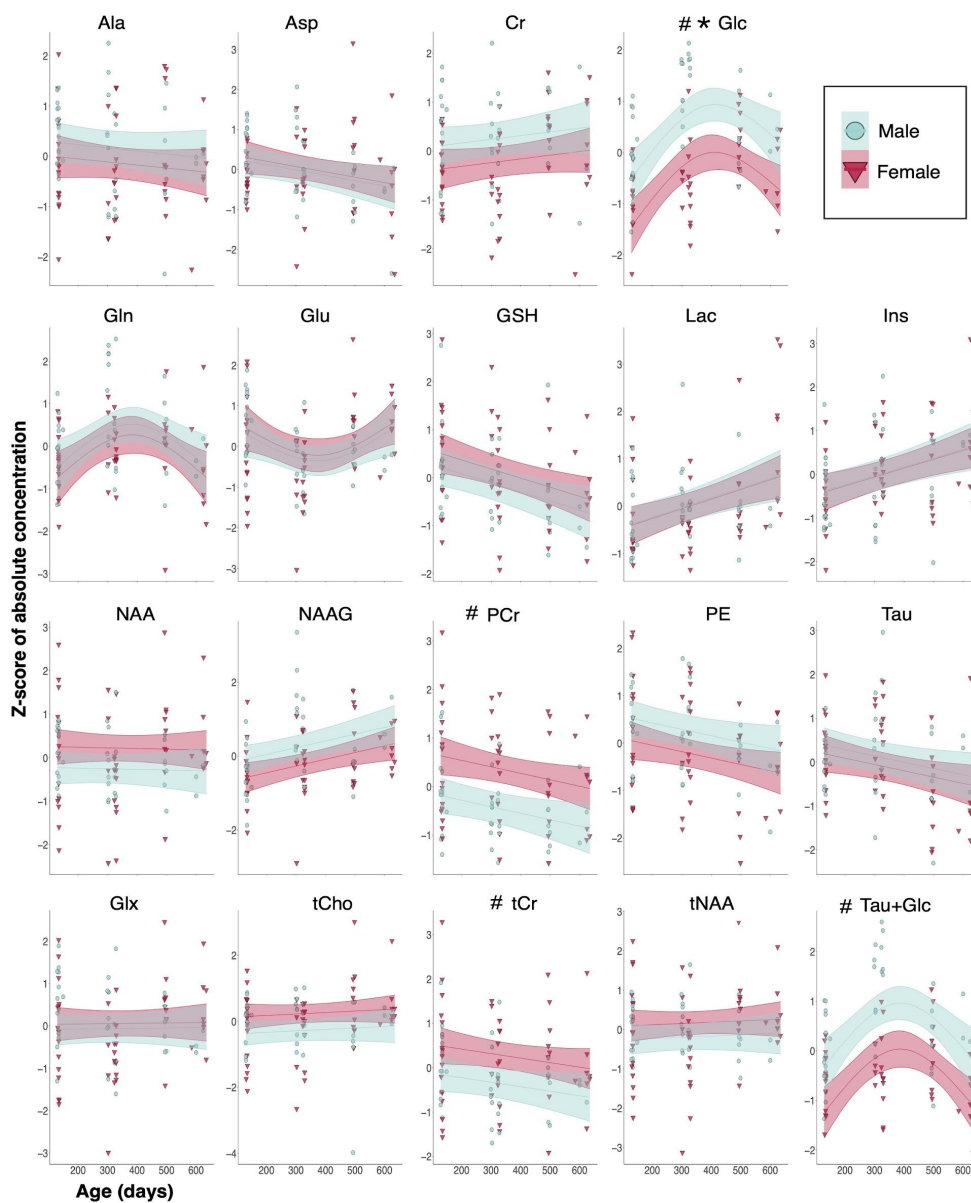


Figure 3.9.5 Differences in hippocampal metabolite concentrations exist between male and female Fischer rats

$^1\text{H-MRS}$ spectra were acquired longitudinally in rats aged 4-, 10-, 16-, and 20-months old. A main effect of sex was determined using linear mixed effects modelling with FDR correction using data collapsed across all four timepoints. Lines of best fit and their 95% confidence intervals are shown (shaded) and represent the linear model used to fit the data. Data corresponding to males and females is shown in teal and red, respectively. Significant effects of sex were seen for Glucose (Glc), Phosphocreatine (PCr), total Creatine (tCr), and Taurine+Glucose (Tau+Glc). * and # indicates significant effects of age and sex, respectively, at $q < 0.05$.

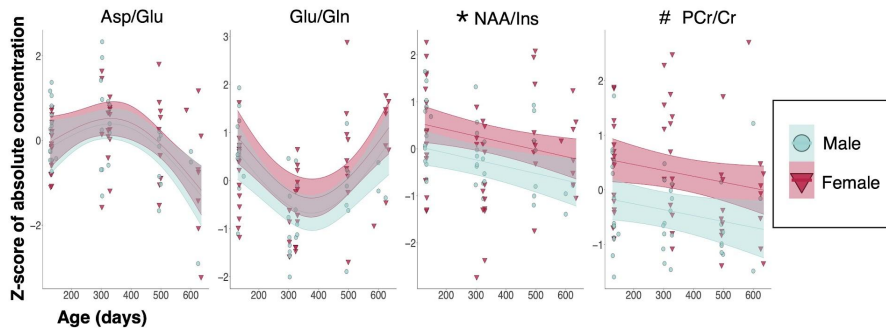


Figure 3.9.6 Differences in brain metabolite ratios exist between male and female F344 rats.

¹H-MRS spectra were acquired longitudinally in rats aged 4-, 10-, 16-, and 20-months old. A main effect of sex was determined using linear mixed effects modelling with FDR correction using data collapsed across all four timepoints. Lines of best fit and their 95% confidence intervals are shown (shaded) and represent the linear model used to fit the data. Data corresponding to males and females is shown in teal and red, respectively. Significant effects of sex were seen for the ratio of Phosphocreatine to Creatine (PCr/Cr). * and # indicates significant effects of age and sex, respectively, at $q < 0.05$.

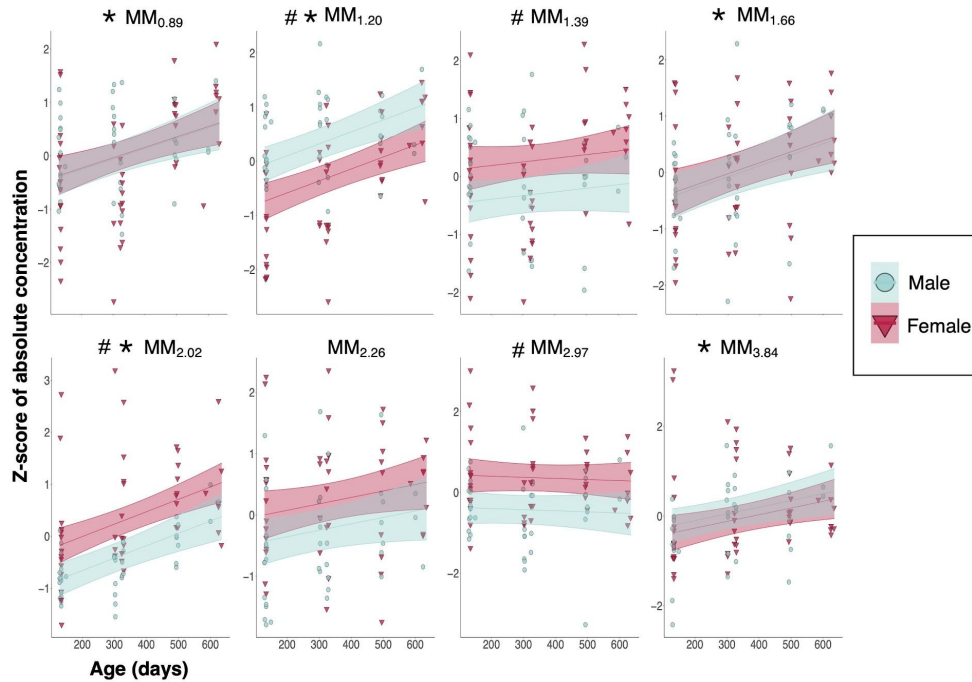


Figure 3.9.7 Differences in brain macromolecules exist between male and female F344 rats

¹H-MRS spectra were acquired longitudinally in rats aged 4-, 10-, 16-, and 20-months old. A main effect of sex was determined using linear mixed effects modelling with FDR correction using data

collapsed across all four timepoints. Lines of best fit and their 95% confidence intervals are shown (shaded) and represent the linear model used to fit the data. Data corresponding to males and females is shown in teal and red, respectively. Significant effects of sex were seen for MM_{1.20}, MM_{1.39}, MM_{2.02}, MM_{2.97}. * and # indicates significant effects of age and sex, respectively, at $q < 0.05$.

3.10 Chapter 3 Tables

	Main effect of age				Main effect of sex	
	Std. Beta ± SE	q value	Std.Beta ± SE*	q value*	Std. Beta ± SE	q value
Ala	-0.092 ± 0.106	0.497			-0.289 ± 0.238	0.330
Asp	-0.222 ± 0.106	0.078			0.108 ± 0.238	0.702
Cr	0.147 ± 0.102	0.230			-0.406 ± 0.244	0.167
Glc	1.872 ± 0.344	< 0.001	-0.147 ± 0.314	0.702	-0.953 ± 0.226	0.002
Gln	1.040 ± 0.422	0.045	-0.599 ± 0.355	0.156	-0.226 ± 0.253	0.494
Glu	-0.663 ± 0.384	0.153	0.663 ± 0.324	0.083	0.185 ± 0.236	0.555
GSH	-0.335 ± 0.100	0.006			0.331 ± 0.239	0.257
Ins	0.363 ± 0.100	0.003			-0.022 ± 0.246	0.944
Lac	0.355 ± 0.101	0.004			-0.033 ± 0.226	0.913
NAA	-0.005 ± 0.102	0.959			0.444 ± 0.234	0.444
NAAG	0.329 ± 0.098	0.006			-0.479 ± 0.223	0.074
PCr	-0.231 ± 0.099	0.056			0.817 ± 0.227	0.003
PE	-0.214 ± 0.102	0.078			-0.500 ± 0.232	0.074
Tau	-0.244 ± 0.105	0.056			-0.177 ± 0.253	0.593
Glx	0.022 ± 0.098	0.872			0.172 ± 0.236	0.587
tCho	0.089 ± 0.093	0.872			0.473 ± 0.212	0.064
tCr	-0.176 ± 0.104	0.156			0.652 ± 0.231	0.018
tNAA	0.064 ± 0.103	0.641			0.358 ± 0.230	0.192
Tau+Glc	1.407 ± 0.355	0.002	-0.677 ± 0.300	0.063	-0.915 ± 0.219	0.002
Asp/Glu	0.236 ± 0.433	0.687	-1.491 ± 0.352	0.001	0.120 ± 0.233	0.120
Glu/Gln	-1.363 ± 0.357	0.003	1.023 ± 0.308	0.006	0.278 ± 0.236	0.346

NAA/Ins	-0.254 ± 0.090	0.018	0.480 ± 0.224	0.078
PCr/Cr	-0.216 ± 0.092	0.056	0.659 ± 0.215	0.014
MM _{0.89}	0.331 ± 0.094	0.004	0.097 ± 0.209	0.702
MM _{1.20}	0.380 ± 0.080	<0.001	-0.654 ± 0.206	0.012
MM _{1.39}	0.113 ± 0.097	0.346	0.592 ± 0.222	0.035
MM _{1.66}	0.357 ± 0.097	0.003	0.050 ± 0.236	0.872
MM _{2.02}	0.423 ± 0.079	<0.001	0.593 ± 0.174	0.005
MM _{2.26}	0.177 ± 0.093	0.108	0.459 ± 0.236	0.108
MM _{2.97}	-0.051 ± 0.098	0.689	0.792 ± 0.253	0.012
MM _{3.84}	0.290 ± 0.093	0.010	-0.226 ± 0.22	0.425

Table 3.10.1 Change in neurochemical concentrations with age and sex in Fischer rats

Std.Beta. represents the standardized beta or coefficient value for the variable of sex or age in the linear model used for analysis, and is accompanied by the standard error (SE). Q-value is the FDR-corrected p-value obtained for each fixed effect. Q-value < 0.05 is denoted in **bold**. Six metabolites were best fit using a second order age term; the linear effect of age, in addition to the second order effect of age, are included, with the second order Std.Beta and q value denoted by *. Abbreviations: Alanine (Ala), Aspartate (Asp), Creatine (Cr), Gamma-aminobutyric acid (GABA), Glucose (Glc), Glutamine (Gln), Glutamate (Glu), Glycerophosphocholine (GPC), Glutathione (GSH), Myo-inositol (Ins); Lactate (Lac), N-acetylaspartate (NAA), N-acetylaspartyl glutamate (NAAG), Phosphocholine (PCh), Phosphocreatine (PCr), Phosphoethanolamine (PE), Serine (Ser), Taurine (Tau), total Choline (tCho), total Creatine (tCr), Glx (Glu+Gln), Macromolecule (MM).

3.11 Supplementary Methods

3.11.1 Quality Control

Each spectrum was visually inspected for quality before and after post-processing with FID-A. The full-width at half-max (FWHM) of the water unsuppressed spectrum and the signal-to-noise ratio (SNR) of the NAA peak in the water suppressed spectrum were extracted from each spectrum using an in-house MATLAB (R2012a) script (below) in conjunction with the FID-A toolkit (relevant commands: `op_getSNR`, and `op_getLW`). Average linewidth and SNR for each timepoint are shown in **Supplementary Table 3.13.5**, alongside values for estimated spectral FWHM and

SNR for water suppressed data provided by LCModel. Quality control resulted in the discarding of a single spectrum at the second time point due to SNR lower than 25, reducing the number of scans from 30 to 29.

3.11.2 Processing of macromolecule spectra

MM scans were obtained in 8 Fischer rats from a separate cohort at 10-months of age (313.8 ± 11.7 days). First, ^1H -MRS scans were acquired after FASTMAP shimming and a water reference scan. Next, “metabolite-suppressed” spectra were acquired using PRESS localization preceded by an inversion recovery (IR) pulse with an inversion time (TI) of 800 ms. In each rat, the metabolite-suppressed IR scan was acquired immediately after the ^1H -MRS scan in order to avoid re-shimming the instrument.

For each rat, water unsuppressed data, water suppressed data, and macromolecule data were imported into the FID-A processing toolbox (version 1.0) in MATLAB (R2012a). Within each dataset, transients were averaged and a zero-order phase shift correction was applied, using the phase of the NAA peak within the metabolite spectra. The NAA peak was also used to determine the frequency shift, and both the determined frequency and phase shifts were then applied to the water suppressed and macromolecule data. The eight macromolecule spectra were then aligned, summed, and scaled to generate an average metabolite-nulled spectra, for parameterization.

3.11.3 Parameterization of the macromolecule spectrum

Parameterization of the MM spectrum was performed in jMRUI using the AMARES fitting tool (Vanhamme, van den Boogaart A, and Van Huffel S 1997; Stefan et al. 2009; Naressi et al. 2001). The water peak was manually removed from the averaged MM spectrum using HLSVD (Hankel-Lanczos singular value decomposition (Pijnappel et al. 1992) in jMRUI and first order phasing was performed. Then, prior knowledge of the chemical shifts of ten MM resonances of interest was used as the input in the initial phase of modeling using Gaussian functions, wherein the subscript denotes the frequency (in ppm) at which the resonance appears: $\text{MM}_{0.89}$, $\text{MM}_{1.20}$, $\text{MM}_{1.39}$, $\text{MM}_{1.66}$, $\text{MM}_{2.02}$, $\text{MM}_{2.26}$, $\text{MM}_{2.97}$, $\text{MM}_{3.18}$, $\text{MM}_{3.84}$, and $\text{MM}_{4.27}$ (Považan et al. 2018; Otazo et al. 2006; Lee and Kim 2017). The MM peak at 4.27 ppm was parameterized but later omitted from basis set simulations due to proximity to the water peak.

As suggested by Craveiro, et al., residual metabolite signals within the MM spectrum can be better accounted for by including advanced prior knowledge of the residual peaks in the fitting process (Craveiro, Cudalbu, and Gruetter 2012; Craveiro et al. 2014). Constraints were therefore manually set for the frequency, phase, and linewidth of residual metabolite peaks (NAA, tCr, Glu, Gln, and Tau), and modelled using Lorentzian functions. Soft constraints on the overall and relative phase, frequency, and linewidth of all peaks were modified iteratively to achieve minimal fitting residuals (**Supplementary Figure 3.12.1**).

3.11.4 Determination of Water and Metabolite Relaxation Constants for Absolute Quantification

T1 and T2 water relaxation constants for use in absolute quantification were measured experimentally in a subset of Fischer rats (n=7) at 10-months of age. The T2 relaxation constant of water was determined by acquiring a series of non-localized water spectra in the same region of interest described above, using the PRESS sequence (TR = 5000 ms, 8 averages) without water suppression and with varying echo times (12, 20, 30, 40, 50, 70, 90, 120, 150, 200, 300, and 500 ms). Mono-exponential fitting of the T2 curves provided an estimated water T2 of 49.13 ms. To determine the T1 relaxation of water, a series of non-localized water spectra were acquired using the PRESS sequence (TR = 5000ms, TE=12 ms, 8 averages) preceded by a 4th order hyperbolic secant adiabatic full passage (AFP) inversion pulse (pulse duration = 1.0ms, bandwidth = 6982.0 Hz). A series of inversion times (TI) (25, 94, 261, 273, 660, 910, 1160, 1409, 1660, 2160, 3160, and 4160 ms) was acquired, with an additional scan performed without the inversion pulse to determine maximum signal intensity. The average maximum signal intensity of water at different inversion times (S(TI)) across the 7 rats were fitted versus their corresponding TIs using the equation below (Dehghani et al. 2020) resulting in an estimated water T1 of 1491ms.

$$S(TI) = S(TI_{off}) \cdot \frac{(1 - (1 + \alpha) \cdot \exp(-TI/T1)) + \alpha \cdot \exp(-TR/T1)}{(1 - \exp(-TR/T1))}, \quad (1)$$

where α represents the factor for the flip angle of the inversion pulse, and $S(TI_{off})$ represents the signal intensity at TE of 12 ms without inversion.

To approximate the T1 and T2 constants of individual metabolites at 7T, we used the curve fitting toolbox in Matlab (R2020b, The MathWorks, Inc., Natick, Massachusetts, United States) with polynomial degree =1 to fit relaxation constant values obtained by de Graaf et al. for tCho, tCr, Glx, NAA, and macromolecules, at 4 and 9.4T(de Graaf et al. 2006). This equation consisted of a simple $y = m*x + b$ format, wherein y was the relaxation constant, and x was the field strength. Once an equation had been derived by the curve-fitting tool, we used $x=7$ to determine the projected relaxation constant at 7T, for tCho, tCr (also applied to Cr and PCr individually), Glx (also applied to Glu and Gln, individually), NAA (also applied to NAAG), and MMs. For relaxation constants in metabolites not specifically measured by de Graaf, we used the average across calculated metabolite relaxation constants. This process of extrapolating from literature values obtained at 4T and 9.4T was performed as there are no existing reported relaxation constants at 7T for both metabolites and macromolecules. We are not the first authors to do this: in 2006, Otazo and colleagues extrapolated from data derived at 1.5, 3, and 4T to obtain an estimate for relaxation constants for 7T (Table 2, (Otazo et al. 2006). The input and output values for the curve fitting tool for each metabolite are reported in **Supplementary Table 3.13.3**.

The following equation was used to account for the T1 and T2 relaxation constants of water, metabolites and macromolecules. **Supplementary Equation 2**, modified from Dhamala et al., (Dhamala et al. 2019), also includes a correction factor to account for the fact that our voxel contained primarily grey matter (with an NMR-visible water concentration of 43300 mM) as opposed to the default for white matter used by LCModel (35880 mM). All relaxation constants and the subsequent correction factors applied, are summarized in **Supplementary Table 3.13.3**.

$$metabolite.abs = \frac{signal_{met}}{signal_{H2O}} \times WCONC_{GM_{H2O}} \times \frac{(exp^{-TE/T2_{H2O}}) \cdot (1 - exp^{-TR/T1_{H2O}})}{(exp^{-TE/T2_{met}}) \cdot (1 - exp^{-TR/T1_{met}})} \quad ,$$

(2)

where *metabolite.abs* is the absolute concentration of a given metabolite.

signal_{met}/signal_{H2O} is the ratio of metabolite signal to water signal, as determined using LCModel. This value is returned by LCModel when the parameters WCONC, ATTH2O, and ATTMET are all set to 1, and water scaling is on.

WCONC_{GMH2O} is the LCModel parameter specifying the tissue water concentration in grey matter (43300 mM) (Ernst, Kreis, and Ross 1993).

TE is the echo time of the experiment (TE = 11.12 ms)

TR is the repetition time of the experiment ($TR = 3000$ ms)

$T2_{H2O}$ is the measured water T2 relaxation time at 7T (49.13 ms)

$T2_{met}$ is the projected metabolite T2 relaxation time at 7T (**Supplementary Table 3.13.3**)

$T1_{H2O}$ is the measured water T1 relaxation time at 7T (1491 ms)

$T1_{met}$ is projected metabolite T2 relaxation time at 7T (**Supplementary Table 3.13.3**)

3.11.5 Retrospective Power Analysis

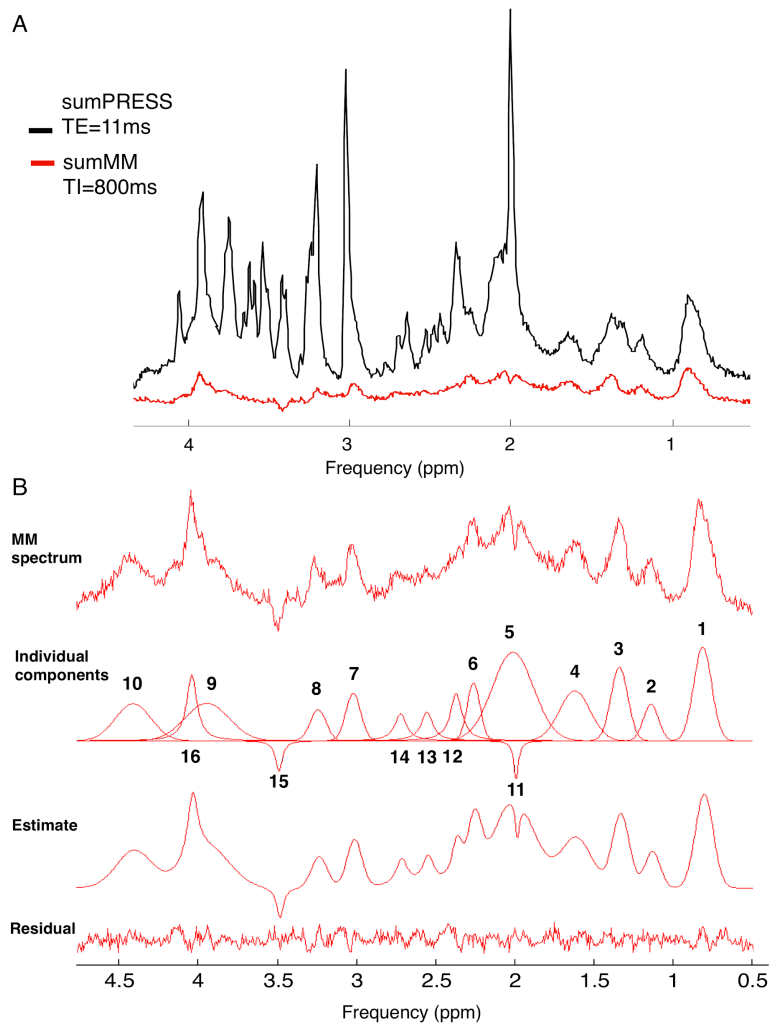
Retrospective power analyses to determine if the absence of an effect was due to lack of power are typically not advised, as there is a direct relationship between observed power and p-values (Hoenig and Heisey, n.d.). However, we are attempting to do the opposite and demonstrate that the effects we do see in our relatively small sample size are, in fact, generalizable to a larger population, i.e. given the variability within our dataset, if the data are simulated x number of times, how often is the effect size of interest statistically significant. This is particularly important because our dataset has a large reduction in subjects at the last two timepoints. As such, power calculations were performed in SIMR using Monte Carlo simulations ($n=1000$) and produced a calculated power and 95% confidence interval for the fixed effects of sex (collapsed across timepoints) and age for each metabolite. Traditionally 80% power is considered adequate, though as this is a somewhat arbitrary cut-off (Bacchetti 2010) we present all results (**Table 3.10.1, Supplementary Tables 3.13.8 and 3.13.9**), including the observed power and effect size (standardized beta) for each metabolite, for the reader to interpret as they wish.

3.11.6 Age- and sex-dependent neurochemical changes over 3 vs 4 timepoints

To ensure our results were not being driven by the last time point wherein we have the fewest subjects (and therefore, the least power), we also analyzed all data from time points 1 through 3 only. Of the 16 neurochemicals with significant age-related changes over the four timepoints, eight remained significant (Glc, Gln, GSH, NAAG, Tau+Glc, Glu/Gln, MM_{1.20}, and MM_{2.02}) at a q-value of <0.05 . Of the eight that were no longer significant, four were trending at a q-value < 0.1 (Ins, MM_{0.89}, MM_{1.66}, MM_{3.84}), while the other four (Lac, NAA/Ins, and the second order age effects for Asp/Glu and Glu/Gln), had q values of 0.183, 0.149, 0.109, and 0.244, respectively. Of the nine neurochemicals with significant differences ($q < 0.05$) between males and females, eight remained significant and the last was trending ($q < 0.1$, MM_{1.39}) when analyzed using data from three timepoints as opposed to four. For more details see **Supplementary Tables 3.13.8 and 3.13.9**.

The majority of significant effects seen at four time points were replicated using three time point data, and those that were no longer significant using the smaller dataset were at trending, or close to it, at the q-value level. The effects of sex remained particularly strong. This additional analysis, in conjunction with the observed power analysis, represents the steps taken towards ensuring our results are robust, despite the decreased sample size towards the end of the study. It is clear that the last timepoint at 20-months constitutes an important piece of the puzzle, both in terms of providing additional power, but also in solidifying age-or sex-related changes in neurochemicals that are trending towards significance in data from the first three timepoints.

3.12 Supplementary Figures



Supplementary Figure 3.12.1 Parameterization of the metabolite-nulled spectrum

(A) Average localized ^1H -MRS spectrum ($n=8$, PRESS sequence) and corresponding metabolite-nulled spectrum ($n=8$, Inversion Recovery PRESS sequence) used for parameterization. (B) Output of AMARES quantification showing the average metabolite-nulled spectrum with all individual components used for fitting, which consisted of 10 macromolecule peaks and 6 residual metabolite peaks, the overall fitting estimate, and the residual difference between the measured and fitted data. Numbers 1 through 10 correspond to macromolecule peaks $\text{MM}_{0.89}$, $\text{MM}_{1.20}$, $\text{MM}_{1.39}$, $\text{MM}_{1.66}$, $\text{MM}_{2.02}$, $\text{MM}_{2.26}$, $\text{MM}_{2.97}$, $\text{MM}_{3.18}$, $\text{MM}_{3.84}$, and $\text{MM}_{4.27}$. Numbers 11 through 16 represent residual metabolite peaks NAA, Glu, Gln, NAA, Tau, and tCr, respectively.

3.13 Supplementary Table Captions

Supplementary Table 3.13.1. SubjectInfo

Subject Information

Supplementary Table 3.13.2. BasisSetSimulation

JMRUI AMARES Output which served as the input for basis set simulation

Supplementary Table 3.13.3. Correction Factors

Relaxation constants and correction factors applied to LCModel outputs. Note that the average metabolite (Avg.Met) value was also used for Glx T2 due to lack of literature values in analysis by deGraaf et al. $\text{Relx.met} = \exp^{-TE/T2_{\text{met}}} \times (1 - \exp^{-TR/T1_{\text{met}}})$; $\text{Relx.water} = \exp^{-TE/T2_{\text{H}_2\text{O}}} \times (1 - \exp^{-TR/T1_{\text{H}_2\text{O}}})$; $\text{WCONC}_{\text{GM}/\text{WM}}$ is a ratio combining the LCModel parameters specifying the tissue water concentration in grey matter (43300mM) and white matter (Harris et al.); Correction factor = $(\text{WCONC}_{\text{GM}}/\text{WCONC}_{\text{WM}}) \times (\text{relx.water}/\text{relx.met})$

Supplementary Table 3.13.4. CRLB

CRLB values (%) for all metabolites

Supplementary Table 3.13.5. SNR_LW

SNR and linewidth values (Hz) across timepoints. LCModel notes that some may use twice the SNR that they report, which is the ratio of the maximum in the spectrum minus baseline over the analysis window to twice the residuals

Supplementary Table 3.13.6. Conc.Summary.Age

Absolute concentrations (mM) of metabolites across all timepoints

Supplementary Table 3.13.7. Conc.Summary.Sex

Absolute concentrations (mM) of metabolites collapsed across timepoints and separated by sex

Supplementary Table 3.13.8. AgeEffect

Analysis of change in neurochemical concentration with age across all 4 timepoints compared to analysis across 3 timepoints

Supplementary Table 3.13.9. SexEffect

Summary of neurochemical differences between males and females analyzed across all 4 timepoints compared to analysis across 3 timepoints

3.14 Supplementary References

- Bacchetti, Peter. 2010. "Current Sample Size Conventions: Flaws, Harms, and Alternatives." *BMC Medicine* 8 (March): 17.
- Craveiro, Mélanie, Virginie Clément-Schatlo, Denis Marino, Rolf Gruetter, and Cristina Cudalbu. 2014. "In Vivo Brain Macromolecule Signals in Healthy and Glioblastoma Mouse Models: 1H Magnetic Resonance Spectroscopy, Post-Processing and Metabolite Quantification at 14.1 T." *Journal of Neurochemistry* 129 (5): 806–15.
- Craveiro, Mélanie, Cristina Cudalbu, and Rolf Gruetter. 2012. "Regional Alterations of the Brain Macromolecule Resonances Investigated in the Mouse Brain Using an Improved Method for the Pre-Processing of the Macromolecular Signal." *Proc. Intl. Soc. Mag. Reson. Med.* 20: 1748.
- Dehghani, Masoumeh, Kim Q. Do, Pierre Magistretti, and Lijing Xin. 2020. "Lactate Measurement by Neurochemical Profiling in the Dorsolateral Prefrontal Cortex at 7T: Accuracy, Precision, and Relaxation Times." *Magnetic Resonance in Medicine: Official Journal of the Society of Magnetic Resonance in Medicine / Society of Magnetic Resonance in Medicine* 83 (6): 1895–1908.
- Dhamala, Elvisha, Ines Abdelkefi, Mavesa Nguyen, T. Jay Hennessy, Hélène Nadeau, and Jamie Near. 2019. "Validation of in Vivo MRS Measures of Metabolite Concentrations in the Human Brain." *NMR in Biomedicine* 32 (3): e4058.
- Ernst, T., R. Kreis, and B. D. Ross. 1993. "Absolute Quantitation of Water and Metabolites in the Human Brain. I. Compartments and Water." *Journal of Magnetic Resonance. Series B* 102 (1): 1–8.
- Graaf, Robin A. de, Peter B. Brown, Scott McIntyre, Terence W. Nixon, Kevin L. Behar, and Douglas L. Rothman. 2006. "High Magnetic Field Water and Metabolite Proton T1 and T2 Relaxation in Rat Brain in Vivo." *Magnetic Resonance in Medicine: Official Journal of the Society of Magnetic Resonance in Medicine / Society of Magnetic Resonance in Medicine* 56 (2): 386–94.
- Hoening, John M., and Dennis M. Heisey. n.d. "The Abuse of Power: The Pervasive Fallacy of Power Calculations for Data Analysis."
- Lee, Hyeong Hun, and Hyeonjin Kim. 2017. "Parameterization of Spectral Baseline Directly from Short Echo Time Full Spectra in 1 H-MRS." *Magnetic Resonance in Medicine: Official Journal of the Society of Magnetic Resonance in Medicine / Society of Magnetic Resonance in Medicine* 78 (3): 836–47.
- Naressi, A., C. Couturier, J. M. Devos, M. Janssen, C. Mangeat, R. de Beer, and D. Graveron-Demilly. 2001. "Java-Based Graphical User Interface for the MRUI Quantitation Package." *Magma* 12 (2-3): 141–52.
- Otazo, Ricardo, Bryon Mueller, Kamil Ugurbil, Lawrence Wald, and Stefan Posse. 2006. "Signal-to-Noise Ratio and Spectral Linewidth Improvements between 1.5 and 7 Tesla in Proton Echo-Planar Spectroscopic Imaging." *Magnetic Resonance in Medicine: Official*

Journal of the Society of Magnetic Resonance in Medicine / Society of Magnetic Resonance in Medicine 56 (6): 1200–1210.

Pijnappel, W. W. F., A. van den Boogaart, R. de Beer, and D. van Ormondt. 1992. “SVD-Based Quantification of Magnetic Resonance Signals.” *Journal of Magnetic Resonance (1969)*. [https://doi.org/10.1016/0022-2364\(92\)90241-x](https://doi.org/10.1016/0022-2364(92)90241-x).

Považan, Michal, Bernhard Strasser, Gilbert Hangel, Eva Heckova, Stephan Gruber, Siegfried Trattinig, and Wolfgang Bogner. 2018. “Simultaneous Mapping of Metabolites and Individual Macromolecular Components via Ultra-Short Acquisition Delay 1 H MRSI in the Brain at 7T : Simultaneous Mapping of Metabolites and Macromolecules.” *Magnetic Resonance in Medicine: Official Journal of the Society of Magnetic Resonance in Medicine / Society of Magnetic Resonance in Medicine* 79 (3): 1231–40.

Stefan, D., F. Di Cesare, A. Andrasescu, E. Popa, A. Lazariiev, E. Vescovo, O. Strbak, et al. 2009. “Quantitation of Magnetic Resonance Spectroscopy Signals: The jMRUI Software Package.” *Measurement Science & Technology* 20 (10): 104035.

Vanhamme, L., van den Boogaart A, and Van Huffel S. 1997. “Improved Method for Accurate and Efficient Quantification of MRS Data with Use of Prior Knowledge.” *Journal of Magnetic Resonance* 129 (1): 35–43.

3.15 Chapter 3 References

Akintola, A.A., van Heemst, D., 2015. Insulin, aging, and the brain: mechanisms and implications. *Front. Endocrinol.* 6, 13.

Bartha, R., 2007. Effect of signal-to-noise ratio and spectral linewidth on metabolite quantification at 4 T. *NMR Biomed.* 20, 512–521.

Béard, E., Braissant, O., 2010. Synthesis and transport of creatine in the CNS: importance for cerebral functions. *J. Neurochem.* 115, 297–313.

Behar, K.L., Ogino, T., 1993. Characterization of macromolecule resonances in the 1H NMR spectrum of rat brain. *Magn. Reson. Med.* 30, 38–44.

Behar, K.L., Rothman, D.L., Spencer, D.D., Petroff, O.A., 1994. Analysis of macromolecule resonances in 1H NMR spectra of human brain. *Magn. Reson. Med.* 32, 294–302.

Benarroch, E.E., 2008. N-Acetylaspartate and N-acetylaspartylglutamate: Neurobiology and clinical significance. *Clinical implications of Neuroscience Research* 70, 1353–1357.

Benjamini, Y., Hochberg, Y., 1995. Controlling the False Discovery Rate: A Practical and Powerful Approach to Multiple Testing. *J. R. Stat. Soc. Series B Stat. Methodol.* 57, 289–300.

Berent-Spillson, A., Robinson, A.M., Golovoy, D., Slusher, B., Rojas, C., Russell, J.W., 2004. Protection against glucose-induced neuronal death by NAAG and GCP II inhibition is regulated by mGluR3. *J. Neurochem.* 89, 90–99.

Best, J.G., Stagg, C.J., Dennis, A., 2014. Chapter 2.5 - Other Significant Metabolites: Myo-Inositol, GABA, Glutamine, and Lactate, in: Stagg, C., Rothman, D. (Eds.), *Magnetic Resonance Spectroscopy*. Academic Press, San Diego, pp. 122–138.

Bettio, L.E.B., Rajendran, L., Gil-Mohapel, J., 2017. The effects of aging in the hippocampus and cognitive decline. *Neurosci. Biobehav. Rev.* 79, 66–86.

Bevilacqua, A., Bizzarri, M., 2018. Inositols in Insulin Signaling and Glucose Metabolism. *Int. J. Endocrinol.* 2018, 1968450.

Boumezbeur, F., Petersen, K.F., Cline, G.W., Mason, G.F., Behar, K.L., Shulman, G.I., Rothman, D.L., 2010. The contribution of blood lactate to brain energy metabolism in humans

measured by dynamic ^{13}C nuclear magnetic resonance spectroscopy. *J. Neurosci.* 30, 13983–13991.

Camandola, S., Mattson, M.P., 2017. Brain metabolism in health, aging, and neurodegeneration. *EMBO J.* 36, 1474–1492.

Chang, L., Ernst, T., Poland, R.E., Jenden, D.J., 1996. In Vivo Proton Magnetic Resonance Spectroscopy of the Normal Aging Human Brain. *Life Sci.* 58, 2049–2056.

Choi, J.-K., Carreras, I., Aytan, N., Jenkins-Sahlin, E., Dedeoglu, A., Jenkins, B.G., 2014. The effects of aging, housing and ibuprofen treatment on brain neurochemistry in a triple transgene Alzheimer's disease mouse model using magnetic resonance spectroscopy and imaging. *Brain Res.* 1590, 85–96.

Clelland, C., Pipingas, A., Scholey, A., White, D., 2019. Neurochemical changes in the aging brain: A systematic review. *Neurosci. Biobehav. Rev.* 98, 306–319.

Craveiro, M., Clément-Schatlo, V., Marino, D., Gruetter, R., Cudalbu, C., 2014. In vivo brain macromolecule signals in healthy and glioblastoma mouse models: ^1H magnetic resonance spectroscopy, post-processing and metabolite quantification at 14.1 T. *J. Neurochem.* 129, 806–815.

Cudalbu, C., Mlynárik, V., Gruetter, R., 2012. Handling macromolecule signals in the quantification of the neurochemical profile. *J. Alzheimers. Dis.* 31 Suppl 3, S101–15.

David, J.P., Ghazali, F., Fallet-Bianco, C., Watzel, A., Delaine, S., Boniface, B., Di Menza, C., Delacourte, A., 1997. Glial reaction in the hippocampal formation is highly correlated with aging in human brain. *Neurosci. Lett.* 235, 53–56.

Dong, Y., Brewer, G.J., 2019. Global Metabolic Shifts in Age and Alzheimer's Disease Mouse Brains Pivot at NAD^+/NADH Redox Sites. *J. Alzheimers. Dis.* 71, 119–140.

Duarte, J.M.N., Do, K.Q., Gruetter, R., 2014. Longitudinal neurochemical modifications in the aging mouse brain measured in vivo by ^1H magnetic resonance spectroscopy. *Neurobiol. Aging* 35, 1660–1668.

Duarte, J.M.N., Lei, H., Mlynárik, V., Gruetter, R., 2012. The neurochemical profile quantified by in vivo ^1H NMR spectroscopy. *Neuroimage* 61, 342–362.

Emir, U.E., Raatz, S., McPherson, S., Hodges, J.S., Torkelson, C., Tawfik, P., White, T., Terpstra, M., 2011. Noninvasive quantification of ascorbate and glutathione concentration in the elderly human brain. *NMR Biomed.* 24, 888–894.

Ernst, T., Kreis, R., Ross, B.D., 1993. Absolute Quantitation of Water and Metabolites in the Human Brain. I. Compartments and Water. *J. Magn. Reson. B* 102, 1–8.

Febo, M., Foster, T.C., 2016. Preclinical Magnetic Resonance Imaging and Spectroscopy Studies of Memory, Aging, and Cognitive Decline. *Front. Aging Neurosci.* 8, 158.

Frazier, H.N., Ghoweri, A.O., Sudkamp, E., Johnson, E.S., Anderson, K.L., Fox, G., Vatthanaphone, K., Xia, M., Lin, R.-L., Hargis-Staggs, K.E., Porter, N.M., Pauly, J.R., Blalock, E.M., Thibault, O., 2020. Long-Term Intranasal Insulin Aspart: A Profile of Gene Expression, Memory, and Insulin Receptors in Aged F344 Rats. *J. Gerontol. A Biol. Sci. Med. Sci.* 75, 1021–1030.

Gillies, G.E., McArthur, S., 2010. Estrogen actions in the brain and the basis for differential action in men and women: a case for sex-specific medicines. *Pharmacol. Rev.* 62, 155–198.

Godbout, J.P., Johnson, R.W., 2009. Age and neuroinflammation: a lifetime of psychoneuroimmune consequences. *Immunol. Allergy Clin. North Am.* 29, 321–337.

Govindaraju, V., Young, K., Maudsley, A.A., 2000. Proton NMR chemical shifts and coupling constants for brain metabolites. *NMR Biomed.* 13, 129–153.

- Green, P., MacLeod, C.J., 2016. SIMR : an R package for power analysis of generalized linear mixed models by simulation. *Methods Ecol. Evol.* 7, 493–498.
- Gruber, S., Pinker, K., Riederer, F., Chmelik, M., Stadlbauer, A., Bittsansky, M., Mlynarik, V., Frey, R., Serles, W., Bodamer, O., Moser, E., 2008. Metabolic changes in the normal ageing brain: Consistent findings from short and long echo time spectroscopy. *Eur. J. Radiol.* 68, 320–327.
- Gruetter, R., 1993. Automatic, Localized in Vivo Adjustment of All First- and Second-Order Shim Coils. *Journal of Magnetic Resonance in Medicine* 29, 804–811.
- Hädel, S., Wirth, C., Rapp, M., Gallinat, J., Schubert, F., 2013. Effects of age and sex on the concentrations of glutamate and glutamine in the human brain: Brain Glutamate and Glutamine With Age and Sex. *J. Magn. Reson. Imaging* 38, 1480–1487.
- Haga, K.K., Khor, Y.P., Farrall, A., Wardlaw, J.M., 2009. A systematic review of brain metabolite changes, measured with 1H magnetic resonance spectroscopy, in healthy aging. *Neurobiol. Aging* 30, 353–363.
- Hagiwara, A., Fujimoto, K., Kamagata, K., Murata, S., Irie, R., Kaga, H., Someya, Y., Andica, C., Fujita, S., Kato, S., Fukunaga, I., Wada, A., Hori, M., Tamura, Y., Kawamori, R., Watada, H., Aoki, S., 2020. Age-Related Changes in Relaxation Times, Proton Density, Myelin, and Tissue Volumes in Adult Brain Analyzed by 2-Dimensional Quantitative Synthetic Magnetic Resonance Imaging. *Invest. Radiol.* <https://doi.org/10.1097/RLI.0000000000000720>
- Harris, J.L., Yeh, H.-W., Swerdlow, R.H., Choi, I.-Y., Lee, P., Brooks, W.M., 2014. High-field proton magnetic resonance spectroscopy reveals metabolic effects of normal brain aging. *Neurobiol. Aging* 35, 1686–1694.
- Hofmann, L., Slotboom, J., Boesch, C., Kreis, R., 2001. Characterization of the Macromolecule Baseline in LocalizedH-MR Spectra of Human Brain. *Magn. Reson. Med.* 46, 855–863.
- Hofmann, L., Slotboom, J., Jung, B., Maloca, P., Boesch, C., Kreis, R., 2002. Quantitative 1H-magnetic resonance spectroscopy of human brain: Influence of composition and parameterization of the basis set in linear combination model-fitting. *Magn. Reson. Med.* 48, 440–453.
- Jansen, J.F.A., Backes, M.S.W.H., Nicolay, K., Eline Kooi, M., 2006. 1H MR Spectroscopy of the Brain: Absolute Quantification of Metabolites. *Radiology* 240.
- Komoroski, R.A., Heimberg, C., Cardwell, D., Karson, C.N., 1999. Effects of gender and region on proton MRS of normal human brain. *Magn. Reson. Imaging* 17, 427–433.
- Kreis, R., 2016. The trouble with quality filtering based on relative Cramér-Rao lower bounds. *Magn. Reson. Med.* 75, 15–18.
- Kreis, R., Slotboom, J., Hofmann, L., Boesch, C., 2005. Integrated data acquisition and processing to determine metabolite contents, relaxation times, and macromolecule baseline in single examinations of individual subjects. *Magn. Reson. Med.* 54, 761–768.
- Kupeli, A., Kocak, M., Goktepel, M., Karavas, E., Danisan, G., 2020. Role of T1 mapping to evaluate brain aging in a healthy population. *Clin. Imaging* 59, 56–60.
- Lee, H.H., Kim, H., 2017. Parameterization of spectral baseline directly from short echo time full spectra in 1 H-MRS. *Magn. Reson. Med.* 78, 836–847.
- Lopez-Kolkovskiy, A.L., Mériaux, S., Boumezeur, F., 2016. Metabolite and macromolecule T1 and T2 relaxation times in the rat brain in vivo at 17.2T. *Magn. Reson. Med.* 75, 503–514.
- Mao, J., Mareci, T.H., Andrew, E.R., 1988. Experimental study of optimal selective 180 radiofrequency pulses. *J. Magn. Reson.* 79, 1–10.
- Marjańska, M., Deelchand, D.K., Hodges, J.S., McCarten, J.R., Hemmy, L.S., Grant, A.,

Terpstra, M., 2018. Altered macromolecular pattern and content in the aging human brain. *NMR Biomed.* 31. <https://doi.org/10.1002/nbm.3865>

Marjańska, M., McCarten, J.R., Hodges, J., Hemmy, L.S., Grant, A., Deelchand, D.K., Terpstra, M., 2017. Region-specific aging of the human brain as evidenced by neurochemical profiles measured noninvasively in the posterior cingulate cortex and the occipital lobe using ¹H magnetic resonance spectroscopy at 7 T. *Neuroscience* 354, 168–177.

Marjańska, M., McCarten, J.R., Hodges, J.S., Hemmy, L.S., Terpstra, M., 2019. Distinctive Neurochemistry in Alzheimer's Disease via 7 T In Vivo Magnetic Resonance Spectroscopy. *J. Alzheimers. Dis.* 68, 559–569.

Marjańska, M., Weigand, S.D., Preboske, G., Wengenack, T.M., Chamberlain, R., Curran, G.L., Poduslo, J.F., Garwood, M., Kobayashi, D., Lin, J.C., Jack, C.R., 2014. Treatment effects in a transgenic mouse model of Alzheimer's disease: A magnetic resonance spectroscopy study after passive immunization. *Neuroscience* 259, 94–100.

Mazure, C.M., Swendsen, J., 2016. Sex differences in Alzheimer's disease and other dementias. *Lancet Neurol.*

McKenna, M.C., Dienel, G.A., Sonnewald, U., Waagepetersen, H.S., Schousboe, A., 2012. Chapter 11 - Energy Metabolism of the Brain, in: Brady, S.T., Siegel, G.J., Albers, R.W., Price, D.L. (Eds.), *Basic Neurochemistry (Eighth Edition)*. Academic Press, New York, pp. 200–231.

Miccheli, A., Puccetti, C., Capuani, G., Di Cocco, M.E., Giardino, L., Calzà, L., Battaglia, A., Battistin, L., Conti, F., 2003. [¹⁻¹³C]Glucose entry in neuronal and astrocytic intermediary metabolism of aged rats: A study of the effects of nicergoline treatment by ¹³C NMR spectroscopy. *Brain Res.* 966, 116–125.

Mlynárik, V., Gambarota, G., Frenkel, H., Gruetter, R., 2006. Localized short-echo-time proton MR spectroscopy with full signal-intensity acquisition. *Magn. Reson. Med.* 56, 965–970.

Morrison, J.H., Stern, P.C., Carstensen, L.L., 2000. *Age-Related Shifts in Neural Circuit Characteristics and Their Impact on Age-Related Cognitive Impairments*. National Academies Press (US).

Mosconi, L., 2013. Glucose metabolism in normal aging and Alzheimer's disease: Methodological and physiological considerations for PET studies. *Clin Transl Imaging* 1. <https://doi.org/10.1007/s40336-013-0026-y>

Murray, M.E., Przybelski, S.A., Lesnick, T.G., Liesinger, A.M., Spsychalla, A., Zhang, B., Gunter, J.L., Parisi, J.E., Boeve, B.F., Knopman, D.S., Petersen, R.C., Jack, C.R., Jr, Dickson, D.W., Kantarci, K., 2014. Early Alzheimer's disease neuropathology detected by proton MR spectroscopy. *J. Neurosci.* 34, 16247–16255.

Naressi, A., Couturier, C., Devos, J.M., Janssen, M., Mangeat, C., de Beer, R., Graveron-Demilly, D., 2001. Java-based graphical user interface for the MRUI quantitation package. *MAGMA* 12, 141–152.

Nilsen, L.H., Melø, T.M., Witter, M.P., Sonnewald, U., 2014. Early differences in dorsal hippocampal metabolite levels in males but not females in a transgenic rat model of Alzheimer's disease. *Neurochem. Res.* 39, 305–312.

Otazo, R., Mueller, B., Ugurbil, K., Wald, L., Posse, S., 2006. Signal-to-noise ratio and spectral linewidth improvements between 1.5 and 7 Tesla in proton echo-planar spectroscopic imaging. *Magn. Reson. Med.* 56, 1200–1210.

Paban, V., Fauvelle, F., Alescio-Lautier, B., 2010. Age-related changes in metabolic profiles of rat hippocampus and cortices. *Eur. J. Neurosci.* 31, 1063–1073.

Pfefferbaum, A., Adalsteinsson, E., Spielman, D., Sullivan, E.V., Lim, K.O., n.d. of Brain Gray

and White Matter: Effects of Normal Aging.

Pfeuffer, J., Tkáč, I., Provencher, S.W., Gruetter, R., 1999. Toward an in Vivo Neurochemical Profile: Quantification of 18 Metabolites in Short-Echo-Time H NMR Spectra of the Rat Brain. *J. Magn. Reson.* 141, 104–120.

Považan, M., Strasser, B., Hangel, G., Heckova, E., Gruber, S., Trattnig, S., Bogner, W., 2018. Simultaneous mapping of metabolites and individual macromolecular components via ultra-short acquisition delay 1 H MRSI in the brain at 7T : Simultaneous Mapping of Metabolites and Macromolecules. *Magn. Reson. Med.* 79, 1231–1240.

Provencher, S., 2019. LCMModel & LCMgui User's Manual.

Provencher, S.W., 1993. Estimation of metabolite concentrations from localized in vivo proton NMR spectra. *Magn. Reson. Med.* 30, 672–679.

Rasgon, N.L., Small, G.W., Siddarth, P., Miller, K., Ercoli, L.M., Bookheimer, S.Y., Lavretsky, H., Huang, S.C., Barrio, J.R., Phelps, M.E., 2001. Estrogen use and brain metabolic change in older adults. A preliminary report. *Psychiatry Res.* 107, 11–18.

Ravera, S., Podestà, M., Sabatini, F., Dagnino, M., Cilloni, D., Fiorini, S., Barla, A., Frassoni, F., 2019. Discrete Changes in Glucose Metabolism Define Aging. *Sci. Rep.* 9, 10347.

Ross, A.J., Sachdev, P.S., 2004. Magnetic resonance spectroscopy in cognitive research. *Brain Res. Brain Res. Rev.* 44, 83–102.

Saunders, D.E., Howe, F.A., van den Boogaart, A., Griffiths, J.R., Brown, M.M., 1997. Discrimination of metabolite from lipid and macromolecule resonances in cerebral infarction in humans using short echo proton spectroscopy. *J. Magn. Reson. Imaging* 7, 1116–1121.

Schuff, N., Amend, D.L., Knowlton, R., Norman, D., Fein, G., Weiner, M.W., 1999. Age-related metabolite changes and volume loss in the hippocampus by magnetic resonance spectroscopy and imaging. *Neurobiol. Aging* 20, 279–285.

Seeger, U., Klose, U., Mader, I., Grodd, W., Nägele, T., 2003. Parameterized evaluation of macromolecules and lipids in proton MR spectroscopy of brain diseases. *Magn. Reson. Med.* 49, 19–28.

Sibson, N.R., Dhankhar, A., Mason, G.F., Behar, K.L., Rothman, D.L., Shulman, R.G., n.d. In vivo ¹³C NMR measurements of cerebral glutamine synthesis as evidence for glutamate–glutamine cycling.

Simpson, R., Devenyi, G.A., Jezard, P., Hennessy, T.J., Near, J., 2017. Advanced processing and simulation of MRS data using the FID appliance (FID-A)-An open source, MATLAB-based toolkit. *Magn. Reson. Med.* 77, 23–33.

Snoussi, K., Gillen, J.S., Horska, A., Puts, N.A.J., Pradhan, S., Edden, R.A.E., Barker, P.B., 2015. Comparison of brain gray and white matter macromolecule resonances at 3 and 7 Tesla. *Magn. Reson. Med.* 74, 607–613.

Stefan, D., Di Cesare, F., Andrasescu, A., Popa, E., Lazariiev, A., Vescovo, E., Strbak, O., Williams, S., Starcuk, Z., Cabanas, M., van Ormondt, D., Graveron-Demilly, D., 2009. Quantitation of magnetic resonance spectroscopy signals: the jMRUI software package. *Meas. Sci. Technol.* 20, 104035.

Tkáč, I., Starcuk, Z., Choi, I., Gruetter, R., 1999. In Vivo H NMR Spectroscopy of Rat Brain at 1 ms Echo Time. *Magn. Reson. Med.* 41, 649–656.

Vanhamme, L., van den Boogaart A, Van Huffel S, 1997. Improved method for accurate and efficient quantification of MRS data with use of prior knowledge. *J. Magn. Reson.* 129, 35–43.

Van Hoesen, G.W., Hyman, B.T., Damasio, A.R., 1991. Entorhinal cortex pathology in Alzheimer's disease. *Hippocampus* 1, 1–8.

- Watanabe, M., Liao, J.H., Jara, H., Sakai, O., 2013. Multispectral quantitative MR imaging of the human brain: lifetime age-related effects. *Radiographics* 33, 1305–1319.
- Wickens, M.M., Bangasser, D.A., Briand, L.A., 2018. Sex Differences in Psychiatric Disease: A Focus on the Glutamate System. *Front. Mol. Neurosci.* 11, 197.
- Yin, F., Sancheti, H., Patil, I., Cadenas, E., 2016. Energy metabolism and inflammation in brain aging and Alzheimer's disease. *Free Radic. Biol. Med.* 100, 108–122.
- Yin, F., Yao, J., Sancheti, H., Feng, T., Melcangi, R.C., Morgan, T.E., Finch, C.E., Pike, C.J., Mack, W.J., Cadenas, E., Brinton, R.D., 2015. The perimenopausal aging transition in the female rat brain: decline in bioenergetic systems and synaptic plasticity. *Neurobiol. Aging* 36, 2282–2295.
- Zahr, N.M., Mayer, D., Rohlfing, T., Chanraud, S., Gu, M., Sullivan, E.V., Pfefferbaum, A., 2013. In vivo glutamate measured with magnetic resonance spectroscopy: behavioral correlates in aging. *Neurobiol. Aging* 34, 1265–1276.
- Zhang, X., Liu, H., Wu, J., Zhang, X., Liu, M., Wang, Y., 2009. Metabonomic alterations in hippocampus, temporal and prefrontal cortex with age in rats. *Neurochem. Int.* 54, 481–487.

CHAPTER 4: LONGITUDINAL CHARACTERIZATION OF NEUROANATOMICAL CHANGES IN THE FISCHER 344 RAT BRAIN DURING NORMAL AGING AND BETWEEN SEXES

4.1 Preface

The work presented in **Chapter 4** represents the first longitudinal exploration of age-related change in neuroanatomy in a mixed-sex cohort of Fischer 344 rats. This publication examines change with age at both the voxel-wise and regional level in 120 brain volumes, capturing structural abnormalities across the whole-brain. Additionally, prior to this study, characterizing the influence of sex on neuroanatomy in the context of aging had not been performed in any rat model.

Similar to the rationale for **Chapter 3**, this study was primarily motivated by the dearth of literature on structural change in the rodent brain from adulthood to senescence. An understanding of the neuroanatomical changes associated with normal aging is necessary before examining compound change due to the presence of both pathology and age, particularly given the frequency with which brain volume measurements are used to support clinical diagnosis of AD in humans.

This publication sought to characterize age- and sex-related changes in neuroanatomy in the Fischer 344 rat. MRI scans of the entire brain were obtained on a 7T preclinical Bruker system at 4, 10, 16, and 20 months in male and female Fischer 344 rats. The volume of 120 regions was estimated and their longitudinal trajectories were compared between male and female rats. This manuscript provides support for the use of MRI to detect volumetric change with age and between sexes, as well as the use of rodent aging studies for developing homologous biomarkers across species.

Longitudinal characterization of neuroanatomical changes in the Fischer 344 rat brain during normal aging and between sexes

Caitlin Fowler^{*a,b}, Dana Goerzen^{*b}, Dan Madularu^{b,c,d}, Gabriel A. Devenyi^{b,d}, M. Mallar Chakravarty^{a,b,d}, Jamie Near^{a,b,d}

- ^a Department of Biological and Biomedical Engineering, McGill University, Montreal, Canada.
- ^b Centre d'Imagerie Cérébrale, Douglas Mental Health University Institute, Montreal, Canada.
- ^c Center for Translational NeuroImaging, Northeastern University, Boston, MA, USA.
- ^d Department of Psychiatry, McGill University, Montreal, Canada.

Published: <https://doi.org/10.1016/j.neurobiolaging.2021.10.003>

4.2 Manuscript Information

Funding Sources: This research was supported by the Canadian Institutes of Health Research (PJT-148751) and the Fonds de la Recherche en Santé du Québec (Chercheur boursiers # 0000035275). C.F.F. is supported in part by funding provided by McGill University's Faculty of Medicine Internal Studentship.

Acknowledgements: Myself (Caitlin Fowler) and Dana Goerzen are co-first authors on this paper. Dana Goerzen hereby acknowledges that I, Caitlin Fowler, will be using this manuscript in my doctoral thesis, and that he cannot use it in his own graduate thesis.

Caitlin Fowler: Signature _____ Date 2021-12-09 _____

Dana Goerzen: Signature  _____ Date 2021-12-09 _____

Disclosure statement: The authors disclose no conflicts of interest.

4.3 Abstract

Animal models are widely used to study the pathophysiology of disease and to evaluate the efficacy of novel interventions, crucial steps towards improving disease outcomes in humans. The Fischer 344 (F344) wildtype rat is a common experimental background strain for transgenic models of disease and is one of the most frequently used models in aging research. Despite frequency of use, characterization of age-related neuroanatomical change has not been performed in the F344 rat. To this end, we present a comprehensive longitudinal examination of morphometric change in 73 brain regions and at a voxel-wise level during normative aging *in vivo* in a mixed-sex cohort of F344 rats. We identified the greatest vulnerability to aging within the cortex, caudoputamen, hindbrain, and internal capsule, while the influence of sex was strongest in the caudoputamen, hippocampus, nucleus accumbens, and thalamus, many of which are implicated in memory and motor control circuits frequently affected by aging and neurodegenerative disease. These findings provide a baseline for neuroanatomical changes associated with aging in male and female F344 rats, to which data from transgenic models or other background strains can be compared.

4.4 Introduction

Aging is the predominant risk factor for the majority of diseases that reduce quality of life and shorten the lifespan, such as neurodegenerative diseases (Hou et al. 2019; Franceschi et al. 2018). Aging and age-related pathologies such as Alzheimer's disease (AD) share many basic molecular and cellular processes including mitochondrial dysfunction, oxidative stress, cellular senescence, and inflammation, to which the brain is particularly susceptible (Franceschi et al. 2018; Farooqui and Farooqui 2009). Given these and other similarities, disentangling pathology from normal aging can be challenging, particularly in the early phases of disease when features such as cognitive impairment may be subclinical.

Preclinical studies in animal models represent an important step towards improving disease outcomes in humans. Importantly, studying aging in wildtype rodents provides a means of separating age-related changes from those arising due to pathology, given that disease phenotypes in rodents are generally introduced by means of transgene insertion or genetic knockout. A commonly used background strain for the development of transgenic lines is the Fischer 344 (F344) rat, which was recently used to generate a rat model of Alzheimer's disease that spontaneously

develops tau pathology (Cohen et al. 2013). The F344 rat is also one of the most frequently used strains for aging research (Gallagher, Stocker, and Koh 2011). Age-related changes in recognition and spatial memory (Marrone, Satvat, and Patel 2018; Guidi et al. 2014), hippocampal neurogenesis (G. A. Shetty, Hattiangady, and Shetty 2013) and inflammatory response (Mawhinney et al. 2011), and brain tissue metabolism (Harris et al. 2014; Fowler et al. 2020) have all previously been explored in the F344 rat. However, characterization of age-related change in brain structure in this rat strain has yet to be performed.

Brain volume measurements obtained through magnetic resonance imaging (MRI) techniques have been widely used to study aging in humans (for reviews, see (Fjell and Walhovd 2010; Hedman et al. 2012; Raz et al. 2005)), with somewhat fewer studies in rodents to date (Maheswaran et al. 2009; Driscoll et al. 2006; Gaser et al. 2012). The non-invasive nature of MRI makes it a unique tool for detecting and monitoring altered brain structure *in vivo*. Additionally, recent advances in MRI co-registration techniques have permitted the development of several widely used processing and analysis pipelines (Friedel et al. 2014; Tustison et al. 2014; Jenkinson et al. 2012) for longitudinal quantification of neuroanatomical change, with demonstrated success in preclinical studies (Rollins et al. 2019; Kong et al. 2018). All of these features, in combination with the significantly shorter lifespan of rodents compared to humans (approximately 21-26 months for the F344 rat (Chesky and Rockstein 1976)), provide a convenient and powerful means to study longitudinal neurobiological changes associated with normal aging across the lifespan.

Previous aging studies examining neuroanatomy in wildtype rodents are limited in number and inconsistent in how data are analyzed, with most studies reporting change in absolute brain volumes with age (von Kienlin et al. 2005; Oberg et al. 2008; Gaser et al. 2012; Hamezah et al. 2017; Casas et al. 2018) and only a few reporting change in relative brain volumes (accounting for total brain volume or intracranial volume), either at a regional level (Maheswaran et al. 2009; Driscoll et al. 2006) or at the level of individual voxels (Alexander et al. 2020). Furthermore, many of these studies are cross-sectional in nature or conducted in a single sex, reducing power and applicability. Additional studies are needed to establish the baseline for normal neuroanatomical change with age in the rodent brain *in vivo*, a necessary step towards understanding structural alterations in the context of pathology using transgenic models.

Studies that examine the influence of sex on brain changes during normal aging are an equally important part of establishing a baseline to which pathology-related neuroanatomical

change can be compared. Significant differences between sexes exist regarding the risk for, and presentation and treatment of, age-related neurodegenerative diseases due to the underlying influence of sex chromosomes and hormones at the structural, functional, and biochemical level of the brain (Mazure and Swendsen 2016; Cosgrove, Mazure, and Staley 2007). Previous studies on the influence of sex on neuroanatomy have been performed cross-sectionally (Spring, Lerch, and Henkelman 2007) or relatively early in the lifespan (Qiu et al. 2018; Sumiyoshi, Nonaka, and Kawashima 2017; Kong et al. 2018; Corre et al. 2016), but to our knowledge, preclinical MRI studies examining the interaction between sex and age on neuroanatomy late into the lifespan do not currently exist. To this end, the present study describes a longitudinal analysis of brain morphometric change in both male and female F344 rats over the majority of the lifespan. *In vivo* morphometric changes are reported both at the voxelwise level, and at the regional level in 73 unique brain regions. This work provides new insight into neuroanatomical trajectories associated with normal aging.

4.5 Methods

4.5.1 Animals and study design

Homozygous Fischer 344/NHsd wildtype (WT) male and female rats were obtained from Envigo Laboratories (Madison, WI, United States; order code: 010) and bred within the Animal Care Facility at the Douglas Hospital Research Centre. Rats were weaned on postnatal day 21 and housed in pairs on a 12 hour light-dark cycle with *ad libitum* access to food and water. Both male and female experimenters handled and tested the rats, while animal staff caring for the rats were primarily female. All animal procedures and experiments were performed in accordance with the guidelines of the McGill University Animal Care Committee and the Douglas Hospital Research Centre Animal Care Committee.

MRI scans were acquired longitudinally at 4-, 10-, 16-, and 20-months of age, covering the majority of the adult rat lifespan. A total of 27 rats, (12M, 15F), were included in the study. 9 of 27 rats were scanned at only 4- and 10-months due to participation in a separate treatment study thereafter, leaving 18 rats (7M, 11F) to be studied at all four time points. Of these 18, 1 female died prior to the 16-month time point, and 4 males died prior to the 20-month time point. Finally, one male and one female scan at 10-months and two female scans at 16-months were discarded after

failing quality control. As such, the final number of scans for the four time points were 27 (12M, 15F), 25 (11M, 14F), 14 (7M, 7F), and 11 (3M, 8F), respectively, for a total of 77 scans (**Supplementary Table 4.12.1**). A linear mixed effects model (LME) was used to handle the imbalance in the number of scans per time point, as LMEs appropriately handle missing values in longitudinal analyses (Bernal-Rusiel et al. 2013).

4.5.2 MRI data acquisition

MRI data were acquired by C.F.F and D.M. at the Douglas Centre d'Imagerie Cérébrale using a 7 Tesla Bruker Biospec 70/30 scanner (Bruker, Billerica, MA, United States) with an 86 mm (diameter) volumetric birdcage coil for transmission and a four-channel surface array coil for signal reception (Bruker). The level of anesthesia (1-4% isoflurane in oxygen gas) was adjusted to maintain a breathing rate between 50-70 breaths per minute throughout the procedure and warm air (37 °C) was blown into the bore of the scanner to maintain a constant body temperature (SA Instruments, Inc., monitoring system, Stony Brook, NY, United States).

High-resolution 3D anatomical MR images were acquired using Rapid Acquisition with Relaxation Enhancement (RARE) using the following scan parameters: TR = 325 ms, echo spacing = 10.8 ms, RARE factor = 6, effective echo time = 32.4 ms, Field of View = 20.6 × 17.9 × 29.3 mm, matrix size = 256 × 180 × 157, slice thickness = 17.9 mm (along the dorsal/ventral direction), readout along the rostral/caudal direction, spatial resolution = 114 μm isotropic, 19m35s acquisition time. Following the scan, animals were allowed to recover from anesthesia and returned to group housing.

4.5.3 MRI pre-processing and registration pipelines

All images were processed in MINC 2.0 format. Preprocessing was performed using minc-toolkit-v2 (Vincent et al. 2016) and the MINC toolkit extras package (<https://github.com/CoBrALab/minc-toolkit-extras>), and the two-level model build Pydpipe module (Friedel et al. 2014) was used to co-register the pre-processed images into a common space. First, an in-house rat MRI preprocessing script within the minc-toolkit-extras package developed by G.A.D. (https://github.com/CoBrALab/minc-toolkit-extras/blob/master/rat-pre_processing-v3.sh) was used to perform the following sequential preprocessing steps: dimension reordering to

standard MINC 2.0 ordering, image centring, whole image N4 bias field correction (Sled and Pike 1998; Tustison et al. 2010), individual foreground mask generation using the Otsu method (Otsu 1979), additional N4 bias field correction using the previously generated mask, affine registration to a Fischer 344 template average image, and a final N4 bias field correction using a template mask in native space. After pre-processing, images were quality controlled by D.G. Images were visualised using the Display program in minc-toolkit-v2 and examined in each of the coronal, sagittal, and axial dimensions for motion artefacts, Gibbs ringing artefacts, proper bias field correction, and other image anomalies. Of the 81 scans acquired, four scans were flagged and excluded from further analysis. Additional details on the QC process are described in the **Supplementary Methods 4.11.2**. A diagram of the pre-processing steps and examples of excluded scans are shown in **Supplementary Figure 4.13.1**.

The remaining 77 scans which passed quality control were then co-registered using the two-level model build pipeline in Pydipper (Friedel et al. 2014). In brief, subject-specific starting averages are created by rigidly registering scans at different time points to the Fischer 344 atlas template, followed by averaging. Iterative affine and non-linear registration and averaging is then repeated to produce an unbiased subject average. Subsequently, each subject specific average is rigidly aligned to the Fischer 344 atlas template space and the process is repeated to create an unbiased population average. This process creates deformation fields for each subject at each time point. The deformation fields can then be used to estimate the Jacobian determinant at each voxel, which reflects the amount of expansion or compression required to deform each individual anatomical image to the subject average (Chung et al. 2001). Deformation fields are then resampled into the common study space allowing comparison between subjects. This registration process generates two sets of Jacobian determinants which were used for subsequent structural analysis. The absolute Jacobian, composed of the sum of the linear plus the non-linear mappings, reflects the global changes in voxel volume. The relative Jacobian, composed of the non-linear mapping with residual affine components estimated and removed, reflects local, or relative changes in voxel volume. The Jacobian deformation fields were then blurred with a 400 micron full width half maximum Gaussian kernel to satisfy assumptions of normality required by the statistical models used to analyze the data.

4.5.4 Regional volume estimation

Using a Fischer 344 rat atlas generated from a 4-month cohort of wildtype Fischer 344 rats (Goerzen et al. 2020) resampled into the study common space, the volumes of 73 unique regions (120 when split across hemispheres, e.g. left and right Caudoputamen) were estimated using the *anatGetAll* function in RMINC_1.5.2.3 (J. Lerch et al. 2017). This function computes the volume of a region by counting the number of voxels with a given label and multiplying the Jacobian with the voxel volume at each voxel. Absolute and brain-size-corrected volumes (mm^3) were generated from the absolute and relative Jacobians, respectively. Of the 120 delineated regions, 76 were classified as GM, 40 as WM, and 4 as CSF. Volumes aggregated within tissue types (grey matter, GM; white matter, WM; cerebrospinal-fluid-filled volumes, CSF) were also calculated to provide an overview of tissue-specific changes across the brain.

4.5.5 Statistical Analysis

Longitudinal changes in a) relative Jacobians at each voxel within the brain, b) absolute and c) brain-size corrected volumes for 73 regions, and d) volumes aggregated within tissue types, were modelled using linear mixed-effects (LME) modeling in R. (version 3.6.3 (R Core Team 2020); attached base packages: stats, graphics, grDevices, utils, datasets, methods, base; other attached packages: effects_4.4-4 (Fox and Weisberg 2019), RColorBrewer_1.1-2 (Neuwirth 2014), readxl_1.3.1 (Wickham and Bryan 2019), lmerTest_3.1-0 (Kuznetsova, Brockhoff, and Christensen 2017), lme4_1.1-23 (Bates et al. 2015), tidyverse_1.3.0 (Wickham et al. 2019), RMINC_1.5.2.3). LME models were used as they appropriately model the covariance structure resulting from repeated measurements in the same subjects and handle data with missing values (Bernal-Rusiel et al. 2013). In the mixed effects model, volumes were predicted by an age by sex interaction with a random intercept for each subject. A random slope for each subject was initially included but the model failed to converge. Age was modelled using a quadratic function ($\text{poly}(\text{age}, 2)$) to account for the possibility of non-linear changes with age, as has previously been demonstrated (Pfefferbaum et al. 2013; Kong et al. 2018; Tullo et al. 2019). To further justify this choice, Akaike information criterion (AIC; (Akaike, Petrov, and Csaki 1973)) was used to test if volume and voxelwise data were better fit using a linear or quadratic age term, using a Δ_i ($\text{AIC}_i - \text{AIC}_{\min}$) threshold of 4, where AIC_{\min} is the minimum of the R (number of models being compared) different

AIC_i values (the minimum is at $i=\min$) (Burnham and Anderson 2004). The larger the Δ_i , the less likely the fitted model i is the best approximating model. Of 120 structures, 65 were best fit by a quadratic model, with 39 of those 65 reaching the Δ_i threshold of 4, indicating substantially less support for the model containing solely linear age term (**Supplementary Table 4.12.2**). Similarly, the majority of voxels demonstrated better fits using a quadratic age term. Thus, for consistency and comparability, all structures and voxelwise data were modelled using a quadratic age term.

The linear and quadratic components of the age term are henceforth abbreviated as poly(age,2)1 and poly(age,2)2, respectively. Main effects of sex (sexF) were evaluated as a group effect of females relative to males, while the interaction between age and sex (poly(age,2)1:sexF and poly(age,2)2:sexF) was also examined, again with males as the reference group. All continuous variables were z-scored so that coefficients (betas (β), or effect sizes) for each fixed effect would be standardized. As such, the standard betas indicate the number of standard deviations a regional volume has changed per standard deviation increase in the predictor variable. The False Discovery Rate (FDR) method (Benjamini and Hochberg 1995) was used to control the family-wise type I error at a level of 5% for each predictor. A fixed effect was considered significant when the FDR-corrected p-value (adjusted p-value or p-adjusted) was < 0.05 .

4.6 Results

4.6.1 Absolute volumes increase with age and are larger in male Fischer rats

Linear mixed effects model results for absolute volumes aggregated within GM and WM tissues, as well as ventricular compartments containing CSF are visualized in **Figure 4.10.1A** and a full LME summary is shown in **Supplementary Table 4.12.3**. Briefly, aggregated absolute volumes all increased and demonstrated negative curvilinear relationships (downward-facing curve) with age, were smaller in females, and demonstrated a negative linear age by sex interaction whereby volumes increased more sharply with age in males than females.

These highly consistent effects across tissue types remained when absolute volumes were decomposed into the individual structures within the Fischer 344 rat brain atlas. All 120 structures increased with linear age, 72 of 120 demonstrated a significant positive quadratic relationship with age (upward-facing curve), and 119 of 120 structures were larger in males. 85 of 120 structures demonstrated a significant negative linear age by sex interaction and 14 of 120 structures

demonstrated significant positive quadratic age by sex interaction, increasing more with age in males than females. LME results and absolute volumes in mm³ for all structures can be found in **Supplementary Tables 4.12.3 and 4.12.4**, respectively.

4.6.2 Brain-size-corrected volumes show heterogeneous change with age and occur in regions implicated in motor control, learning, and memory

As shown in **Figure 4.10.1B** and **Supplementary Table 4.12.5**, aggregated brain-size-corrected volumes demonstrated different age-related effects depending on tissue type: total GM volume decreased significantly and demonstrated a positive curvilinear relationship with age, while total WM volume increased sharply with linear age, and CSF volume increased subtly with linear age.

Aggregated volumes were then decomposed into the individual structures delineated by the Fischer 344 atlas. Whole-brain age- and sex-related changes were visualized using the *mincPlotSliceSeries* function in RMINC, wherein t-statistic heatmaps were created for each term in the LME model and overlaid on the average anatomy background (**Figure 4.10.2**). LME results for selected structures, chosen for the strength of their effects or relevance of the brain region in aging and neurodegeneration (basal forebrain, caudoputamen, cingulum, commissure of the inferior colliculus, frontal cortex, dentate gyrus, hippocampus, internal capsule, nucleus accumbens, periaqueductal grey, and thalamus), are shown in **Table 4.9.1**. Visualization of the longitudinal trajectories for these selected structures, split by sex, was performed using the effects package in R (version 4.2-0, (Fox and Weisberg 2019)) and is shown in **Figure 4.10.3**. For simplicity and since effects were highly consistent across hemispheres, for structures that exist within both hemispheres, such as the hippocampus, only the trajectory within the right hemisphere is shown. LME results are included in **Supplementary Table 4.12.5** and volumetric trajectory visualization for all 120 structures are shown **Supplementary Figures 4.13.2 to 4.13.9**.

GM structures showed a nearly even split of increased versus decreased volumes with age, while WM and ventricular system volumes generally increased with age. Specifically, of the 76 GM volumes analyzed, 20 regions increased linearly with age, while 24 decreased. 15 of 76 GM structures demonstrated a significant positive curvilinear relationship with age while 4 structures demonstrated a negative curvilinear relationship. Of the 40 WM volumes analyzed, 20 increased and 3 decreased linearly with age, while 4 of 40 regions demonstrated a negative curvilinear

relationship with age. Of the 4 volumes that were categorized as part of the ventricular system, only the aqueduct and fourth ventricle increased significantly with age. Additionally, GM structures comprised the vast majority of the strongest age-related changes overall. Upon ranking the structures by adjusted p-value within the linear and quadratic age terms, of the top 20 strongest linear changes with age, 14 were in GM structures. For curvilinear changes the top 20 comprised 15 GM, 4 WM, and 1 CSF region(s). All structures ranked by adjusted p-value within each model term are shown in **Supplementary Table 4.12.6**.

The strongest linear changes with age in GM structures were decreases in the temporal-parietal cortex, caudoputamen, and frontal cortex, and increases in the hindbrain and substantia nigra. In WM, the strongest linear changes with age were identified in the internal capsule, cerebral peduncle, and fimbria, all of which increased in volume. Age-related changes in CSF volumes were limited to the aqueduct and fourth ventricle, both of which increased.

Regarding curvilinearity, the strongest effects in GM structures were positive curvilinear changes in the frontal cortex and caudoputamen, and a negative curvilinear relationship between age and volume in the hindbrain. Curvilinear effects in WM structures were less common and were only significant in the optic chiasm, right optic tract, right fasciculus retroflexus, and left olfactory tract, all of which were negative. Significant curvilinearity with age was not present in ventricular system volumes. All linear model results are shown in **Supplementary Table 4.12.5**, with results for each model term ranked by adjusted p-value in **Supplementary Table 4.12.6**.

4.6.3 The influence of sex on neuroanatomy is strongest in grey matter structures

Of the brain-size-corrected volumes aggregated across tissue type, only total GM demonstrated significant sex-related effects with larger volume in females, as shown in **Figure 4.10.1B** and **Supplementary Table 4.12.5**. None of total GM, WM, or CSF volumes demonstrated age by sex interactions. Upon examination of 120 regional volumes (split across hemispheres), GM structures comprised the majority of the sex effects identified in aging Fischer rats. 31 of 76 GM volumes showed significant effects of sex, with 23 of 31 being larger in females. 13 of 40 WM volumes had significant sex effects, with 9 of 13 being larger in females. Additionally, of the top 20 smallest (most significant) adjusted p-values, 13 were in GM structures and 7 in WM structures (regions ranked by adjusted p-values shown in **Supplementary Table 4.12.6**). The strongest main effects of sex in GM structures were in the caudoputamen, thalamus, periaqueductal grey, and basal

forebrain, all of which were larger in females. The most significant main effects of sex in WM structures were larger optic chiasm volume and smaller commissure of the inferior colliculus volume in females relative to males.

Age by sex effects were present in grey and white matter volumes but not the ventricular system, and were generally observed bilaterally; 14 of 76 GM structures and 8 of 40 WM structures demonstrated linear age by sex interactions, with a positive interaction occurring in 8 of 14 GM regions, and 6 of 8 WM regions, reflecting increasing volume in females relative to males as a function of age. A second order age by sex interaction was present for 8 of 76 GM regions and 3 of 40 WM regions; this interaction was negative for 7 of 8 GM regions, reflecting a more negative curvilinear relationship with age in females than in males, while all 3 WM regions showed a positive curvilinear relationship with age.

The linear interaction between age and sex in GM structures was strongest in the crus 2 ansiform lobule and cerebellar lobule 7, which were smaller over time in females, and the hippocampus and olfactory nuclei which were larger over time in females. In WM structures a linear age by sex interaction was present in fewer structures and included the left lateral olfactory tract and commissure of the inferior colliculus, which were smaller over time in females, and the optic chiasm, intrabulbar part of the anterior commissure, and optic tract, which were larger over time in females. Second order age by sex interactions in GM structures were strongest in the caudoputamen, right hippocampus (the left hippocampus neared significance), and left frontal cortex, all of which demonstrated negative curvilinear relationships with age. In WM structures the only significant quadratic age by sex interactions were in the left cingulum, optic chiasm, and right lateral olfactory tract, all of which were positive. Linear model results for all structures are included in **Supplementary Table 4.12.5**, with results ranked by adjusted p-value in **Supplementary Table 4.12.6**.

4.6.4 Whole-brain voxel-wise and volumetric analyses provide complementary results

In conjunction with the volumetric analyses described above, a whole-brain voxel-wise analysis was performed to assess changes at the voxel level. Whole-brain age- and sex-related voxelwise changes were visualized using the *mincPlotSliceSeries* function in RMINC, wherein t-statistic heatmaps of LME modeling results at each voxel were overlaid on the average anatomy

background, split by model term (**Figure 4.10.4**). Side-by-side comparisons of volumetric and voxel-wise results are shown in **Supplementary Figures 4.13.10 and 4.13.11**. Overall, voxel-wise results correspond well with those identified using volumetric analyses. However, the volumetric analysis—whereby the relative Jacobians shown in the voxel-wise data were integrated across each structure in the Fischer atlas—identified changes not visible at the individual voxel level, and similarly, several focal changes exist that were not visible at the whole-structure level.

For example, the voxel-wise analysis identified both significant focal increases and decreases with linear age within cerebellar lobule 4 and 5. These changes were offset when summing the volume over the whole region, resulting in a lack of linear age effect in the volumetric analysis. When examining second order effects of age, the most noticeable contrast between the two methods was throughout the cortex whereby only the volumetric analysis identified significant positive curvilinear effects in cortical volumes with age. Voxel-wise analysis identified significant sex-related increases in the posterior cerebellar lobule 3, and decreases in the anterior cerebellar lobule 3, resulting in a lack of overall effect of sex at the level of the whole structure. Regarding linear age by sex interactions, there were positive bilateral effects in the hippocampal formations that were not strongly reflected at a voxel-wise level, whereas conversely, focal changes within the medial hindbrain appeared to drive the strong positive interaction in the hindbrain identified in the regional analysis. Finally, upon examining the interaction of curvilinear age and sex identified by each method, there were bilateral decreases in the caudoputamen at a volumetric level which were not reflected at a voxel-wise level.

4.7 Discussion

The purpose of this study was to characterize brain volumetric changes and whole-brain voxelwise changes in a commonly used rat model of aging (Gallagher, Stocker, and Koh 2011). This work establishes a baseline for normative neuroanatomical change with age in the rat brain, and informs studies examining pathology-related change in transgenic models developed on the Fischer 344 background strain. It is particularly important to study both sexes in this context, given the progression and presentation of many age-related diseases, such as Alzheimer's disease, are influenced by sex. Our study is among the few aging studies to assess structural change longitudinally as opposed to cross-sectional or *ex-vivo* study designs, allowing for exploration of

non-linear effects, providing increased power to detect small differences in neuroanatomy, and increasing preclinical to clinical translatability.

119 of 120 absolute volumes increased linearly with age, with 72 of 120 structures also demonstrating a positive curvilinear relationship with age. These trends were also seen in the total aggregated volumes for GM, WM, and CSF. This consistent volumetric increase with age matches the few studies that have tracked absolute change in regional and/or total brain volume with age in wildtype rodents (Casas et al. 2018; Gaser et al. 2012; Maheswaran et al. 2009). Our finding that 119 of 120 absolute brain volumes were larger in males can be explained by the documented relationship between brain size and body size (Welniak-Kaminska et al. 2019; Valdés-Hernández et al. 2011), and matches previous studies comparing absolute volumes between males and females at various periods during the lifespan in rodents (Sumiyoshi, Nonaka, and Kawashima 2017; Qiu et al. 2018; Spring, Lerch, and Henkelman 2007; Reichel et al. 2017), and in humans (Scahill et al. 2003; Walhovd et al. 2005; Jay N. Giedd et al. 2012). Interestingly, this progressive increase in brain volume throughout the Fischer rat lifespan is in contrast to that in humans, which plateaus in the mid-teens and then declines later in life (J. N. Giedd et al. 1999). The difference between rodent and human brain growth is generally hypothesized to be facilitated by the delay in growth plate closure in rodents, permitting continuous expansion of brain volume (Sandner et al. 2010; Kilborn, Trudel, and Uthoff 2002).

The analysis of brain-size-corrected volumes offers a much more interesting and relevant perspective on how the brain is altered locally during normal aging and between sexes. The majority of other studies examining relative volumetric change do so by normalizing (dividing) regional volumes to intracranial volume (ICV) or total brain volume (TBV). We employed an alternative method to explore volumetric change that avoids the inherent alteration of the distribution of variance, as well as the increase in measurement uncertainty that occurs when error propagation is performed, as is necessary when dividing a regional volume by ICV or TBV. Our corrected volumes were obtained by integrating relative Jacobians across voxels within a given structure, thus providing a value representative of local regional change independent of affine scaling factors for global brain volume, while avoiding violating assumptions regarding the distribution and variance incurred by computing a ratio of total volume.

The age-related changes in total GM, WM, and CSF volumes in the Fischer rat brain that we report are generally consistent with the few existing aging studies in rodents that examine

relative volumetric change. Total CSF compartmental volume increased with age, as has previously been documented in both rodents (Maheswaran et al. 2009; von Kienlin et al. 2005) and humans, particularly in the lateral ventricles (Fjell et al. 2009; Scahill et al. 2003; Driscoll et al. 2009; Walhovd et al. 2005; Narvacan et al. 2017). Regionally, only the aqueduct and fourth ventricle increased significantly with age, indicating the majority of ventricular enlargement occurred in the more caudal parts of the Fischer 344 rat brain.

Total WM volume increased linearly in aging Fischer 344 rats. The strongest linear changes with age were identified in the internal capsule, cerebral peduncle, and fimbria, all of which increased. These structures are spatially distributed across the brain and are implicated in a number of physiological functions, including motor function (internal capsule, (Wen et al. 2019), episodic and spatial memory formation (fimbria, (Aggleton and Brown 1999; Okada and Okaichi 2006)), and transmission of visual information (optic tract, (Mehra and Moshirfar 2020)). In humans, WM volume appears to increase until approximately age 45 and then plateaus and decreases (Hedman et al. 2012; Walhovd et al. 2005; Pfefferbaum et al. 2013), in opposition to our finding that total WM increased consistently with age. Unfortunately our ability to understand this discrepancy is limited by the lack of volumetric analyses of the majority of white matter regions, particularly at the preclinical level. One longitudinal study in C57BL6 mice demonstrated significant age-related volumetric increases in the corpus callosum, corticospinal tract, and the fornix system up until 14 months of age but did not perform scans later into the lifespan (Maheswaran et al. 2009). Additional longitudinal studies in rodents that extend late into their lifespan and that document both whole-brain and regional tissue-specific change are clearly needed to characterize age-related change in WM volumes, and to better understand differences in WM changes between aging rodents and humans.

Total GM volume decreased in aging Fischer 344 rats, and also demonstrated a positive curvilinear relationship with age, similar to the linear and curvilinear decreases in GM volume in humans post-adolescence that have been consistently shown in human aging studies (Hedman et al. 2012; Hasan et al. 2010; Walhovd et al. 2005; Narvacan et al. 2017; Pfefferbaum et al. 2013). Our age-related findings within specific GM structures closely match those reported by other authors at the preclinical and clinical level. The longitudinal study in male C57BL6 mice by Maheswaran et al. that reported slight, non-significant decreases in the cortex, hippocampus, caudoputamen, and thalamus, and increases in the midbrain-hindbrain and hypothalamus ((Maheswaran et al. 2009).

The increases they identified in the midbrain-hindbrain and hypothalamus of aging C57BL6 mice are similar to those seen in our Fischer rats, while the non-significant decreases they report were significant in our study, possibly because we explored changes 6 months later into the lifespan. Another comparable study is a cross-sectional voxel-wise study in Fischer rats at 10 and 25 months that revealed an increase in select hippocampal regions which appeared to be primarily within the dentate gyrus (Alexander et al. 2020). While this is comparable to our findings, it is at odds with an early study in Fischer rats (A. K. Shetty and Turner 1999), and the majority of human aging literature (Small et al. 2004; Dillon et al. 2017; Hayek et al. 2020; Wisse et al. 2014; Malykhin et al. 2017). Given the sparsity of literature on relative volumetric change with age in the rodent brain, additional studies are required to improve the interpretation of our findings.

Although several of our findings have not yet been reported in preclinical literature, there are some similarities compared to human aging literature. Aging studies in humans have identified highly heterogeneous age-related change across the brain, including atrophy in many subcortical gray matter structures, including the thalamus, nucleus accumbens, caudate, and putamen, (Long et al. 2012; Walhovd et al. 2005; Narvacan et al. 2017; Tullo et al. 2019), and decreased cerebellar volume (Bernard and Seidler 2013; Han et al. 2020), all of which we also report in our aging Fischer rats. Hypertrophy of the substantia nigra (Cabello et al. 2002; Rudow et al. 2008), and either stable or increased hippocampal volume until mid-life followed by a sharp decline have also been reported (Narvacan et al. 2017; Malykhin et al. 2017; Raz et al. 2010; Bussy et al. 2021), again, similar to our findings. For reviews on age-related structural changes in humans see (Sowell, Thompson, and Toga 2004) and (Fjell and Walhovd 2010).

Regarding the cellular and molecular basis for altered brain structure with age, it has previously been shown that altered axonal/dendritic branching, synapse, spine, or cell numbers are sufficient to alter brain volume (J. P. Lerch et al. 2011; Qiu et al. 2013; Spring et al. 2010). The current study design did not allow us to identify these underlying mechanisms. However, experiments in aging Fischer 344 x Brown Norway hybrid rats (Driscoll et al. 2006), Wistar rats (Mortera and Herculano-Houzel 2012), and rhesus monkeys (Dumitriu et al. 2010) report that age-related brain atrophy may result from some combination of dendritic regression, neuronal death and decreased neurogenesis, similar to the loss of dendritic and synaptic density reported in human post-mortem studies (Raz and Rodrigue 2006). Additionally, we recently published a longitudinal analysis of hippocampal neurochemical concentrations in the same cohort of aging rats as studied

here (Fowler et al. 2020) where we identified altered concentrations of metabolites implicated in neuroinflammation, cell membrane turnover, bioenergetics, and antioxidant capacity, which are indicative of major changes at the cellular level during normal aging (Mattson and Arumugam 2018; McKenna et al. 2012). Given that we report age-related increases and decreases in regional volumes whereas much of the aging literature focuses only on mechanisms for neurodegeneration, future studies combining *in vivo* and *ex-vivo* techniques are needed to better characterize the cellular and molecular basis of volumetric change.

Structures influenced by sex were widespread across the Fischer rat brain and more commonly found in GM than WM structures, for both the main effect of sex and its interaction with age. In our cohort of aging Fischer rats, females displayed larger volumes in the frontal cortex, caudoputamen, thalamus, and periaqueductal grey relative to males, similar to findings by Qui et al. in young C57BL/6J mice (post-natal day 3-65, (Qiu et al. 2018), while in contrast, Spring et al. noted smaller thalamic volumes in adolescent female Wistar rats (Spring, Lerch, and Henkelman 2007). The influence of sex on hippocampal volumes in rodents is also inconsistently reported. We identified a positive linear age by sex interaction in hippocampal volume, indicating larger hippocampi in female rats relative to males across the life span, while the opposite has been reported in 6-10 week-old Wistar rats (Sumiyoshi, Nonaka, and Kawashima 2017). Given the lack of studies examining the influence of sex in relative brain volumes in rodents at ages comparable to those studied here, it is difficult to determine if discrepancies between our findings and the three aforementioned studies are due to inherent differences between mouse and rat brains, differences between strains of rats (particularly related to inbreeding versus outbreeding), or due to the younger age of the rodents studied by the other authors compared to our cohort. As such, many of our sex-related findings require additional preclinical research for confirmation, particularly as many are being reported for the first time.

There are only a few subcortical structures for which sex differences during aging have been identified in humans. For example, it has previously been reported that women have larger hippocampal volumes (Cosgrove, Mazure, and Staley 2007; Jay N. Giedd et al. 2012; Goldstein et al. 2001), while men have been shown to have steeper age-related volumetric declines (Armstrong et al. 2019), similar to our identification of larger hippocampal volume in females with atrophy occurring primarily in male rats. We also report larger thalamic volume in female Fischer rats, with atrophy occurring at a similar rate in males and females, comparable to human aging cohorts

(Ruigrok et al. 2014; Sullivan et al. 2004). For reviews see (Cosgrove, Mazure, and Staley 2007; Jay N. Giedd et al. 2012; Ruigrok et al. 2014).

The origin and subsequent impact of sex chromosomes and hormones on the brain have been studied at the cellular, molecular, structural, and behavioural level. Sex hormones influence the outgrowth of axons and dendrites, the amount of cell death, and the number and type of synapses that a cell makes (Juraska, Sisk, and DonCarlos 2013; Juraska and Lowry 2012), all of which are sufficient to alter brain volume (J. P. Lerch et al. 2011; Qiu et al. 2013; Spring et al. 2010). For reviews, see (Cooke et al. 1998; Cahill 2006; Osterlund and Hurd 2001). Previous studies have shown that in addition to hormone levels fluctuating with age, topographic distribution, binding capacity, and associated enzyme levels of sex steroid receptor systems also vary as a function of age (Sholl and Kim 1990; MacLusky et al. 1987), likely contributing to differing trajectories of aging in males and females in specific regions. Going forward, ensuring proper age and sex-matching in study design will be important as the research community works towards understanding the influences of sex on age- and pathology-related changes in brain structure. Additionally, given the effect of sex on brain volumes reported here, it will also be important to intentionally study and account for both sexes when characterizing biological outcome measures known to be associated with altered neuroanatomy. For example, changes to spatial learning and memory with age may differ between males and females as a result of differing hippocampal volume trajectories.

Finally, a whole-brain voxel-wise analysis was performed in conjunction with the volumetric analysis to explore if the two methods would provide complementary information. There were instances where the regional analysis masked finer-grained details of morphological change identified in the voxel-wise analysis, while conversely, analysis at the level of whole structures was capable of identifying changes that were only weakly present at the individual voxel level, but overall the voxel-wise and regional analyses resulted in comparable findings.

This study has a few important limitations that warrant discussion. First, due to some of the rats being part of a treatment study at 10 months and therefore not included in this analysis, the number of animals decreased considerably at the last two time points. This may have decreased our power to detect differences between sexes or change with age. To confirm the robustness of our findings, we performed the same analysis for the brain-size-corrected volumes across only three time points as opposed to four, compared side by side in **Supplementary Table 4.12.7**. The majority of age and sex effects remained in the three time point analysis, particularly the main

effects of sex. Despite some changes in significance, the direction of change (sign of beta coefficient) was unaltered for all effects. Overall, while it is clear that the last time point at 20 months is particularly important for consolidating curvilinear change, the majority of the results are consistent across the two analyses, demonstrating the robustness of our findings despite the decreased sample size towards the end of the study. The longitudinal nature of the study, the number of time points over which data were collected, and the implementation of a 5% false discovery rate correction also improve the confidence with which we report our findings.

Secondly, it should be acknowledged that inbred models such as the Fisher 344 rat do not completely recapitulate aging as it occurs in humans due to the extreme genetic homogeneity of inbred strains. While studying inbred strains reduces experimental variability and increases study reproducibility, it is necessary to consider that studies using these inbred animals do not replicate the genetic diversity in human aging studies and results may therefore not be completely representative of the aging process in humans. Strain-specific neuroanatomical features likely also exist as a result of in-breeding and may contribute to difficulty in replicating results from one strain to another. A multi-strain aging study examining both inbred and outbred strains could be of great interest to the research community.

Finally, the image resolution in this study (114 μm) prevented the delineation of very small structures and/or adjacent grey matter nuclei, such as the thalamic, cortical, and amygdalar nuclei. To address this limitation, we performed a whole-brain voxel-wise analysis to identify focal changes that may not have been identified in the volumetric analysis, which confirmed that the two methods revealed complementary information regarding neuroanatomical change, and even found some focal effects masked by regional averaging.

4.8 Conclusion

In order to better understand and address age-related pathologies in transgenic models of disease, it is necessary to first characterize the features of normal aging in common experimental background strains, such as the Fischer 344 wildtype rat. To this end, this work presents a comprehensive analysis of MRI-derived brain changes at the voxelwise and whole-structure level during normative aging in a mixed-sex cohort of F344 rats. These findings contribute to our understanding of the neuroanatomical changes associated with normal aging in male and female

F344 rats, critical for informing future studies in transgenic models of age-related diseases, which frequently present and progress differently in males versus females.

4.9 Chapter 4 Tables

Table 4.9.1 Linear mixed effects model summary for selected brain-size-corrected volumes, listed in alphabetical order.

Volumes were predicted by an age by sex interaction with a random intercept for each subject. Age was modelled using a quadratic polynomial function. The linear and quadratic components of the age term with age are written as poly(age,2)1 and poly(age,2)2, respectively. Effects of sex were evaluated in females relative to males. Betas are standardized. Bold font denotes significance after FDR-correction at 5%. L or R represent the structure in the left or right hemisphere, respectively.

Structure	poly(age,2)1		poly(age,2)2		sexF		poly(age,2)1:sexF		poly(age,2)2:sexF	
	std.beta	p-adjusted	std.beta	p.adjusted	std.beta	p.adjusted	std.beta	p.adjusted	std.beta	p.adjusted
Basal Forebrain	2.295	6.15E-02	1.753	1.68E-01	1.308	1.51E-06	-0.536	7.81E-01	0.357	8.60E-01
Caudoputamen -L	-6.885	1.11E-20	3.068	3.36E-08	1.186	4.17E-10	0.985	1.64E-01	-1.831	5.34E-03
Caudoputamen -R	-7.225	3.19E-21	3.326	3.20E-09	0.967	9.57E-07	0.731	3.13E-01	-2.067	1.17E-03
Cingulum -L	5.731	3.93E-06	-2.427	5.37E-02	-0.110	0.788	-1.267	4.76E-01	3.881	9.90E-03
Cingulum -R	6.311	1.02E-08	-1.027	3.76E-01	-0.659	5.43E-02	-2.533	5.75E-02	2.431	6.11E-02
Commissure of the Inferior Colliculus	6.208	1.44E-06	0.069	9.73E-01	1.051	1.50E-04	-5.610	4.68E-04	0.259	9.04E-01
Dentate Gyrus -L	3.180	5.70E-03	-1.755	1.41E-01	-0.836	1.27E-02	1.131	4.93E-01	1.379	3.78E-01
Dentate Gyrus -R	3.864	4.25E-04	-2.006	7.04E-02	-0.502	0.186	0.386	8.31E-01	1.663	2.48E-01
Frontal Cortex -L	-5.738	1.38E-20	3.027	1.73E-10	1.047	1.09E-07	-0.753	1.93E-01	-1.161	2.91E-02
Frontal Cortex -R	-6.022	2.90E-17	3.278	9.44E-09	0.717	7.81E-04	-0.979	1.71E-01	-1.079	1.13E-01
Hippocampus -L	-3.597	6.43E-04	0.911	4.42E-01	0.782	8.07E-02	4.769	2.79E-04	-2.512	5.27E-02
Hippocampus -R	-1.683	7.80E-02	2.238	1.43E-02	0.966	1.32E-02	2.705	2.02E-02	-2.566	2.29E-02
Internal Capsule -L	7.031	2.98E-16	-0.881	2.44E-01	0.047	0.844	0.971	3.15E-01	-0.412	7.03E-01
Internal Capsule -R	8.008	4.48E-20	-0.678	3.42E-01	0.279	0.110	-0.706	4.45E-01	-0.285	7.80E-01
Nucleus Accumbens -L	-4.996	2.04E-08	2.239	7.79E-03	1.259	8.52E-06	0.855	4.83E-01	-0.475	7.22E-01
Nucleus Accumbens -R	6.183	5.98E-11	1.202	1.73E-01	1.161	3.87E-04	2.806	7.54E-03	0.364	7.81E-01
Periaqueductal Grey	-0.518	7.27E-01	1.519	2.29E-01	1.534	7.11E-09	-2.415	1.07E-01	-1.525	3.40E-01
Thalamus -L	-2.932	6.31E-04	0.299	7.82E-01	1.390	2.45E-05	-0.861	4.82E-01	-1.287	2.53E-01
Thalamus -R	-4.227	6.84E-07	0.788	4.11E-01	1.519	4.87E-09	-0.300	8.31E-01	-0.658	6.04E-01

4.10 Chapter 4 Figures

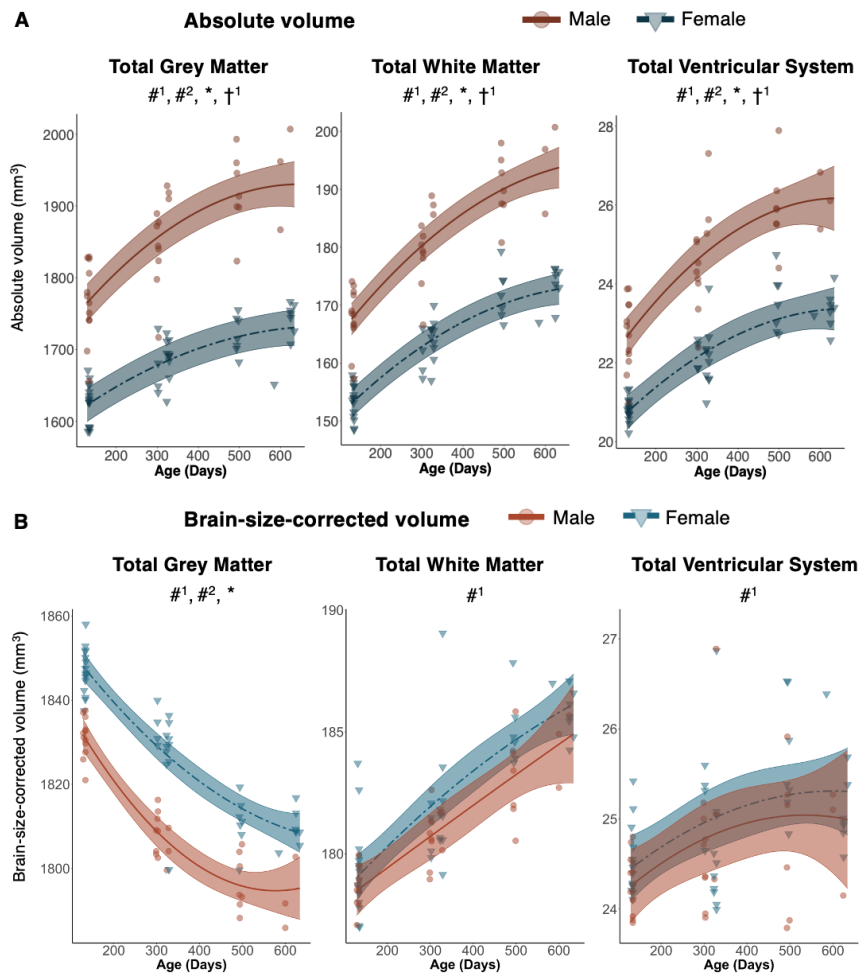


Figure 4.10.1 Absolute volumes summed across tissue type increase with age and are larger in males, while brain-size corrected volumes reveal different age and sex-dependent trends across tissue types

MRI data were acquired longitudinally in rats aged 4-, 10-, 16- and 20-months old. Main effects of age and sex, as well as age by sex interactions, were determined using linear mixed effects modelling. Each data point represents a single rat. The linear mixed effects model used to fit the data is represented by a line of best fit and 95% interval (shaded), split by sex. Data corresponding to males is shown using red circles with a solid line of best fit, while females are shown using blue triangles and a dashed line of best fit. Significance symbols are shown for each term in the model, where #¹ and #² represent the linear and quadratic age terms, * denotes a main effect of sex, and †¹ and †² represent age by sex interactions with a linear and quadratic age term, respectively. Multiple comparisons were corrected for using a 5% false discovery rate. Significance was determined by $q < 0.05$.

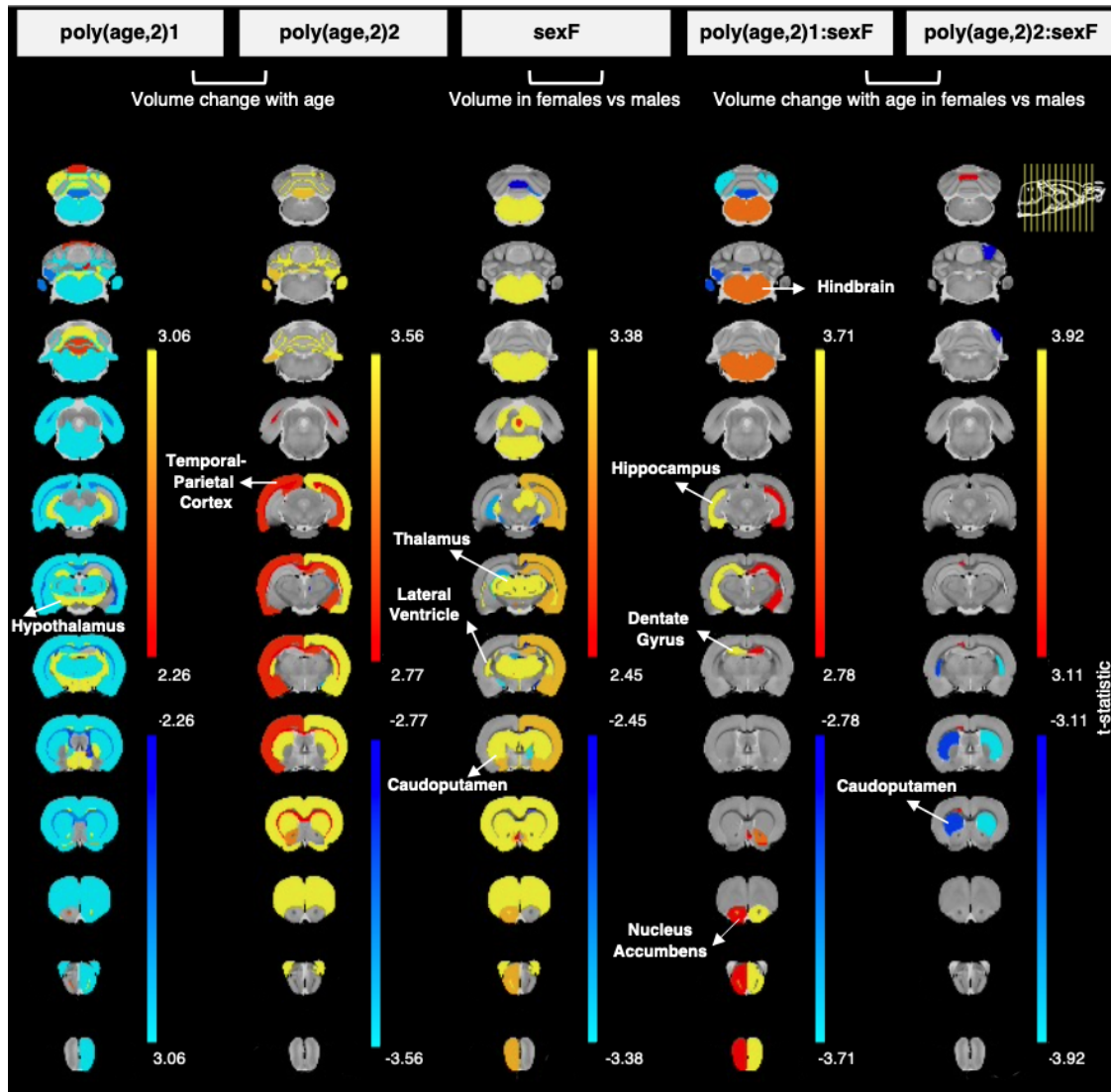


Figure 4.10.2 Visualization of age and sex effects, along with their interaction, on brain size-corrected brain volumes (LME results) in healthy aging Fischer rats, overlaid on the average anatomy background.

In the mixed effects model, volumes were each predicted by an age by sex interaction with a random intercept for each subject. Age was modelled using a quadratic polynomial function to account for the possibility of non-linear changes with age. The linear and quadratic components of age are written as $\text{poly}(\text{age},2)1$ or $\text{poly}(\text{age},2)2$, respectively. Effects of sex (sexF) were evaluated in females relative to males, and the interaction between age and sex was also examined ($\text{poly}(\text{age},2)1:\text{sexF}$ and $\text{poly}(\text{age},2)2:\text{sexF}$, with males as the reference group). Each column shows significant volume effects specific to each model term. The regional t-values for each term in the mixed effects model are indicated by the colour bars in columns 1 through 5. The plot range for each set of t-values is specific to each model term and displays effects significant between 5 and 1% FDR, with t-values above 1% thresholded at the 1% value, except for the $\text{poly}(\text{age},2)2:\text{sexF}$ column which displays values significant at 10% FDR.

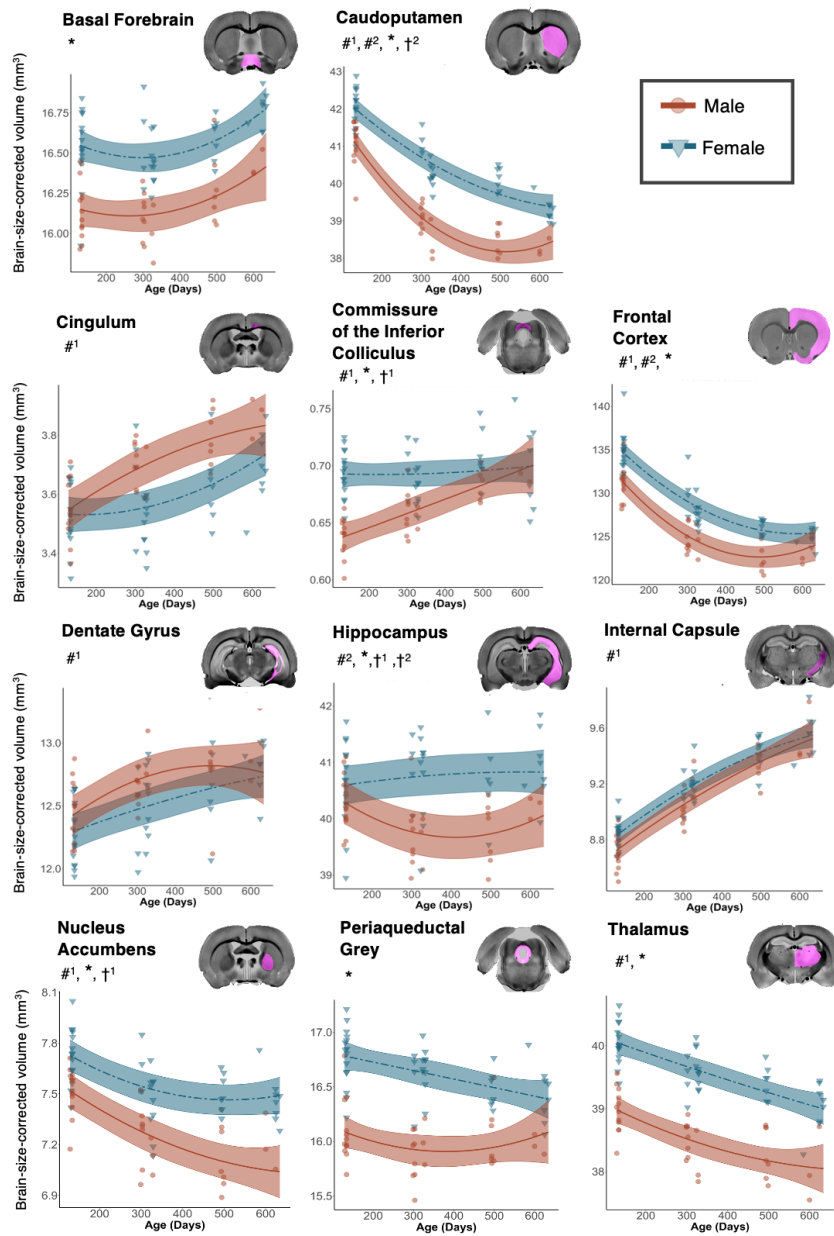


Figure 4.10.3 Prominent age and sex-dependent changes in brain-size-corrected volumes are present throughout the brain in both grey and white matter regions, suggesting a multitude of physiological functions are affected by aging

MRI data were acquired longitudinally in rats aged 4-, 10-, 16- and 20-months old. Main effects of age and sex, as well as age by sex interactions, were determined using linear mixed effects modelling. Each data point represents a single rat. The mixed effects model used to fit the data is represented by a line of best fit and 95% interval (shaded), split by sex. Data corresponding to males is shown using red circles with a solid line of best fit, while females are shown using blue triangles and a dashed line of best fit. Significance symbols are shown for each term in the model, where #¹

and #² represent the linear and second order age terms, * denotes a main effect of sex, and †¹ and †² represent age by sex interactions with a linear and second order age term, respectively. Multiple comparisons were corrected for using a 5% false discovery rate.

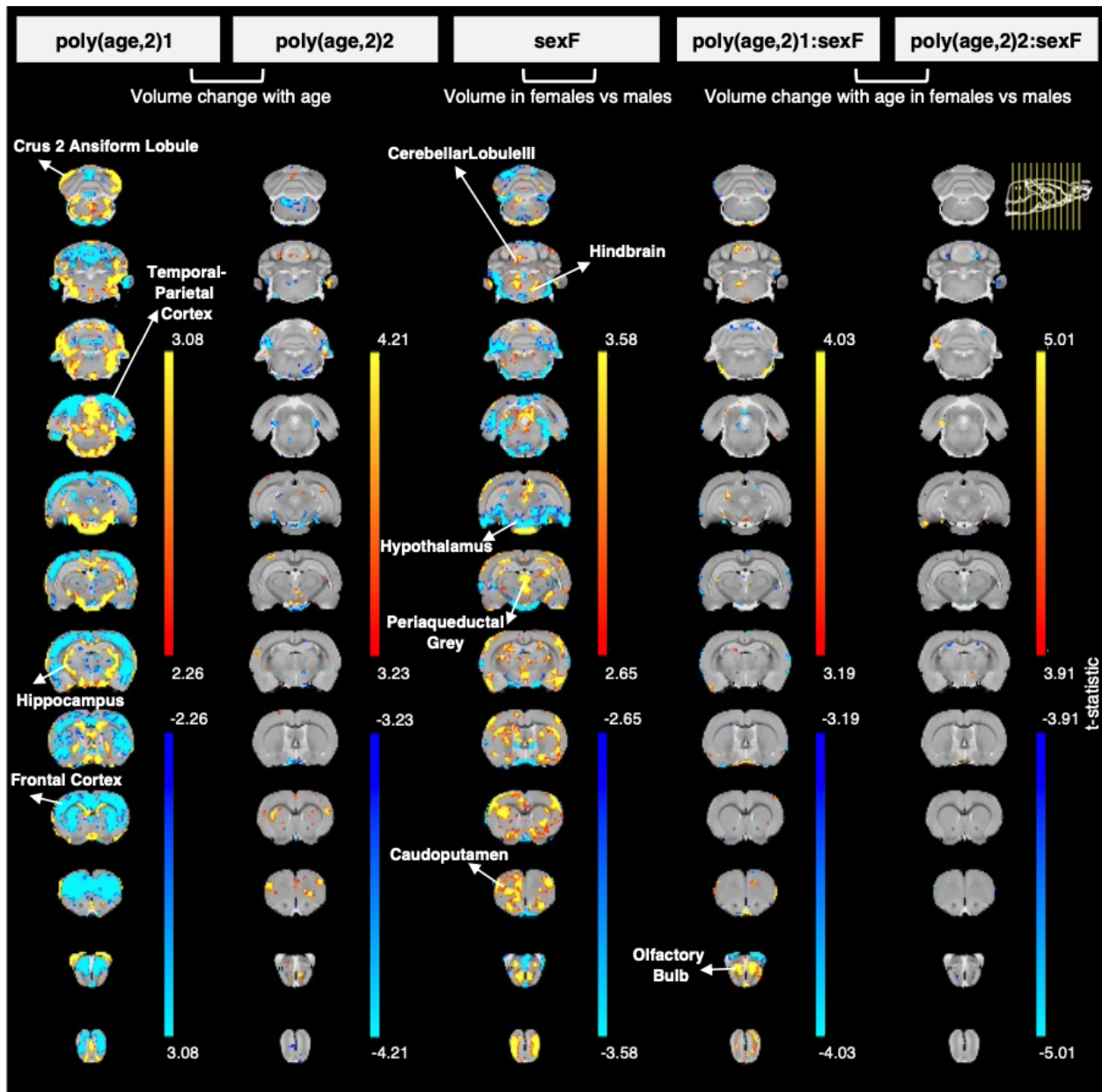


Figure 4.10.4 Statistical maps demonstrating local brain size-corrected volume differences due to age, sex, and their interaction in healthy aging Fischer rats, overlaid on the average anatomy background

A mixed effects model was run at each voxel across the brain, whereby relative Jacobians were predicted by an age by sex interaction with a random intercept for each subject. Age was modelled using a quadratic polynomial function to account for the possibility of non-linear changes with age. The linear and quadratic components of age are written as poly(age,2)1 or poly(age,2)2,

respectively. Effects of sex (sexF) were evaluated in females relative to males, and the interaction between age and sex was also examined ($\text{poly}(\text{age},2)1:\text{sexF}$ and $\text{poly}(\text{age},2)2:\text{sexF}$, with males as the reference group. Each column shows significant voxel-wise effects specific to each model term. The t-values for each term in the mixed effects model are indicated by the colour bars in columns 1 through 5. The plot range for each set of t-values is specific to each model term and displays effects significant between 5 and 1% FDR, with t-values above 1% thresholded at the 1% value.

4.11 Supplementary Methods

4.11.1 Age- and sex-dependent change in brain-size-corrected volumes over three time points as compared to four time points

To ensure our results were not being driven by the last time point wherein we have the fewest subjects (and therefore, the least power), we also analyzed all data from the first three time points only. 68 of 70 regions that originally indicated linear effects of age maintained those effects over three time points as opposed to four, while five new regions demonstrated significant linear effects. Curvilinear effects were seen in 20 regions as opposed to 22 in the original analysis, losing significance in six regions but becoming significant in four. The main effects of sex remained particularly strong, with only three regions losing significance when analyzed over three timepoints. Four additional regions showed linear age by sex interactions, while one region was no longer significant. Quadratic age by sex interactions differed somewhat (nine new regions, seven regions no longer significant, four remained the same), which was to be expected given the aforementioned differences in curvilinear effects of age over three timepoints versus four. For a comparison of LME results obtained using data from three versus four time points see **Supplementary Table 4.12.6**. This additional analysis represents the steps taken towards ensuring our results are robust, despite the decreased sample size towards the end of the study. It is clear that the last timepoint at 20-months constitutes an important data point solidifying the curvilinear effects of age, and especially age by sex interactions, in brain structure present between 4 and 16 months.

4.11.2 Detailed description of the quality control process

A 4-point scoring scale was applied to each scan by D.G, who was blinded to all subject demographic data. Scans with whole-brain motion or Gibb's ringing were given a score of 0, scans with localized motion or Gibb's ringing that severely blurred regional boundaries were given a score of 1, scans with minor motion or Gibb's ringing that did not obstruct regional boundaries

were given a score of 2, and scans without motion or Gibb's ringing or with only very minor artifacts were given a score of 3. Scans given a score of 0 or 1 were excluded from co-registration and further analysis, scans given a score of 2 were flagged for review for corroboration by C.F.F before inclusion in the study, and scans with a score of 3 were included in the study without corroboration from C.F.F. Of the 81 scans acquired, four scans were flagged and excluded from further analysis.

4.12 Supplementary Table Captions

Supplementary Table 4.12.1. Subject Data

Number of subjects scanned at each timepoint, split by sex, with reasons for removal of scans indicated. -QC represents the number of scans removed due to failing quality control (QC), D represents death of a rat prior to that time point, and Tx denotes the removal of a rat after the 10-month time point due to participation in a separate treatment study. F and M denote female or male rats, respectively.

Supplementary Table 4.12.2. Comparison between models containing a linear versus quadratic age term using Akaike information criterion (AIC)

In both models, volume was predicted using an age by sex interaction with a random effect per subject. In model 1, the age term was modelled using a linear age term ($\text{poly}(\text{age},1)$) while in model 2, a quadratic age term ($\text{poly}(\text{age},2)$) was used. Both used the polynomial function, but with differing degrees, to ensure proper model nesting for AIC comparison. Δ_i ($\text{AIC}_i - \text{AIC}_{\min}$) was calculated using the AIC value for each model, whereby a $\Delta_i \geq 4$ indicated substantially less support for model 1 (first order age term) than model 2 (second order age term). The smallest AIC between model 1 and 2 is shown in grey, while $\Delta_i \geq 4$ and AIC_{\min} are denoted by shaded blue boxes.

Supplementary Table 4.12.3. Linear mixed effects model results for 73 absolute volumes derived from integrated absolute Jacobians

Absolute volumes were modelled using an age by sex interaction with a random effect per subject. Age was expressed using a polynomial function of degree 2 to allow for non-linear change with age. The linear and quadratic components of the age term are written as $\text{poly}(\text{age},2)_1$ and $\text{poly}(\text{age},2)_2$, respectively. Effects of sex (sexF) were evaluated in females relative to males, along with the interaction of age and sex ($\text{poly}(\text{age},2)_1:\text{sexF}$ and $\text{poly}(\text{age},2)_2:\text{sexF}$). Std.Beta represents the standardized beta or coefficient value for each model term, with the adjacent column, Std.Error indicating the error associated with the standard beta measurement. The t-value for each model term is also included. Significant adjusted p-values, after 5% FDR correction, are denoted by blue shaded boxes, while those between 5 and 10% are shown by shaded grey boxes. L and R indicate a structure that is split over the left and right hemispheres, and was therefore reported and analyzed as two separate volumes.

Supplementary Table 4.12.4. Absolute volumes of 73 brain regions in mm³, split by timepoint and sex

Average volume and standard deviation for each structure across all subjects are recorded, with separate columns for the same data split by sex. L and R indicate a structure that is split over the left and right hemispheres, and was therefore analyzed and reported as two separate volumes.

Supplementary Table 4.12.5. Linear mixed effects model results for 73 brain-size-corrected volumes derived from integrated relative Jacobians

Brain-size-corrected volumes were modelled using an age by sex interaction with a random effect per subject. Age was expressed using a polynomial function of degree 2 to allow for non-linear change with age. The linear and quadratic components of the age term are written as poly(age,2)1 and poly(age,2)2, respectively. Effects of sex (sexF) were evaluated in females relative to males, along with the interaction of age and sex (poly(age,2)1:sexF and poly(age,2)2:sexF). Std.Beta represents the standardized beta or coefficient value for each model term, with the adjacent column, Std.Error indicating the error associated with the standard beta measurement. The t-value for each model term is also included. Significant adjusted p-values, after 5% FDR correction, are denoted by blue shaded boxes, while those between 5 and 10% are shown by shaded grey boxes. L and R indicate a structure that is split over the left and right hemispheres, and was therefore reported and analyzed as two separate volumes.

Supplementary Table 4.12.6. Linear mixed effects model results for 73 unique brain-size-corrected volumes derived from integrated relative Jacobians, ranked by adjusted p-value within each model term

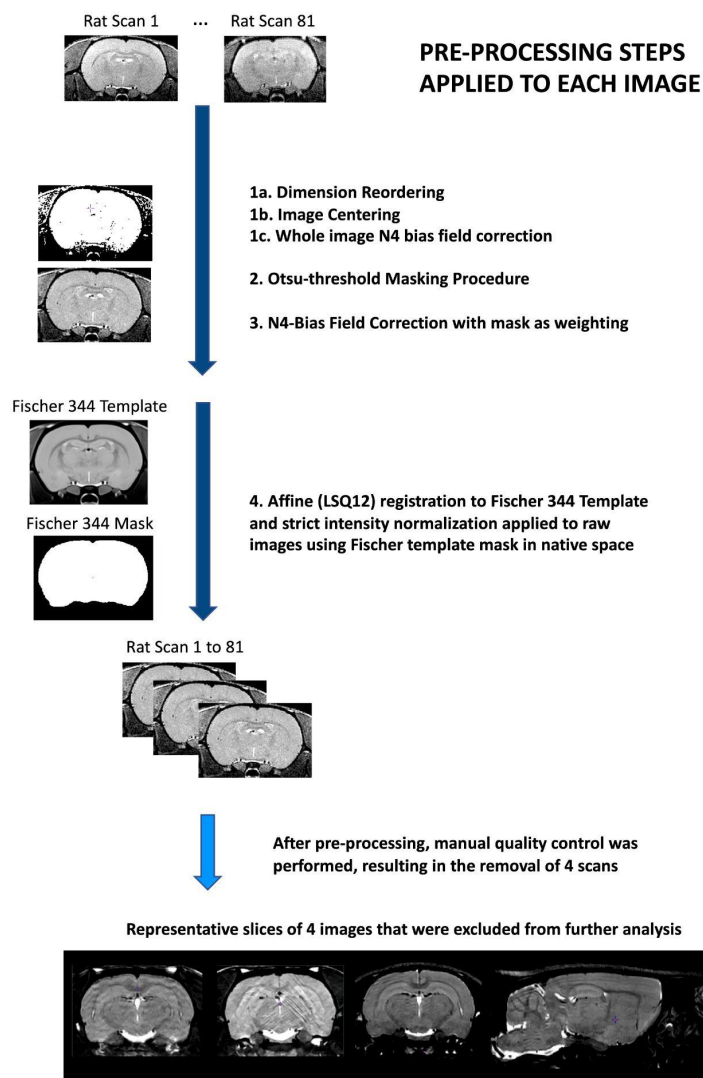
Brain-size-corrected volumes were modelled using an age by sex interaction with a random effect per subject. Age was expressed using a polynomial function of degree 2 to allow for non-linear change with age. The linear and quadratic components of the age term are written as poly(age,2)1 and poly(age,2)2, respectively. Effects of sex (sexF) were evaluated in females relative to males, along with the interaction of age and sex (poly(age,2)1:sexF and poly(age,2)2:sexF). Std.Beta represents the standardized beta or coefficient value for each model term, with the adjacent column, Std.Error indicating the error associated with the standard beta measurement. The t-value for each model term is also included. Significant adjusted p-values, after 5% FDR correction, are denoted by blue shaded boxes, while those between 5 and 10% are shown by shaded grey boxes. L and R indicate a structure that is split over the left and right hemispheres, and was therefore reported and analyzed as two separate volumes. Structures are ranked by adjusted p-value, from smallest (most significant) to largest.

Supplementary Table 4.12.7. Linear mixed effects model results for brain-size-corrected volumes analyzed over 3 time points as compared to four

LME results are compared between two separate analyses, with the first using data from only the first three time points (4, 10, and 16 months) and the second using data from all four time points (4, 10, 16, and 20 months), as is presented elsewhere in the manuscript. Brain-size-corrected volumes were modelled using an age by sex interaction with a random effect per subject. Age was expressed using a quadratic polynomial function to allow for non-linear change with age. The linear and

quadratic components of age are written as $\text{poly}(\text{age},2)1$ or $\text{poly}(\text{age},2)2$, respectively. Effects of sex (sexF) were evaluated in females relative to males, along with the interaction of age and sex ($\text{poly}(\text{age},2)1:\text{sexF}$ and $\text{poly}(\text{age},2)2:\text{sexF}$). Std.Beta represents the standardized beta or coefficient value for each model term, with the adjacent column, Std.Error indicating the error associated with the standard beta measurement. The t-value for each model term is also included. Significant adjusted p-values, after 5% FDR correction, are denoted by blue shaded boxes, while those between 5 and 10% are shown by shaded grey boxes. L and R indicate a structure that is split over the left and right hemispheres, and was therefore reported and analyzed as two separate volumes.

4.13 Supplementary Figures



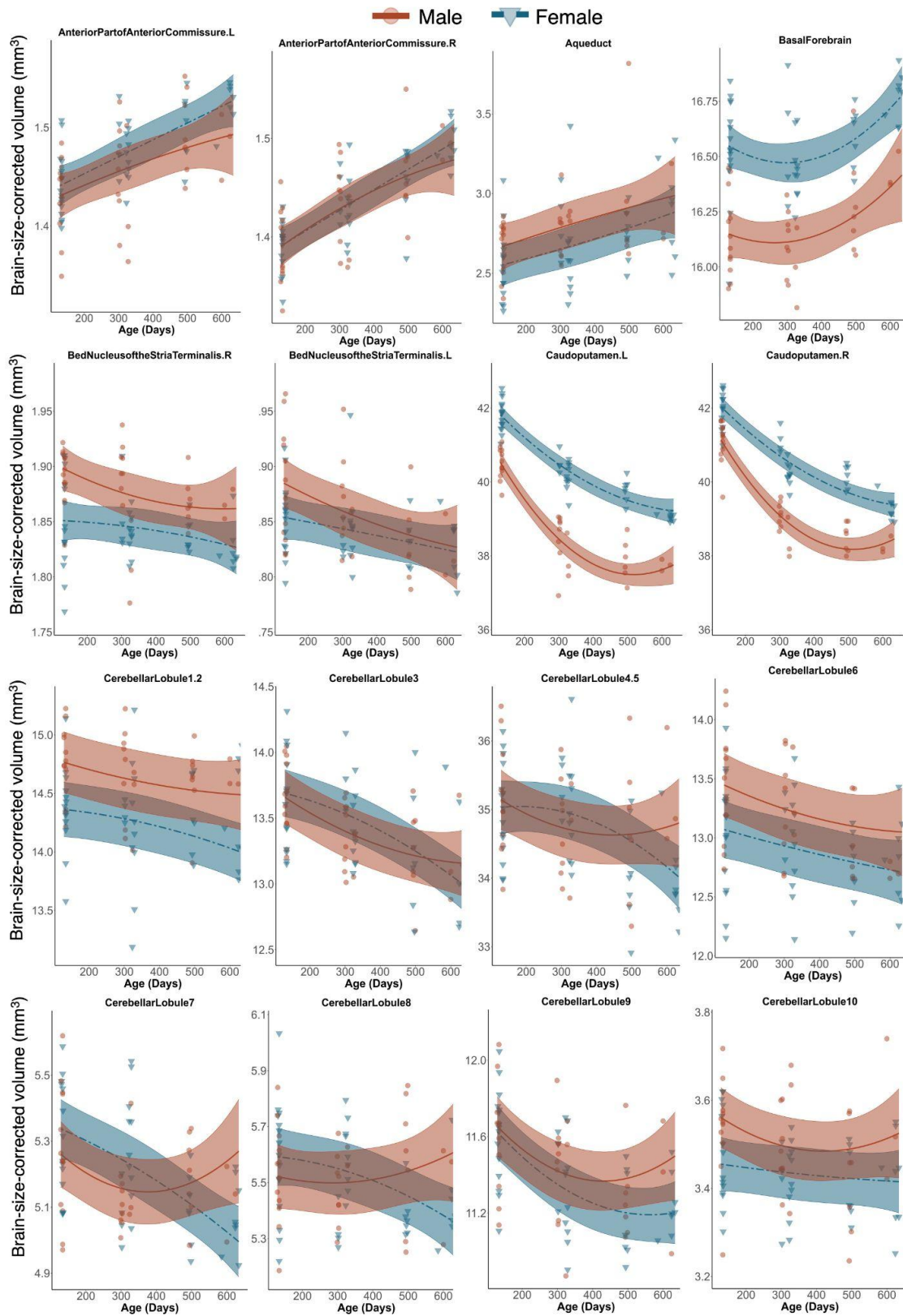
Supplementary Figure 4.13.1 Workflow illustrating the steps involved in preprocessing anatomical MR images.

Representative images of the scans removed during the quality control process are also shown.

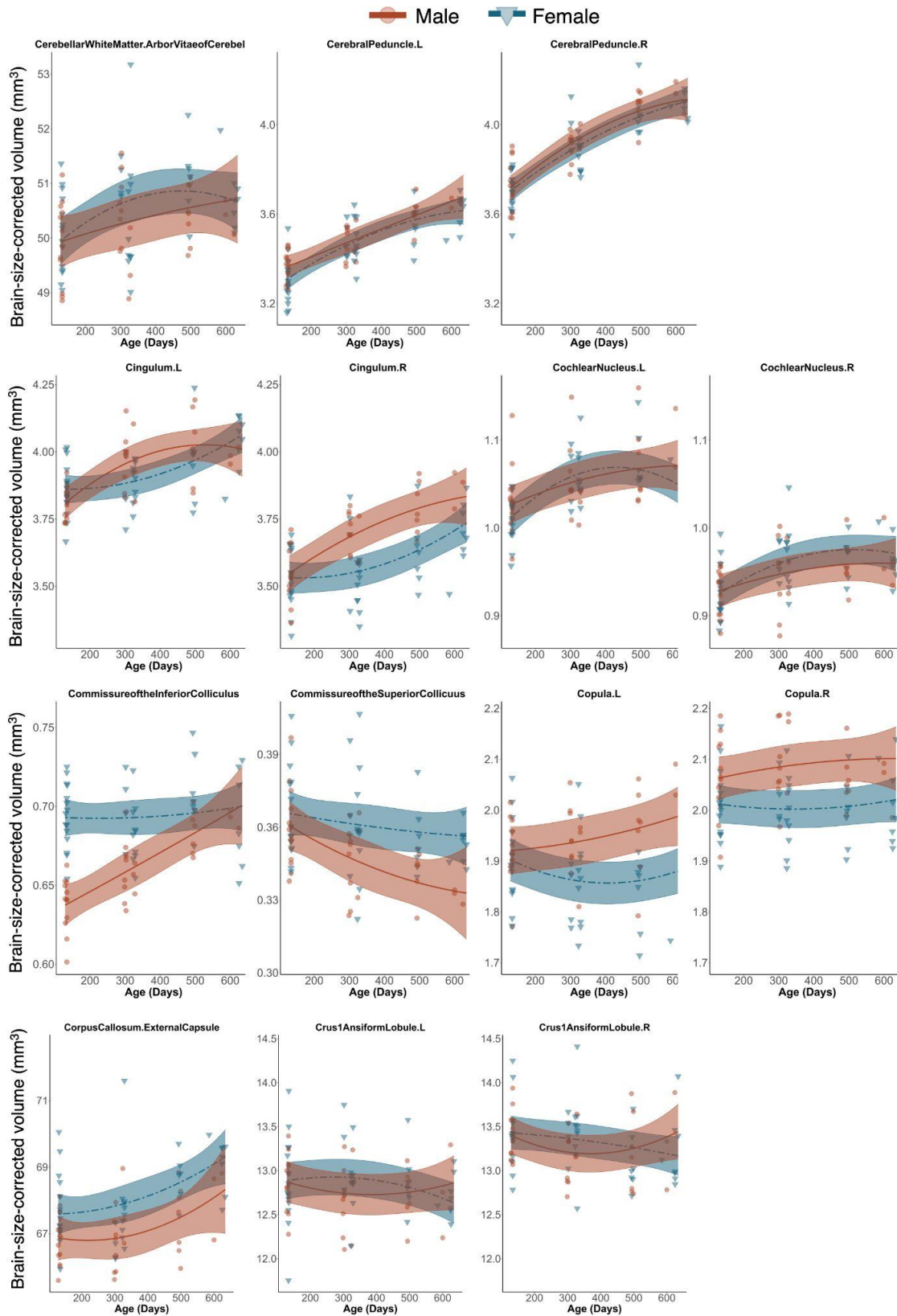
Supplementary Figures 4.13.2 to 4.13.9: Longitudinal trajectory of brain volumes with age and split by sex, for 71 unique brain regions in the aging Fischer rat

MRI data were acquired longitudinally in rats aged 4-, 10-, 16- and 20-months old. Main effects of age and sex, as well as age by sex interactions, were determined using linear mixed effects modelling. Each rat is depicted by a single data point. The mixed effects model used to fit the data is represented by a line of best fit and 95% interval (shaded), split by sex. Data corresponding to

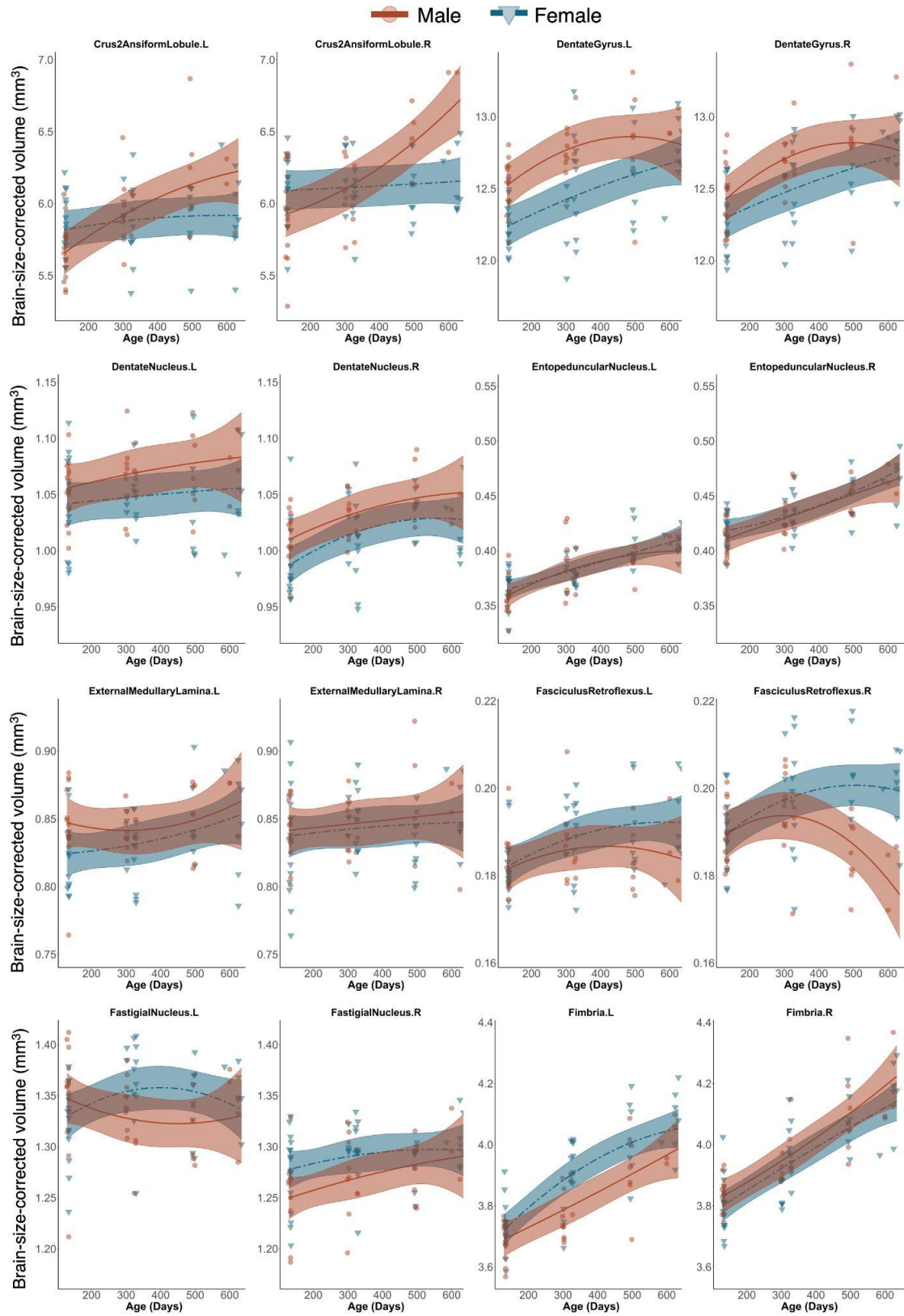
males is shown using red circles with a solid line of best fit, while females are shown using blue triangles and a dashed line of best fit. Significance symbols are shown for each term in the model, where #¹ and #² represent the linear and second order age components of the natural spline with age, * denotes a main effect of sex in females relative to males, and †¹ and †² represent age by sex interactions with a linear or second order component of the natural spline with age, respectively. Multiple comparisons were corrected for using a 5% false discovery rate. (Supplementary Figures 4.13.2 through 4.13.9 are shown below, in order).



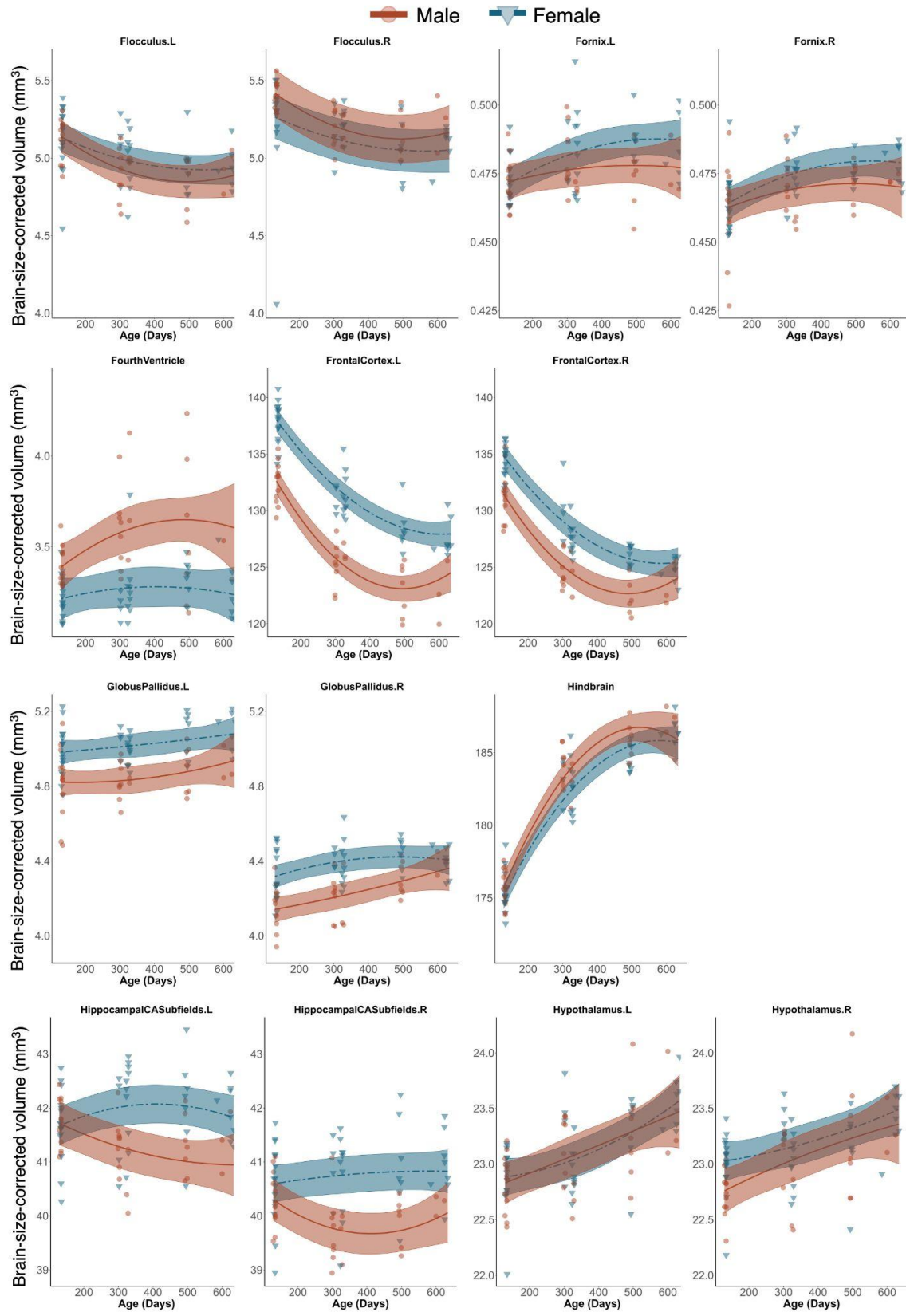
Supplementary Figure 4.13.2



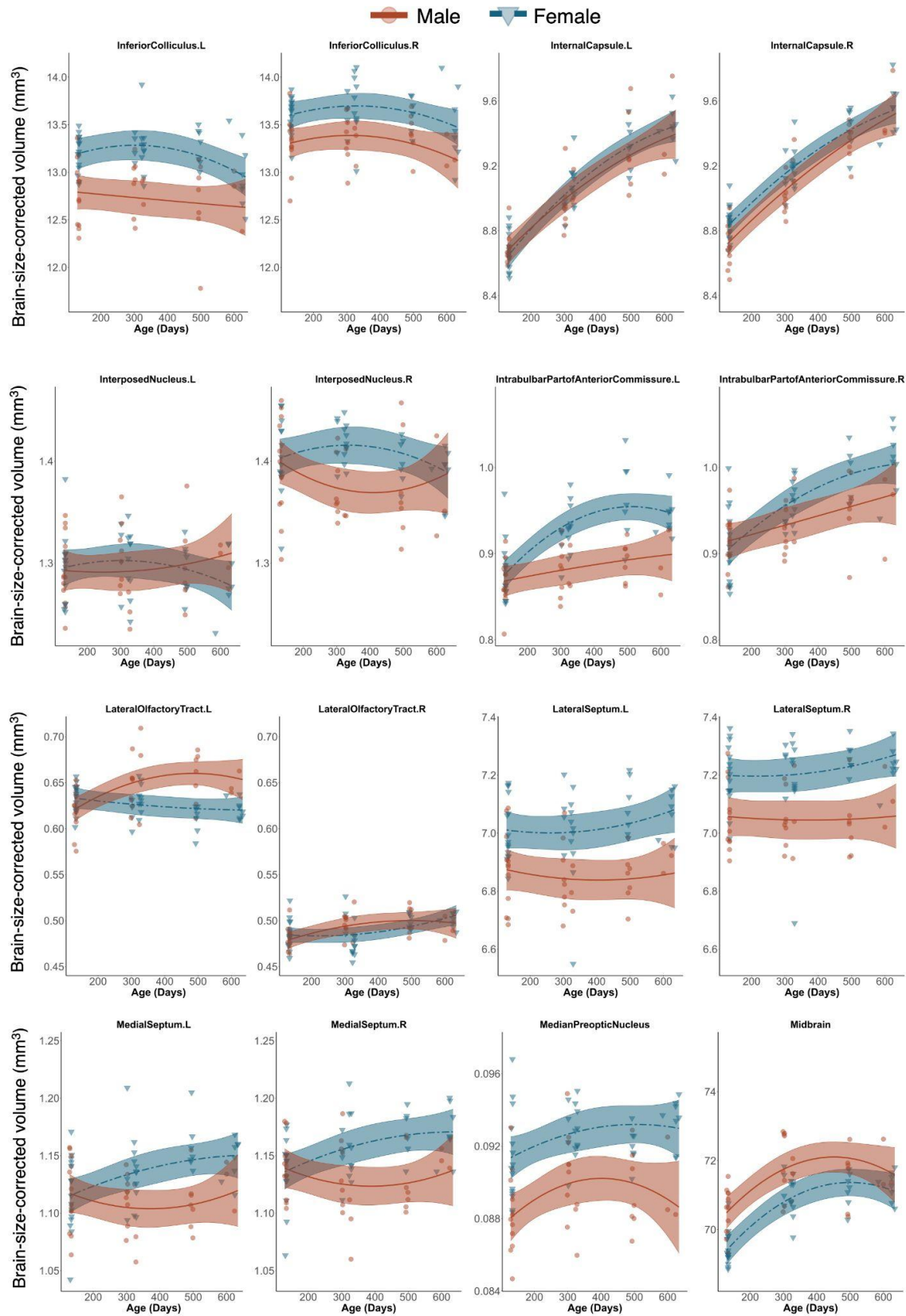
Supplementary Figure 4.13.3



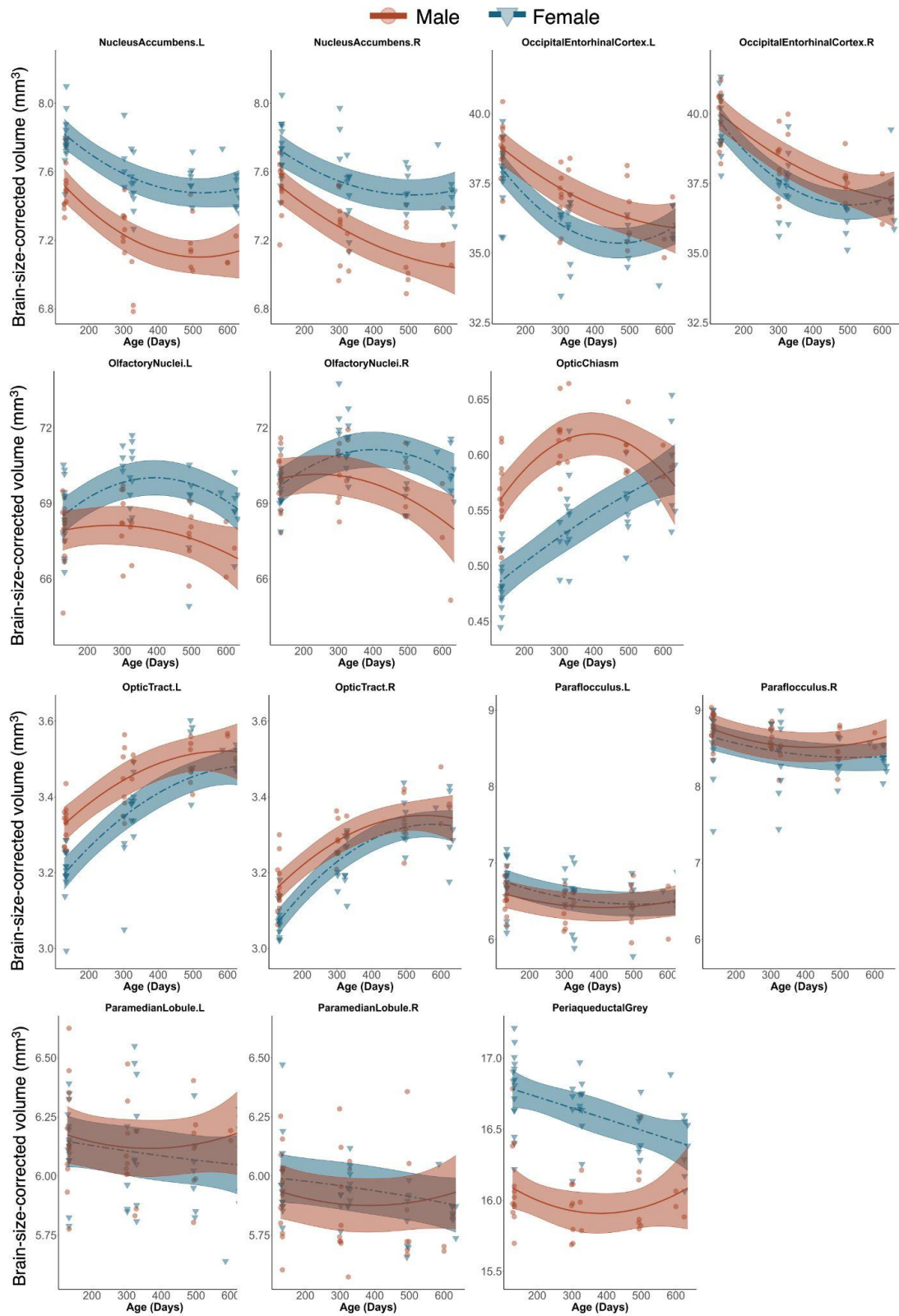
Supplementary Figure 4.13.4



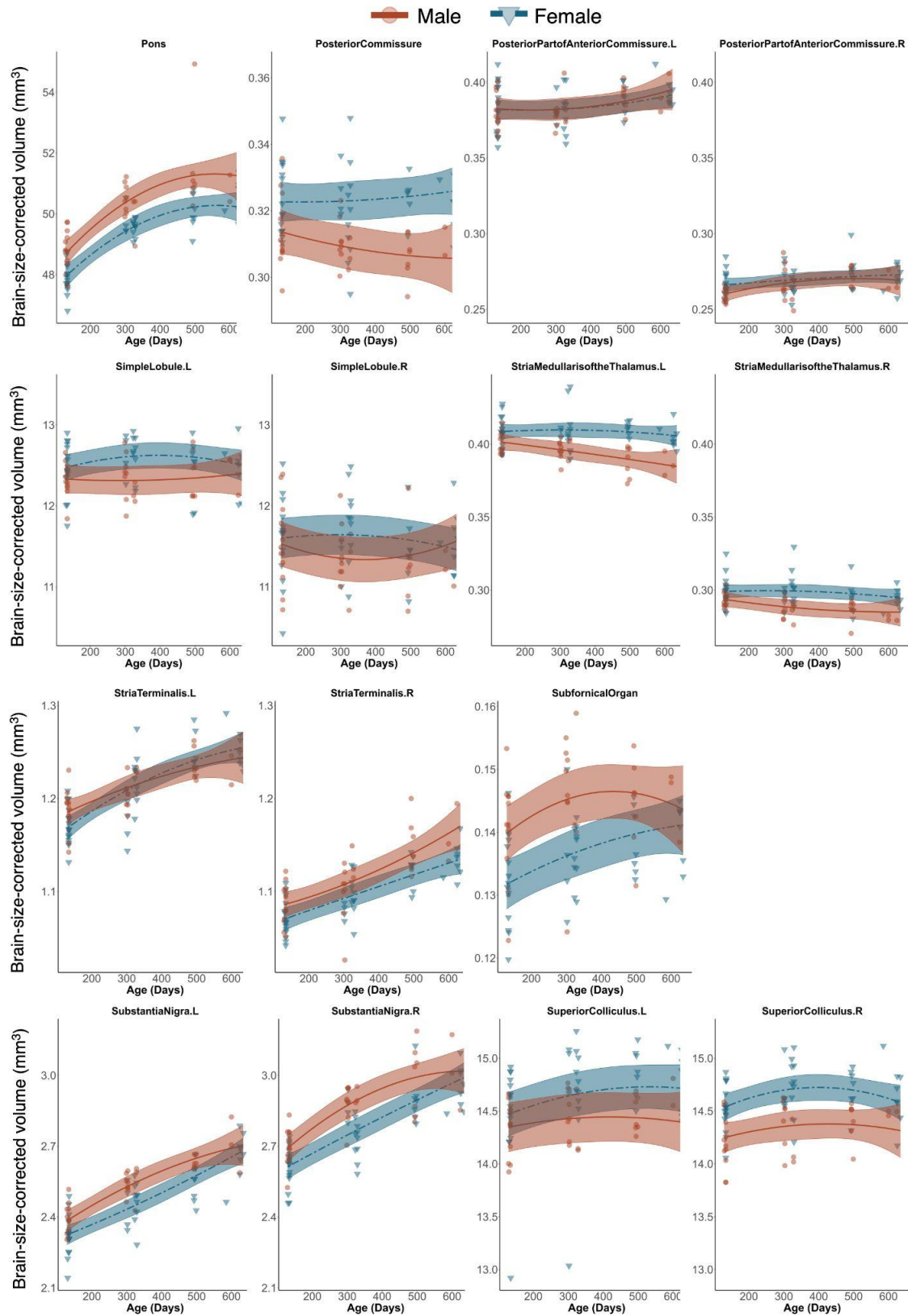
Supplementary Figure 4.13.5



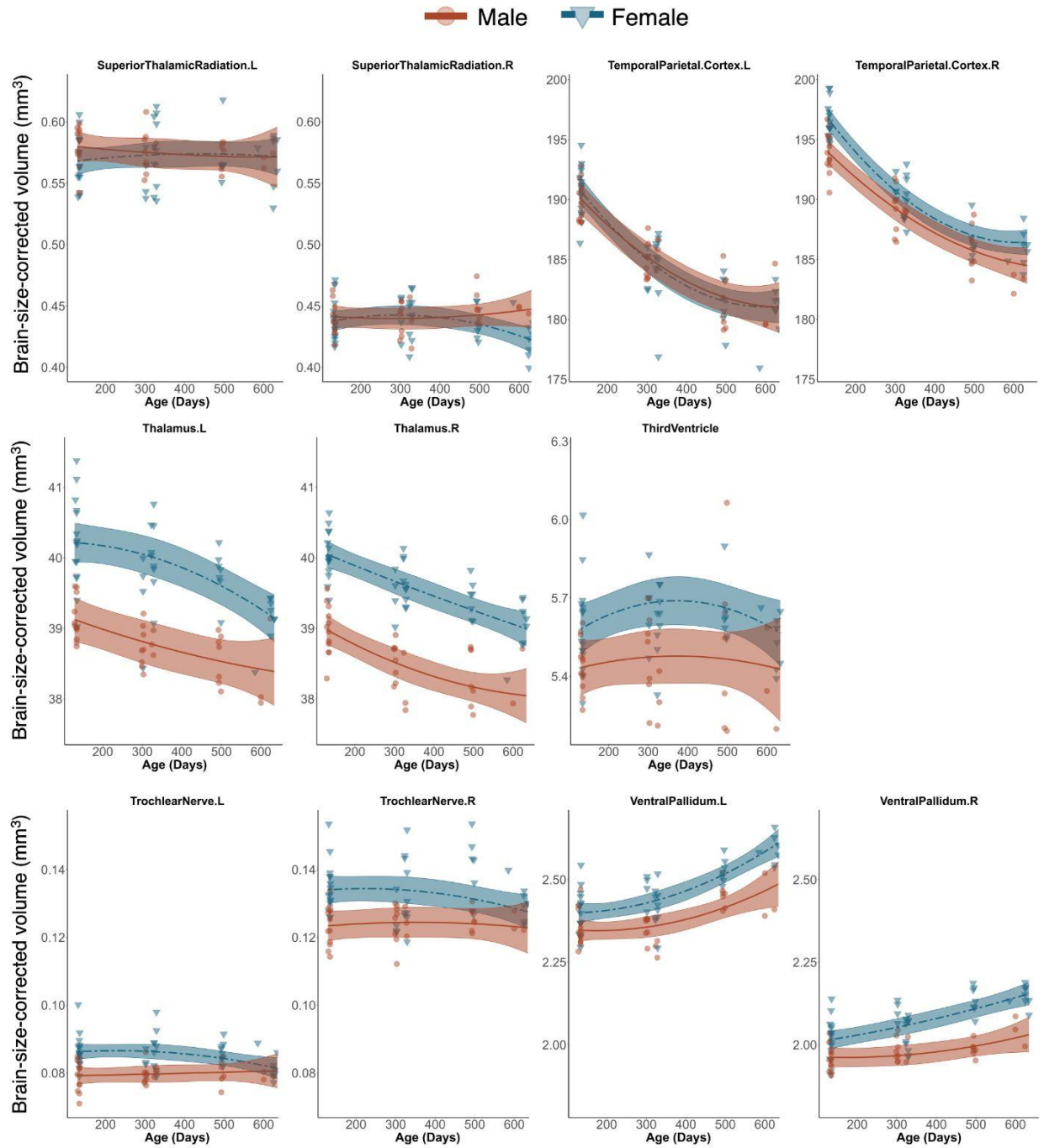
Supplementary Figure 4.13.6



Supplementary Figure 4.13.7



Supplementary Figure 4.13.8

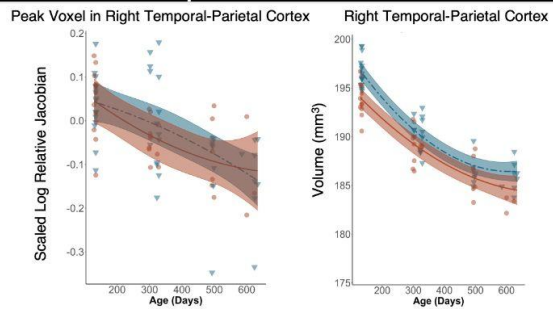
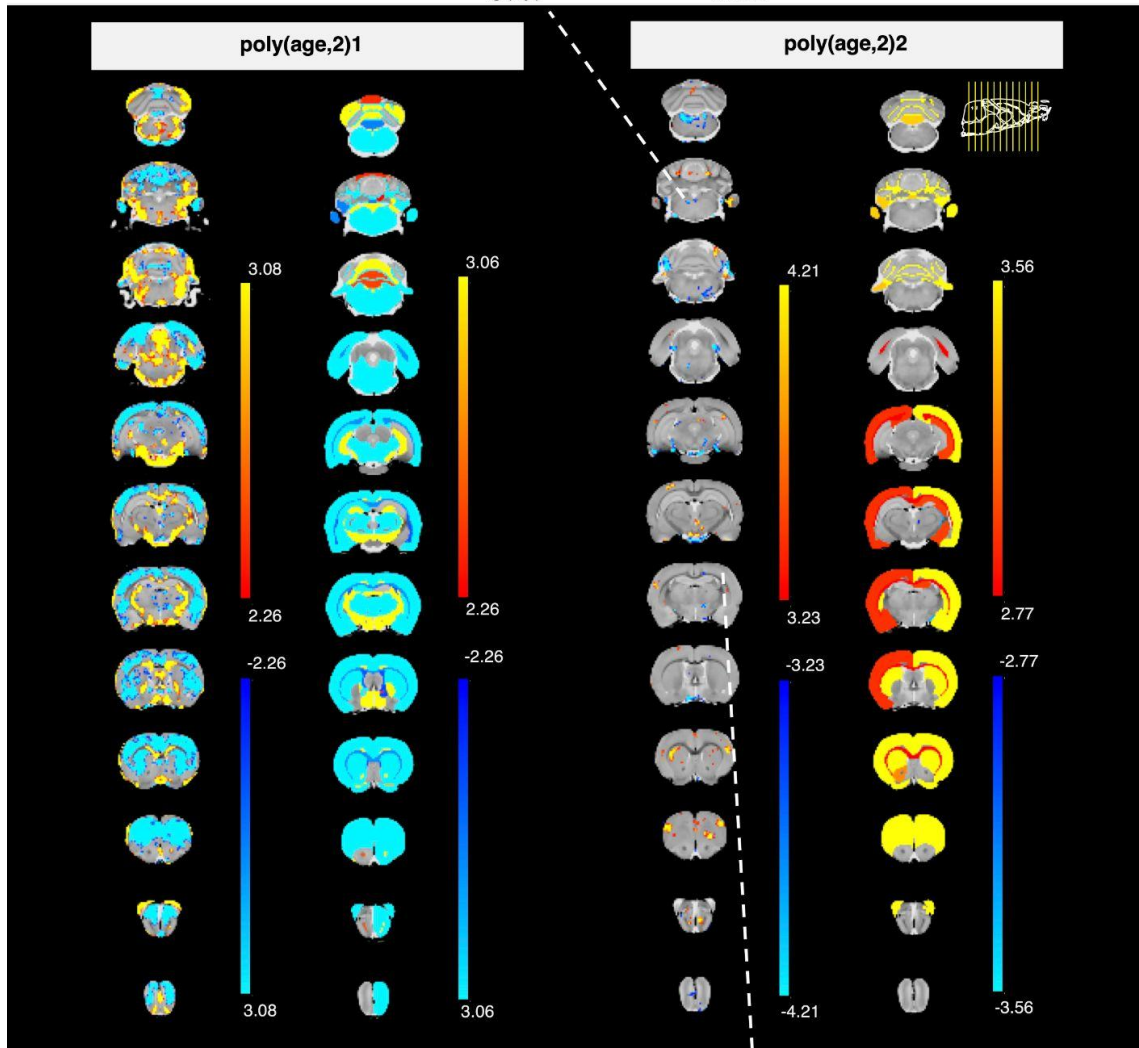
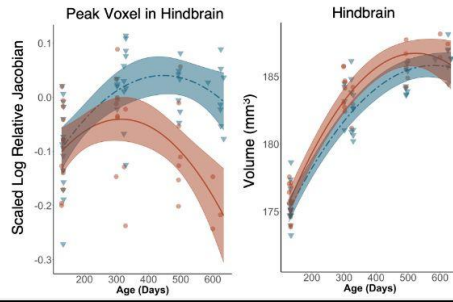


Supplementary Figure 4.13.9

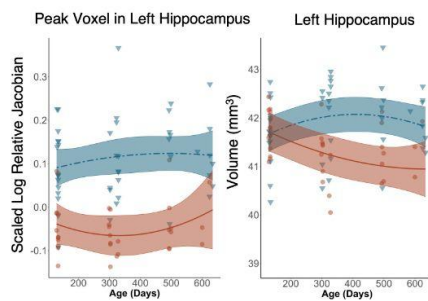
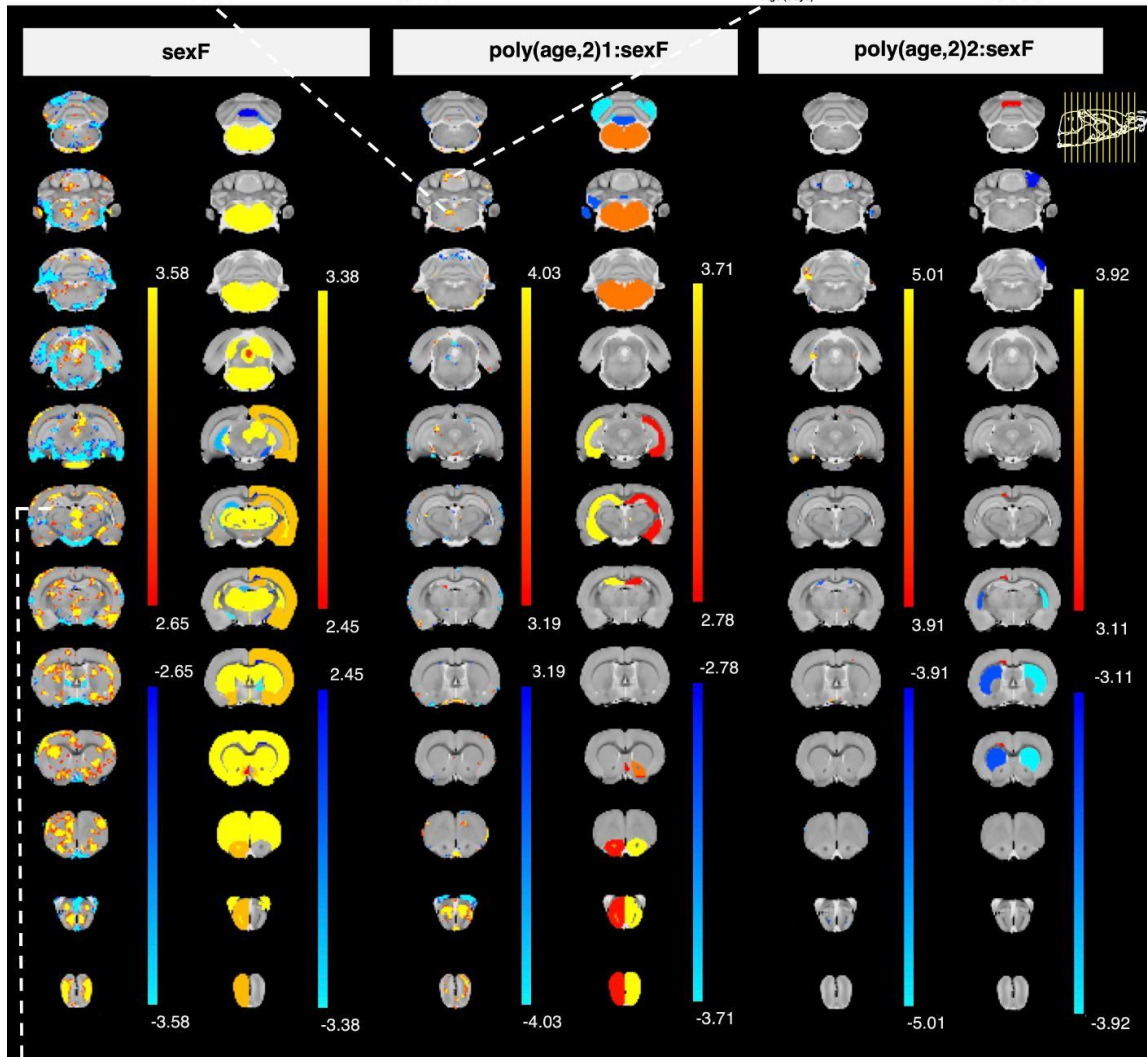
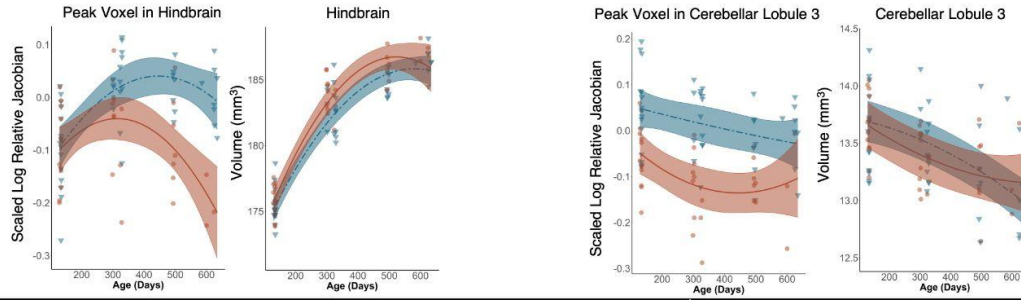
Supplementary Figures 4.13.10 and 4.13.11: A side by side comparison between whole-brain voxel-wise changes and regional changes as a result of age, sex, and their interaction, overlaid on the average anatomy background

Brain-size-corrected volumes and relative Jacobians at each voxel were both modelled using an age by sex interaction with a random effect per subject. Age was expressed using a quadratic polynomial function to allow for non-linear change with age. The linear and quadratic components of the age term are written as $\text{poly}(\text{age},2)1$ and $\text{poly}(\text{age},2)2$, respectively. Effects of sex (sexF) were evaluated in females relative to males, along with the interaction of age and sex ($\text{poly}(\text{age},2)1:\text{sexF}$ and $\text{poly}(\text{age},2)2:\text{sexF}$). The t-values for each term in the mixed effects model at either the voxelwise or structural level are plotted over the average anatomy background. t-value maps for the linear and quadratic age terms are shown in Figure 10, while those for the main effect of sex, and the interaction of age and sex are shown in Figure 11. The plot range for each set of t-values is specific to each model term and displays effects significant between 5 and 1% FDR, with t-values above 1% thresholded at the 1% value. The only exception to this is the t-statistic map for brain volumes under the $\text{poly}(\text{age},2)2:\text{sexF}$ heading, which are displayed with a 10% FDR cut-off. The scaled log relative Jacobian of peak voxels in the hindbrain, cerebellar lobule 3, and the hippocampus were visualized alongside the volume plots of the same structures, to highlight findings identified only at the voxel-wise level. A voxel from the temporal-parietal cortex is also visualized, alongside the volume data, to demonstrate findings only visible at the whole-volume level. For voxel and volume plots, the mixed effects model used to fit the data is represented by a line of best fit and 95% interval (shaded), split by sex. Data corresponding to males is shown using red circles with a solid line of best fit, while females are shown using blue triangles and a dashed line of best fit.

(Supplementary Figures 4.13.10 and 4.13.11 are shown below, in order).



Supplementary Figure 4.13.10



Supplementary Figure 4.13.11

4.14 References

- Aggleton, John P., and Malcolm W. Brown. 1999. "Episodic Memory, Amnesia, and the Hippocampal–anterior Thalamic Axis." *The Behavioral and Brain Sciences* 22 (3): 425–44.
- Akaike, Hirotugu, Boris Nikolaevich Petrov, and F. Csaki. 1973. "Second International Symposium on Information Theory." Akadémiai Kiadó, Budapest.
- Alexander, Gene E., Lan Lin, Eriko S. Yoshimaru, Pradyumna K. Bharadwaj, Kaitlin L. Bergfield, Lan T. Hoang, Monica K. Chawla, et al. 2020. "Age-Related Regional Network Covariance of Magnetic Resonance Imaging Gray Matter in the Rat." *Frontiers in Aging Neuroscience* 12: 267.
- Armstrong, Nicole M., Yang An, Lori Beason-Held, Jimit Doshi, Guray Erus, Luigi Ferrucci, Christos Davatzikos, and Susan M. Resnick. 2019. "Sex Differences in Brain Aging and Predictors of Neurodegeneration in Cognitively Healthy Older Adults." *Neurobiology of Aging* 81 (September): 146–56.
- Bates, Douglas, Martin Mächler, Ben Bolker, and Steve Walker. 2015. "Fitting Linear Mixed-Effects Models Using lme4." *Journal of Statistical Software, Articles* 67 (1): 1–48.
- Benjamini, Yoav, and Yosef Hochberg. 1995. "Controlling the False Discovery Rate: A Practical and Powerful Approach to Multiple Testing." *Journal of the Royal Statistical Society. Series B, Statistical Methodology* 57 (1): 289–300.
- Bernal-Rusiel, Jorge L., Douglas N. Greve, Martin Reuter, Bruce Fischl, Mert R. Sabuncu, and Alzheimer's Disease Neuroimaging Initiative. 2013. "Statistical Analysis of Longitudinal Neuroimage Data with Linear Mixed Effects Models." *NeuroImage* 66 (February): 249–60.
- Bernard, Jessica A., and Rachael D. Seidler. 2013. "Relationships between Regional Cerebellar Volume and Sensorimotor and Cognitive Function in Young and Older Adults." *Cerebellum* 12 (5): 721–37.
- Burnham, Kenneth P., and David R. Anderson. 2004. "Multimodel Inference: Understanding AIC and BIC in Model Selection." *Sociological Methods & Research* 33 (2): 261–304.
- Bussy, Aurelie, Eric Plitman, Raihaan Patel, Stephanie Tullo, Alyssa Salaciak, Saashi A. Bedford, Sarah Farzin, et al. 2021. "Hippocampal Subfield Volumes across the Healthy Lifespan and the Effects of MR Sequence on Estimates." *NeuroImage*, March, 117931.
- Cabello, C. R., J. J. Thune, H. Pakkenberg, and B. Pakkenberg. 2002. "Ageing of Substantia Nigra in Humans: Cell Loss May Be Compensated by Hypertrophy." *Neuropathology and Applied Neurobiology* 28 (4): 283–91.
- Cahill, Larry. 2006. "Why Sex Matters for Neuroscience." *Nature Reviews. Neuroscience* 7 (6): 477–84.
- Casas, Rafael, Siva Muthusamy, Paul G. Wakim, Sanhita Sinharay, Margaret R. Lentz, William C. Reid, and Dima A. Hammoud. 2018. "MR Brain Volumetric Measurements Are Predictive of Neurobehavioral Impairment in the HIV-1 Transgenic Rat." *NeuroImage. Clinical* 17: 659–66.
- Chesky, J. A., and M. Rockstein. 1976. "Life Span Characteristics in the Male Fischer Rat." *Experimental Aging Research* 2 (5): 399–407.
- Chung, M. K., K. J. Worsley, T. Paus, C. Cherif, D. L. Collins, J. N. Giedd, J. L. Rapoport, and A. C. Evans. 2001. "A Unified Statistical Approach to Deformation-Based Morphometry." *NeuroImage* 14 (3): 595–606.
- Cohen, Robert M., Kavon Rezai-Zadeh, Tara M. Weitz, Altan Rentsendorj, David Gate, Inna Spivak, Yasmin Bholat, et al. 2013. "A Transgenic Alzheimer Rat with Plaques, Tau Pathology,

Behavioral Impairment, Oligomeric A β , and Frank Neuronal Loss.” *The Journal of Neuroscience: The Official Journal of the Society for Neuroscience* 33 (15): 6245–56.

Cooke, B., C. D. Hegstrom, L. S. Villeneuve, and S. M. Breedlove. 1998. “Sexual Differentiation of the Vertebrate Brain: Principles and Mechanisms.” *Frontiers in Neuroendocrinology* 19 (4): 323–62.

Corre, Christina, Miriam Friedel, Dulcie A. Vousden, Ariane Metcalf, Shoshana Spring, Lily R. Qiu, Jason P. Lerch, and Mark R. Palmert. 2016. “Separate Effects of Sex Hormones and Sex Chromosomes on Brain Structure and Function Revealed by High-Resolution Magnetic Resonance Imaging and Spatial Navigation Assessment of the Four Core Genotype Mouse Model.” *Brain Structure & Function* 221 (2): 997–1016.

Cosgrove, Kelly P., Carolyn M. Mazure, and Julie K. Staley. 2007. “Evolving Knowledge of Sex Differences in Brain Structure, Function, and Chemistry.” *Biological Psychiatry* 62 (8): 847–55.

Dillon, Serena E., Demitra Tsivos, Michael Knight, Bryony McCann, Catherine Pennington, Anna I. Shiel, Myra E. Conway, Margaret A. Newson, Risto A. Kauppinen, and Elizabeth J. Coulthard. 2017. “The Impact of Ageing Reveals Distinct Roles for Human Dentate Gyrus and CA3 in Pattern Separation and Object Recognition Memory.” *Scientific Reports* 7 (1): 14069.

Driscoll, I., C. Davatzikos, Y. An, X. Wu, D. Shen, M. Kraut, and S. M. Resnick. 2009. “Longitudinal Pattern of Regional Brain Volume Change Differentiates Normal Aging from MCI.” *Neurology* 72 (22): 1906–13.

Driscoll, I., S. R. Howard, J. C. Stone, M. H. Monfils, B. Tomanek, W. M. Brooks, and R. J. Sutherland. 2006. “The Aging Hippocampus: A Multi-Level Analysis in the Rat.” *Neuroscience* 139 (4): 1173–85.

Dumitriu, Dani, Jiandong Hao, Yuko Hara, Jeffrey Kaufmann, William G. M. Janssen, Wendy Lou, Peter R. Rapp, and John H. Morrison. 2010. “Selective Changes in Thin Spine Density and Morphology in Monkey Prefrontal Cortex Correlate with Aging-Related Cognitive Impairment.” *The Journal of Neuroscience: The Official Journal of the Society for Neuroscience* 30 (22): 7507–15.

Farooqui, Tahira, and Akhlaq A. Farooqui. 2009. “Aging: An Important Factor for the Pathogenesis of Neurodegenerative Diseases.” *Mechanisms of Ageing and Development* 130 (4): 203–15.

Fjell, Anders M., and Kristine B. Walhovd. 2010. “Structural Brain Changes in Aging: Courses, Causes and Cognitive Consequences.” *Reviews in the Neurosciences* 21 (3): 187–221.

Fjell, Anders M., Kristine B. Walhovd, Christine Fennema-Notestine, Linda K. McEvoy, Donald J. Hagler, Dominic Holland, James B. Brewer, and Anders M. Dale. 2009. “One-Year Brain Atrophy Evident in Healthy Aging.” *The Journal of Neuroscience: The Official Journal of the Society for Neuroscience* 29 (48): 15223–31.

Fowler, Caitlin F., Dan Madularu, Masoumeh Dehghani, Gabriel A. Devenyi, and Jamie Near. 2020. “Longitudinal Quantification of Metabolites and Macromolecules Reveals Age- and Sex-Related Changes in the Healthy Fischer 344 Rat Brain.” *Neurobiology of Aging* 101 (December): 109–22.

Fox, John, and Sanford Weisberg. 2019. “An R Companion to Applied Regression.” Thousand Oaks CA: Sage. <https://socialsciences.mcmaster.ca/jfox/Books/Companion/index.html>.

Franceschi, Claudio, Paolo Garagnani, Cristina Morsiani, Maria Conte, Aurelia Santoro, Andrea Grignolio, Daniela Monti, Miriam Capri, and Stefano Salvioli. 2018. “The Continuum of Aging and Age-Related Diseases: Common Mechanisms but Different Rates.” *Frontiers of Medicine*

5 (March): 61.

Friedel, Miriam, Matthijs C. van Eede, Jon Pipitone, M. Mallar Chakravarty, and Jason P. Lerch. 2014. "Pyd Piper: A Flexible Toolkit for Constructing Novel Registration Pipelines." *Frontiers in Neuroinformatics* 8 (July): 67.

Gallagher, Michela, Amy M. Stocker, and Ming Teng Koh. 2011. "Mindspan: Lessons from Rat Models of Neurocognitive Aging." *ILAR Journal / National Research Council, Institute of Laboratory Animal Resources* 52 (1): 32–40.

Gaser, Christian, Silvio Schmidt, Martin Metzler, Karl-Heinz Herrmann, Ines Krumbein, Jürgen R. Reichenbach, and Otto W. Witte. 2012. "Deformation-Based Brain Morphometry in Rats." *NeuroImage* 63 (1): 47–53.

Giedd, Jay N., Armin Raznahan, Kathryn L. Mills, and Rhoshel K. Lenroot. 2012. "Review: Magnetic Resonance Imaging of Male/female Differences in Human Adolescent Brain Anatomy." *Biology of Sex Differences* 3 (1): 19.

Giedd, J. N., J. Blumenthal, N. O. Jeffries, F. X. Castellanos, H. Liu, A. Zijdenbos, T. Paus, A. C. Evans, and J. L. Rapoport. 1999. "Brain Development during Childhood and Adolescence: A Longitudinal MRI Study." *Nature Neuroscience* 2 (10): 861–63.

Goerzen, Dana, Caitlin Fowler, Gabriel A. Devenyi, Jürgen Germann, Dan Madularu, M. Mallar Chakravarty, and Jamie Near. 2020. "An MRI-Derived Neuroanatomical Atlas of the Fischer 344 Rat Brain." *Scientific Reports* 10 (1): 6952.

Goldstein, J. M., L. J. Seidman, N. J. Horton, N. Makris, D. N. Kennedy, V. S. Caviness Jr, S. V. Faraone, and M. T. Tsuang. 2001. "Normal Sexual Dimorphism of the Adult Human Brain Assessed by in Vivo Magnetic Resonance Imaging." *Cerebral Cortex* 11 (6): 490–97.

Guidi, Michael, Ashok Kumar, Asha Rani, and Thomas C. Foster. 2014. "Assessing the Emergence and Reliability of Cognitive Decline over the Life Span in Fisher 344 Rats Using the Spatial Water Maze." *Frontiers in Aging Neuroscience* 6 (January): 2.

Hamezah, Hamizah Shahirah, Lina Wati Durani, Nor Faeizah Ibrahim, Daijiro Yanagisawa, Tomoko Kato, Akihiko Shiino, Sachiko Tanaka, Hanafi Ahmad Damanhuri, Wan Zurinah Wan Ngah, and Ikuo Tooyama. 2017. "Volumetric Changes in the Aging Rat Brain and Its Impact on Cognitive and Locomotor Functions." *Experimental Gerontology* 99 (December): 69–79.

Han, Shuo, Yang An, Aaron Carass, Jerry L. Prince, and Susan M. Resnick. 2020. "Longitudinal Analysis of Regional Cerebellum Volumes during Normal Aging." *NeuroImage* 220 (October): 117062.

Harris, Janna L., Hung-Wen Yeh, Russell H. Swerdlow, In-Young Choi, Phil Lee, and William M. Brooks. 2014. "High-Field Proton Magnetic Resonance Spectroscopy Reveals Metabolic Effects of Normal Brain Aging." *Neurobiology of Aging* 35 (7): 1686–94.

Hasan, Khader M., Indika S. Walimuni, Larry A. Kramer, and Richard E. Frye. 2010. "Human Brain Atlas-Based Volumetry and Relaxometry: Application to Healthy Development and Natural Aging." *Magnetic Resonance in Medicine: Official Journal of the Society of Magnetic Resonance in Medicine / Society of Magnetic Resonance in Medicine* 64 (5): 1382–89.

Hayek, Dayana, Friederike Thams, Agnes Flöel, and Daria Antonenko. 2020. "Dentate Gyrus Volume Mediates the Effect of Fornix Microstructure on Memory Formation in Older Adults." *Frontiers in Aging Neuroscience* 12 (March): 79.

Hedman, Anna M., Neeltje E. M. van Haren, Hugo G. Schnack, René S. Kahn, and Hilleke E. Hulshoff Pol. 2012. "Human Brain Changes across the Life Span: A Review of 56 Longitudinal Magnetic Resonance Imaging Studies." *Human Brain Mapping* 33 (8): 1987–2002.

Hou, Yujun, Xiuli Dan, Mansi Babbar, Yong Wei, Steen G. Hasselbalch, Deborah L. Croteau,

- and Vilhelm A. Bohr. 2019. "Ageing as a Risk Factor for Neurodegenerative Disease." *Nature Reviews. Neurology* 15 (10): 565–81.
- Jenkinson, Mark, Christian F. Beckmann, Timothy E. J. Behrens, Mark W. Woolrich, and Stephen M. Smith. 2012. "FSL." *NeuroImage* 62 (2): 782–90.
- Juraska, Janice M., and Nioka C. Lowry. 2012. "Neuroanatomical Changes Associated with Cognitive Aging." In *Behavioral Neurobiology of Aging*, edited by Marie-Christine Pardon and Mark W. Bondi, 137–62. Berlin, Heidelberg: Springer Berlin Heidelberg.
- Juraska, Janice M., Cheryl L. Sisk, and Lydia L. DonCarlos. 2013. "Sexual Differentiation of the Adolescent Rodent Brain: Hormonal Influences and Developmental Mechanisms." *Hormones and Behavior* 64 (2): 203–10.
- Kienlin, Markus von, Basil Künnecke, Friedrich Metzger, Guido Steiner, J. Grayson Richards, Laurence Ozmen, Helmut Jacobsen, and Hansruedi Loetscher. 2005. "Altered Metabolic Profile in the Frontal Cortex of PS2APP Transgenic Mice, Monitored throughout Their Life Span." *Neurobiology of Disease* 18 (1): 32–39.
- Kilborn, Susan H., Guy Trudel, and Hans Uthoff. 2002. "Review of Growth Plate Closure Compared with Age at Sexual Maturity and Lifespan in Laboratory Animals." *Contemporary Topics in Laboratory Animal Science / American Association for Laboratory Animal Science* 41 (5): 21–26.
- Kong, Vincent, Gabriel A. Devenyi, Daniel Gallino, Gülebru Ayranci, Jürgen Germann, Colleen Rollins, and M. Mallar Chakravarty. 2018. "Early-in-Life Neuroanatomical and Behavioural Trajectories in a Triple Transgenic Model of Alzheimer's Disease." *Brain Structure & Function* 223 (7): 3365–82.
- Kuznetsova, Alexandra, Per B. Brockhoff, and Rune H. B. Christensen. 2017. "lmerTest Package: Tests in Linear Mixed Effects Models." *Journal of Statistical Software, Articles* 82 (13): 1–26.
- Lerch, Jason P., Adelaide P. Yiu, Alonso Martinez-Canabal, Tetyana Pekar, Veronique D. Bohbot, Paul W. Frankland, R. Mark Henkelman, Sheena A. Josselyn, and John G. Sled. 2011. "Maze Training in Mice Induces MRI-Detectable Brain Shape Changes Specific to the Type of Learning." *NeuroImage* 54 (3): 2086–95.
- Lerch, J., C. Hammill, M. van Eede, and D. Cassel. 2017. "Statistical Tools for Medical Imaging NetCDF (MINC) Files. R Package Version 1.5.2.3." 2017. <http://mouse-imaging-centre.github.io/RMINC/>.
- Long, Xiaojing, Weiqi Liao, Chunxiang Jiang, Dong Liang, Bensheng Qiu, and Lijuan Zhang. 2012. "Healthy Aging: An Automatic Analysis of Global and Regional Morphological Alterations of Human Brain." *Academic Radiology* 19 (7): 785–93.
- MacLusky, N. J., A. S. Clark, F. Naftolin, and P. S. Goldman-Rakic. 1987. "Estrogen Formation in the Mammalian Brain: Possible Role of Aromatase in Sexual Differentiation of the Hippocampus and Neocortex." *Steroids* 50 (4-6): 459–74.
- Maheswaran, Satheesh, Hervé Barjat, Daniel Rueckert, Simon T. Bate, David R. Howlett, Lorna Tilling, Sean C. Smart, et al. 2009. "Longitudinal Regional Brain Volume Changes Quantified in Normal Aging and Alzheimer's APP X PS1 Mice Using MRI." *Brain Research* 1270 (May): 19–32.
- Malykhin, Nikolai V., Yushan Huang, Stanislaw Hrybouski, and Fraser Olsen. 2017. "Differential Vulnerability of Hippocampal Subfields and Anteroposterior Hippocampal Subregions in Healthy Cognitive Aging." *Neurobiology of Aging* 59 (November): 121–34.
- Marrone, Diano F., Elham Satvat, and Anuj Patel. 2018. "Age-Related Deficits in Recognition

Memory Are Protocol-Dependent.” *Aging and Disease* 9 (5): 798–807.

Mattson, Mark P., and Thiruma V. Arumugam. 2018. “Hallmarks of Brain Aging: Adaptive and Pathological Modification by Metabolic States.” *Cell Metabolism* 27 (6): 1176–99.

Mawhinney, Lana J., Juan Pablo de Rivero Vaccari, Gordon A. Dale, Robert W. Keane, and Helen M. Bramlett. 2011. “Heightened Inflammation Activation Is Linked to Age-Related Cognitive Impairment in Fischer 344 Rats.” *BMC Neuroscience* 12 (December): 123.

Mazure, Carolyn M., and Joel Swendsen. 2016. “Sex Differences in Alzheimer’s Disease and Other Dementias.” *Lancet Neurology*.

McKenna, Mary C., Gerald A. Dienel, Ursula Sonnewald, Helle S. Waagepetersen, and Arne Schousboe. 2012. “Chapter 11 - Energy Metabolism of the Brain.” In *Basic Neurochemistry (Eighth Edition)*, edited by Scott T. Brady, George J. Siegel, R. Wayne Albers, and Donald L. Price, 200–231. New York: Academic Press.

Mehra, Divy, and Majid Moshirfar. 2020. “Neuroanatomy, Optic Tract.” In *StatPearls*. Treasure Island (FL): StatPearls Publishing.

Mortera, Priscilla, and Suzana Herculano-Houzel. 2012. “Age-Related Neuronal Loss in the Rat Brain Starts at the End of Adolescence.” *Frontiers in Neuroanatomy* 6 (October): 45.

Narvacan, Karl, Sarah Treit, Richard Camicioli, Wayne Martin, and Christian Beaulieu. 2017. “Evolution of Deep Gray Matter Volume across the Human Lifespan.” *Human Brain Mapping* 38 (8): 3771–90.

Neuwirth, Erich. 2014. “RColorBrewer: ColorBrewer Palettes.” <https://CRAN.R-project.org/package=RColorBrewer>.

Oberg, Johanna, Christian Spenger, Fu-Hua Wang, Anders Andersson, Eric Westman, Peter Skoglund, Dan Sunnemark, et al. 2008. “Age Related Changes in Brain Metabolites Observed by 1H MRS in APP/PS1 Mice.” *Neurobiology of Aging* 29 (9): 1423–33.

Okada Kana, and Okaichi Hiroshige. 2006. “[The functional cooperation of the hippocampus and anterior thalamus via the fimbria-fornix in spatial memory in rats].” *Shinrigaku kenkyu: The Japanese journal of psychology* 77 (3): 261–70.

Osterlund, M. K., and Y. L. Hurd. 2001. “Estrogen Receptors in the Human Forebrain and the Relation to Neuropsychiatric Disorders.” *Progress in Neurobiology* 64 (3): 251–67.

Otsu, N. 1979. “A Threshold Selection Method from Gray-Level Histograms.” *IEEE Transactions on Systems, Man, and Cybernetics* 9 (1): 62–66.

Pfefferbaum, Adolf, Torsten Rohlfing, Margaret J. Rosenbloom, Weiwei Chu, Ian M. Colrain, and Edith V. Sullivan. 2013. “Variation in Longitudinal Trajectories of Regional Brain Volumes of Healthy Men and Women (ages 10 to 85 Years) Measured with Atlas-Based Parcellation of MRI.” *NeuroImage* 65 (January): 176–93.

Qiu, Lily R., Darren J. Fernandes, Kamila U. Szulc-Lerch, Jun Dazai, Brian J. Nieman, Daniel H. Turnbull, Jane A. Foster, Mark R. Palmert, and Jason P. Lerch. 2018. “Mouse MRI Shows Brain Areas Relatively Larger in Males Emerge before Those Larger in Females.” *Nature Communications* 9 (1): 2615.

Qiu, Lily R., Jürgen Germann, Shoshana Spring, Christina Alm, Dulcie A. Vousden, Mark R. Palmert, and Jason P. Lerch. 2013. “Hippocampal Volumes Differ across the Mouse Estrous Cycle, Can Change within 24 Hours, and Associate with Cognitive Strategies.” *NeuroImage* 83 (December): 593–98.

Raz, Naftali, Paolo Ghisletta, Karen M. Rodrigue, Kristen M. Kennedy, and Ulman Lindenberger. 2010. “Trajectories of Brain Aging in Middle-Aged and Older Adults: Regional and Individual Differences.” *NeuroImage* 51 (2): 501–11.

- Raz, Naftali, Ulman Lindenberger, Karen M. Rodrigue, Kristen M. Kennedy, Denise Head, Adrienne Williamson, Cheryl Dahle, Denis Gerstorff, and James D. Acker. 2005. "Regional Brain Changes in Aging Healthy Adults: General Trends, Individual Differences and Modifiers." *Cerebral Cortex* 15 (11): 1676–89.
- Raz, Naftali, and Karen M. Rodrigue. 2006. "Differential Aging of the Brain: Patterns, Cognitive Correlates and Modifiers." *Neuroscience and Biobehavioral Reviews* 30 (6): 730–48.
- R Core Team. 2020. "R: A Language and Environment for Statistical Computing." Vienna, Austria: R Foundation for Statistical Computing. <https://www.R-project.org/>.
- Reichel, J. M., B. T. Bedenk, M. Czisch, and C. T. Wotjak. 2017. "Age-Related Cognitive Decline Coincides with Accelerated Volume Loss of the Dorsal but Not Ventral Hippocampus in Mice." *Hippocampus* 27 (1): 28–35.
- Rollins, Colleen P. E., Daniel Gallino, Vincent Kong, Gülebru Ayranci, Gabriel A. Devenyi, Jürgen Germann, and M. Mallar Chakravarty. 2019. "Contributions of a High-Fat Diet to Alzheimer's Disease-Related Decline: A Longitudinal Behavioural and Structural Neuroimaging Study in Mouse Models." *NeuroImage. Clinical* 21: 101606.
- Rudow, Gay, Richard O'Brien, Alena V. Savonenko, Susan M. Resnick, Alan B. Zonderman, Olga Pletnikova, Laura Marsh, et al. 2008. "Morphometry of the Human Substantia Nigra in Ageing and Parkinson's Disease." *Acta Neuropathologica* 115 (4): 461–70.
- Ruigrok, Amber N. V., Gholamreza Salimi-Khorshidi, Meng-Chuan Lai, Simon Baron-Cohen, Michael V. Lombardo, Roger J. Tait, and John Suckling. 2014. "A Meta-Analysis of Sex Differences in Human Brain Structure." *Neuroscience and Biobehavioral Reviews* 39 (February): 34–50.
- Sandner, Guy, Marie-Josée Angst, Thierry Guiberteau, Blandine Guignard, and David Brasse. 2010. "MRI and X-Ray Scanning Images of the Brain of 3-, 6- and 9-Month-Old Rats with Bilateral Neonatal Ventral Hippocampus Lesions." *NeuroImage* 53 (1): 44–50.
- Scahill, Rachael I., Chris Frost, Rhian Jenkins, Jennifer L. Whitwell, Martin N. Rossor, and Nick C. Fox. 2003. "A Longitudinal Study of Brain Volume Changes in Normal Aging Using Serial Registered Magnetic Resonance Imaging." *Archives of Neurology* 60 (7): 989–94.
- Shetty, A. K., and D. A. Turner. 1999. "Vulnerability of the Dentate Gyrus to Aging and Intracerebroventricular Administration of Kainic Acid." *Experimental Neurology* 158 (2): 491–503.
- Shetty, Geetha A., Bharathi Hattiangady, and Ashok K. Shetty. 2013. "Neural Stem Cell- and Neurogenesis-Related Gene Expression Profiles in the Young and Aged Dentate Gyrus." *Age* 35 (6): 2165–76.
- Sholl, S. A., and K. L. Kim. 1990. "Aromatase, 5-Alpha-Reductase, and Androgen Receptor Levels in the Fetal Monkey Brain during Early Development." *Neuroendocrinology* 52 (1): 94–98.
- Sled, J. G., and G. B. Pike. 1998. "Standing-Wave and RF Penetration Artifacts Caused by Elliptic Geometry: An Electrodynamics Analysis of MRI." *IEEE Transactions on Medical Imaging* 17 (4): 653–62.
- Small, Scott A., Monica K. Chawla, Michael Buonocore, Peter R. Rapp, and Carol A. Barnes. 2004. "Imaging Correlates of Brain Function in Monkeys and Rats Isolates a Hippocampal Subregion Differentially Vulnerable to Aging." *Proceedings of the National Academy of Sciences of the United States of America* 101 (18): 7181–86.
- Sowell, Elizabeth R., Paul M. Thompson, and Arthur W. Toga. 2004. "Mapping Changes in the Human Cortex throughout the Span of Life." *The Neuroscientist: A Review Journal Bringing*

- Neurobiology, Neurology and Psychiatry* 10 (4): 372–92.
- Spring, Shoshana, Jason P. Lerch, and R. Mark Henkelman. 2007. “Sexual Dimorphism Revealed in the Structure of the Mouse Brain Using Three-Dimensional Magnetic Resonance Imaging.” *NeuroImage* 35 (4): 1424–33.
- Spring, Shoshana, Jason P. Lerch, Monica K. Wetzel, Alan C. Evans, and R. Mark Henkelman. 2010. “Cerebral Asymmetries in 12-Week-Old C57Bl/6J Mice Measured by Magnetic Resonance Imaging.” *NeuroImage* 50 (2): 409–15.
- Sullivan, Edith V., Margaret Rosenbloom, Kathleen L. Serventi, and Adolf Pfefferbaum. 2004. “Effects of Age and Sex on Volumes of the Thalamus, Pons, and Cortex.” *Neurobiology of Aging* 25 (2): 185–92.
- Sumiyoshi, Akira, Hiroi Nonaka, and Ryuta Kawashima. 2017. “Sexual Differentiation of the Adolescent Rat Brain: A Longitudinal Voxel-Based Morphometry Study.” *Neuroscience Letters* 642 (March): 168–73.
- Tullo, Stephanie, Raihaan Patel, Gabriel A. Devenyi, Alyssa Salaciak, Saashi A. Bedford, Sarah Farzin, Nancy Wlodarski, et al. 2019. “MR-Based Age-Related Effects on the Striatum, Globus Pallidus, and Thalamus in Healthy Individuals across the Adult Lifespan.” *Human Brain Mapping* 40 (18): 5269–88.
- Tustison, Nicholas J., Brian B. Avants, Philip A. Cook, Yuanjie Zheng, Alexander Egan, Paul A. Yushkevich, and James C. Gee. 2010. “N4ITK: Improved N3 Bias Correction.” *IEEE Transactions on Medical Imaging* 29 (6): 1310–20.
- Tustison, Nicholas J., Philip A. Cook, Arno Klein, Gang Song, Sandhitsu R. Das, Jeffrey T. Duda, Benjamin M. Kandel, et al. 2014. “Large-Scale Evaluation of ANTs and FreeSurfer Cortical Thickness Measurements.” *NeuroImage* 99 (October): 166–79.
- Valdés-Hernández, Pedro Antonio, Akira Sumiyoshi, Hiroi Nonaka, Risa Haga, Eduardo Aubert-Vásquez, Takeshi Ogawa, Yasser Iturria-Medina, Jorge J. Riera, and Ryuta Kawashima. 2011. “An in Vivo MRI Template Set for Morphometry, Tissue Segmentation, and fMRI Localization in Rats.” *Frontiers in Neuroinformatics* 5 (November): 26.
- Vincent, Robert D., Peter Neelin, Najmeh Khalili-Mahani, Andrew L. Janke, Vladimir S. Fonov, Steven M. Robbins, Leila Baghdadi, et al. 2016. “MINC 2.0: A Flexible Format for Multi-Modal Images.” *Frontiers in Neuroinformatics* 10 (August): 35.
- Walhovd, Kristine B., Anders M. Fjell, Ivar Reinvang, Arvid Lundervold, Anders M. Dale, Dag E. Eilertsen, Brian T. Quinn, David Salat, Nikos Makris, and Bruce Fischl. 2005. “Effects of Age on Volumes of Cortex, White Matter and Subcortical Structures.” *Neurobiology of Aging* 26 (9): 1261–70; discussion 1275–78.
- Welniak-Kaminska, Marlena, Michal Fiedorowicz, Jaroslaw Orzel, Piotr Bogorodzki, Klaudia Modlinska, Rafal Stryjek, Anna Chrzanowska, Wojciech Pisula, and Pawel Grieb. 2019. “Volumes of Brain Structures in Captive Wild-Type and Laboratory Rats: 7T Magnetic Resonance in Vivo Automatic Atlas-Based Study.” *PloS One* 14 (4): e0215348.
- Wen, Tong-Chun, Anil Sindhurakar, Violeta Contreras Ramirez, Honggeun Park, Disha Gupta, and Jason B. Carmel. 2019. “Targeted Infarction of the Internal Capsule in the Rat Using Microstimulation Guidance.” *Stroke; a Journal of Cerebral Circulation* 50 (9): 2531–38.
- Wickham, Hadley, Mara Averick, Jennifer Bryan, Winston Chang, Lucy McGowan, Romain François, Garrett Grolemond, et al. 2019. “Welcome to the Tidyverse.” *Journal of Open Source Software* 4 (43): 1686.
- Wickham, Hadley, and Jennifer Bryan. 2019. “Readxl: Read Excel Files.” <https://CRAN.R-project.org/package=readxl>.

Wisse, Laura E. M., Geert Jan Biessels, Sophie M. Heringa, Hugo J. Kuijf, Dineke H. L. Koek, Peter R. Luijten, Mirjam I. Geerlings, and Utrecht Vascular Cognitive Impairment (VCI) Study Group. 2014. "Hippocampal Subfield Volumes at 7T in Early Alzheimer's Disease and Normal Aging." *Neurobiology of Aging* 35 (9): 2039–45.

CHAPTER 5: NEUROCHEMICAL AND COGNITIVE CHANGES PRECEDE STRUCTURAL ABNORMALITIES IN THE TGF344-AD RAT MODEL

5.1 Preface

The work presented in **Chapter 5** is a comprehensive longitudinal analysis of multiple pathological features in the TgF344-AD rat model of Alzheimer's disease. This rat model is unique in its ability to spontaneously develop tau pathology without insertion of a human tau transgene, and thus more closely replicates how the disease occurs in humans than most other rodent models. Despite the model being studied extensively since its emergence in 2013, we are the first to characterize disease-dependent changes in neuroanatomy and the full neurochemical profile, and ours is the earliest assessment of cognitive function. This multimodal testing approach, applied at 4, 10, and 16 months, allowed us to determine the relative timing of the appearance and progression of neuroanatomical, neurochemical, and cognitive abnormalities in this model. These results contribute to the accurate staging of disease progression in the TgF344-AD rat, a necessary step towards improving diagnosis methods and designing appropriate treatment, particularly given the converging consensus on early as opposed to late intervention.

In addition, we examined the intersection between sex and pathology on neuroimaging and cognitive markers. While few significant effects were detected, the intentional statistical analysis of sex-dependent differences represents one of few performed in this model and is a consideration often overlooked in preclinical studies. Intentional inclusion of males and females is of particular importance in preclinical AD research given the documented differences between men and women in disease manifestation and progression.

Overall, the findings in this chapter support the use of MRI and MRS for the development of non-invasive biomarkers of AD progression, clarify the timing of pathological feature presentation in the TgF344-AD model, and advance the validation of the TgF344-AD rat as a highly relevant model for preclinical AD research, all of which represent significant contributions to the scientific community.

Neurochemical and cognitive changes precede structural abnormalities in the TgF344-AD rat model

Caitlin F. Fowler^{*a,b}, Dana Goerzen^b, Gabriel A. Devenyi^{b,c}, Dan Madularu^{b,c,d}, Katrina Cruickshank^{b,e}, Augustine Vinh-Phuc Pham^{b,e}, Kristin Ellerbeck^{b,f}, Kristi Drudik^{b,e}, Naguib Mechawar^{c,g}, Maria Antonietta Davoli^g, M. Mallar Chakravarty^{a,b,c}, Jamie Near^{a,b,c,h,i}

^a Department of Biological and Biomedical Engineering, McGill University, Montreal, QC, Canada.

^b Centre d'Imagerie Cérébrale, Douglas Mental Health University Institute, Verdun, QC, Canada.

^c Department of Psychiatry, McGill University, Montreal, QC, Canada.

^d Center for Translational NeuroImaging, Northeastern University, Boston, MA, USA.

^e Department of Neuroscience, McGill University, Montreal, QC, Canada

^f Department of Physiology, McGill University, Montreal, QC, Canada

^g McGill Group for Suicide Studies, Douglas Mental Health University Institute, Verdun, QC, Canada

^h Physical Sciences Platform, Sunnybrook Research Institute, Toronto, ON, Canada

ⁱ Department of Medical Biophysics, University of Toronto, Toronto, ON, Canada

Modified version published in Brain Communications: <https://doi.org/10.1093/braincomms/fcac072>

5.2 Manuscript Information

Funding

This research was supported by the Canadian Institutes of Health Research (PJT-148751) and the Fonds de la Recherche en Santé du Québec (Chercheur boursiers # 0000035275). C.F.F. is supported by funding provided by McGill University's Faculty of Medicine Internal Studentship and Healthy Brains for Healthy Lives Doctoral Fellowship.

Declaration of Interests

The authors disclose no conflicts of interest.

5.3 Abstract

Alzheimer's disease is a progressive neurodegenerative disorder with a decades-long pre-symptomatic phase, substantiating the need for prodromal biomarker development and early intervention. To deconstruct the processes underlying disease progression and identify potential biomarkers, we used neuroimaging techniques with high translational potential to human clinical studies in the TgF344-AD rat model which recapitulates the full spectrum of Alzheimer's neuropathology (progressive amyloid deposition, tauopathy, frank neuronal loss, gliosis, and cognitive dysfunction). We employed longitudinal magnetic resonance imaging (MRI) and spectroscopy (MRS) in conjunction with behavioural testing to characterize multiple facets of disease pathology in male and female TgF344-AD rats (n=26, 14M/12F) relative to wildtype littermates (n=24, 12M/12F). Testing was performed at 4-, 10-, 16-, and 18-months, covering much of the adult rat lifespan and multiple stages of disease progression. Immunofluorescence experiments were performed at 18-months of age to probe the relationship between tissue pathological load, neuroimaging markers, and cognition. The TgF344-AD model demonstrated impaired spatial reference memory in the Barnes Maze by 4 months of age, followed by neurochemical abnormalities by 10 months and major structural changes by 16 months. These included increased total choline and lactate, and decreased total creatine, taurine, and N-acetylaspartate to myo-inositol ratio, dentate gyrus hypertrophy, and atrophy in the hippocampus, hypothalamus, and nucleus accumbens. Immunofluorescence experiments indicated that major neuroimaging markers (N-acetylaspartate, myo-inositol, hippocampal volume) and behavioural testing outcome metrics did not correlate with neuronal or microglial cell counts. This suggests that change in cellular function (as opposed to structure or density) may underlie neurochemical and cognitive abnormalities, and that altered regional volumes may be better reflected by morphological characteristics other than cell count. Overall, these findings support the use of MRI and MRS for the development of non-invasive biomarkers of disease progression, clarify the timing of pathological feature presentation in this model, and contribute to the validation of the TgF344-AD rat as a highly relevant model for preclinical Alzheimer's disease research.

5.4 Introduction

Alzheimer's disease is a progressive neurodegenerative disorder that accounts for 60-80% of the 50 million dementia cases worldwide (Patterson 2018). Aspects of Alzheimer's pathology can occur decades before clinical onset (Clifford R. Jack Jr et al. 2010, 2013; Bateman et al. 2012), substantiating the need for prodromal biomarker development and early intervention.

Early-stage disease characterization in transgenic animal models represents one promising avenue towards the development of new biomarkers and intervention approaches at a clinical level. The most common transgenic models are rodents expressing human genes harbouring mutations known to drive amyloid- β accumulation and cause familial or early-onset Alzheimer's disease in humans, such as presenilin-1 (*PS1*), presenilin-2 (*PS2*), and amyloid precursor protein (*APP*) (Drummond and Wisniewski 2017; Do Carmo and Cuellar 2013; Dennis J. Selkoe 2011). Amyloid- β -overproducing rodents are considered “gold standard” models but most do not display robust tauopathy or neuronal loss—two major hallmarks of Alzheimer's disease—unless additional human transgenes are expressed that are not associated with familial Alzheimer's disease (typically microtubule-associated protein tau, *MAPT* (Dennis J. Selkoe 2011; Lewis et al. 2001)), as is the case with the widely used 3xTg mouse (Oddo et al. 2003).

To date, one of the only rodent models to recapitulate the full spectrum of Alzheimer's disease neuropathology without insertion of a human tau transgene is the TgF344-AD rat which displays progressive amyloid- β deposition, tauopathy, gliosis, neuronal loss, and cognitive impairment, despite only expressing mutant human *APP* (*APP*^{swe}, KM670/671NL) and *PS1* (Δ E9) genes (Cohen et al. 2013). Not only does the TgF344-AD model represent a major advancement for Alzheimer's disease research, but the numerous advantages of studying rats over mice—they are physiologically and genetically closer to humans, display a richer behavioural phenotype, and have larger brains (Ellenbroek and Youn 2016)—make the TgF344-AD rat a particularly salient option for preclinical biomarker development.

Magnetic resonance (MR) techniques such as MR Imaging (MRI) and Spectroscopy (MRS) enable non-invasive, longitudinal assays of brain structure and tissue chemistry at the preclinical and clinical level (Gao and Barker 2014; Frisoni et al. 2010; Mueller, Schuff, and Weiner 2006). MRI studies have identified reduced cortical thickness and atrophy of the medial temporal lobe as prominent features of Alzheimer's disease in human subjects (Frisoni et al. 2010; Pini et al. 2016)

that may precede clinical diagnosis (C. R. Jack Jr et al. 2005; van de Pol et al. 2007). Similar studies in transgenic models have replicated some of these findings (Lau et al. 2008; Kong et al. 2018; Badhwar et al. 2013; Spencer et al. 2013; Maheswaran et al. 2009). Proton MRS studies in rodent models of Alzheimer's disease have identified altered brain metabolic profiles, including reduced N-acetylaspartate (NAA) and glutamate (Glu), and increased myo-inositol (Ins), glutamine (Gln), and total choline (tCho) (Dedeoglu et al. 2004; Choi et al. 2014; Marjanska et al. 2005; Nilsen et al. 2012). These changes parallel those observed in human Alzheimer's patients (Marjańska et al. 2019; Murray et al. 2014). while also informing on physiological processes involved in disease pathogenesis, including neuronal viability, cell membrane turnover, antioxidant capacity, neuroinflammation, energy metabolism, and neurotransmission (McKenna et al. 2012; Ross and Sachdev 2004). Despite the relevance of MRI and MRS in Alzheimer's disease research, few studies have simultaneously examined the longitudinal progression of anatomical, neurochemical, and cognitive changes in either rodent models or humans. As such, a gap in knowledge exists regarding the relative timing of the appearance of these pathological features, limiting the understanding of disease stages and subsequent design of therapeutic approaches.

The primary aim of this study was to characterize the manifestation and time course of pathological change in neuroimaging biomarkers and cognition in the TgF344-AD rat model *in vivo*. We employed MRI, MRS, and Barnes Maze testing at 4-, 10-, 16-, and 18-months of age to distinguish longitudinal changes in neuroanatomy, neurochemistry, and cognitive function in male and female TgF344-AD rats relative to wildtype littermates. Immunofluorescence experiments were performed at 18-months to probe the relationship between tissue pathological load, neuroimaging markers of disease progression, and behavioural metrics.

5.5 Materials and Methods

5.5.1 Animal care and study design

The TgF344-AD model (Tg) is a double transgenic line created on a Fischer 344 background that expresses the “Swedish” mutant human *APP* (*APP^{swe}: APP KM670/671NL*) and deletion of exon 9 mutant of human *PS1* (*PS1ΔE9*). Male hemizygous TgF344-AD rats (Terrence Town Laboratory, University Southern California) and female homozygous Fischer 344/NHsd wildtype rats (Envigo, Madison, WI, United States) were bred in-house. Offspring were a mixture of

hemizygous Tg and homozygous wildtype (WT) rats. Tail snips were obtained from each rat to identify the presence of the *APP^{swE}* and *PS1 Δ E9* transgenes (genotyping by Transnetyx, Memphis, TN). Rats were weaned on postnatal day 21 and housed in same-sex pairs on a 12 hour light-dark cycle with *ad libitum* access to food (Envigo, Teklad Global 18% Protein Rodent Diet) and water. All animal procedures and experiments were performed in accordance with the guidelines of the local institutional Animal Care Committee.

24 WT rats (12M/12F) and 26 Tg rats (14M/12F) were studied longitudinally, with Barnes Maze testing and neuroimaging performed at 4-, 10-, 16-, and 18-months of age. Behavioural testing was performed prior to neuroimaging to avoid confounds of anesthesia on behaviour. Sample size calculations were performed using a population simulation-based power analysis tool (J. P. Lerch et al. 2012) and can be found in the **Supplementary Methods 5.9.1**. Group sizes at each time point are included in **Supplementary Table 5.10.1**. We also present an exploratory analysis of the intersecting effect of genotype and sex on neuroimaging and behavioural markers.

7 WT rats (4M/3F) and 6 Tg rats (3M/3F) were sacrificed for immunofluorescence experiments at 18 months, after completion of longitudinal testing. One additional Tg rat (1M) was also included that had been part of a parallel paradigm where rats were aged but did not complete neuroimaging or behavioural testing. Sex was only employed as a covariate for histological analyses due to the small group sizes and non-longitudinal design.

5.5.2 MRI data acquisition and regional volume estimation

MRI data were acquired using a 7 Tesla Bruker Biospec 70/30 scanner (Bruker, Billerica, MA, United States) with an 86 mm (diameter) volumetric birdcage coil for transmission and a four-channel surface array coil for signal reception (Bruker). The level of anesthesia (1-4% isoflurane in oxygen gas) was adjusted to maintain a breathing rate between 50-75 breaths per minute throughout the procedure and warm air (37 °C) was blown into the bore of the scanner to maintain a constant body temperature (SA Instruments, Inc., monitoring system, Stony Brook, NY, United States).

High-resolution 3D anatomical MR images were acquired using Rapid Acquisition with Relaxation Enhancement (RARE) using scan parameters identical to those described previously (C. Fowler, Goerzen, Madularu, Devenyi, Chakravarty, et al. 2021; Goerzen et al. 2020). Scan resolution was 114 μ m isotropic. All pre-processing methodology is described in detail elsewhere (C. Fowler, Goerzen, Madularu, Devenyi, Mallar Chakravarty, et al. 2021) and in the

Supplementary Methods 5.9.2. After pre-processing, images were examined for motion artefacts, Gibbs ringing artefacts, and other image anomalies, following which 15 of a total 179 scans were excluded from further analysis. 7 rats (4Tg (1M/3F), 3 WT (2M/1F)) were excluded at 4-months, 1 at 10-months (1TgM), and 5 at 16-months (3Tg (1M/2F), 2WT (1M/1F)). The remaining 164 scans were co-registered using the two-level deformation-based morphometry pipeline in Pydipper, as described by Friedel et al., (Friedel et al. 2014) and in the **Supplementary Methods 5.9.2**. This process creates deformation fields for each subject at each timepoint, reflecting the amount of expansion or compression required to deform each individual anatomical image to the subject average (Chung et al. 2001). Deformation fields are then resampled into the common study space allowing comparison between subjects. The Fischer 344 rat atlas was used to estimate the volume of 120 regions (J. Lerch et al. 2017).

5.5.3 ¹H-MRS data acquisition and quantification

Immediately following MRI data acquisition, MRS data acquisition was performed using the same methodology as described previously (C. F. Fowler et al. 2020). Automated localized shimming was performed using the FASTMAP method (Gruetter 1993) (ParaVision 5.1, Bruker). Proton MRS scans were acquired from a 2.5x3.5x3.5 mm³ voxel in the dorsal hippocampus using a Point RESsolved Spectroscopy sequence (acquisition time=13m0s0ms, TR=3000 ms, TE=11.12 ms, 2048 acquisition data points, spectral width=4006 Hz) in combination with outer volume suppression. 256 averages were acquired with VAPOR water suppression (Tkac̆ et al. 1999) and 8 averages were acquired without water suppression for eddy current correction and as a reference for absolute metabolite quantification.

Spectral preprocessing was performed in the FID-A toolbox (github.com/CIC-methods/FID-A, version 1.0 (Simpson et al. 2017)) in Matlab (R2012a, The MathWorks, Inc., Natick, MA, USA), and consisted of removal of motion corrupted scans and spectral registration to correct frequency and phase drift errors (Simpson et al. 2017). Processed spectra were analyzed using LCMoDel (version 6.3, Stephen Provencher Inc, Oakville, Ontario, Canada), with a neurochemical basis set consisting of 18 simulated metabolite resonances and 9 macromolecule basis functions. Methods detailing the acquisition of macromolecule spectra for parameterization and inclusion into the quantification basis set are described elsewhere (C. F. Fowler et al. 2020).

Absolute quantification was performed using the unsuppressed water signal as a reference. A correction was applied to account for T1 and T2 relaxation constants of water and measured neurochemicals, and an assumed NMR-visible water concentration of 4300 mM given that our voxel contained mostly grey matter.(Ernst, Kreis, and Ross 1993) For details on the correction formula, see the supplementary material in our previous publication (C. F. Fowler et al. 2020). Neurochemical concentrations are reported in mmol/L (mM). Details regarding the basis set and quality control methods are included in the **Supplementary Methods 5.9.3**.

5.5.4 Behavioural phenotyping via the Barnes Maze test

We assessed hippocampus-dependent spatial reference memory using a shortened variation (Attar et al. 2013) of the popular Barnes Maze protocol (Barnes 1979). Detailed methodology is described in the **Supplementary Methods 5.9.4**. Briefly, a circular maze with 20 holes was used, and rats were trained to locate a single escape hole that led to a box underneath. Rats were given three 3-minute trials on Day 1 and two 3-minute trials on Day 2, for a total of five training trials. A probe trial was used to test long term spatial reference memory. The probe trial was conducted 48 hours after the last training trial and involved blocking the escape hole so that no escape was possible. All sessions were recorded using a Logitech QuickCam Pro 9000. The following metrics were measured during the probe trial using EthoVision XT Software (Noldus Information Technology, Wageningen, The Netherlands): % time in target quadrant, % time in target holes, success or failure to locate the escape hole, average speed (cm/s), and number of holes searched.

5.5.5 Immunofluorescence experiments and stereology

50 μm sections from 7 WT and 7 Tg rats at 18-months were collected throughout the hippocampus (1.20 mm through -7.30 Bregma) and stored in cryoprotectant solution at -20°C . Every eighth hippocampal section was selected to be stained and used for stereology for a total of 10 sections, as this volume ($\sim 3.5\text{mm}$) best approximated the voxel used for MRS data acquisition. Staining for microglia and mature neurons was performed simultaneously using neuron-specific neuronal nuclear protein (NeuN) and ionized calcium-binding adaptor molecule-1 (Iba1), respectively. Sections were then mounted and stained with Thioflavin-S (ThioS), which binds to the characteristic β -pleated sheet conformation of amyloid, directly detecting amyloid- β plaques

(Rajamohamedsait and Sigurdsson 2012). Immunofluorescence was imaged on a ZEISS Axio Imager M.2 with an MBF Bioscience microscope stage and Apotome 2. Stereology for cell counts and % plaque volume was performed using the Optical Fractionator probe and the Area Fraction Fractionator probe, respectively. Details for perfusion procedures, reagents, and imaging/stereology are in the **Supplementary Methods 5.9.5**.

5.5.6 Statistical analysis

Statistical analyses and visualizations were performed in R (version 3.6.3(R Core Team 2020)). Brain volume and metabolite concentration data were modelled using linear mixed-effects models as they appropriately model the covariance structure resulting from repeated measurements in the same subjects and handle data with missing values (Bernal-Rusiel et al. 2013). Brain volumes were predicted by a quadratic-age-by-genotype interaction (model 1), and metabolite concentrations were predicted by a linear age-by-genotype interaction (model 2), with sex covaried and a random intercept for each subject. Genotype effects were evaluated as a group effect of Tg rats relative to WT rats at each time point using four age-centered models, with age centered at the average cohort age (129.6, 310.7, 494.3, and 572.9 days). All continuous variables were z-scored. For MRS data, the fixed effect of water linewidth was included to control for the effect of linewidth on metabolite concentration estimates (Bartha 2007). A weighting factor of the inverse absolute CRLB for each metabolite accounted for differences in fitting reliability between samples. We also examined a three-way interaction of age by genotype by sex with the same covariates as mentioned above for brain volumes (model 3) and metabolite concentrations (model 4).

For all linear models, the False Discovery Rate (FDR) method (Benjamini and Hochberg 1995) was used to control the family-wise type I error at a level of 5% for each predictor of interest. Details on attached base packages in R, Akaike information criterion comparisons and linear models 1 through 4 are included in the **Supplementary Methods 5.9.6**.

Barnes Maze data were analyzed cross-sectionally. % success, number of holes searched, and speed were analyzed using a linear model with genotype as a fixed effect and sex covaried, or genotype and sex interacting (secondary analysis). % time in the target quadrant and % time in target holes were assessed using a one-sample t-test or a wilcoxon signed rank test (if test residuals were non-normal) against a mean of 25% (chance amount of time) within WT and Tg rats, as well as for genotypes split by sex (WT males, WT females, Tg males, and Tg females). Bonferroni

correction was applied at each time point for the primary and secondary analyses separately, whereby the p-value threshold was set at 0.05/7 tests ($P < 0.00714$) or 0.05/11 tests ($P < 0.00455$), respectively.

Counts of NeuN and Iba1 at 18-months were analyzed using a linear model with genotype as a fixed effect, covarying for sex, age at sacrifice, paradigm, and time between staining and imaging. Bonferroni correction was applied with a significance threshold of $P < 0.025$ (0.05/2 markers).

Spearman's rank correlations between tissue pathological markers (microglial and neuronal cell counts), neuroimaging markers (hippocampus and dentate gyrus volumes, concentrations of Ins, NAA, NAA/Ins, tCho, Tau), and behavioural metrics (% time in target quadrant, % time in target holes). Bonferroni correction was applied across the 18 tests (0.05/18tests, $P < 0.0028$).

5.5.7 Data Availability

Data are reported within the text, figures, and Supplementary material. Raw data will be published to the publicly available repository, Zenodo, upon acceptance of this manuscript.

5.6 Results

5.6.1 TgF344-AD rats display altered local brain volume, primarily in grey matter structures

Volume changes for the age-by-genotype interaction term of model 1 are illustrated as t-statistic maps in **Figure 5.8.1A** for voxel-wise (**left**) and regional (**right**) analyses. Significant effects were generally consistent between the two methods and the majority were bilateral. As summarized in **Supplementary Table 5.10.2**, 27 of 120 regions demonstrated significant linear age by genotype interactions, 19 of which occurred in grey matter (GM) regions, 7 in white matter (WM) regions, and one in the ventricular system. Most interactions (16 of 19 for GM, 5 of 7 for WM) were negative, indicating decreased volume with age in Tgs relative to WTs. The strongest interactions were atrophy in the basal forebrain, caudoputamen, fimbria, hippocampus, and nucleus accumbens, unilateral atrophy in the right fornix, and hypertrophy in the dentate gyrus. Weaker effects were present as increases in cerebellar white matter and aqueduct volume, and decreased ventral pallidum, lateral septum, and hypothalamus volume. The basal forebrain was the only

structure to demonstrate a significant quadratic interaction, indicating different curvilinearity in the volume trajectory of Tg rats relative to WT. Whole-brain GM, WM, and CSF volumes were also quantified but did not differ by genotype.

Four age-centered models examining the main effect of genotype at each time point were used to provide group difference snapshots of the timeline along which structural changes occur in the TgF344-AD model. As shown in **Supplementary Table 5.10.2**, volume differences between WTs and Tgs were present at 4-months for the aqueduct, caudoputamen, dentate gyrus, nucleus accumbens, and fimbria. Hippocampal atrophy was not significant until 16 and 18 months of age and was preceded by a period of marginally increased volume relative to WTs. Volume trajectories for selected structures are shown in **Figure 5.8.1B**.

Figure 5.8.1C shows trajectories for several structures split by sex and depicts results from the analysis using a three-way interaction between quadratic age, genotype, and sex (model 2) to predict regional volume. Linear age-by-genotype-by-sex interaction terms for the right caudoputamen and left hypothalamus were positive and negative, respectively, and the left dentate gyrus demonstrated a positive quadratic age-by-genotype-by-sex effect. However, neither these effects nor any other structures evaluated with model 2 survived FDR correction.

A summary of linear model results for brain regions analyzed using model 1 and 2 is shown in **Supplementary Table 5.10.2**. Brain volumes in mm³ at each timepoint, both collapsed across and split by sex, are summarized in **Supplementary Table 5.10.3**. Trajectories of brain structures showing a significant age by genotype interaction via model 1 can be found in **Supplementary Fig. 5.11.1 and 5.11.2**. Those demonstrating significant three-way interactions via model 2 (prior to FDR correction) are shown in **Supplementary Fig. 5.11.3 and 5.11.4**.

5.6.2 The TgF344-AD model recapitulates neurochemical features of human AD

27 hippocampal neurochemicals were quantified longitudinally in Tg rats relative to WT littermates. The neurochemical profile contained 9 macromolecule resonances which have yet to be quantified in this model. High quality spectra were consistently obtained, as shown by the representative spectrum obtained from a 10-month WT female (**Figure 5.8.2, inset**), and by the low % CRLB values shown in **Supplementary Table 5.10.4**. The average signal-to-noise ratio of the NAA peak at 2.02 ppm was 61.77 (± 13.96 (\pm standard deviation), range: 24.51 to 107.35), and the

average linewidth of water was 9.21 Hz (\pm 0.73, range: 7.74 to 12.79; measured as the full width at half max of the unsuppressed water peak in the reference scan).

The primary analysis explored the interaction between linear age and genotype while controlling for sex (model 3). As shown in **Supplementary Table 5.10.4** and **Figure 5.8.2A**, tCho and Ins demonstrated significant positive age-by-genotype interactions, whereby metabolite concentration increased more steeply with age in Tg rats than in WT rats, but did not survive FDR correction. Upon examining the main effect of genotype at each time point using age-centered models, several metabolites differed between WT and Tg rats, with the earliest differences detected at 10 months. Total creatine (tCr), taurine (Tau), and the ratio of NAA to Ins (NAA/Ins) were decreased in Tg rats at 10 months of age and remained lower at 16 and 18 months, whereas the ratio of aspartate (Asp) to Glu (Asp/Glu) was significantly lower at 10 months only. NAA was significantly lower at 10, 16, and 18 months but not after FDR correction. Higher concentrations of Lactate (Lac) and tCho were evident at 10, 16, and 18 months, while Ins was significantly higher in Tg rats only at 16 and 18 months of age. None of the macromolecule peaks differed between Tg and WT rats.

A secondary analysis explored a three-way interaction between age, genotype, and sex (model 4). Both glucose (Glc) and Ins demonstrated three-way interactions but were not significant after FDR correction. Neurochemical trajectories for these metabolites, along with tCho and Gln, which showed sub-threshold ($p < 0.15$) three-way interactions prior to FDR correction, are shown in **Figure 5.8.2B**. A full summary of linear model results is shown in **Supplementary Table 5.10.4**, with the concentration of each neurochemical (mM) included in **Supplementary Table 5.10.5**. Trajectories of select metabolites are shown in **Supplementary Fig. 5.11.5**.

5.6.3 The TgF344-AD rat model displays cognitive impairment by 4-months of age

Long-term spatial reference memory in Tg and WT rats was evaluated at each time point via the probe trial of the Barnes Maze test, conducted 48 hours after the last training trial. Cognitive impairment in Tg rats was evident as early as 4-months of age, as determined by testing the percentage of time WT and Tg rats spent in the target quadrant against the chance amount of time a rat would spend in each quadrant. A mean significantly above 25% is suggestive of intact spatial memory recall, which WT rats demonstrated throughout the study, while Tg rats did not meet the significance threshold at any time points (**Figure 5.8.3A(left)**). A similar effect was seen when

testing the percentage of time spent exploring holes within the target quadrant (**Figure 5.8.3B(left)**). WT rats consistently spent more than a chance amount of time exploring holes in the target quadrant, whereas Tg rats did not. Additionally, as shown in **Figure 5.8.3C(left)** the rate of success versus failure in locating the escape hole was lower among Tg rats throughout the study, though this difference was not statistically significant. The number of holes searched and average speed were also measured during the probe trial to characterize level of exploration and mobility, respectively. As shown in **Figures 5.8.3D(left) and 5.8.3E(left)**, both metrics differed between WT and Tg rats, with Tgs searching fewer holes throughout the study and moving more slowly than their WT littermates. However, after Bonferroni correction, the differences in holes searched was only significant at 10 and 16 months, while the difference in speed was only significant at 10-months.

A secondary analysis examining the interaction between genotype and sex was also performed. As shown in **Figure 5.8.3A(right)**, only WT males consistently spent significantly more than 25% of the time in the target quadrant, although the 4-month time point did not reach the significance threshold after Bonferroni correction. WT males generally also spent a higher percentage of time in the target holes than WT females, Tg males, or Tg females, but only reached the significance threshold at 16-months (**Figure 5.8.3B(right)**). Interestingly, and as shown in **Figure 5.8.3C(right) and 5.8.3D(right)**, Tg females demonstrated the lowest success rate across all timepoints, and the lowest rates of exploration (fewest holes searched) at three of four time points, though no significant genotype-by-sex interactions were found for either metric. Finally, as seen in **Figure 5.8.3E(right)**, no genotype-by-sex interactions were found for speed at any time point. All Barnes Maze statistics can be found in **Supplementary Table 5.10.6**, with summary data for each metric, split by timepoint, genotype, and sex in **Supplementary Table 5.10.7**.

5.6.4 No genotype-dependent differences detected in microglia and neuronal cell counts

Immunofluorescence experiments to quantify the number of microglia and neurons in hippocampal tissue were performed in a subset of 18-month old WT and Tg rats that had completed the longitudinal testing paradigm. % volume of plaque was calculated for Tg rats only since WT rats do not manifest amyloid pathology. While extensive amyloid pathology was present in Tg rats (**Figure 5.8.4C**), mean % area: 0.73 ± 0.24), and microglia could be seen aggregating around amyloid plaques (**Figure 5.8.4D, E**), there were no significant differences in microglial cell count

(WT $5.14E05 \pm 2.49E05$; Tg $4.89E05 \pm 3.66E05$) or neuronal cell count (WT $1.06E06 \pm 5.86E05$; Tg $8.39E05 \pm 5.54E05$) between WT and Tg rats (**Figure 5.8.4A,B**). Linear model results for microglial and neuronal counts are shown in **Supplementary Table 5.10.8**.

Spearman's rank correlations were performed between tissue pathological markers (microglial and neuronal counts), hippocampal and dentate gyrus volumes, metabolites with strong genotype-dependent effects (Ins, NAA, NAA/Ins, tCho, Tau), and behavioural metrics (% time in target quadrant, % time in target holes) at 18-months. Importantly, stereology was performed on specific slices that best approximated the voxel used for MRS. Similarly, only the hippocampus and dentate gyrus were used for correlations as they were the only regions in which stereology was performed. As shown in **Supplementary Table 5.10.9**, of the 18 correlation tests conducted, only neuronal cell count and taurine were significantly correlated but did not survive Bonferroni correction. Select correlations are shown in **Figure 5.8.4B and C iii**.

5.7 Discussion

The TgF344-AD rat is unique in its manifestation of amyloid and tau pathology despite only expressing mutant *APP* and *PS1*, and therefore closely replicates human Alzheimer's disease. Thorough characterization of the manifestation and progression of physiological abnormalities—particularly those that can be measured non-invasively—comprising each disease stage in this rat model is required for designing effective therapeutic approaches. While other authors have characterized pathological features in this model, the majority of our neuroimaging findings are being reported for the first time and ours is the earliest assessment of cognitive function. This study also explores the intersecting influence of sex and genotype on neuroimaging and behavioural markers, which is crucial for improving diagnostic methods and interventions given that Alzheimer's disease prevalence and manifestation can differ between men and women (Mazure and Swendsen 2016).

As determined via post-mortem histology studies, decreased brain volume detected via MRI is an accurate marker of Alzheimer's disease-related neurodegeneration that can be used to support a clinical diagnosis in humans (Clifford R. Jack et al. 2011; Frisoni et al. 2010; Bobinski et al. 2000). Models of human disease progression indicate early tissue pathology and atrophy in the entorhinal cortex (Braak and Braak 1995) and other regions that comprise the limbic system, particularly the hippocampus (Callen et al. 2001; Braak and Braak 1991; Clifford R. Jack et al.

2011). The TgF344-AD model does not demonstrate significant cortical atrophy by 18 months, but does recapitulate volume reductions in limbic structures, including the hippocampus, basal forebrain, fimbria, fornix, hypothalamus, and lateral septum. In opposition to dentate gyrus atrophy reported in human Alzheimer's disease (Wisse et al. 2014; Pini et al. 2016) we observed hypertrophy in the TgF344-AD model, with significantly larger volume at 16 and 18 months in Tgs relative to WTs. This is not entirely unexpected given that Fischer 344 rats display increased dentate gyrus volume during normal aging, (C. Fowler, Goerzen, Madularu, Devenyi, Mallar Chakravarty, et al. 2021; Alexander et al. 2020) and therefore further hypertrophy during Alzheimer's disease may represent a pathological feature, similar to how normal hippocampal atrophy with age is exacerbated in Alzheimer's disease (Fjell et al. 2014). Importantly, neither hippocampal nor dentate gyrus volume correlated with neuronal cell counts at 18 months, suggesting that altered regional volumes may be better reflected by morphological characteristics other than cell count. Additional structures with significant atrophy were the nucleus accumbens, caudoputamen, and ventral pallidum, all of which display amyloid and tau pathology and structural changes in human Alzheimer's disease (Pini et al. 2016; Braak and Braak 1991; de Jong et al. 2008).

Age-centered analyses revealed that while many structures atrophied faster in Tgs, this was occasionally preceded by hypertrophy. For example, Tg rats demonstrate larger caudoputamen, fimbria, and nucleus accumbens volumes until 10 months, and then smaller volumes at 16 and 18 months relative to WTs. Supporting these findings, a neuroimaging study in PS1 mutation carriers reported increased caudate volume in asymptomatic individuals but decreased volume in symptomatic individuals (Fortea et al. 2010), suggesting different processes underlie morphometric change at different stages of disease progression. Reactive neuronal hypertrophy in the hippocampal CA1 region has been shown in Alzheimer's disease subjects prior to symptom onset (Riudavets et al. 2007) supporting early regional volume increases, either as a cellular response to amyloid and tau deposition, or a compensatory process prior to degeneration of neurons and synapses. (Mattson 2004) Future work combining MRI-based volumetric analysis and design-based stereology, similar to studies in transgenic mice (West et al. 2009; Oh et al. 2009), would help fill critical gaps in knowledge regarding mechanisms underlying pathological morphometric change in the TgF344-AD model.

MRS allows for quantification of brain tissue metabolites, providing insight into the biochemical underpinnings of altered brain structure and function (Gao and Barker 2014). Similar

changes in NAA, Ins, and NAA/Ins to what we report have been shown in the TgF344-AD rat (A. M. Chaney et al. 2021), the McGill-R-Thy1-APP rat model (Nilsen et al. 2012), mouse models (Oberge et al. 2008; Marjańska et al. 2005; Güell-Bosch et al. 2020), and in human studies (Marjańska et al. 2019; Murray et al. 2014; Wang et al. 2015), Decreased NAA reflects reduced neuronal viability—specifically mitochondrial dysfunction—as opposed to purely neuronal density (McKenna et al. 2012; Ross and Sachdev 2004). The possible mechanisms behind increased Ins are more varied and may reflect increased glial cell activation and/or inflammation, increased phagocytic activity, or cellular membrane disruption, as Ins is a precursor for inositol lipid synthesis, a constituent of membrane lipids, and an osmolyte (Ross and Sachdev 2004; Best, Stagg, and Dennis 2014; Brand, Richter-Landsberg, and Leibfritz 1993). Given neither NAA or Ins correlated with neuronal or microglial counts, it is likely that disease-dependent changes in these two metabolites reflect altered cellular function as opposed to density.

Decreased Tau (taurine) in the TgF344-AD rat is in agreement with literature supporting the role of Tau in neurite outgrowth, synaptogenesis, and synaptic transmission (Mersman et al. 2020), all of which are dysfunctional in Alzheimer's disease (Camandola and Mattson 2017). Other differences between Tg rats and WT controls included a lower Asp/Glu ratio, lower tCr, and higher Lac at 10 months of age. These differences suggest the TgF344-AD model replicates the well-documented phenomenon of altered bioenergetics in human Alzheimer's disease (Yin et al. 2016; Mosconi 2013) specifically, disrupted excitatory neurotransmission and a shift towards non-oxidative energy metabolism (McKenna et al. 2012). These findings also indicate tCr should not be used as an internal reference in this model. Finally, our report of increased tCho is in agreement with studies in human Alzheimer's disease patients (A. Pfefferbaum et al. 1999; Kantarci et al. 2004; Marjańska et al. 2019) and likely reflects increased cell membrane turnover (a feature characteristic of neuronal degeneration (Lin and Gant 2014)) and/or inflammation and astrocytosis (D. J. Selkoe 2001; Ross and Sachdev 2004). Overall, the neurochemical profile of the TgF344-AD rat closely replicates that of human patients and provides insight into numerous pathological processes, substantiating its application in Alzheimer's disease research.

Deficits in hippocampus-dependent spatial learning and memory are among the earliest complaints in Alzheimer's disease subjects (Chan et al. 2016; Bianchini et al. 2014; Lithfous, Dufour, and Després 2013). Previous studies indicate 5-month-old TgF344-AD rats require more trials to learn a delayed nonmatch-to-sample task (Muñoz-Moreno et al. 2018) and impaired

reversal learning on the Morris Water Maze (Rorabaugh et al. 2017) and Barnes Maze (Cohen et al. 2013) by 6 months. To test spatial navigation in our TgF344-AD rats, we used a shortened version of the Barnes Maze test (Barnes 1979) which detected impairment in 3xTg mice earlier than traditional protocols (Attar et al. 2013). Fittingly, ours is the earliest report of cognitive disturbance in this model, with impairments in long term spatial reference memory present by 4-months of age. We also noted genotype-dependent differences in speed and number of holes searched, substantiating the choice to use speed- and motivation-independent measures rather than the frequently chosen escape latency or number of errors (Gawel et al. 2019; Pitts 2018). No correlations existed between behavioural metrics and neuronal or microglial count, suggesting altered cellular function as opposed to density may underlie cognitive dysfunction.

Regarding the interaction between sex and genotype, Tg females demonstrated stronger pathological effects in several brain volumes and more cognitive decline than Tg males, whereas sex effects on metabolite concentration were also present but did not consistently impact Tg females. Sex differences in the TgF344-AD rat exist in open field and buried food tasks (Saré et al. 2020) and the Morris Water Maze test (Berkowitz et al. 2018), and sex differences in neuroanatomy and hippocampal tissue chemistry during normal aging in the Fischer 344 rat have been reported (C. F. Fowler et al. 2020; C. Fowler, Goerzen, Madularu, Devenyi, Chakravarty, et al. 2021). These findings generally recapitulate human Alzheimer's disease data. Sex-specific patterns of neurodegeneration exist in human patients (Podcasy and Epperson 2016; Martínez-Pinilla et al. 2016) and men frequently present with later and less severe cognitive deficits than women (Filon et al. 2016; Rahman et al. 2019). There is also an established role for estrogen in regulation of metabolic pathways affected by Alzheimer's disease such as glucose transport, aerobic glycolysis, and mitochondrial function (Camandola and Mattson 2017; Rahman et al. 2019; Rettberg, Yao, and Brinton 2014). While additional work is required to corroborate our findings, the TgF344-AD model appears to recapitulate known sex differences in several aspects of disease presentation.

Thorough characterization of tissue pathological load of disease hallmarks in the TgF344-AD model has been performed, confirming the presence of amyloid- β deposition, gliosis, neuronal loss, and tauopathy (Cohen et al. 2013; Wu et al. 2020; Aisling M. Chaney et al. 2021) in regions and along a time course similar to that of human Alzheimer's disease (D. J. Selkoe 2001). While we report extensive amyloid pathology at 18 months, we did not detect differences in neuronal or microglial cell counts between WT and Tg rats. Other authors have failed to detect decreased

neuronal counts in this model with the NeuN antibody (Anckaerts et al. 2019; Lelplus et al. 2019; Voorhees et al. 2018; Aisling M. Chaney et al. 2021), though some authors noted amyloid plaques created a void of stable neurons around them, demonstrating highly localized neuronal disruption. This observation supports our findings of decreased NAA and Tau, given their roles regarding neuronal viability and synaptic transmission. The lack of difference in microglial load was surprising given the clear accumulation of microglia around ThioS+ plaques. A possible explanation is the large variation in cell count, likely resulting from inconsistent time between staining and imaging due to COVID-19 restrictions on the microscopy facility. Given previous publications support extensive gliosis in the TgF344-AD rat (Cohen et al. 2013; Aisling M. Chaney et al. 2021; Anckaerts et al. 2019), it is likely that similar microglial counts in WT and Tg rats are not representative of the processes occurring in this model.

Regarding corroboration of the timing of pathological changes that we report in the TgF344-AD rat, previous studies show by 5-6 months of age, TgF344-AD rats display disruption in hippocampal-dependent synaptic circuits (Muñoz-Moreno et al. 2018; Stoiljkovic et al. 2019), dysfunction of the noradrenergic system (Rorabaugh et al. 2017), and loss of functional connectivity prior to the appearance of microstructural alterations (Anckaerts et al. 2019). Reduced maximum synaptic transmission in the hippocampus occurs between 9 and 12 months, in the absence of reduced dendritic spine density (Smith and McMahon 2018), continuing to support a timeline of functional change prior to significant morphometric change. Profound cerebral microvascular and neuronal network dysfunction is present at 9 months (Joo et al. 2017; Bazzigaluppi et al. 2018), along with reduced antioxidant capacity, and increased reactive oxygen species and pro-inflammatory cytokines at 10 months (Wu et al. 2020). Our report of neurochemical changes by 10 months is consistent with these previously described molecular events. At 13 months, TgF344-AD rats demonstrate deficits in hippocampal neuronal differentiation, migration, and survival (Morrone et al. 2020), and display significant tau pathology, neuronal damage, and cognitive impairment between 16 and 26 months (Cohen et al. 2013; Voorhees et al. 2018; Aisling M. Chaney et al. 2021). Given that reduced synaptic density and neuronal loss are associated with MRI-detectable volume changes (Bobinski et al. 2000; Apostolova et al. 2015), these reports of altered neurogenesis and neuronal damage may reflect some of the processes underlying the volumetric changes we report.

This timeline of biochemical changes preceding substantive structural abnormalities is corroborated by models of disease progression (Clifford R. Jack Jr et al. 2013), and studies

exploring upstream and downstream processes of amyloid and tau deposition (Mattson and Arumugam 2018; Mattson 2004; Camandola and Mattson 2017). Additionally, the timing of biochemical and structural changes around midlife to the beginning of senescence suggests altered neurochemistry and neuroanatomy may be in response to amyloid and tau pathological load (Cohen et al. 2013; Rorabaugh et al. 2017), and are not evident before the appearance of gross tissue pathology. In contrast, early cognitive impairment differs from disease progression in humans where cognitive complaints are among the last pathological features to manifest. Given numerous studies have validated the consistency with which this model mimics the spread of components of human Alzheimer's pathology, this difference in timing of cognitive dysfunction may reflect inconsistencies in how cognition is tested or presents in rodent models versus humans. Behavioural testing is also extremely variable and subjective. Neuroimaging is considerably more objective and less variable, thus providing a better powered, sensitive, accurate, and efficient means to characterize disease progression.

There are limitations to consider when interpreting the results of the present study. First, the use of a polynomial age term in the volumetric analyses, which was necessary given the non-linear change with age that we and others report (Adolf Pfefferbaum et al. 2013; Kong et al. 2018; Tullo et al. 2019; C. Fowler, Goerzen, Madularu, Devenyi, Mallar Chakravarty, et al. 2021), likely reduced our power to detect age by genotype by sex interactions. Given that most structures demonstrated volume change towards 16 months, a paradigm where brain volumes are quantified from mid life onwards may permit the use of a linear age term and provide more power to detect three-way interactions. Second, restrictions on facility access due to the COVID-19 pandemic resulted in fewer animals being tested and increased variation in testing dates at the final time point, as well as inconsistency in the time between staining and imaging during immunofluorescence experiments. While these inconsistencies were accounted for in the statistical modelling, this is likely to have increased the overall variation in the data, possibly masking or muting some of the effects at the final time point. Finally, the lack of histological analyses at early time points meant we were unable to determine if pathological changes in neuroimaging markers precede those at the cellular level in the TgF344-AD rat. This gap in knowledge limits our ability to interpret the origin of the altered neuroimaging and cognitive markers that we report.

Altogether, our results provide a comprehensive review of multiple phenotypic components of pathology in the TgF344-AD model, characterized from early to late stages of disease

progression. This longitudinal multimodal study demonstrates that the TgF344-AD rat recapitulates major neurochemical, neuroanatomical, and cognitive features of human Alzheimer's disease, and furthers our understanding of the many processes comprising disease progression. These findings support the use of MRI and MRS to monitor disease progression in rodent models of Alzheimer's disease *in vivo*, and contribute to the growing body of work validating the TgF344-AD rat as a highly relevant model of Alzheimer's disease.

5.8 Chapter 5 Figures

Figure 5.8.1: Genotype-dependent differences in local brain volume with age

A) Voxel-wise (left) and regional (right) statistical maps for the linear age by genotype interaction term are shown. The plot range for each set of t-values displays effects significant between 5 and 1% FDR, with t-values above 1% displayed at the 1% value. Select regional volume trajectories in wildtype (WT) and TgF344-AD (Tg) rats are shown in **B)**. The mixed effects model used to fit the data is represented by a line of best fit and 95% prediction interval (shaded). Significance symbols are shown for the linear age by genotype interaction term (\ddagger) and quadratic age by genotype interaction term (\ddagger^2). The main effect of genotype as determined by the four age-centered models is shown by (\dagger), with the subscript denoting at which age the main effect was significant. **C)** A three-way interaction between age, genotype, and sex was also explored, with a 5% false discovery rate correction applied. Significance symbols for the linear and second order age-by-genotype-by-sex interaction terms are denoted by X and X² respectively. ● denotes an effect significant at the p-value level but not after FDR correction.

Figure 5.8.2: Trajectory of neurochemical changes with age in TgF344-AD and WT rats

Select neurochemical concentration trajectories in wildtype (WT) and TgF344-AD (Tg) rats are shown in **A)**. The mixed effects model used to fit the data is represented by a line of best fit and 95% prediction interval (shaded). Significance symbols are shown for the linear age by genotype interaction term (\ddagger), and the main effect of genotype (\dagger) at each time point as determined by age-centered models. The subscript denotes the age at which the genotype effect was significant. **A, Inset:** A representative MRS spectrum obtained from a female Tg rat at 4-months, with individual metabolite fit components shown below. Positioning of the voxel around the hippocampus is shown in red. **B)** A three-way interaction between age, genotype, and sex was also explored, with a 5% false discovery rate correction applied. A significant 3-way interaction term is denoted by X. ● denotes an effect significant at the p-value level but not after FDR correction.

Figure 5.8.3: Barnes Maze probe trial data reveal cognitive impairment as early as 4-months of age

(A) % time spent in the target quadrant and **(B)** % time in target holes were analyzed via a one-sample t-test for each group against a mean of 25% (chance % of time, indicated by a dotted line),

where significance indicates normal cognitive function, and lack of significance indicates impairment. **(C)** % success, **(D)** number of holes searched, and **(E)** speed (cm/s) were analyzed via a linear model that included either a main effect of genotype, covarying for sex (**left side of figure**), or an interaction between genotype and sex (**right side of figure**). Bonferroni correction was applied at each time point for data with sex covaried whereby the threshold for significance was $\alpha=0.05/7=0.00714$. * $p<0.00714$, ** $p<0.005$, *** $p<0.001$. Similarly, the threshold for significance for data split by genotype and sex was $\alpha=0.05/11=0.00455$. # $p<0.00455$, ## $p<0.001$. Abbreviations: wildtype (WT), transgenic (Tg), male (M), female (F).

Figure 5.8.4. Despite extensive amyloid pathology at 18 months, neuronal and microglial cell counts do not differ significantly between Tg344-AD and wildtype rats

Tissue burden of NeuN+ neurons **(A)**, Iba1+ microglia **(B)**, and ThioS+ amyloid- β plaques **(C)** was quantified in hippocampal sections of 18-month old rats ($n=7$ WT, $n=7$ Tg) via stereology. Representative photomicrographs are shown in **(i)**. Insets depict the same section but at a higher magnification. Boxplots in **(ii)** depict cell counts of microglia, neurons, and % immunolabeled volume of amyloid- β plaques. β and p-values for the effect of genotype are shown. The threshold for significance was $\alpha=0.05/2=0.025$. Spearman rank correlations between cell counts and neuroimaging markers are shown in **(iii)**, along with the corresponding correlation coefficient (ρ) and p-value. A line of best fit is shown with the 95% confidence interval (shaded). None of the correlations reached the significance threshold ($\alpha=0.05/18$ tests= 0.003 , not all tests are pictured). Photomicrographs showing simultaneous staining with Iba1, NeuN, and ThioS **(D)**, with a higher magnification image depicting microglia aggregating around amyloid plaques **(E)**. All scale bars denote 25 μ m.

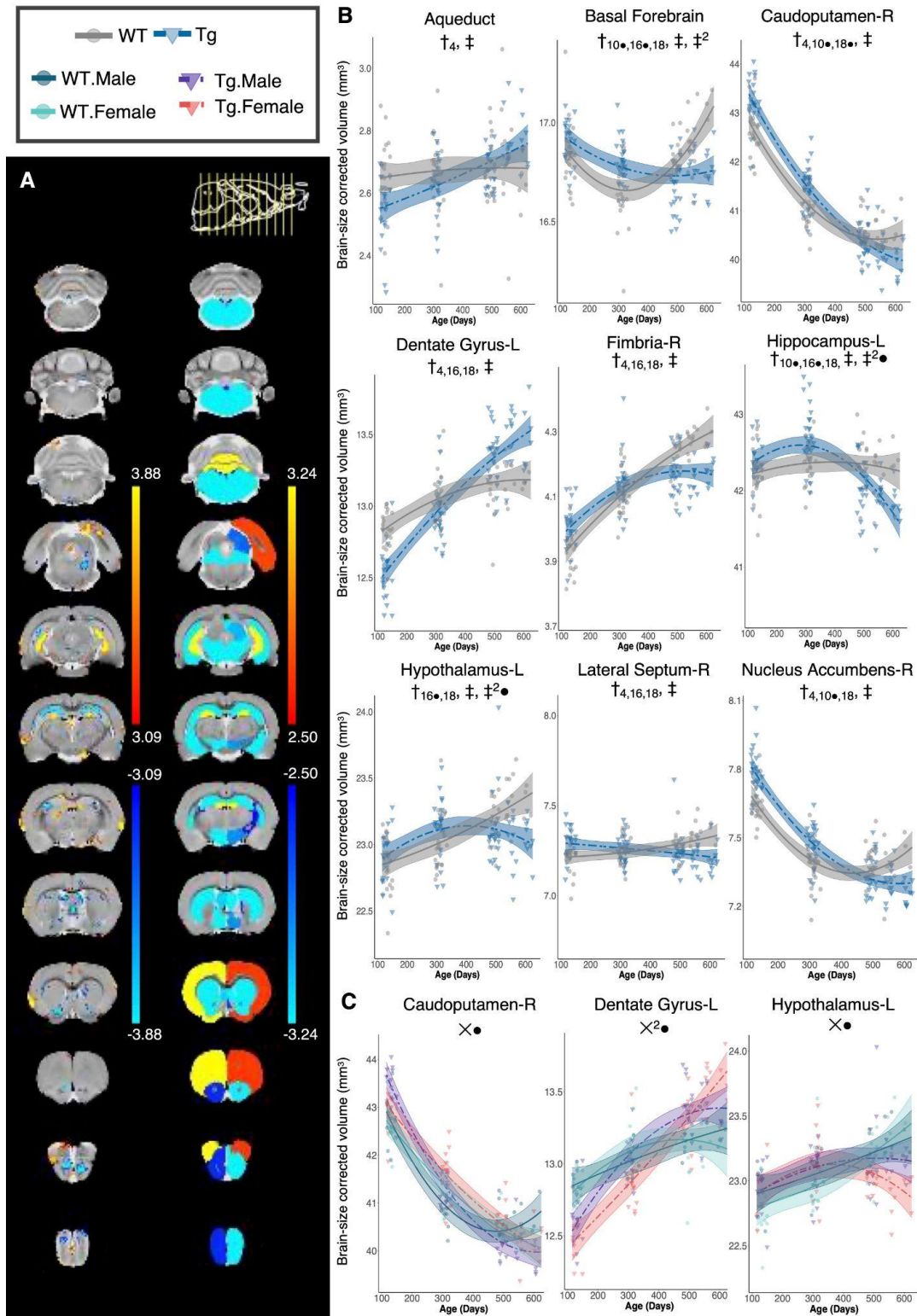


Figure 5.8.1

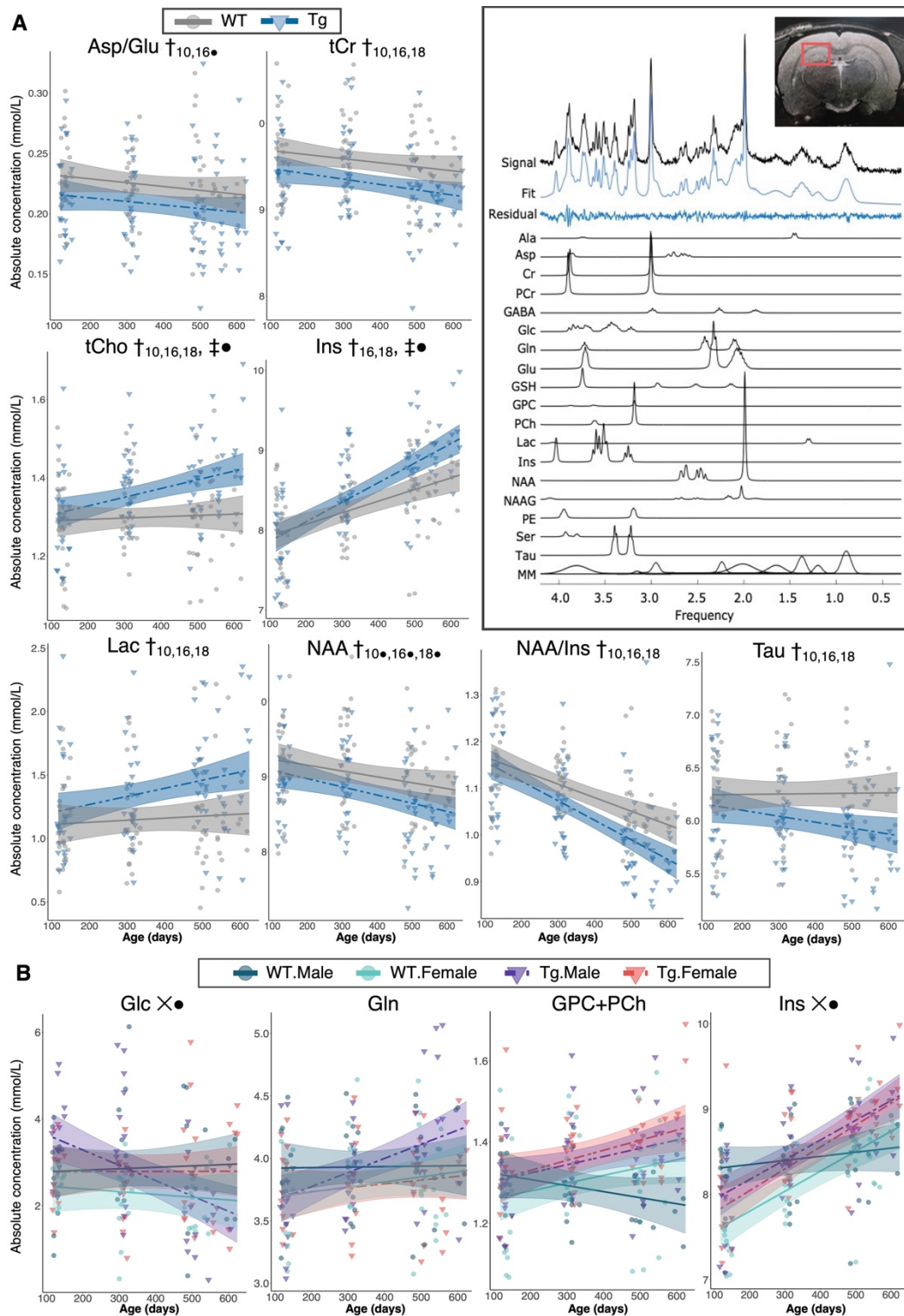


Figure 5.8.2

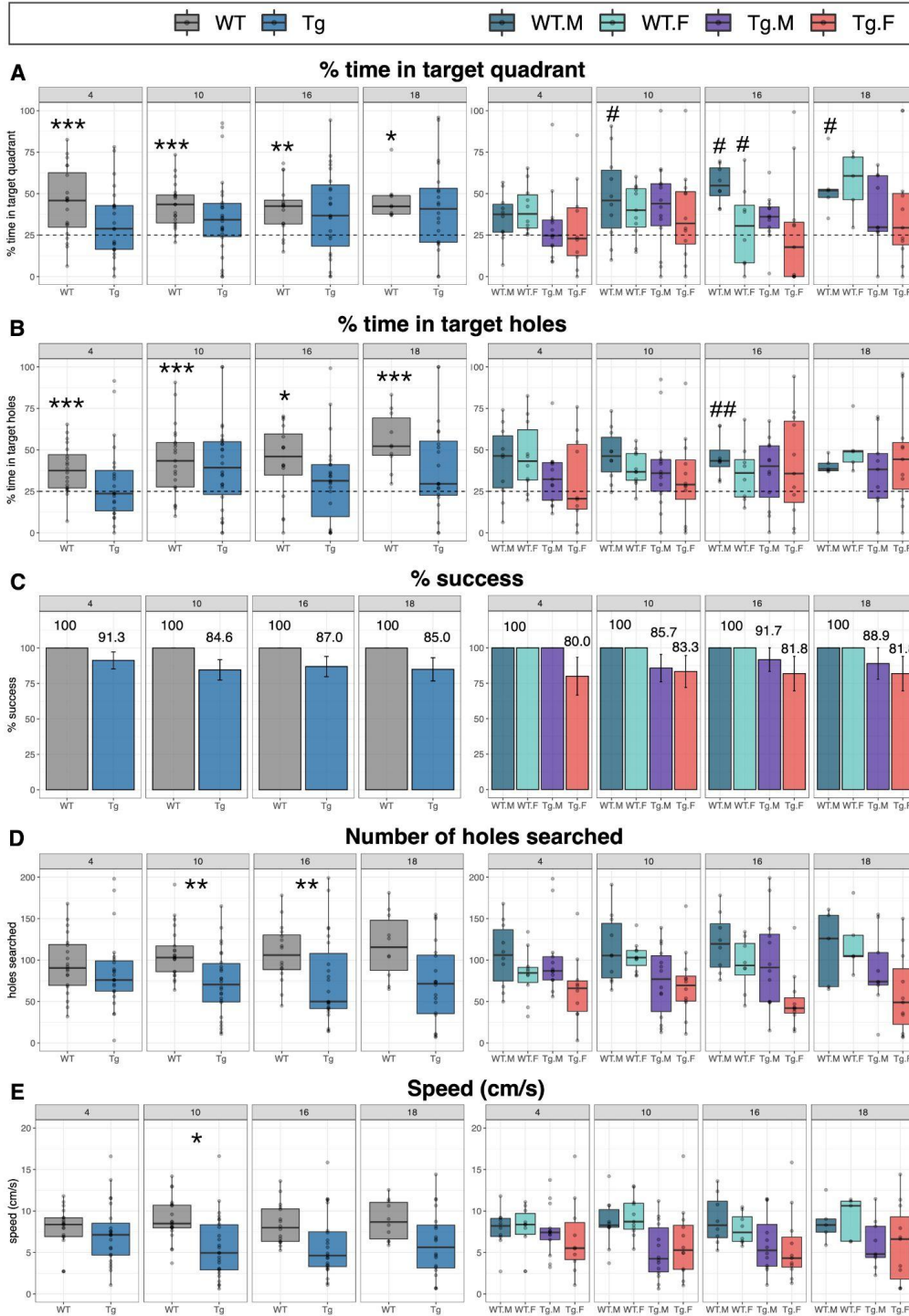


Figure 5.8.3

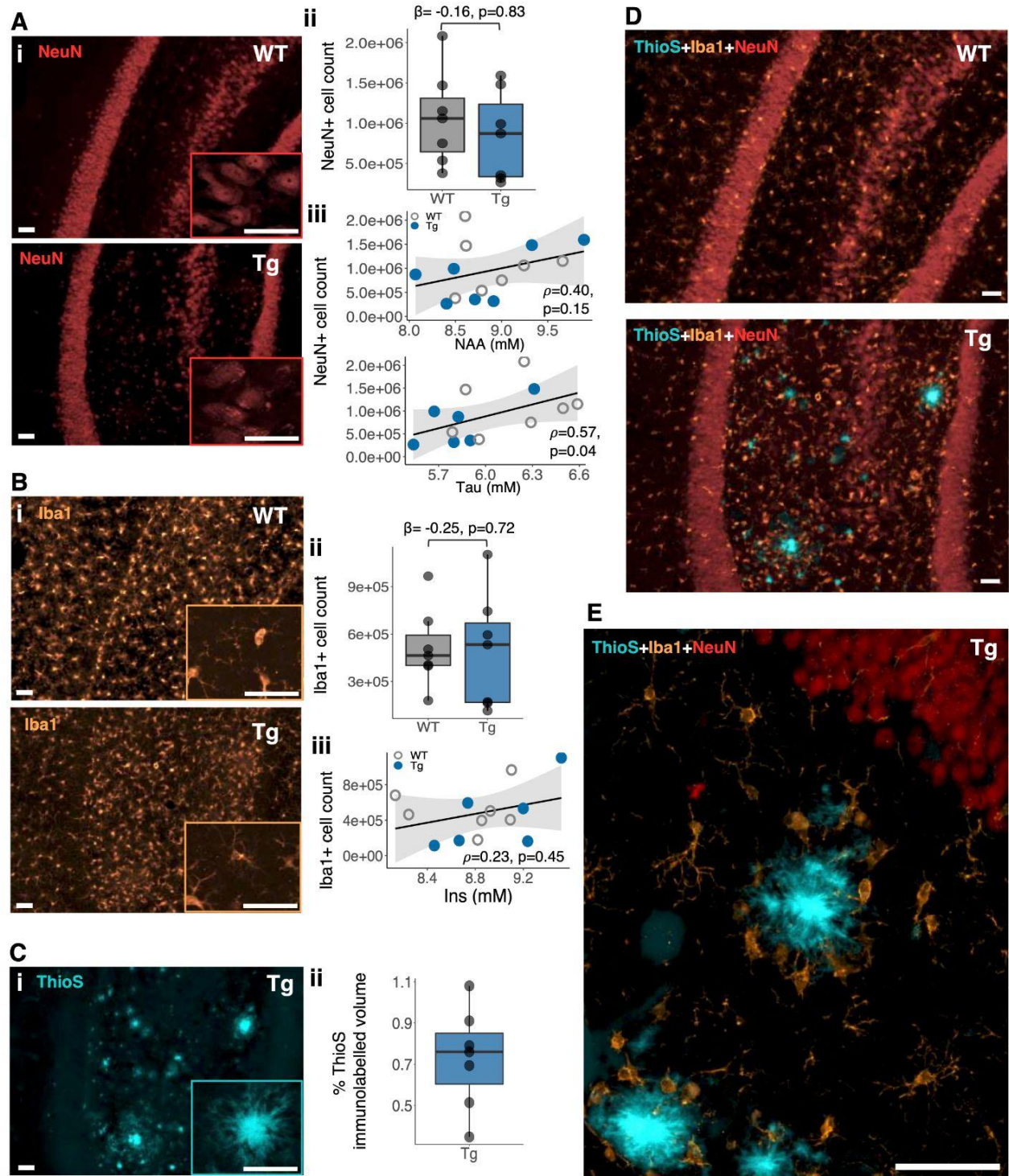


Figure 5.8.4

5.9 Supplementary Methods

Additional methodological information for sample size calculations/group sizes, MRI, MRS, Barnes Maze, immunofluorescence experiments, and statistical analysis

5.9.1 Sample Size Calculations and Group Sizes

The primary hypothesis for this study involved characterizing differences between Tg and WT rats while controlling for sex. Based on test-retest experiments performed in our lab examining intra- and inter-subject variation in hippocampal volume, this study was designed to have 80% power to detect an effect size of 3% with data collected from $n=17$ animals per genotype over four time points with an estimated type-1 error rate of less than 0.05¹. Test-retest results for major metabolites of interest (NAA, Ins, tCr, Glu, Gln, tCho) were comparable to those obtained for hippocampal volume and thus the power simulation above generally applies to the main metabolites quantified here. Group sizes were increased from 17 to 24 and 26 for WTs and Tgs, respectively, to account for an estimated attrition rate of approximately 15%. These group sizes (~20 or more) align well with behavioural analyses previously performed in this model², which were adequate to determine significant differences between genotypes in a cross-sectional analysis.

Group sizes for all modalities changed over the course of the study due to normal attrition with age, occasional malfunction of the camera and/or tracking software used for behavioural testing, and restricted access to our facility during COVID-19, particularly at the last time point. Additionally, if animals only had data from one time point for any modality (typically due to failure of quality control metrics at one time point combined with death prior to 18 months), that animal was removed from the dataset for that modality. This occurred for one rat within the MRS dataset, three rats within the MRI dataset, and two rats within the Barnes Maze dataset. Group sizes and average age at each timepoint, before and after exclusions during quality control, split by modality and sex, are summarized in **Supplementary Table 5.10.1**.

5.9.2 MRI methods

High-resolution 3D anatomical MR images were acquired using Rapid Acquisition with Relaxation Enhancement (RARE) using the following scan parameters: TR = 325 ms, echo spacing = 10.8 ms, RARE factor = 6, effective echo time = 32.4 ms, Field of View = $20.6 \times 17.9 \times 29.3$ mm,

matrix size = $256 \times 180 \times 157$, slice thickness 17.9 mm (along the dorsal/ventral direction), readout along the rostral/caudal direction, scanner resolution = 114 μm isotropic, 19m35s acquisition time.

All pre-processing methodology is described in detail elsewhere (Fowler et al., 2021). Briefly, preprocessing was performed using minc-toolkit-v2 (Vincent et al., 2016) with the MINC toolkit extras package (<https://github.com/CoBrALab/minc-toolkit-extras>), and the two-level model build Pydipper module (Friedel et al., 2014) was used to co-register the pre-processed images into a common space. First, an in-house rat MRI preprocessing script within the minc-toolkit-extras package developed by G.A.D. (<https://github.com/CoBrALab/minc-toolkit-extras>, `rat-preprocessing-v4.sh`) was used to perform the following sequential preprocessing steps: dimension reordering to standard MINC 2.0 ordering, image centring, whole image N4 bias field correction (Sled and Pike, 1998; Tustison et al., 2010), individual foreground mask generation using the Otsu method (Otsu, 1979), additional N4 bias field correction using the previously generated mask, registration to a Fischer 344 template average image, and a final N4 bias field correction using a template mask. After pre-processing, images were quality controlled by D.G. Images were visualised using the Display program in minc-toolkit-v2 and examined in each of the coronal, sagittal, and axial dimensions for motion artefacts, Gibbs ringing artefacts, and other image anomalies. 15 of a total 179 scans were excluded from further analysis. 7 rats (4Tg (1M/3F), 3 WT (2M/1F)) were excluded at 4-months, 1 at 10-months (1TgM), and 5 at 16-months (3Tg (1M/2F), 2WT (1M/1F)).

The remaining 164 scans were co-registered using the two-level model build pipeline in Pydipper. This co-registration paradigm uses deformation-based morphometry techniques and is described fully by Friedel et al. (Friedel et al., 2014). In brief, subject-specific starting averages are created by rigidly registering scans at different time points to a Fischer 344 atlas template (Goerzen et al., 2020), followed by averaging. Iterative affine and non-linear registration and averaging is then repeated to produce an unbiased subject average. Subsequently, each subject specific average is rigidly aligned to the Fischer 344 atlas template space and the process is repeated to create an unbiased population average. This process creates deformation fields for each subject at each time point. The deformation fields can then be used to estimate the Jacobian determinant at each voxel, which reflects the amount of expansion or compression required to deform each individual anatomical image to the subject average (Chung et al., 2001). Deformation fields are then resampled into the common study space allowing comparison between subjects. This registration process

generates two sets of Jacobian determinants, though only the relative Jacobian—composed solely of the non-linear mapping and thus reflects local or relative changes in voxel volume—was used for subsequent analysis. The Jacobian deformation fields were then blurred with a 400 micron full width half maximum Gaussian kernel to satisfy assumptions of normality required by the statistical models used to analyze the data.

Using the Fischer 344 rat atlas resampled into the common space of this study, the volumes of 120 regions were estimated using the *anatGetAll* function in RMINC_1.5.2.3 (Lerch et al., 2017). This function computes the volume of a region by counting the number of voxels with a given label and multiplying the Jacobian with the voxel volume at each voxel.

5.9.3 MRS methods

5.9.3.1 Basis Set

The neurochemical basis set consisting of 18 simulated metabolite resonances and 9 macromolecule (MM) basis functions: alanine (Ala), aspartate (Asp), creatine (Cr), γ -aminobutyrate (GABA), glucose (Glc), glutamine (Gln), glutamate (Glu), glycerophosphocholine (GPC), glutathione (GSH), lactate (Lac), myo-Inositol (Ins), N-acetylaspartate (NAA), N-acetylaspartylglutamate (NAAG), phosphocholine (PCh), phosphocreatine (PCr), phosphoethanolamine (PE), serine (Ser), taurine (Tau), MM_{0.89}, MM_{1.20}, MM_{1.39}, MM_{1.66}, MM_{2.02}, MM_{2.26}, MM_{2.97}, MM_{3.18}, and MM_{3.84}. The subscript of each MM indicates the ppm value at which the peak appears in the MRS spectrum. We also report summed Cr+PCr (tCr), GPC+PCh (tCho), NAA+NAAG (tNAA) and Glu+Gln (Glx) and the ratios of Glu to Gln, Asp to Glu, and NAA to Ins.

5.9.3.2 Quality Control

To ensure high quality MRS data, we visually inspected each spectrum and removed three scans that generated the RFALSI 4 error during LCModel fitting, which is indicative of particularly noisy data. These scans also had the lowest signal-to-noise ratio (SNR) of all 178 scans, with SNR of 13, 13, and 15, when the average was 23.13 (\pm 3.30, standard deviation).

The Cramer-Rao lower bound (CRLB) provided by LCModel was used as a measure of reliability of neurochemical quantification on a per-metabolite basis.³ We employed a strict cut-off

of 20% CRLB averaged across all scans, which resulted in the removal of GABA (CRLB 41.56), Serine (CRLB 33.59), and MM_{3.18} (CRLB 44.96) from our analysis. Finally, after visual inspection of all graphed data, there were several extreme outliers. In two cases, the entire animal was removed from that time point, the first because MRS data was indicative of cancer (high total Choline, low NAA) and the second because the data points from that animal were outliers for all metabolites. A very conservative median absolute deviation (MAD) threshold of 3.5^{4,5} was applied to all remaining data points, resulting in the removal of 34 of 4671 data points, or 0.728% of the data.

5.9.4 Barnes Maze Testing

Due to the large number of animals in this study and the desire to identify early memory deficits in the TgF344-AD rat model, we followed a shortened and thus more cognitively challenging protocol while keeping the time per trial (3 minutes) and the maze set-up consistent with protocols designed for rats.^{2,6} The maze consisted of a circular platform (122 cm diameter) constructed of PVC material with 20 holes (4 inches diameter) evenly spaced around the perimeter. A bottom layer was placed underneath such that 19 of 20 holes would have a false bottom (too shallow for the rat to enter but otherwise identical to the escape hole), and to allow for rotation of the the top of the maze between trials, ensuring rats could not track any scent cues or navigate using small markings on the maze surface itself. An escape box consisting of a dark chamber with a ramp was placed underneath one of the holes (target hole). The maze and escape box were coated with black waterproof epoxy paint to ensure they would be easily cleanable with Peroxyguard (hydrogen peroxide sanitizer). The maze was mounted on top of a large plastic box such that it stood 35" above the ground and was lit by two bright spotlights positioned to reduce shadows projected onto the maze. White curtains were drawn in a square around the maze and three simple visual cues were attached to three of the four curtain "walls".

In the week prior to Barnes Maze testing, rats were introduced to the escape box by placing them in it and allowing them to climb around and explore during their weekly handling session. This exploration session was introduced after pilot testing where rats showed extreme hesitancy to enter the box during the training trials. Their fear of entering the escape hole was mitigated by introducing them to the box prior to testing and was therefore retained for the animals tested in this study.

The rats interacted with the Barnes Maze in three consecutive phases: habituation (2 trials over 1 day), training (5 trials over 2 days), and probe (1 trial). Before each phase, rats were acclimated to the testing room for one hour. For habituation trial 1, rats were placed directly into the escape cage underneath the maze and allowed to remain there or independently exit the escape cage and explore the maze for a maximum of 3 minutes. If the rat exited the box and re-entered it, or if 3 minutes elapsed without the rat exiting the box, the escape hole was immediately covered and the rat was kept in the box for 30 to 60 seconds to mimic the end of the trial before returning them to their home cage. For habituation trial 2, the process was similar but rats were placed directly in the centre of the maze and allowed to explore until they either entered the escape hole or 3 minutes had elapsed. Rats that did not enter the escape hole after 3 minutes were guided to the hole and nudged until they entered it or manually placed in the box if they did not enter it independently.

In the training phase, the escape hole location was changed by at least 90 degrees from its location during habituation. Rats were placed in the centre of the maze underneath an opaque bucket for 10 seconds so they would be facing a random direction upon the start of the trial. The trial began as soon as the experimenter lifted the bucket. Rats were given 3 minutes to locate and enter the escape hole. If they located the hole (end point of test) but turned away to explore further, or if they did not enter after 3 minutes, they were guided to the hole and nudged to enter, or manually placed in the hole if they did not enter independently. The hole was covered and the rat remained in the escape hole for 30-60 seconds before being returned to their home cage. The maze and escape box was cleaned in between each rat, and the top of the maze was rotated between cages of rats. This process typically took 5 minutes per rat and was performed with 4-6 rats at a time, providing a 20-30 minute inter-trial interval. Training was repeated 3 times on day 1, and 2 times the subsequent day for a total of 5 training trials.

The probe trial, used to assess long-term spatial reference memory (Pitts, 2018), took place 48 hours after the last training trial. The escape cage was replaced with a false bottom such that all 20 holes appeared the same and escape was not possible. Rats were again placed in the centre of the maze under an opaque bucket and, upon removal of the bucket, were allowed to explore the maze for 3 minutes before being returned to their home cage. The maze was cleaned and the maze top was rotated between each rat.

5.9.5 Immunofluorescence experiments

5.9.5.1 Perfusion

After completion of testing at the final time point at 18 months, 7 WT rats and 7 Tg rats were anesthetized using an intraperitoneal injection of ketamine-xylazine-acepromazine cocktail (0.1mL/10g rat body weight, contains: 100mg/kg ketamine, 10 mg/kg xylazine, 3 mg/kg acepromazine) and fixed by transcardiac perfusion with 0.9% heparinized saline followed by 4% paraformaldehyde (PFA) in 0.1M phosphate buffer (PB). Brains were collected, postfixed in 4% PFA in 0.1M PB for 2 to 7 days at 4°C, equilibrated in 30% sucrose solution for 2 to 7 days to cryoprotect the tissue, and then flash frozen in isopentane and stored at -80°C until ready for sectioning.

5.9.5.2 Sectioning

Free-floating sections (~90 to 100 per animal) were collected into a 24-well plate containing phosphate buffered saline PBS, 10mM, and then transferred to a new 24-well plate containing cryoprotectant solution (glycerol, ethylene glycol, and 10mM PBS in a 3:3:4 ratio) for storage at -20°C. Of the collected sections, only 12 sections per subject were selected to be stained, starting with section 1 and advancing in intervals of 8 (section 1, 9, 17, 25, 33, 41, 49, 57, 65, 73, 81, 89). The last 10 sections (17 to 89) were used for stereology, as this volume (~3.5 mm) best approximated the voxel used for MRS data acquisition.

5.9.5.3 Application of primary and secondary antibodies and detection solutions

Sections were first incubated in mouse anti-neuron primary antibody (target antigen: neuron-specific neuronal nuclear protein, NeuN, Millipore Sigma, 1:400) and rabbit anti-microglia primary antibody (target antigen: ionized calcium-binding adaptor molecule-1, Iba1, Wako Chemical, 1:500) for 19 hours, followed by anti-mouse secondary 647 antibody for NeuN detection (Jackson ImmunoResearch Laboratory, 1:500) and biotinylated anti-rabbit secondary antibody (Vector Laboratories, 1:500), followed by streptavidin Cy3 for detection of Iba1 (Jackson

Immunoresearch Laboratory). Sections were then mounted and stained with Thioflavin-S (ThioS, 0.5% ThioS in 50% ethanol).

5.9.5.4 Imaging and Stereology

Imaging was performed using a ZEISS Axio Imager M.2 with a MBF Bioscience microscope stage and Apotome 2. A 63x oil lens was used with the DsRed Widefield filter and Cy5 Widefield filter for microglia and neurons, respectively. Multichannel acquisition in a Systematic Random Sampling (SRS) image stack series was enabled so that the same site would be imaged for Iba1 and NeuN simultaneously. A step size of 2 μm was used, in order to produce 20-24 images per sampling site. The grid size for the SRS grid was 650x650 μm within a voxel of 2500x3500 μm anchored at the top corner of the corpus callosum and extending over the hippocampus. Stereology was performed using the Optical Fractionator (OF) probe within the Stereo Investigator software (MBF Bioscience) with a counting frame of 40x40 μm . Traditional design-based stereology rules were followed, with any marker touching the red line being excluded and only counting a specimen when the top of its cell body came into focus. Plaque imaging and stereology was conducted separately, also on the ZEISS Axio Imager M.2 with Apotome 2, but with a 20x air lens. The GFP Widefield filter was implemented on a SRS image series on a 550x550 μm grid. Stereology was performed using the Area Fraction Fractionator (AFF) probe with a counting frame of 200x200 μm . To approximate the volume of plaques, the Cavalieri settings were set at a grid spacing of 6.00 μm and a grid rotation of 0.00 degrees.

5.9.6 Statistical Analysis

5.9.6.1 Base Packages in R

The following base packages were attached in R: splines, stats, graphics, grDevices, utils, datasets, methods, base; other attached packages: effects_4.4-4⁷, RColorBrewer_1.1-2⁸, readxl_1.3.1⁹, lmerTest_3.1-0¹⁰, lme4_1.1-23¹¹, tidyverse_1.3.0¹², RMINC_1.5.2.3).

5.9.6.2 Linear model comparison

Akaike information criterion (AIC) comparisons were performed for both volume and metabolite data to determine if age was best modelled using a linear or quadratic age term, given

that non-linear change with age has previously been demonstrated with brain volumes^{13–15} and metabolite concentrations.¹⁶ AIC comparison using a threshold of Δ_i ($AIC - AIC_{\min}$) > 4¹⁷ demonstrated that brain volumes were best fit using a quadratic age term ($\text{poly}(\text{age}, 2)$), while all metabolite concentrations were best fit using a linear age term.

5.9.6.3 Final linear models

The full linear models for longitudinal analysis of brain structure and chemistry are shown below. For MRS data only (models 2 and 4), the fixed effect of water linewidth (water.lw) was included to control for the effect of linewidth on metabolite concentration estimates.⁴⁸ A weighting factor of the inverse absolute CRLB for each metabolite ($1/\text{metabolite.sdab}$) accounted for differences in fitting reliability between samples and allowed us to include all observations with $\text{CRLB} < 999$.

Model 1: $\text{lmer}(\text{volume}) \sim \text{poly}(\text{age}, 2) * \text{genotype} + \text{sex} + (1 | \text{subject})$

Model 2: $\text{lmer}(\text{metabolite}) \sim \text{age} * \text{genotype} + \text{sex} + \text{water.lw} + (1 | \text{subject}), \text{weights} = 1 / \text{metabolite.sdab}$

Model 3: $\text{lmer}(\text{volume}) \sim \text{poly}(\text{age}, 2) * \text{genotype} * \text{sex} + (1 | \text{subject})$

Model 4: $\text{lmer}(\text{metabolite}) \sim \text{age} * \text{genotype} * \text{sex} + \text{water.lw} + (1 | \text{subject}), \text{weights} = 1 / \text{metabolite.sdab}$

5.10 Supplemental Table Captions

Supplementary Table 5.10.1. Summary of subject demographic data at each timepoint, split by modality and sex

Number of subjects is shown both before and after exclusions during quality control. Squares highlighted in pink indicate where quality control reduced the number of rats with usable data. Average age in days is shown, with the standard deviation included after the plus minus symbol. Abbreviations: M, male; F, female.

Supplementary Table 5.10.2: LME_MRI: Akaike's information criterion (AIC) analysis and linear model summary for 120 brain volumes

AIC was used to determine whether or not the majority of structures were better fit using a linear versus quadratic age term. Model A predicted volume via $\text{poly}(\text{age}, 1) * \text{genotype} + \text{sex} + (1 | \text{subject})$ while model B predicted volume via $\text{poly}(\text{age}, 2) * \text{genotype} * \text{sex} + (1 | \text{subject})$. For each structure, delta AIC ($AIC_i - AIC_{\text{minimum}}$) > 4 was indicative of a better fit using a quadratic age term, which was the case for the majority of structures. Model B was therefore applied to all brain volumes and

each term from model B is shown under the primary hypothesis heading, whereby the model terms of interest were the linear (poly(age,2)1:genotypeTg) and quadratic (poly(age,2)2:genotypeTg) interaction terms. Model B was also run in the form of four age-centered models, wherein the model term of interest was the main effect of genotype, denoted by genotypeTg(age). Standard beta values, standard error, and p-values are shown for all model terms, while model terms of interest are highlighted with a black border and include a column with adjusted p-values after 5% FDR correction. For these terms of interest, p-values and adjusted p-values that meet the significance threshold of 0.05 are highlighted in blue, while those between 0.05 and 0.1 are highlighted in grey. A secondary analysis was also performed whereby the model included a 3-way interaction between quadratic age, genotype, and sex, with a random intercept per subject. The model terms of interest for this analysis were genotypeTg:sexF, poly(age,2)1:genotypeTg:sexF, and poly(age,2)2:genotypeTg:sexF. All model terms are shown under the secondary hypothesis heading.

Supplementary Table 5.10.3: MRI_volume_summary_mm3

Summary of brain volumes in mm³ measured longitudinally in TgF344-AD (Tg) rats and wildtype (WT) controls, as well as split by sex. Volumes are expressed as mean ± standard deviation. N indicates the number of subjects per group. Abbreviations: WT male (WTM), WT female (WTF), Tg male (TgM), Tg female (TgF).

Supplementary Table 5.10.4: LME_MRS: CRLB values, Akaike's information criterion (AIC) analysis, and linear model summary for 27 neurochemicals

Cramer-Rao Lower Bounds were averaged across all scans and used as a quality control metric with a strict threshold of 20%, resulting in the removal of GABA (CRLB 41.56), Serine (CRLB 33.59), and MM_{3,18} (CRLB 44.96) from further analysis. AIC was used to determine whether or not the majority of neurochemicals were better fit using a linear versus quadratic age term. Model A predicted concentration via poly(age,1)*genotype + sex + water.linewidth (lw) + (1|subject) while model 2 predicted concentration via poly(age,2)*genotype*sex + water.lw + (1|subject). For each neurochemical, delta AIC (AIC_i-AIC_{minimum}) > 4 was indicative of a better fit using a quadratic age term. All neurochemicals demonstrated a better fit using Model A with a linear age term. Model A was therefore applied to all neurochemicals and each model term is shown under the primary hypothesis heading, whereby the model term of interest was the age by genotype interaction term (age:genotypeTg). Model A was also applied in the form of four age-centered models, whereby the term of interest was the main effect of genotype, evaluated at four time points (genotypeTg(age)). Standard beta values, standard error, and p-values are shown for all model terms, while model terms of interest are highlighted with a black border and include a column with adjusted p-values after 5% FDR correction. For these terms of interest, p-values and adjusted p-values that meet the significance threshold of 0.05 are highlighted in blue, while those between 0.05 and 0.1 are highlighted in grey. A secondary analysis was also performed whereby the model included a 3-way

interaction between age, genotype, and sex, with water linewidth covaried and a random intercept per subject. The model terms of interest for this analysis were genotypeTg:sexF and age:genotypeTg:sexF. All model terms are shown under the secondary hypothesis heading.

Supplementary Table 5.10.5: MRS_conc_summary_mMol

Summary of neurochemical concentrations in mMol measured longitudinally in TgF344-AD (Tg) rats and wildtype (WT) controls, as well as split by sex. Concentrations are expressed as mean \pm standard deviation. 'n' indicates the number of subjects per group. Abbreviations: WT male (WTM), WT female (WTF), Tg male (TgM), Tg female (TgF).

Supplementary Table 5.10.6: Barnes_stats

All statistics run on Barnes Maze probe data for both primary (main effect of genotype) and secondary analyses (genotype by sex). The statistical test for each of the five metrics (% time in target quadrant, % time in target holes, % success, number of holes searched, and speed) is shown, along with the effect size (either cohen's d or standardized beta) for all terms in the model. Statistics are split by time point. Bonferroni correction was applied at each time point for primary analyses and secondary analysis separately. For primary analyses, the number of tests run per time point was 7 (4 one-sample t-tests and 3 linear models) so the significance threshold was $0.05/7=0.00714$. For secondary analyses the number of tests per time point was 11 (8 one-sample t-tests and 3 linear models), so the significance threshold was $0.05/11 = 0.00455$. P-values that reached the appropriate significance threshold are highlighted in blue.

Supplementary Table 5.10.7: Barnes_data_summary

Summary of Barnes maze statistics measured at 4 time points in TgF344-AD (Tg) rats and wildtype (WT) controls, as well as split by sex. N represents the number of subjects per group. For each metric the average, standard deviation (SD), standard error (SE), and 95% confidence interval (CI) are shown. Abbreviations: WT male (WTM), WT female (WTF), Tg male (TgM), Tg female (TgF).

Supplementary Table 5.10.8: Histology_LME: LME results for microglial and neuronal cell counts

Cell counts were modelled using a main effect of genotype while controlling for sex, age at sacrifice, paradigm, and time between staining and imaging. Standard beta values, standard error, and p-values are shown for all model terms, while model terms of interest (genotype) are highlighted with a black border. Bonferroni correction was applied such that the significance threshold was $0.05/2 = 0.025$.

Supplementary Table 5.10.9: Correlations_18months: Correlations between microglial and neuronal burden, metabolite concentrations, brain volumes, and behavioural metrics

The correlation coefficient (ρ) and 95% confidence interval (CI) are shown, along with the p-value for each correlation. Number of subjects (n) differ slightly due to exclusion of MRI or MRS scans during quality control, as well as removal of outliers on a per-metric basis. Bonferroni correction for multiple comparisons was applied such that the significance threshold was $\alpha=0.05/18$ tests=0.0028, resulting in none of the correlations reaching statistical significance.

5.11 Supplemental Figures

Supplementary Figures 5.11.1 and 5.11.2. Visualization of the longitudinal volume trajectories of all brain structures that display a significant age by genotype interaction

Brain-size-corrected volumes were predicted via linear mixed effects modelling using a second order age by genotype interaction with sex covaried and a random intercept for each subject. Multiple comparisons were corrected for using a 5% false discovery rate. The mixed effects model used to fit the data is represented by a line of best fit and 95% interval (shaded). Each data point represents a single rat. Data corresponding to wildtype (WT) rats are shown using grey circles and a solid line of best fit, while data corresponding to TgF344-AD (Tg) rats are shown using blue triangles and a dashed line of best fit. Significance symbols are shown for the linear age by genotype interaction term (\ddagger), quadratic age by genotype interaction term (\ddagger^2), and the main effect of genotype (\dagger) at each time point as determined by the age-centered models, with the subscript denoting at which age the genotype effect was significant. ● denotes an effect significant at the original p-value level but not after FDR correction.

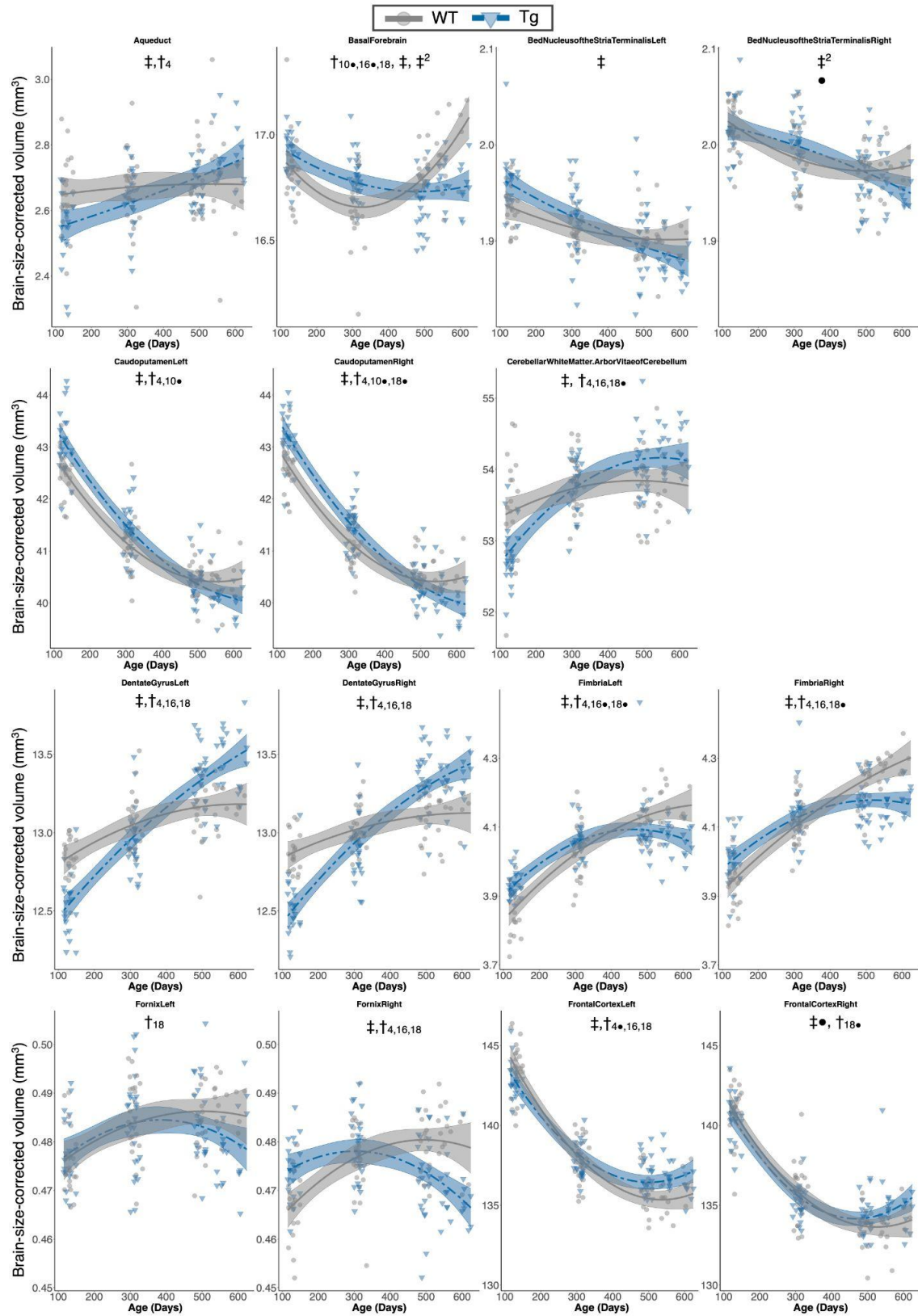
Supplementary Figures 5.11.3 and 5.11.4. Visualization of the longitudinal volume trajectories of all brain structures that display a significant age by genotype by sex interaction, prior to FDR correction

Brain-size-corrected volumes were predicted via linear mixed effects modelling using a second order age by genotype by sex interaction and a random intercept for each subject. Multiple comparisons were corrected for using a 5% false discovery rate. The mixed effects model used to fit the data is represented by a line of best fit and 95% interval (shaded). Each data point represents a single rat. Data corresponding to wildtype (WT) rats are shown using circles and a solid line of best fit, while data corresponding to TgF344-AD (Tg) rats are shown using triangles and a dashed line of best fit. Significance symbols are shown for the linear age by genotype by sex interaction term (X) and quadratic age by genotype interaction term (X^2). A single symbol indicates an adjusted p-value <0.05. ● denotes an effect significant at the original p-value level but not after FDR

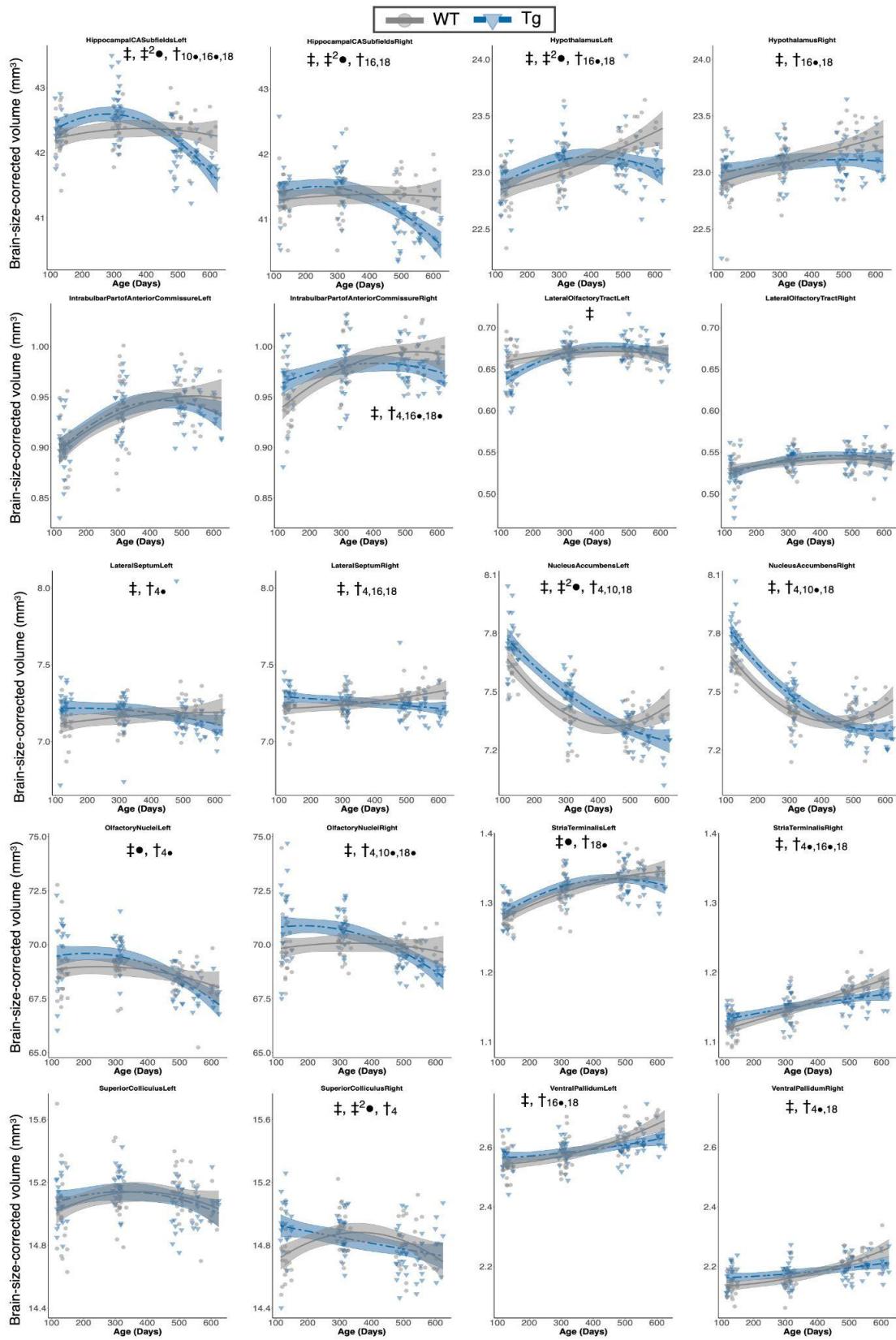
correction. Abbreviations: wildtype male, WT.M; wildtype female, WT.F; TgF344-AD male, Tg.M; TgF344-AD female, Tg.F.

Supplementary Figure 5.11.5. Longitudinal trajectory of neurochemicals in TgF344-AD and wildtype rats, with some split by sex

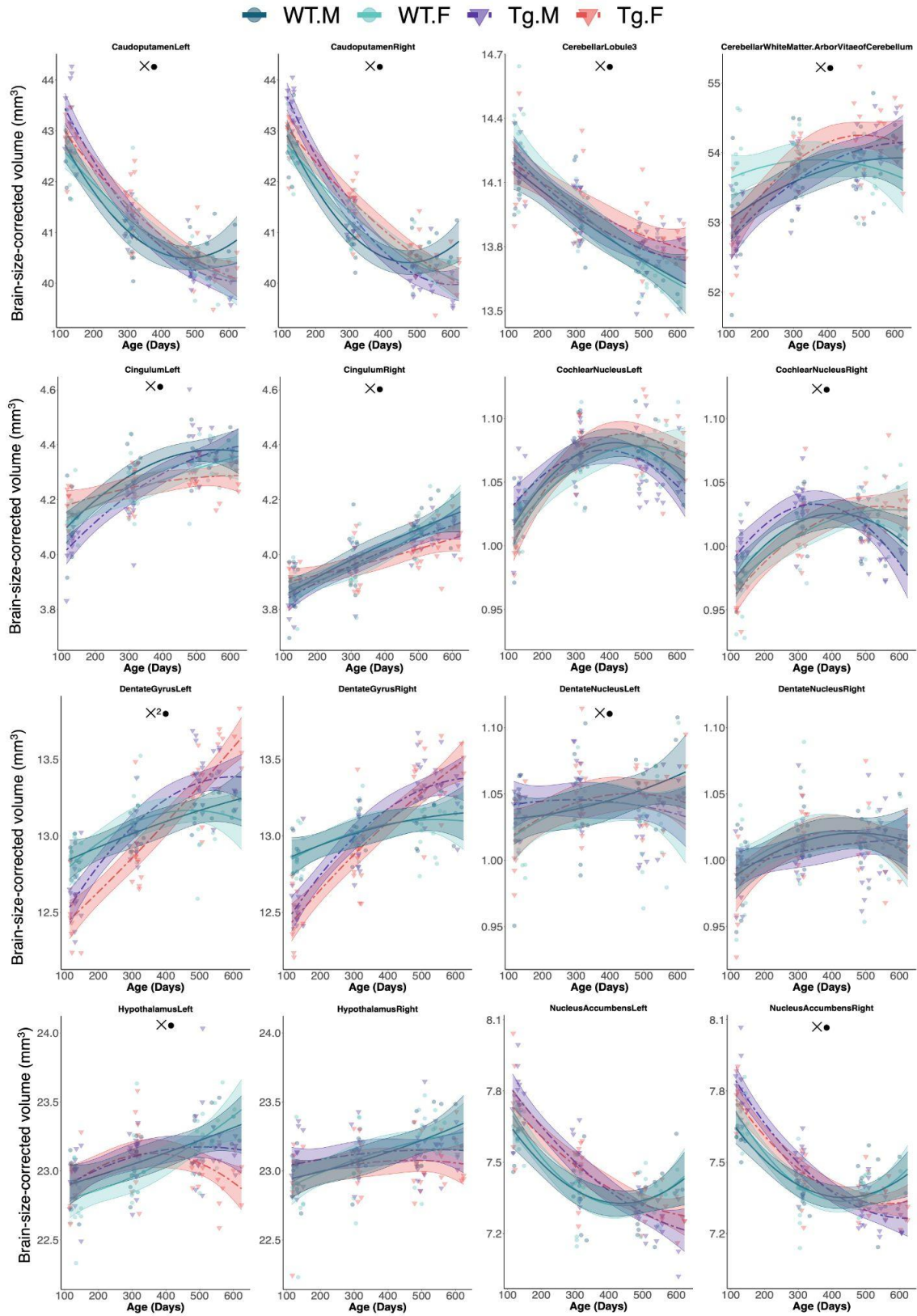
Absolute concentration (mM) of neurochemicals were predicted via linear mixed effects modelling using either **A**) an age by genotype interaction with sex covaried (model 3), or **B**) a three-way interaction between age, genotype, and sex (model 4). In both cases, water linewidth was also covaried and a random intercept for each subject was included. Multiple comparisons were corrected for using a 5% false discovery rate. The mixed effects model used to fit the data is represented by a line of best fit and 95% interval (shaded). Each data point represents a single rat. Data corresponding to WT rats are shown using circles and a solid line of best fit, while data corresponding to TgF344-AD rats are shown using triangles and a dashed line of best fit, respectively. Significance symbols in **A** are shown for the linear age by genotype interaction term (\ddagger) and the main effect of genotype (\dagger) at each time point as determined by the age-centered models, with the subscript denoting at which age the genotype effect was significant. The significance symbol for the age by genotype by sex interaction term (\times) from model 4 shown in **B** was not necessary as none of the results were significant. \bullet denotes an effect significant at the p-value level but not after FDR correction. Abbreviations: Alanine (Ala), Aspartate (Asp), Glucose (Glc), Glutamine (Gln), Glutamate (Glu), Glutathione (GSH), N-acetylaspartate (NAA), N-acetylaspartylglutamate (NAAG), Phosphoethanolamine (PE), Taurine (Tau), Macromolecule (MM). The subscript of each MM indicates the ppm value at which the peak appears in the MRS spectrum.



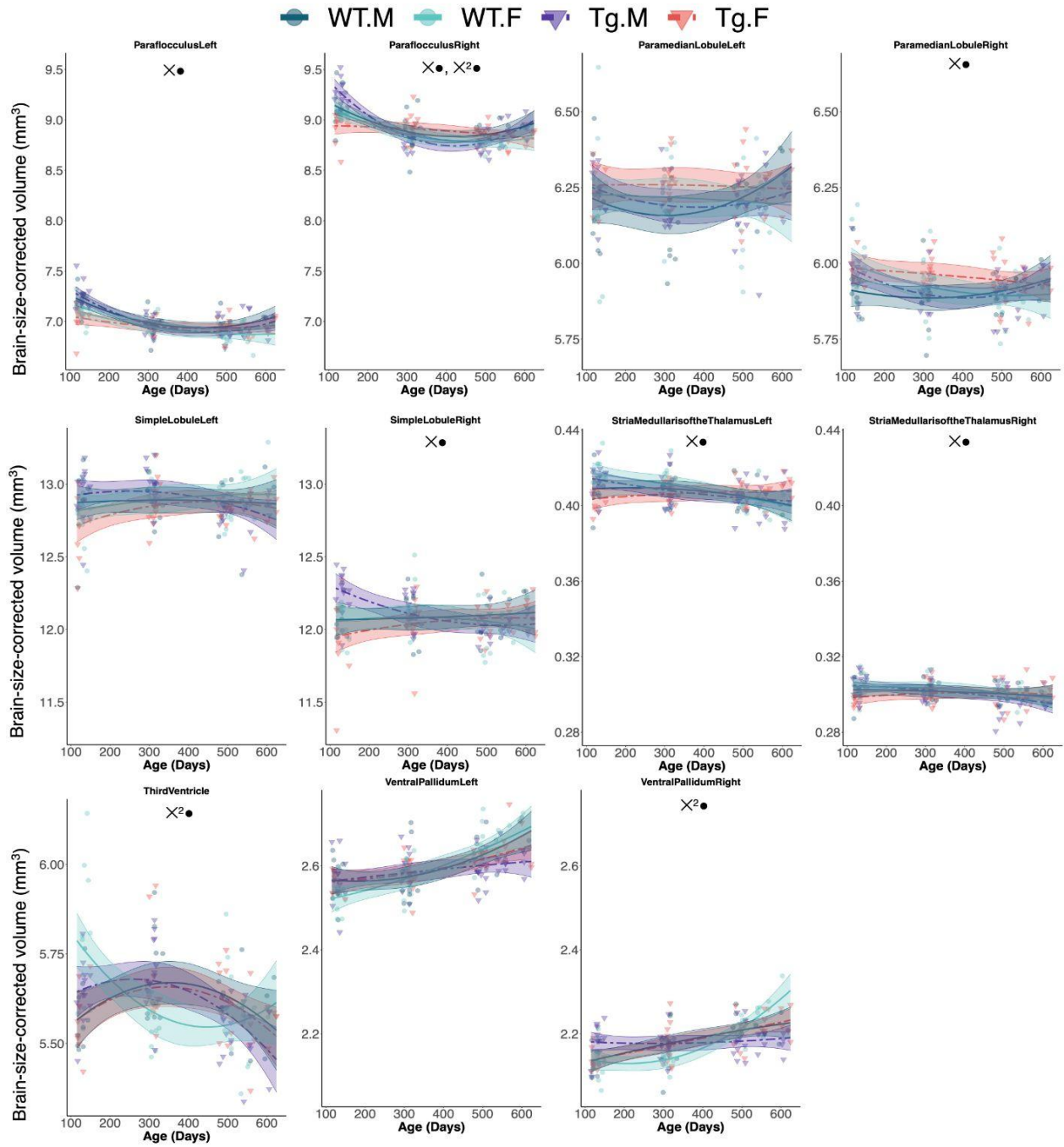
Supplementary Figure 5.11.1



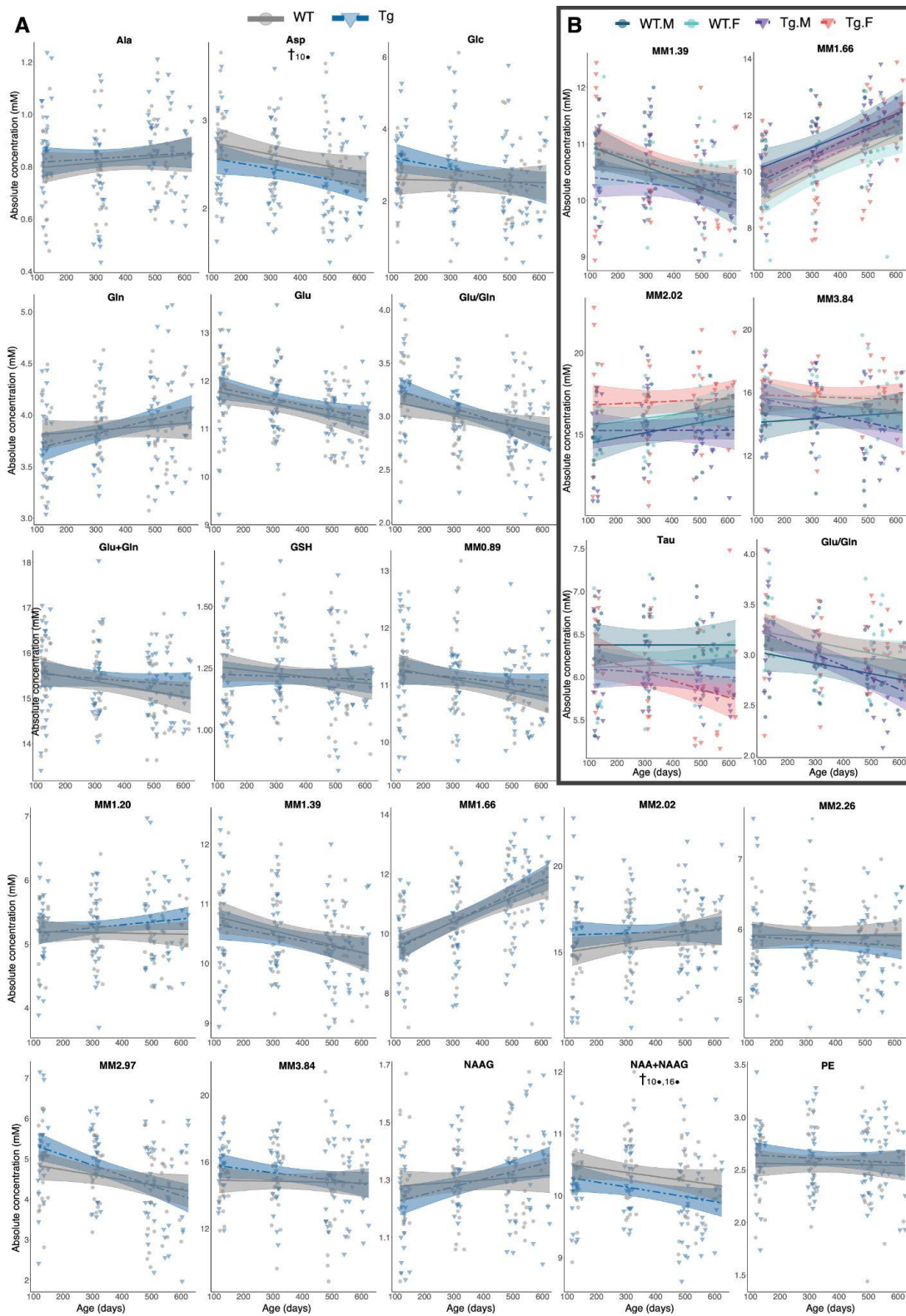
Supplementary Figure 5.11.2



Supplementary Figure 5.11.3



Supplementary Figure 5.11.4



Supplementary Figure 5.11.5

5.12 Chapter 5 Supplementary References

1. Lerch JP, Gazdzinski L, Germann J, Sled JG, Henkelman RM, Nieman BJ. Wanted dead or alive? The tradeoff between in-vivo versus ex-vivo MR brain imaging in the mouse. *Front Neuroinform.* 2012;6:6.
2. Cohen RM, Rezai-Zadeh K, Weitz TM, et al. A transgenic Alzheimer rat with plaques, tau pathology, behavioral impairment, oligomeric $\text{A}\beta$, and frank neuronal loss. *J Neurosci.* 2013;33(15):6245-6256.
3. Kreis R. The trouble with quality filtering based on relative Cramér-Rao lower bounds. *Magn Reson Med.* 2016;75(1):15-18.
4. Iglewicz B, Hoaglin DC. *How to Detect and Handle Outliers.* Vol 16. (Mykytka EF, Westergard S, Wall A, eds.). ASQC/Quality Press; 1997.
5. Leys C, Ley C, Klein O, Bernard P, Licata L. Detecting outliers: Do not use standard deviation around the mean, use absolute deviation around the median. *J Exp Soc Psychol.* 2013;49(4):764-766.
6. Pitts MW. Barnes Maze Procedure for Spatial Learning and Memory in Mice. *Bio Protoc.* 2018;8(5). doi:10.21769/bioprotoc.2744
7. Fox J, Weisberg S. An R Companion to Applied Regression. Published online 2019. <https://socialsciences.mcmaster.ca/jfox/Books/Companion/index.html>
8. Neuwirth E. *RColorBrewer: ColorBrewer Palettes.*; 2014. <https://CRAN.R-project.org/package=RColorBrewer>
9. Wickham H, Bryan J. *Readxl: Read Excel Files.*; 2019. <https://CRAN.R-project.org/package=readxl>
10. Kuznetsova A, Brockhoff PB, Christensen RHB. lmerTest Package: Tests in Linear Mixed Effects Models. *Journal of Statistical Software, Articles.* 2017;82(13):1-26.
11. Bates D, Mächler M, Bolker B, Walker S. Fitting Linear Mixed-Effects Models Using lme4. *Journal of Statistical Software, Articles.* 2015;67(1):1-48.
12. Wickham H, Averick M, Bryan J, et al. Welcome to the tidyverse. *J Open Source Softw.* 2019;4(43):1686.
13. Pfefferbaum A, Rohlfing T, Rosenbloom MJ, Chu W, Colrain IM, Sullivan EV. Variation in longitudinal trajectories of regional brain volumes of healthy men and women (ages 10 to 85 years) measured with atlas-based parcellation of MRI. *Neuroimage.* 2013;65:176-193.
14. Kong V, Devenyi GA, Gallino D, et al. Early-in-life neuroanatomical and behavioural trajectories in a triple transgenic model of Alzheimer's disease. *Brain Struct Funct.* 2018;223(7):3365-3382.
15. Tullo S, Patel R, Devenyi GA, et al. MR-based age-related effects on the striatum, globus pallidus, and thalamus in healthy individuals across the adult lifespan. *Hum Brain Mapp.* 2019;40(18):5269-5288.
16. Fowler CF, Madularu D, Dehghani M, Devenyi GA, Near J. Longitudinal quantification of metabolites and macromolecules reveals age- and sex-related changes in the healthy Fischer 344 rat brain. *Neurobiol Aging.* 2020;101:109-122.
17. Burnham KP, Anderson DR. Multimodel Inference: Understanding AIC and BIC in Model Selection. *Sociol Methods Res.* 2004;33(2):261-304.

5.13 Chapter 5 References

- Alexander, Gene E., Lan Lin, Eriko S. Yoshimaru, Pradyumna K. Bharadwaj, Kaitlin L. Bergfield, Lan T. Hoang, Monica K. Chawla, et al. 2020. "Age-Related Regional Network Covariance of Magnetic Resonance Imaging Gray Matter in the Rat." *Frontiers in Aging Neuroscience* 12: 267.
- Anckaerts, Cynthia, Ines Blockx, Priska Summer, Johanna Michael, Julie Hamaide, Christina Kreutzer, Hervé Boutin, Sébastien Couillard-Després, Marleen Verhoye, and Annemie Van der Linden. 2019. "Early Functional Connectivity Deficits and Progressive Microstructural Alterations in the TgF344-AD Rat Model of Alzheimer's Disease: A Longitudinal MRI Study." *Neurobiology of Disease* 124 (April): 93–107.
- Apostolova, Liana G., Chris Zarow, Kristina Biado, Sona Hurtz, Marina Boccardi, Johanne Somme, Hedieh Honarpisheh, et al. 2015. "Relationship between Hippocampal Atrophy and Neuropathology Markers: A 7T MRI Validation Study of the EADC-ADNI Harmonized Hippocampal Segmentation Protocol." *Alzheimer's & Dementia: The Journal of the Alzheimer's Association* 11 (2): 139–50.
- Attar, Aida, Tingyu Liu, Wai-Ting Coco Chan, Jane Hayes, Mona Nejad, Kaichyuan Lei, and Gal Bitan. 2013. "A Shortened Barnes Maze Protocol Reveals Memory Deficits at 4-Months of Age in the Triple-Transgenic Mouse Model of Alzheimer's Disease." *PloS One* 8 (11): e80355.
- Badhwar, Amanpreet, Jason P. Lerch, Edith Hamel, and John G. Sled. 2013. "Impaired Structural Correlates of Memory in Alzheimer's Disease Mice." *NeuroImage. Clinical* 3 (September): 290–300.
- Barnes, C. A. 1979. "Memory Deficits Associated with Senescence: A Neurophysiological and Behavioral Study in the Rat." *Journal of Comparative and Physiological Psychology* 93 (1): 74–104.
- Bartha, Robert. 2007. "Effect of Signal-to-Noise Ratio and Spectral Linewidth on Metabolite Quantification at 4 T." *NMR in Biomedicine* 20 (5): 512–21.
- Bateman, Randall J., Chengjie Xiong, Tammie L. S. Benzinger, Anne M. Fagan, Alison Goate, Nick C. Fox, Daniel S. Marcus, et al. 2012. "Clinical and Biomarker Changes in Dominantly Inherited Alzheimer's Disease." *The New England Journal of Medicine* 367 (9): 795–804.
- Bazzigaluppi, Paolo, Tina L. Beckett, Margaret M. Koletar, Aaron Y. Lai, Illsung L. Joo, Mary E. Brown, Peter L. Carlen, Joanne McLaurin, and Bojana Stefanovic. 2018. "Early-Stage Attenuation of Phase-Amplitude Coupling in the Hippocampus and Medial Prefrontal Cortex in a Transgenic Rat Model of Alzheimer's Disease." *Journal of Neurochemistry* 144 (5): 669–79.
- Benjamini, Yoav, and Yosef Hochberg. 1995. "Controlling the False Discovery Rate: A Practical and Powerful Approach to Multiple Testing." *Journal of the Royal Statistical Society. Series B, Statistical Methodology* 57 (1): 289–300.
- Berkowitz, Laura E., Ryan E. Harvey, Emma Drake, Shannon M. Thompson, and Benjamin J. Clark. 2018. "Progressive Impairment of Directional and Spatially Precise Trajectories by TgF344-Alzheimer's Disease Rats in the Morris Water Task." *Scientific Reports* 8 (1): 16153.
- Bernal-Rusiel, Jorge L., Douglas N. Greve, Martin Reuter, Bruce Fischl, Mert R. Sabuncu, and Alzheimer's Disease Neuroimaging Initiative. 2013. "Statistical Analysis of Longitudinal Neuroimage Data with Linear Mixed Effects Models." *NeuroImage* 66 (February): 249–60.
- Best, Jonathan G., Charlotte J. Stagg, and Andrea Dennis. 2014. "Chapter 2.5 - Other

- Significant Metabolites: Myo-Inositol, GABA, Glutamine, and Lactate.” In *Magnetic Resonance Spectroscopy*, edited by Charlotte Stagg and Douglas Rothman, 122–38. San Diego: Academic Press.
- Bianchini, F., A. Di Vita, L. Palermo, L. Piccardi, C. Blundo, and C. Guariglia. 2014. “A Selective Egocentric Topographical Working Memory Deficit in the Early Stages of Alzheimer’s Disease: A Preliminary Study.” *American Journal of Alzheimer’s Disease and Other Dementias* 29 (8): 749–54.
- Bobinski, M., M. J. de Leon, J. Wegiel, S. Desanti, A. Convit, L. A. Saint Louis, H. Rusinek, and H. M. Wisniewski. 2000. “The Histological Validation of Post Mortem Magnetic Resonance Imaging-Determined Hippocampal Volume in Alzheimer’s Disease.” *Neuroscience* 95 (3): 721–25.
- Braak, H., and E. Braak. 1991. “Alzheimer’s Disease Affects Limbic Nuclei of the Thalamus.” *Acta Neuropathologica* 81 (3): 261–68.
- . 1995. “Staging of Alzheimer’s Disease-Related Neurofibrillary Changes.” *Neurobiology of Aging* 16 (3): 271–78; discussion 278–84.
- Brand, A., C. Richter-Landsberg, and D. Leibfritz. 1993. “Multinuclear NMR Studies on the Energy Metabolism of Glial and Neuronal Cells.” *Developmental Neuroscience* 15: 289–98.
- Callen, D. J., S. E. Black, F. Gao, C. B. Caldwell, and J. P. Szalai. 2001. “Beyond the Hippocampus: MRI Volumetry Confirms Widespread Limbic Atrophy in AD.” *Neurology* 57 (9): 1669–74.
- Camandola, Simonetta, and Mark P. Mattson. 2017. “Brain Metabolism in Health, Aging, and Neurodegeneration.” *The EMBO Journal* 36 (11): 1474–92.
- Chan, Dennis, Laura Marie Gallaher, Kuven Moodley, Ludovico Minati, Neil Burgess, and Tom Hartley. 2016. “The 4 Mountains Test: A Short Test of Spatial Memory with High Sensitivity for the Diagnosis of Pre-Dementia Alzheimer’s Disease.” *Journal of Visualized Experiments: JoVE*, no. 116 (October). <https://doi.org/10.3791/54454>.
- Chaney, Aisling M., Francisco R. Lopez-Picon, Sophie Serrière, Rui Wang, Daniela Bochicchio, Samuel D. Webb, Matthias Vandesquille, et al. 2021. “Prodromal Neuroinflammatory, Cholinergic and Metabolite Dysfunction Detected by PET and MRS in the TgF344-AD Transgenic Rat Model of AD: A Collaborative Multi-Modal Study.” *Theranostics* 11 (14): 6644–67.
- Chaney, A. M., F. R. Lopez-Picon, S. Serriere, R. Wang, D. Bochicchio, S. D. Webb, M. Vandesquille, et al. 2021. *Prodromal Neuroinflammatory, Cholinergic and Metabolite Dysfunction Detected by PET and MRS in the TgF344-AD Transgenic Rat Model of AD: A Collaborative Multi-Modal Study*. <https://zenodo.org/record/4710273>.
- Choi, Ji-Kyung, Isabel Carreras, Nur Aytan, Eric Jenkins-Sahlin, Alpaslan Dedeoglu, and Bruce G. Jenkins. 2014. “The Effects of Aging, Housing and Ibuprofen Treatment on Brain Neurochemistry in a Triple Transgene Alzheimer’s Disease Mouse Model Using Magnetic Resonance Spectroscopy and Imaging.” *Brain Research* 1590 (November): 85–96.
- Chung, M. K., K. J. Worsley, T. Paus, C. Cherif, D. L. Collins, J. N. Giedd, J. L. Rapoport, and A. C. Evans. 2001. “A Unified Statistical Approach to Deformation-Based Morphometry.” *NeuroImage* 14 (3): 595–606.
- Cohen, Robert M., Kavon Rezai-Zadeh, Tara M. Weitz, Altan Rentsendorj, David Gate, Inna Spivak, Yasmin Bholat, et al. 2013. “A Transgenic Alzheimer Rat with Plaques, Tau Pathology, Behavioral Impairment, Oligomeric A β , and Frank Neuronal Loss.” *The Journal of Neuroscience: The Official Journal of the Society for Neuroscience* 33 (15): 6245–56.

- Dedeoglu, Alpaslan, Ji-Kyung Choi, Kerry Cormier, Neil W. Kowall, and Bruce G. Jenkins. 2004. "Magnetic Resonance Spectroscopic Analysis of Alzheimer's Disease Mouse Brain That Express Mutant Human APP Shows Altered Neurochemical Profile." *Brain Research* 1012 (1-2): 60–65.
- Do Carmo, Sonia, and A. Claudio Cuello. 2013. "Modeling Alzheimer's Disease in Transgenic Rats." *Molecular Neurodegeneration* 8 (October): 37.
- Drummond, Eleanor, and Thomas Wisniewski. 2017. "Alzheimer's Disease: Experimental Models and Reality." *Acta Neuropathologica* 133 (2): 155–75.
- Ellenbroek, Bart, and Jiun Youn. 2016. "Rodent Models in Neuroscience Research: Is It a Rat Race?" *Disease Models & Mechanisms* 9 (10): 1079–87.
- Ernst, T., R. Kreis, and B. D. Ross. 1993. "Absolute Quantitation of Water and Metabolites in the Human Brain. I. Compartments and Water." *Journal of Magnetic Resonance. Series B* 102 (1): 1–8.
- Filon, Jessica R., Anthony J. Intorcchia, Lucia I. Sue, Elsa Vazquez Arreola, Jeffrey Wilson, Kathryn J. Davis, Marwan N. Sabbagh, et al. 2016. "Gender Differences in Alzheimer Disease: Brain Atrophy, Histopathology Burden, and Cognition." *Journal of Neuropathology and Experimental Neurology* 75 (8): 748–54.
- Fjell, Anders M., Linda McEvoy, Dominic Holland, Anders M. Dale, Kristine B. Walhovd, and Alzheimer's Disease Neuroimaging Initiative. 2014. "What Is Normal in Normal Aging? Effects of Aging, Amyloid and Alzheimer's Disease on the Cerebral Cortex and the Hippocampus." *Progress in Neurobiology* 117 (June): 20–40.
- Fortea, Juan, Roser Sala-Llonch, David Bartrés-Faz, Beatriz Bosch, Albert Lladó, Nuria Bargalló, José Luis Molinuevo, and Raquel Sánchez-Valle. 2010. "Increased Cortical Thickness and Caudate Volume Precede Atrophy in PSEN1 Mutation Carriers." *Journal of Alzheimer's Disease: JAD* 22 (3): 909–22.
- Fowler, Caitlin F., Dan Madularu, Masoumeh Dehghani, Gabriel A. Devenyi, and Jamie Near. 2020. "Longitudinal Quantification of Metabolites and Macromolecules Reveals Age- and Sex-Related Changes in the Healthy Fischer 344 Rat Brain." *Neurobiology of Aging* 101 (December): 109–22.
- Fowler, Caitlin, Dana Goerzen, Dan Madularu, Gabriel A. Devenyi, M. Mallar Chakravarty, and Jamie Near. 2021. "LONGITUDINAL CHARACTERIZATION OF NEUROANATOMICAL CHANGES IN THE FISCHER 344 RAT BRAIN DURING NORMAL AGING AND BETWEEN SEXES." *Neurobiology of Aging*, October. <https://doi.org/10.1016/j.neurobiolaging.2021.10.003>.
- Fowler, Caitlin, Dana Goerzen, Dan Madularu, Gabriel A. Devenyi, M. Mallar Chakravarty, and Jamie Near. 2021. "Longitudinal Characterization of Neuroanatomical Changes in the Fischer 344 Rat Brain during Normal Aging and between Sexes." *bioRxiv*. <https://doi.org/10.1101/2021.04.12.439510>.
- Friedel, Miriam, Matthijs C. van Eede, Jon Pipitone, M. Mallar Chakravarty, and Jason P. Lerch. 2014. "Pydpiper: A Flexible Toolkit for Constructing Novel Registration Pipelines." *Frontiers in Neuroinformatics* 8 (July): 67.
- Frisoni, Giovanni B., Nick C. Fox, Clifford R. Jack Jr, Philip Scheltens, and Paul M. Thompson. 2010. "The Clinical Use of Structural MRI in Alzheimer Disease." *Nature Reviews. Neurology* 6 (2): 67–77.
- Gao, F., and P. B. Barker. 2014. "Various MRS Application Tools for Alzheimer Disease and Mild Cognitive Impairment." *AJNR. American Journal of Neuroradiology* 35 (6 Suppl): S4–

11.

Gawel, Kinga, Ewa Gibula, Marta Marszalek-Grabska, Joanna Filarowska, and Jolanta H. Kotlinska. 2019. "Assessment of Spatial Learning and Memory in the Barnes Maze Task in Rodents-Methodological Consideration." *Naunyn-Schmiedeberg's Archives of Pharmacology* 392 (1): 1–18.

Goerzen, Dana, Caitlin Fowler, Gabriel A. Devenyi, Jurgen Germann, Dan Madularu, M. Mallar Chakravarty, and Jamie Near. 2020. "An MRI-Derived Neuroanatomical Atlas of the Fischer 344 Rat Brain." *Scientific Reports* 10 (1): 6952.

Gruetter, Rolf. 1993. "Automatic, Localized in Vivo Adjustment of All First- and Second-Order Shim Coils." *Journal of Magnetic Resonance in Medicine* 29: 804–11.

Güell-Bosch, J., S. Lope-Piedrafita, G. Esquerda-Canals, L. Montoliu-Gaya, and S. Villegas. 2020. "Progression of Alzheimer's Disease and Effect of scFv-h3D6 Immunotherapy in the 3xTg-AD Mouse Model: An in Vivo Longitudinal Study Using Magnetic Resonance Imaging and Spectroscopy." *NMR in Biomedicine* 33 (5): e4263.

Jack, Clifford R., Frederik Barkhof, Matt A. Bernstein, Marc Cantillon, Patricia E. Cole, Charles DeCarli, Bruno Dubois, et al. 2011. "Steps to Standardization and Validation of Hippocampal Volumetry as a Biomarker in Clinical Trials and Diagnostic Criterion for Alzheimer's Disease." *Alzheimer's & Dementia: The Journal of the Alzheimer's Association* 7 (4): 474–85.e4.

Jack, Clifford R., Jr, David S. Knopman, William J. Jagust, Ronald C. Petersen, Michael W. Weiner, Paul S. Aisen, Leslie M. Shaw, et al. 2013. "Tracking Pathophysiological Processes in Alzheimer's Disease: An Updated Hypothetical Model of Dynamic Biomarkers." *Lancet Neurology* 12 (2): 207–16.

Jack, Clifford R., Jr, David S. Knopman, William J. Jagust, Leslie M. Shaw, Paul S. Aisen, Michael W. Weiner, Ronald C. Petersen, and John Q. Trojanowski. 2010. "Hypothetical Model of Dynamic Biomarkers of the Alzheimer's Pathological Cascade." *Lancet Neurology* 9 (1): 119–28.

Jack, C. R., Jr, M. M. Shiung, S. D. Weigand, P. C. O'Brien, J. L. Gunter, B. F. Boeve, D. S. Knopman, et al. 2005. "Brain Atrophy Rates Predict Subsequent Clinical Conversion in Normal Elderly and Amnesic MCI." *Neurology* 65 (8): 1227–31.

Jong, L. W. de, K. van der Hiele, I. M. Veer, J. J. Houwing, R. G. J. Westendorp, E. L. E. M. Bollen, P. W. de Bruin, H. A. M. Middelkoop, M. A. van Buchem, and J. van der Grond. 2008. "Strongly Reduced Volumes of Putamen and Thalamus in Alzheimer's Disease: An MRI Study." *Brain: A Journal of Neurology* 131 (Pt 12): 3277–85.

Joo, Illsung L., Aaron Y. Lai, Paolo Bazzigaluppi, Margaret M. Koletar, Adrienne Dorr, Mary E. Brown, Lysie A. M. Thomason, John G. Sled, Joanne McLaurin, and Bojana Stefanovic. 2017. "Early Neurovascular Dysfunction in a Transgenic Rat Model of Alzheimer's Disease." *Scientific Reports* 7 (1): 1–14.

Kantarci, K., R. C. Petersen, B. F. Boeve, D. S. Knopman, D. F. Tang-Wai, P. C. O'Brien, S. D. Weigand, et al. 2004. "1H MR Spectroscopy in Common Dementias." *Neurology* 63 (8): 1393–98.

Kong, Vincent, Gabriel A. Devenyi, Daniel Gallino, Gülebru Ayranci, Jürgen Germann, Colleen Rollins, and M. Mallar Chakravarty. 2018. "Early-in-Life Neuroanatomical and Behavioural Trajectories in a Triple Transgenic Model of Alzheimer's Disease." *Brain Structure & Function* 223 (7): 3365–82.

Lau, Jonathan C., Jason P. Lerch, John G. Sled, R. Mark Henkelman, Alan C. Evans, and Barry

- J. Bedell. 2008. “Longitudinal Neuroanatomical Changes Determined by Deformation-Based Morphometry in a Mouse Model of Alzheimer’s Disease.” *NeuroImage* 42 (1): 19–27.
- Leplus, Aurelie, Inger Lauritzen, Christophe Melon, Lydia Kerkerian-Le Goff, Denys Fontaine, and Frederic Checler. 2019. “Chronic Fornix Deep Brain Stimulation in a Transgenic Alzheimer’s Rat Model Reduces Amyloid Burden, Inflammation, and Neuronal Loss.” *Brain Structure & Function* 224 (1): 363–72.
- Lerch, Jason P., Lisa Gazdzinski, Jürgen Germann, John G. Sled, R. Mark Henkelman, and Brian J. Nieman. 2012. “Wanted Dead or Alive? The Tradeoff between in-Vivo versus Ex-Vivo MR Brain Imaging in the Mouse.” *Frontiers in Neuroinformatics* 6 (March): 6.
- Lerch, J., C. Hammill, M. van Eede, and D. Cassel. 2017. “Statistical Tools for Medical Imaging NetCDF (MINC) Files. R Package Version 1.5.2.3.” 2017. <http://mouse-imaging-centre.github.io/RMINC/>.
- Lewis, J., D. W. Dickson, W. L. Lin, L. Chisholm, A. Corral, G. Jones, S. H. Yen, et al. 2001. “Enhanced Neurofibrillary Degeneration in Transgenic Mice Expressing Mutant Tau and APP.” *Science* 293 (5534): 1487–91.
- Lin, Joanne C., and Nicholas Gant. 2014. “Chapter 2.3 - The Biochemistry of Choline.” In *Magnetic Resonance Spectroscopy*, edited by Charlotte Stagg and Douglas Rothman, 104–10. San Diego: Academic Press.
- Lithfous, Ségolène, André Dufour, and Olivier Després. 2013. “Spatial Navigation in Normal Aging and the Prodromal Stage of Alzheimer’s Disease: Insights from Imaging and Behavioral Studies.” *Ageing Research Reviews* 12 (1): 201–13.
- Maheswaran, Satheesh, Hervé Barjat, Daniel Rueckert, Simon T. Bate, David R. Howlett, Lorna Tilling, Sean C. Smart, et al. 2009. “Longitudinal Regional Brain Volume Changes Quantified in Normal Aging and Alzheimer’s APP X PS1 Mice Using MRI.” *Brain Research* 1270 (May): 19–32.
- Marjanska, Malgorzata, Geoffrey L. Curran, Thomas M. Wengenack, Pierre-Gilles Henry, Robin L. Bliss, Joseph F. Poduslo, Clifford R. Jack Jr, Kâmil Ugurbil, and Michael Garwood. 2005. “Monitoring Disease Progression in Transgenic Mouse Models of Alzheimer’s Disease with Proton Magnetic Resonance Spectroscopy.” *Proceedings of the National Academy of Sciences of the United States of America* 102 (33): 11906–10.
- Marjańska, Malgorzata, J. Riley McCarten, James S. Hodges, Laura S. Hemmy, and Melissa Terpstra. 2019. “Distinctive Neurochemistry in Alzheimer’s Disease via 7 T In Vivo Magnetic Resonance Spectroscopy.” *Journal of Alzheimer’s Disease: JAD* 68 (2): 559–69.
- Martínez-Pinilla, Eva, Cristina Ordóñez, Eva Del Valle, Ana Navarro, and Jorge Tolivia. 2016. “Regional and Gender Study of Neuronal Density in Brain during Aging and in Alzheimer’s Disease.” *Frontiers in Aging Neuroscience* 8 (September): 213.
- Mattson, Mark P. 2004. “Pathways towards and Away from Alzheimer’s Disease.” *Nature* 430 (7000): 631–39.
- Mattson, Mark P., and Thiruma V. Arumugam. 2018. “Hallmarks of Brain Aging: Adaptive and Pathological Modification by Metabolic States.” *Cell Metabolism* 27 (6): 1176–99.
- Mazure, Carolyn M., and Joel Swendsen. 2016. “Sex Differences in Alzheimer’s Disease and Other Dementias.” *Lancet Neurology*.
- McKenna, Mary C., Gerald A. Dienel, Ursula Sonnewald, Helle S. Waagepetersen, and Arne Schousboe. 2012. “Chapter 11 - Energy Metabolism of the Brain.” In *Basic Neurochemistry (Eighth Edition)*, edited by Scott T. Brady, George J. Siegel, R. Wayne Albers, and Donald L. Price, 200–231. New York: Academic Press.

- Mersman, Brittany, Wali Zaidi, Naweed I. Syed, and Fenglian Xu. 2020. "Taurine Promotes Neurite Outgrowth and Synapse Development of Both Vertebrate and Invertebrate Central Neurons." *Frontiers in Synaptic Neuroscience* 12 (July): 29.
- Morrone, Christopher D., Paolo Bazzigaluppi, Tina L. Beckett, Mary E. Hill, Margaret M. Koletar, Bojana Stefanovic, and Joanne McLaurin. 2020. "Regional Differences in Alzheimer's Disease Pathology Confound Behavioural Rescue after Amyloid- β Attenuation." *Brain: A Journal of Neurology* 143 (1): 359–73.
- Mosconi, Lisa. 2013. "Glucose Metabolism in Normal Aging and Alzheimer's Disease: Methodological and Physiological Considerations for PET Studies." *Clinical and Translational Imaging* 1 (4). <https://doi.org/10.1007/s40336-013-0026-y>.
- Mueller, S. G., N. Schuff, and M. W. Weiner. 2006. "Evaluation of Treatment Effects in Alzheimer's and Other Neurodegenerative Diseases by MRI and MRS." *NMR in Biomedicine* 19 (6): 655–68.
- Muñoz-Moreno, Emma, Raúl Tudela, Xavier López-Gil, and Guadalupe Soria. 2018. "Early Brain Connectivity Alterations and Cognitive Impairment in a Rat Model of Alzheimer's Disease." *Alzheimer's Research & Therapy* 10 (1): 16.
- Murray, Melissa E., Scott A. Przybelski, Timothy G. Lesnick, Amanda M. Liesinger, Anthony Spychalla, Bing Zhang, Jeffrey L. Gunter, et al. 2014. "Early Alzheimer's Disease Neuropathology Detected by Proton MR Spectroscopy." *The Journal of Neuroscience: The Official Journal of the Society for Neuroscience* 34 (49): 16247–55.
- Nilsen, Linn H., Torun M. Melø, Oddbjørn Saether, Menno P. Witter, and Ursula Sonnewald. 2012. "Altered Neurochemical Profile in the McGill-R-Thy1-APP Rat Model of Alzheimer's Disease: A Longitudinal in Vivo 1 H MRS Study." *Journal of Neurochemistry* 123 (4): 532–41.
- Oberg, Johanna, Christian Spenger, Fu-Hua Wang, Anders Andersson, Eric Westman, Peter Skoglund, Dan Sunnemark, et al. 2008. "Age Related Changes in Brain Metabolites Observed by 1H MRS in APP/PS1 Mice." *Neurobiology of Aging* 29 (9): 1423–33.
- Oddo, Salvatore, Antonella Caccamo, Jason D. Shepherd, M. Paul Murphy, Todd E. Golde, Rakez Kaye, Raju Metherate, Mark P. Mattson, Yama Akbari, and Frank M. LaFerla. 2003. "Triple-Transgenic Model of Alzheimer's Disease with Plaques and Tangles: Intracellular Abeta and Synaptic Dysfunction." *Neuron* 39 (3): 409–21.
- Oh, Esther S., Alena V. Savonenko, Julie F. King, Stina M. Fangmark Tucker, Gay L. Rudow, Guilian Xu, David R. Borchelt, and Juan C. Troncoso. 2009. "Amyloid Precursor Protein Increases Cortical Neuron Size in Transgenic Mice." *Neurobiology of Aging* 30 (8): 1238–44.
- Patterson, Christina. 2018. "World Alzheimer Report 2018. The State of the Art of Dementia Research: New Frontiers." *Alzheimer's Disease International*. <https://apo.org.au/sites/default/files/resource-files/2018-09/apo-nid260056.pdf>.
- Pfefferbaum, A., E. Adalsteinsson, D. Spielman, E. V. Sullivan, and K. O. Lim. 1999. "In Vivo Brain Concentrations of N-Acetyl Compounds, Creatine, and Choline in Alzheimer Disease." *Archives of General Psychiatry* 56 (2): 185–92.
- Pfefferbaum, Adolf, Torsten Rohlfing, Margaret J. Rosenbloom, Weiwei Chu, Ian M. Colrain, and Edith V. Sullivan. 2013. "Variation in Longitudinal Trajectories of Regional Brain Volumes of Healthy Men and Women (ages 10 to 85 Years) Measured with Atlas-Based Parcellation of MRI." *NeuroImage* 65 (January): 176–93.
- Pini, Lorenzo, Michela Pievani, Martina Bocchetta, Daniele Altomare, Paolo Bosco, Enrica Cavedo, Samantha Galluzzi, Moira Marizzoni, and Giovanni B. Frisoni. 2016. "Brain Atrophy

in Alzheimer's Disease and Aging." *Ageing Research Reviews* 30 (September): 25–48.

Pitts, Matthew W. 2018. "Barnes Maze Procedure for Spatial Learning and Memory in Mice." *Bio-Protocol* 8 (5). <https://doi.org/10.21769/bioprotoc.2744>.

Podcasy, Jessica L., and C. Neill Epperson. 2016. "Considering Sex and Gender in Alzheimer Disease and Other Dementias." *Dialogues in Clinical Neuroscience* 18 (4): 437–46.

Pol, L. A. van de, W. M. van der Flier, E. S. C. Korf, N. C. Fox, F. Barkhof, and P. Scheltens. 2007. "Baseline Predictors of Rates of Hippocampal Atrophy in Mild Cognitive Impairment." *Neurology* 69 (15): 1491–97.

Rahman, Aneela, Hande Jackson, Hollie Hristov, Richard S. Isaacson, Nabeel Saif, Teena Shetty, Orli Etingin, Claire Henschliffe, Roberta Diaz Brinton, and Lisa Mosconi. 2019. "Sex and Gender Driven Modifiers of Alzheimer's: The Role for Estrogenic Control Across Age, Race, Medical, and Lifestyle Risks." *Frontiers in Aging Neuroscience* 11 (November): 315.

Rajamohamedsait, Hameetha B., and Einar M. Sigurdsson. 2012. "Histological Staining of Amyloid and Pre-Amyloid Peptides and Proteins in Mouse Tissue." *Methods in Molecular Biology* 849: 411–24.

R Core Team. 2020. "R: A Language and Environment for Statistical Computing." Vienna, Austria: R Foundation for Statistical Computing. <https://www.R-project.org/>.

Rettberg, Jamaica R., Jia Yao, and Roberta Diaz Brinton. 2014. "Estrogen: A Master Regulator of Bioenergetic Systems in the Brain and Body." *Frontiers in Neuroendocrinology* 35 (1): 8–30.

Riudavets, Miguel Angel, Diego Iacono, Susan M. Resnick, Richard O'Brien, Alan B. Zonderman, Lee J. Martin, Gay Rudow, Olga Pletnikova, and Juan C. Troncoso. 2007. "Resistance to Alzheimer's Pathology Is Associated with Nuclear Hypertrophy in Neurons." *Neurobiology of Aging* 28 (10): 1484–92.

Rorabaugh, Jacki M., Termpanit Chalermpanupap, Christian A. Botz-Zapp, Vanessa M. Fu, Natalie A. Lembeck, Robert M. Cohen, and David Weinshenker. 2017. "Chemogenetic Locus Coeruleus Activation Restores Reversal Learning in a Rat Model of Alzheimer's Disease." *Brain: A Journal of Neurology* 140 (11): 3023–38.

Ross, Amy J., and Perminder S. Sachdev. 2004. "Magnetic Resonance Spectroscopy in Cognitive Research." *Brain Research. Brain Research Reviews* 44 (2-3): 83–102.

Saré, Rachel Michelle, Spencer K. Cooke, Leland Krych, Patricia M. Zervas, Robert M. Cohen, and Carolyn Beebe Smith. 2020. "Behavioral Phenotype in the TgF344-AD Rat Model of Alzheimer's Disease." *Frontiers in Neuroscience* 14 (June): 601.

Selkoe, Dennis J. 2011. "Alzheimer's Disease." *Cold Spring Harbor Perspectives in Biology* 3 (7). <https://doi.org/10.1101/cshperspect.a004457>.

Selkoe, D. J. 2001. "Alzheimer's Disease: Genes, Proteins, and Therapy." *Physiological Reviews* 81 (2): 741–66.

Simpson, Robin, Gabriel A. Devenyi, Peter Jezzard, T. Jay Hennessy, and Jamie Near. 2017. "Advanced Processing and Simulation of MRS Data Using the FID Appliance (FID-A)-An Open Source, MATLAB-Based Toolkit." *Magnetic Resonance in Medicine: Official Journal of the Society of Magnetic Resonance in Medicine / Society of Magnetic Resonance in Medicine* 77 (1): 23–33.

Smith, Lindsey A., and Lori L. McMahon. 2018. "Deficits in Synaptic Function Occur at Medial Perforant Path-Dentate Granule Cell Synapses prior to Schaffer Collateral-CA1 Pyramidal Cell Synapses in the Novel TgF344-Alzheimer's Disease Rat Model." *Neurobiology of Disease* 110 (February): 166–79.

- Spencer, N. G., L. R. Bridges, K. Elderfield, K. Amir, B. Austen, and F. A. Howe. 2013. "Quantitative Evaluation of MRI and Histological Characteristics of the 5xFAD Alzheimer Mouse Brain." *NeuroImage* 76 (August): 108–15.
- Stoiljkovic, Milan, Craig Kelley, Bernardo Stutz, Tamas L. Horvath, and Mihály Hajós. 2019. "Altered Cortical and Hippocampal Excitability in TgF344-AD Rats Modeling Alzheimer's Disease Pathology." *Cerebral Cortex* 29 (6): 2716–27.
- Tkac̆, I., Z. Starc̆uk, I. -Y. Choi, and R. Gruetter. 1999. "In Vivo H NMR Spectroscopy of Rat Brain at 1 Ms Echo Time." *Magnetic Resonance in Medicine: Official Journal of the Society of Magnetic Resonance in Medicine / Society of Magnetic Resonance in Medicine* 41: 649–56.
- Tullo, Stephanie, Raihaan Patel, Gabriel A. Devenyi, Alyssa Salaciak, Saashi A. Bedford, Sarah Farzin, Nancy Wlodarski, et al. 2019. "MR-Based Age-Related Effects on the Striatum, Globus Pallidus, and Thalamus in Healthy Individuals across the Adult Lifespan." *Human Brain Mapping* 40 (18): 5269–88.
- Voorhees, Jaymie R., Matthew T. Remy, Coral J. Cintrón-Pérez, Eli El Rassi, Michael Z. Khan, Laura M. Dutca, Terry C. Yin, et al. 2018. "(-)-P7C3-S243 Protects a Rat Model of Alzheimer's Disease From Neuropsychiatric Deficits and Neurodegeneration Without Altering Amyloid Deposition or Reactive Glia." *Biological Psychiatry* 84 (7): 488–98.
- Wang, Hui, Lan Tan, Hui-Fu Wang, Ying Liu, Rui-Hua Yin, Wen-Ying Wang, Xiao-Long Chang, Teng Jiang, and Jin-Tai Yu. 2015. "Magnetic Resonance Spectroscopy in Alzheimer's Disease: Systematic Review and Meta-Analysis." *Journal of Alzheimer's Disease: JAD* 46 (4): 1049–70.
- West, Mark J., Georg Bach, Andreas Söderman, and Jens Ledet Jensen. 2009. "Synaptic Contact Number and Size in Stratum Radiatum CA1 of APP/PS1DeltaE9 Transgenic Mice." *Neurobiology of Aging* 30 (11): 1756–76.
- Wisse, Laura E. M., Geert Jan Biessels, Sophie M. Heringa, Hugo J. Kuijf, Dineke H. L. Koek, Peter R. Luijten, Mirjam I. Geerlings, and Utrecht Vascular Cognitive Impairment (VCI) Study Group. 2014. "Hippocampal Subfield Volumes at 7T in Early Alzheimer's Disease and Normal Aging." *Neurobiology of Aging* 35 (9): 2039–45.
- Wu, Chongyun, Luodan Yang, Yong Li, Yan Dong, Baocheng Yang, Lorelei Donovan Tucker, Xuemei Zong, and Quanguang Zhang. 2020. "Effects of Exercise Training on Anxious-Depressive-like Behavior in Alzheimer Rat." *Medicine and Science in Sports and Exercise* 52 (7): 1456–69.
- Yin, Fei, Harsh Sancheti, Ishan Patil, and Enrique Cadenas. 2016. "Energy Metabolism and Inflammation in Brain Aging and Alzheimer's Disease." *Free Radical Biology & Medicine* 100 (November): 108–22.

CHAPTER 6: DISCUSSION AND CONCLUSIONS

6.1 Summary of results and main conclusions

A major challenge to the advancement of options for AD diagnosis and treatment has been a lack of biomarkers that can distinguish the effects of normal aging from those manifesting due to pathology, specifically at an early stage of the disease, and in the presence of differences between sexes. In an attempt to address this limitation, we characterized longitudinal neuroanatomical and neurochemical processes underlying normal aging in a mixed-sex cohort of Fischer 344 rats; and the chronological order and extent of disease-related neurochemical, neuroanatomical, and cognitive abnormalities in a mixed-sex cohort of TgF344-AD rats, using methods with high translational potential to human studies. Specifically, this thesis addressed the following questions:

1. How do age and sex affect hippocampal tissue chemistry throughout the adult rat lifespan?
2. How do age and sex influence brain volume trajectories throughout the adult rat lifespan?
3. Does the TgF344-AD rat model recapitulate major cognitive, neurochemical, and neuroanatomical features of human Alzheimer's disease and in what chronological order do these pathological changes appear?
4. How does sex influence the pathological features of AD in the TgF344-AD rat model?

We addressed the first question in **Chapter 3**. Motivated by the lack of preclinical literature describing longitudinal neurochemical change with age, and even less literature examining the influence of sex on neurochemistry, we acquired *in vivo* MRS data from the hippocampus of a mixed-sex cohort of Fischer 344 rats at 4, 10, 16, and 20 months. We also developed and implemented methodology to quantify individual MM resonances, which provided additional valuable metabolic information. We identified linear age-dependent decreases in GSH and NAA/Ins concentrations and increases in Ins, Lac, NAAG. Other notable changes with age were curvilinear changes in Asp/Glu and Glu/Gln. Several neurochemicals also differed by sex, with Glc seen in higher concentrations in males while PCr and tCr were present in lower concentrations in males. Finally, several MMs increased with age and differed by sex. These findings demonstrate a significant metabolic shift with age and a role of sex in defining those changes. Specifically, the age-related metabolic changes indicated a shift towards anaerobic energy metabolism (Glc, Lac),

decreased antioxidant capacity (GSH), compensatory attempts at neuroprotection (NAAG), possible neuroinflammation (Ins), altered neurotransmission and/or impaired mitochondrial energetics (Glu/Gln, Asp/Glu), and possibly increased cell death (MMs). Sex effects were primarily seen in metabolites involved in energy metabolism (Glc, tCr, PCr), which fits with findings of hormonal influence on glucose metabolism and mitochondrial function in aging rats ([Yin et al. 2015](#)). This published work represents the first longitudinal characterization of age-related change in neurochemistry in the Fischer 344 rat. This study provides detailed insight into the many metabolic processes affected by age and the influence of sex on these processes in a commonly used rat model of aging. We anticipate that many of these findings may be applicable to human aging populations, given that many of the processes affected by aging in the Fischer rat brain have been shown to be similarly affected in humans ([Camandola and Mattson 2017](#); [Mattson and Magnus 2006](#)), and sex differences have been reported for several neurotransmitter systems at the clinical level ([Cosgrove et al. 2007](#)). Importantly, these findings also represent a neurochemical baseline for studies in transgenic models of disease, particularly those developed on a Fischer 344 background.

Chapter 4 represents a natural follow-up to the investigation of highly localized effects of brain aging in **Chapter 3**, and explores the effect of age and sex on rat neuroanatomy across the whole brain. The motivation for this study was similar to that for **Chapter 3**: despite aging research being vital to the understanding and management of age-related diseases, there is a paucity of literature regarding neuroanatomical change during normal aging at the preclinical level, and the impact of sex on those changes. As such, the work presented in **Chapter 4** is the first longitudinal investigation of age-related change in neuroanatomy in a mixed-sex cohort of Fischer 344 rats. This publication examines longitudinal neuroanatomical change at both the voxel-wise and regional level in 120 brain volumes at 4, 10, 16, and 20 months in male and female Fischer 344 rats, capturing structural abnormalities across the whole brain and covering much of the adult and senescent rat lifespan. The majority of age-related changes were seen in grey matter structures, with strong decreases in areas such as the caudoputamen, frontal cortex, and thalamus, and increased volume in the dentate gyrus. Some white matter structures were also altered with age but tended to increase in volume, such as the internal capsule, and cingulum. The influence of sex on these changes was not consistent, with some structures showing parallel trajectories but with one sex having a larger relative volume overall (basal forebrain, thalamus), and other structures showing an

interaction between sex and age, such as the hippocampus, whereby female hippocampal volume was stable with increasing age and males showed signs of atrophy after mid-life. Overall, structures showing volume changes were spatially distributed across the brain and implicated in a wide variety of physiological functions (motor control, visual processing, memory, autonomic functions, etc) ([Rolls 2015](#); [Malinowski 2019](#)), suggesting that numerous systems are affected by the aging process, and further modified by sex. Given how rarely subcortical structures aside from the hippocampus are examined in human studies, only a few of the age- and sex-related results in this chapter have been shown in humans. That said, the overall findings of widespread neuroanatomical changes with age and the influence of sex are consistent with the existing literature ([Cosgrove et al. 2007](#); [Armstrong et al. 2019](#); [Pini et al. 2016](#); [Fjell and Walhovd 2010](#)). Perhaps more importantly, and similar to **Chapter 3**, the findings presented here can be considered a neuronanatomical baseline for future work examining the compound effect of age, pathology, and sex on brain structure in transgenic models of disease.

Finally, **Chapter 5** builds upon the work in the previous two chapters by applying the same neuroimaging modalities, along with behavioural testing, to perform a comprehensive longitudinal analysis of multiple pathological features in the TgF344-AD rat model of Alzheimer's disease. This manuscript aimed to determine if this rat model recapitulated major cognitive, neurochemical, and neuroanatomical features of human AD; the chronological order in which they appear; and the intersection of sex, genotype, and age. MRI, MRS, and behavioural testing were employed at 4, 10, 16, and 18 months of age in male and female TgF344-AD rats. The TgF344-AD model demonstrated impaired spatial reference memory in the Barnes Maze by 4 months of age, followed by neurochemical abnormalities by 10 months and major structural changes by 16 months. This is the earliest report of cognitive dysfunction in this model and our detection of impaired spatial memory in particular fits well with documented complaints of early deficits in hippocampus-dependent spatial learning and memory in human AD subjects ([Chan et al. 2016](#); [Lithfous et al. 2013](#)). This study is also the first to quantify the full neurochemical profile, including individual MM resonances. Metabolic changes included increased tCho and Lac, decreased tCr, Tau, and NAA/Ins, suggesting cell membrane degradation (tCho), increased anaerobic energy metabolism and/or altered mitochondrial energetics (Lac, tCr), and possibly neuroinflammation and/or neuronal dysfunction (NAA/Ins, Tau), all of which replicate well-documented phenomena in human AD ([Yin et al. 2016](#); [Mosconi 2013](#); [Camandola and Mattson 2017](#); [Marjańska et al. 2019](#)).

Interestingly, MMs were previously shown to be modified with age in **Chapter 3** but no significant differences were present between aging WT and TgF344-AD rats, suggesting that MM abnormalities are primarily a feature of aging and not AD pathology specifically. All neuroanatomical findings presented in this chapter are also novel, as the only existing study exploring brain structure in TgF344-AD rats was performed in a single-sex cohort ([Anckaerts et al. 2019](#)). While TgF344-AD rats did not display notable cortical atrophy in our study, they did demonstrate atrophy in numerous limbic structures known to be affected by disease progression in humans ([Jack et al. 2011](#); [Callen et al. 2001](#)), such as the hippocampus, basal forebrain, and hypothalamus. Finally, mild sex effects were present in MRI, MRS, and behavioural data, supporting previous reports indicating a role for sex hormones in the pathogenesis of AD ([Podcasy and Epperson 2016](#); [Filon et al. 2016](#); [Rahman et al. 2019](#)); Tg females demonstrated stronger pathological effects in several brain volumes and more cognitive impairment than Tg males, whereas sex effects on metabolite concentrations appeared to be the result of WT or Tg males differing from the other groups. The findings in this chapter support the use of MRI and MRS for the development of non-invasive biomarkers of AD progression, clarify the timing of pathological feature presentation in the TgF344-AD model, and advance the validation of the TgF344-AD rat as a highly relevant model for preclinical AD research, all of which represent significant contributions to the scientific community.

In summary, the original work presented in this thesis describes the application of whole-brain MRI and localized MRS to comprehensively investigate age- and sex-related changes in neurochemistry and neuroanatomy in the Fischer 344 rat, and the subsequent integration of these techniques with behavioural testing in the TgF344-AD rat model to distinguish the effects of aging versus Alzheimer's disease pathology on neuroimaging and cognitive markers. This thesis thoroughly characterizes multiple neurobiological features of aging and AD in mixed-sex cohorts of two highly relevant rat models, contributing to our understanding of the complex changes underlying the aging process and progression of AD in both sexes. Importantly, the neuroimaging techniques employed throughout the three manuscripts are highly translatable to the study of other transgenic models of disease, as well as to human clinical studies, supporting the development of homologous biomarkers across species. This thesis therefore provides support for the use of MRI and MRS to detect age, disease, or intervention-related change which may be used to improve age- and disease-related outcomes in humans.

6.2 Limitations

There are several limitations to the work described in this thesis that should be considered when interpreting the results and designing studies for further investigation of the topics addressed herein.

First, there are limitations in translating findings in rodents to studies in humans given differences between species in neuronal network complexity, grey to white matter ratios, expression of gene polymorphisms, neurotransmitter distribution, and the complexity of cognitive functions and behaviour ([Geerts 2009](#); [Shineman et al. 2011](#)). Behavioural findings in rodents are particularly difficult to translate to humans for a variety of reasons, including the high variability of behavioural metrics in both rodents and humans; a lack of standardization for testing protocols; and inherent difficulties in interpretation of subtle behavioural traits (e.g. does floating in the MWM reflect lack of motivation, reduced motor function, or cognitive impairment? Do human behavioural domains such as episodic memory, working memory, executive function, activities of daily living, etc., have reasonable endophenotypic analogs in animal models?) ([Stephan et al. 2019](#); [Vitek et al. 2020](#)). Additionally, even in strains without transgene insertion, such as the Fischer 344 rat, their generation through inbreeding reduces genetic diversity and may reduce applicability to humans compared to outbred strains with more genetic variability, such as the Wistar rat ([Gallagher et al. 2011](#)). As such, the extent of translation between preclinical and clinical results may vary depending on the strain of rodent used, the disease being modelled, and the outcome metrics being analyzed, and these factors should be taken into consideration when designing future studies.

Second, while the TgF344-AD transgenic model, leveraged in this thesis, is a highly valuable tool for preclinical AD research and has been used extensively since its emergence in 2013 ([Cohen et al. 2013](#)), translatability is limited as a result of how it was generated. As with most transgenic models of AD, the TgF344-AD rat was developed by means of insertion of mutant human transgenes known to cause familial AD, and therefore does not reflect the more common form of sporadic AD, which, while genetic risk factors exist, does not currently have a clear genetic cause ([Selkoe 2011](#)). Additionally, there have been discussions on whether a model developed in less genetically invasive ways, such as the McGill-R-Thy1-APP rat (reproduces extensive AD amyloid pathology with a single transgene ([Leon et al. 2010](#))) is a closer model of sporadic AD than models like the TgF344-AD rat (developed using two transgenes) ([Do Carmo and Cuello](#)

[2013](#)). Finally, rodent models of sporadic AD exist and neuropathology develops as a result of expressing variants of genes known to be strong genetic risk factors (*APOE*, *TREM2*), but none of these models develops tau pathology or widespread neuronal loss ([Nakai et al. 2021](#); [Foidl and Humpel 2020](#)). Therefore, given that no other rat or mouse model of AD, familial or sporadic, develops tau pathology without insertion of a human tau transgene, the TgF344-AD rat still represents an extremely useful and unique tool for preclinical research provided the caveat of only reflecting FAD is acknowledged. This model can still contribute to our understanding of the etiology and pathogenesis of sporadic AD without being directly translatable, just as studies in individuals with familial AD have informed studies on sporadic AD ([Bateman et al. 2012](#); [Gordon et al. 2018](#); [Lee et al. 2013](#)).

Third, there are inherent limitations to the interpretation of outcome metrics obtained from the MR techniques employed in this thesis, generally as a result of spatial resolution. For example, while MRS is a unique and powerful method for directly quantifying brain tissue chemistry, the voxel is too large to determine the exact cellular origin (cell type) or location (intracellular or extracellular) of the MRS signal. This kind of cellular localization can be inferred using advanced diffusion-weighted MRS ([Ligneul et al. 2019](#)), but not using conventional *in vivo* MRS as employed in this thesis. With MRI we do not directly measure the cellular compartments whose properties we are trying to describe, but rather image contrast is used—which depends on tissue proton density and local tissue microenvironment—to make indirect neurobiological conclusions ([Lerch et al. 2017](#)). Studies that combine MR techniques and immunohistochemistry experiments, genomic pathway analysis, and/or forms of *in vitro* metabolic profiling such as mass spectrometry ([Kostidis et al. 2017](#); [Bobinski et al. 2000](#)), have contributed significantly to our understanding and contextualization of the cellular and molecular properties of MRI and MRS signals. *In vivo* neuroimaging (ideally using more than one MR modality) should continue to be combined with *ex-vivo* or *in-vitro* studies to enhance interpretability whenever possible.

6.3 Future directions

6.3.1 Identifying multivariate features of aging and AD

Throughout this thesis we identified neurochemical and neuroanatomical changes that occurred as a result of aging (**Chapter 3 and 4**) and AD pathology (**Chapter 5**), many of which

were reported for the first time. Upon comparison of the individual manuscripts, a consistent theme appeared: some changes were specific to the TgF344-AD genotype, while others appeared in both the aging and TgF344-AD cohorts but were further exacerbated by the AD genotype.

For example, Ins and Lac, both of which were increased during normal aging (**Chapter 3**), were further increased in TgF344-AD rats relative to WT littermates (**Chapter 5**). Additionally, the ratios of NAA/Ins and Asp/Glu were decreased and Tau was trending towards a decrease in aging Fischer 344 rats, and both were further decreased in TgF344-AD rats. Changes specific to TgF344-AD rats were increased total choline and decreased tCr. Similarly, several neuroanatomical changes with age described in **Chapter 4** were intensified in the presence of pathology, as examined in **Chapter 5**, but with some exceptions that distinguished the two processes. For example, increased volume with age was identified within the aqueduct, dentate gyrus, and fimbria, while decreases were noted in the caudoputamen, hippocampus, and nucleus accumbens, and these changes were amplified in TgF344-AD rats. Structural trajectories that were distinct between aging rats and those with AD were decreased lateral septum, basal forebrain, and hypothalamus volumes in TgF344-AD rats, whereby the former two were unaltered with age in the Fischer 344 rat and the latter actually increased in the aging cohort.

While qualitatively these patterns are present in the data, statistical examination and/or classification was not performed outside of using univariate methods. To explore the importance of these patterns in differentiating TgF344-AD rats from control rats, classification methods such as a random forest algorithm could be implemented on the separate imaging datasets or both together. This kind of analysis has previously been performed using neurochemical (14 metabolites) and neuroanatomical data from two brain regions in healthy controls and individuals with clinically confirmed AD ([Marjańska et al. 2019](#)). Random forests distinguished between the two groups with 88% sensitivity and 97% specificity, using only neurochemical data, and the main predictors of clinical status were Asc, Ins, tCho, and NAAG. Interestingly, adding grey matter, white matter, and CSF volumes did not change the classification or increase performance, indicating the neurochemical profile was better suited for classification purposes in this particular study cohort.

Data from this thesis would be well-suited for this type of classification analysis, particularly since a multi-modal approach has been shown to improve classification accuracy compared to a single modality approach ([Tong et al. 2017](#)). In particular, the comprehensive volumetric data (120 brain regions) and expanded neurochemical dataset (18 metabolites and 9

MMs) generated herein may improve classification sensitivity and specificity, and/or reveal previously unidentified neurochemicals or structures important for distinguishing between aging and AD phenotypes at the preclinical level.

6.3.2 Developing a more comprehensive translational research platform

As reviewed by several authors ([Scearce-Levie et al. 2020](#); [Shineman et al. 2011](#); [Vitek et al. 2020](#)), there have been difficulties regarding translatability of preclinical findings to clinical outcomes, particularly regarding therapeutic approaches. The best-documented example are the many studies showing comparable reduction of A β levels in rodents and humans using anti-A β antibodies or secretase inhibitors, but the subsequent inability of these therapies to slow, halt, or reverse cognitive decline in AD patients while cognitive improvement was seen in the rodent models ([Fitz et al. 2014](#); [Boutajangout et al. 2019](#); [Henley et al. 2009](#)). Among the many reasons for the lack of translatability are the use of different modalities for assessing disease progression at the preclinical versus clinical level, and the nearly ubiquitous use of rodent models that do not capture the full spectrum of AD pathological features.

While MRI and MRS serve as important non-invasive modalities capable of detecting and monitoring structural and biochemical abnormalities, MRS biomarkers are not currently widely used in clinical research settings due to the complexities of data acquisition, processing and interpretation ([Cecil 2013](#)). As discussed in section 2.1.3, the most widely used imaging modalities for AD in a clinical research setting are PET-based amyloid markers, and markers of neuronal injury, including FDG-PET and structural MRI ([Teipel et al. 2015](#)), while CSF levels of amyloid and tau are also frequently examined. Tau-based PET is also beginning to be employed in rodent models and in clinical studies ([Schöll et al. 2016](#); [Saint-Aubert et al. 2017](#); [Chaney et al. 2021](#)). Implementing these techniques longitudinally in relevant transgenic models of AD would be highly analogous to the design of clinical studies and would enable the translatability of novel therapeutics to be determined using the same biomarkers as are used in human clinical trials. Compared to mice, rat models are better-suited for these techniques due to their larger size, thus offering better spatial resolution for imaging, as well as easier CSF collection and analysis ([Ellenbroek and Youn 2016](#); [Vitek et al. 2020](#)).

Two studies have recently been published that employed imaging techniques typically used in human AD studies in transgenic rat models. Parent et al. used resting state functional MRI (rs-

fMRI) to characterize brain connectivity, PET[¹⁸F]FDG to detect glucose hypometabolism, PET[¹⁸F]NAV4694 to detect fibrillar amyloid, structural MRI to quantify hippocampal atrophy, behavioural testing to identify cognitive impairment, and CSF sampling to examine A β concentrations in male and female McGill-R-Thy1-APP rats at 9-11 and 16-19 months ([Parent et al. 2017](#)). Given that the McGill-R-Thy1-APP model does not display tau pathology, the authors were able to examine the effect of only brain amyloid on aspects of disease progression and concluded that this model recapitulates an abnormal biomarker profile, similar to that shown in human AD patients using the same techniques, despite lacking NFTs and widespread neuronal loss. A similarly comprehensive study by Chaney et al., used [¹⁸F]DPA-714, [¹⁸F]ASEM, [¹⁸F]Florbetan, and (S)-[¹⁸F]THK5117 PET imaging to assess neuroinflammation, the acetylcholine system, A β plaque deposition, and tau aggregation, respectively, along with MRS, behavioural testing, and immunohistochemistry in the TgF344-AD rat model at 6, 12, and 18 months ([Chaney et al. 2021](#)). This latter paper demonstrated, among other findings, that tau pathology in the TgF344-AD model could be detected via PET, which adds another modality with which disease progression can be monitored in this model. However, several of the experiments conducted in this study used only single sex groups, so much of this data needs to be replicated in mixed-sex cohorts. Regardless, both studies indicated the ability to obtain meaningful neurobiological data by applying typically clinical-level techniques in rat models of AD and demonstrate the benefit of a multimodal approach to disease characterization. Both studies also took advantage of the opportunity provided by working with rodent models to perform immunohistochemical analyses, although unfortunately, correlative analyses with neuroimaging outcome measures were not performed. We attempted to perform correlative analyses between immunofluorescence data and neuroimaging and cognitive measures in **Chapter 5** but were limited by a small sample size, so a larger study would be highly informative.

As authors Chaney and Parent showed above, employing commonly used methods for studying human AD in rat models, particularly longitudinally, directly mimics the clinical approach. Knowing that methods such as amyloid and tau imaging, FDG-PET, or CSF sampling are equally applicable in rat models will allow for future work to use these techniques in other contexts, such as monitoring therapeutic efficacy or more closely staging the early or late aspects of disease progression. Additionally, combining longitudinal amyloid and tau imaging and CSF sampling with MRS (using the extended neurochemical profile employed here), and structural MRI

in the TgF344-AD rat (using the 120 brain regions examined in this thesis and recently developed rat atlas ([Goerzen et al. 2020](#))), as well as employing age-centered models for analysis, would expand our understanding of the relative timing of imaging biomarker abnormalities in the TgF344-AD model, and may support the development of MRS-based biomarkers in a clinical setting. Finally, given that MRS is the only imaging modality described here that remains “investigational” and is not routinely used to support AD diagnosis, despite evidence that it would prove helpful ([Lin et al. 2005](#); [Graff-Radford and Kantarci 2013](#); [Marjańska et al. 2019](#)), it could also be interesting to perform multimodal *in vivo* imaging in the TgF344-AD rat and then apply a classifier algorithm to determine if MRS performed similarly well to amyloid and tau PET imaging, or CSF markers.

In addition to using biomarkers that are directly translatable to those used in humans, another way to facilitate more reliable translation between preclinical and clinical studies is the use of appropriate transgenic models of disease. While no transgenic model will perfectly capture the entirety of a human disease, there are several that recapitulate most features, and some that are better used for testing of specific disease targets and pathways (for extensive reviews, see ([Vitek et al. 2020](#); [Shineman et al. 2011](#))). As discussed in Section 2.2.3 of this thesis, the majority of existing rodent models only capture both disease hallmarks if a human tau transgene is inserted into their genome, such as the 3xTg rat ([Oddo et al. 2003](#)), which is not causative of AD in humans. The TgF344-AD model overcomes this limitation and develops tau pathology despite only harbouring mutated *APP* and *PS1* transgenes. Finally, while writing the final sections of this thesis, a report was published that describes a new *APP* knock-in rat model of AD that spontaneously develops tau pathology, similar to the TgF344-AD rat ([Pang et al. 2021](#)). Extensive characterization of tissue pathology has been performed, and revealed the deposition of A β plaques, gliosis, tau pathology, neuronal apoptosis, progressive synaptic degeneration, brain atrophy, and cognitive deficits ([Pang et al. 2021](#)), indicating that this new *APP* knock-in model may serve as a second highly relevant transgenic rat model for studying the combined effect of amyloid and tau pathology on disease manifestation and progression. Knock-in models maintain the original murine genomic structure, except for the introduced mutations, and were developed to overcome issues intrinsic to models developed via overexpression of transgenes method, such as those used to generate the TgF344-AD and McGill-R-Thy1-APP models ([Searce-Levie et al. 2020](#)). For more information on knock-in models, please see ([Searce-Levie et al. 2020](#); [Saito et al. 2014](#); [Sasaguri et al. 2017](#)). Future work should include using *in vivo* imaging methods to study the *APP* knock-in rat, particularly in

comparison with equivalent experiments in the TgF344-AD rat model and/or the McGill-R-Thy1-APP model. Comparison of multiple transgenic rat models would provide insight into the effect of only amyloid pathology versus amyloid and tau compounded (McGill-R-Thy1-APP versus TgF344-AD models) on *in vivo* biomarker profiles, as well as the effect of transgene overexpression versus genetic knock-in on phenotype development (TgF344-AD versus *APP* knock-in models). Even more interesting could be research comparing a model of familial AD to a model of sporadic AD, such as the *APOE* rat ([Kulkarni et al. 2020](#)) to examine the differences in disease manifestation and progression as a result of genotype. Excitingly, the *APOE* rat and the *APP* knock-in model were both developed on a Sprague Dawley background, meaning strain differences would not confound the results.

Finally, and this applies to all potential studies addressed in this section, intentionally including and investigating the influence of sex on outcome metrics at the preclinical level is incredibly important for ensuring translatability to human clinical studies. Only by including and studying both sexes can we capture the diversity of the pathophysiological mechanisms of disease, particularly when studying AD given that clear evidence exists for differences between the sexes regarding disease prevalence, presentation, and progression ([Filon et al. 2016](#); [Rahman et al. 2019](#)). The consideration of sex as a variable would thus seem a necessary part of preclinical AD research, yet very few preclinical studies include both males and females, and even fewer explicitly examine the influence of sex ([Coiro and Pollak 2019](#)). For example, the incredibly comprehensive investigation of multiple *in vivo* biomarkers of disease in the TgF344-AD rat by Chaney et al. mentioned above included multiple experiments that were only performed in one sex, and the remaining experiments did not indicate the sex of the rats ([Chaney et al. 2021](#)), instantly reducing the interpretability and translatability of the data. Future preclinical studies in transgenic models must include both sexes for the findings to inform clinical research.

6.3.3 Delving into molecular mechanisms and histological underpinnings of aging and AD pathology

While existing *in vivo* biomarkers are incredibly useful for detecting pathological features, they do not provide much mechanistic information about the cellular and molecular processes underlying the pathology. This is where a variety of different histological, biochemical, and genetic

approaches come in, underlining the unique advantages of research at the preclinical level, where both *in vivo* and *ex vivo* approaches can be employed within the same subjects.

Perhaps the most large-scale method for future preclinical research is the use of transcriptomics and proteomics to identify specific genes and pathways implicated in the onset of AD in transgenic models. In humans, early genetic linkage studies led to the association of *APP*, *PS1*, and *PS2* gene mutations with disease pathogenesis ([Castanho et al. 2020](#)). Since those discoveries, many genome-wide association studies (GWAS) have identified numerous gene loci that increase a person's vulnerability to late-onset AD, the most well-known of which is *APOE*. Many other susceptibility genes have been identified that involve lipid homeostasis, immune regulation, mitochondrial function, cellular metabolism, and synaptic signaling, as well as several that are either directly or indirectly involved in the regulation of inflammatory mechanisms ([Sleegers et al. 2010](#); [Vitek et al. 2020](#); [De Strooper and Karran 2016](#); [Mattson 2004](#)). Interestingly, the proteome and transcriptome can offer up distinct but complementary information; clusters of proteins correlating with AD phenotypes were distinct from those in RNA-directed networks, but many AD risk loci were identified in glial-related molecules in both the proteome and transcriptome of individuals with AD ([Seyfried et al. 2017](#)), further supporting the implication of microglial response pathways in disease pathogenesis ([Scheltens et al. 2021](#); [Lutz et al. 2019](#)). Excitingly, at least two studies of this nature have been performed in transgenic models of AD. Castanho et al., studied the transcriptional signatures of two different mouse models of AD pathology, one expressing primary amyloid and the other expressing only tau neuropathology, across the majority of the mouse lifespan. Among their many findings, they identified gene co-expression networks associated with the progression of tau pathology that were enriched for pathways related to synaptic transmission, the immune system, and glial cell activation, many of which are similar to networks identified in human AD ([Castanho et al. 2020](#)). In a separate study, genome-wide transcriptional profiling of the insular cortex in 3xTg mice was performed, along with behavioural and biochemical profiling and identified specific sets of genes associated with amyloid deposition and cognitive decline ([Yin et al. 2020](#)). It is clear that transcriptional and proteomic profiling can provide significant insight into the mechanisms underlying disease progression, and thus would complement the use of *in vivo* methods in transgenic models.

Findings from transcriptional or proteomic studies could also be used to inform what markers to look for using other methods, such as histology or biochemical assays. For example,

genes involved in mitochondrial and bioenergetic function have been identified in a number of the aforementioned genome studies ([Slegers et al. 2010](#); [Lambert et al. 2013](#); [Vitek et al. 2020](#)). Mitochondrial dysfunction can produce other AD-associated molecular features, such as increased oxidative stress ([Swerdlow et al. 2014](#)). Measures of oxidative stress can be obtained by monitoring lipid peroxidation or the presence of oxidized proteins by high-performance liquid chromatography (HPLC) ([Sultana and Butterfield 2011](#); [Shineman et al. 2011](#)); these metrics could be compared to levels of GSH, a known antioxidant, measured by MRS. Other potentially important processes include ectopic cell cycle events (CCEs) and dysfunctional lysosomal and autophagy pathways. Varvel et al., examined the presence of CCEs in AD transgenic mice using cell cycle proteins cyclin A and D, along with NeuN ([Varvel et al. 2009](#)). CCEs play a major role in the loss of neurons in AD dementia ([Yang et al. 2003](#)), but it remains unclear if disrupted cell cycling plays a role in early disease progression as well. Similarly, defective autophagy (the major degradative pathway for organelles and proteins) and abnormal lysosomal system function has been identified in neurons in the brains of AD patients and evidence suggests dysfunction in these pathways at very early disease stages ([Nixon and Yang 2011](#); [Nixon and Cataldo 2006](#)). Immunolabelling and western blot analysis of brain tissue from APP^{E693Q} mice identified increased lysosomal proteins (LAMP-2, cathepsin D, and LC3), as well as increased conversion of LC3-1 to LC3-II, which is an autophagosomal/autolysosomal marker, indicating lysosomal pathology in this transgenic model ([Kaur et al. 2017](#)). Any of the aforementioned experiments could be performed in the TgF344-AD rat or *APP* knock-in model.

There are also non-invasive ways to obtain more mechanistic information that could complement MRI and MRS findings. For example, inflammatory pathways have been heavily implicated in AD pathogenesis ([Lambert et al. 2013](#); [Slegers et al. 2010](#); [Krstic and Knuesel 2013](#); [Heneka and O'Banion 2007](#)), but authors often fall back on using histological methods to quantify microglial or astrocytic activation. However, 11C-PK11195 or 18F-DPA-714 PET imaging has been developed and used in rats to assess neuroinflammation *in vivo*, specifically microglial activation ([Kong et al. 2016](#); [Cui et al. 2009](#)). Perhaps even more interesting is the use of diffusion weighted MRS (DW-MRS), which investigates the diffusion process of metabolites, a property that has been shown to differ depending on the structure of their microenvironment (i.e. is diffusion indicative of a metabolite being localized to a smaller space, like an astrocyte, or a large space, like a neuron) ([Palombo et al. 2016](#)). Excitingly, in a mouse model of reactive astrocytes, DW-MRS

was used to identify Ins as a specific astrocytic marker, enabling non-invasive detection of astrocyte hypertrophy based on its diffusion properties, results that were then confirmed by confocal microscopy *ex vivo*. On the other hand, lactate was found to be primarily astrocytic under control conditions but became predominantly neuronal in the case of astrocytic activity, suggesting remodeling of lactate metabolism ([Ligneul et al. 2019](#)). This type of approach in a transgenic rat model of AD could provide information on metabolic remodeling, as well as cell morphology.

It is clear that any of the aforementioned methods could be used in conjunction with MRI, MRS, or other imaging modalities to improve interpretation of *in vivo* findings. In particular, a comprehensive study involving *in vivo* and *ex vivo* techniques could be leveraged to answer important questions regarding which features are the earliest to appear, and which represent suitable targets for disease-modifying therapies.

6.3.4 Examination of early preclinical stage to identify earliest disease features and targets for preventative treatment

The studies performed in this thesis were conducted from 4 to 18 or 20 months, covering much of the rodent lifespan after development to the beginning of senescence. The next step towards identifying the etiology of AD and identifying new targets for treatment is to perform comprehensive investigations of the earliest stages of the disease in transgenic models, before the accumulation of neuropathological hallmarks have even begun. There is substantial evidence demonstrating that amyloid deposition begins up to decades prior to the appearance of cognitive symptoms ([Bateman et al. 2012](#); [Jack et al. 2013](#)), and if amyloid is not the causative factor, then the initiating event(s) will occur even earlier. The overwhelming lack of success of agents administered to patients already in MCI or dementia stages of AD (particularly anti-amyloid therapies) indicates that the most effective strategy for disease management will likely be to treat at very early stages of the disease, or even in a preventative manner for individuals who are at high risk ([Sperling et al. 2014](#)). Studies using early treatment paradigms have shown promise over treatment administered late into disease progression. For example, administration of anti-amyloid antibodies in 3xTg mice reduced plaque load and even cleared tau pathology, but tau clearance was dependent on phosphorylation state and treatment once tau was hyperphosphorylated was ineffective ([Oddo et al. 2004](#)). Similarly, only early administration of non-steroidal anti-inflammatory drugs (NSAIDs) (Naproxen and Ibuprofen) blocked ectopic neuronal cell cycle

events (CCE) which mark vulnerable neuronal populations, whereas late treatment failed to reverse existing CCEs ([Varvel et al. 2009](#)), again suggesting early intervention is more effective at mitigating aspects of disease progression. In fact, our lab has also examined the effect of early versus late administration of NSAIDs in the TgF344-AD model on the progression of neuroimaging markers and cognition. While this study is not yet published, preliminary results suggest early treatment is more effective than late treatment at mitigating disease-dependent changes in metabolite concentrations. The analysis and publication of that data, along with the MRI and behavioural results, will represent the first study to examine the outcome of early versus late NSAID treatment in the TgF34-AD model. Even in humans, this hypothesis of effective early treatment has been shown: administration of Naproxen in cognitively normal individuals reduced their risk of developing AD over a 3-year span, whereas treatment in individuals with MCI and AD resulted in accelerated cognitive decline ([Breitner et al. 2011](#)).

Given the promising results in these and other early treatment paradigms, there is a need to continue to explore alternative biomarkers that reflect early pathological changes and may represent new therapeutic targets, such as CCEs or the inflammatory response, while also working to develop non-invasive biomarkers that can be translated from preclinical to clinical studies. There has been much discussion in previous sections and throughout this thesis of MRS meeting these needs, as it may detect changes reflecting many biological processes at earlier stages than other neuroimaging methods and is a non-invasive technique. However, MRS or other non-invasive modalities should be combined with additional methods that can provide more mechanistic information, such as immunohistochemistry or transcriptional analysis of brain tissue. As such, these initial experiments will need to be performed in transgenic models. In order to avoid the majority of the developmental stage (which could confound biomarker readings) while still taking place before amyloid or tau pathology appears, these experiments could be performed as early as six to eight weeks in the TgF344-AD model, McGill-R-Thy1-APP model, and *APP* knock-in models ([Cohen et al. 2013](#); [Leon et al. 2010](#); [Pang et al. 2021](#)). These early-stage studies, incorporating as many of the suggestions identified in this Future Directions section as possible (multiple and or new transgenic rat models, studying both sexes, using several imaging methods combined with genomic, biochemical, and histological analyses) represent the best next step towards better understanding AD etiology, developing early biomarkers, and identifying new targets for disease-modifying therapies.

COMPLETE BIBLIOGRAPHY

- Aggleton, John P., and Malcolm W. Brown. 1999. "Episodic Memory, Amnesia, and the Hippocampal–anterior Thalamic Axis." *The Behavioral and Brain Sciences* 22 (3): 425–44.
- Akaike, Hirotugu, Boris Nikolaevich Petrov, and F. Csaki. 1973. "Second International Symposium on Information Theory." Akadémiai Kiadó, Budapest.
- Akintola, Abimbola A., and Diana van Heemst. 2015. "Insulin, Aging, and the Brain: Mechanisms and Implications." *Frontiers in Endocrinology* 6 (February): 13.
- Alexander, Gene E., Lan Lin, Eriko S. Yoshimaru, Pradyumna K. Bharadwaj, Kaitlin L. Bergfield, Lan T. Hoang, Monica K. Chawla, et al. 2020. "Age-Related Regional Network Covariance of Magnetic Resonance Imaging Gray Matter in the Rat." *Frontiers in Aging Neuroscience* 12: 267.
- Allemand-Grand, R., J. Scholz, J. Ellegood, L. S. Cahill, C. Laliberté, P. E. Fraser, S. A. Josselyn, J. G. Sled, and J. P. Lerch. 2015. "Altered Brain Development in an Early-Onset Murine Model of Alzheimer's Disease." *Neurobiology of Aging* 36 (2): 638–47.
- Anckaerts, Cynthia, Ines Blockx, Priska Summer, Johanna Michael, Julie Hamaide, Christina Kreutzer, Hervé Boutin, Sébastien Couillard-Després, Marleen Verhoye, and Annemie Van der Linden. 2019. "Early Functional Connectivity Deficits and Progressive Microstructural Alterations in the TgF344-AD Rat Model of Alzheimer's Disease: A Longitudinal MRI Study." *Neurobiology of Disease* 124 (April): 93–107.
- Andres, Robert H., Angélique D. Ducray, Uwe Schlattner, Theo Wallimann, and Hans Rudolf Widmer. 2008. "Functions and Effects of Creatine in the Central Nervous System." *Brain Research Bulletin* 76 (4): 329–43.
- Apostolova, Liana G., Chris Zarow, Kristina Biado, Sona Hurtz, Marina Boccardi, Johanne Somme, Hedieh Honarpisheh, et al. 2015. "Relationship between Hippocampal Atrophy and Neuropathology Markers: A 7T MRI Validation Study of the EADC-ADNI Harmonized Hippocampal Segmentation Protocol." *Alzheimer's & Dementia: The Journal of the Alzheimer's Association* 11 (2): 139–50.
- Ardekani, Babak A., Antonio Convit, and Alvin H. Bachman. 2016. "Analysis of the MIRIAD Data Shows Sex Differences in Hippocampal Atrophy Progression." *Journal of Alzheimer's Disease: JAD* 50 (3): 847–57.
- Armstrong, Nicole M., Yang An, Lori Beason-Held, Jimit Doshi, Guray Erus, Luigi Ferrucci, Christos Davatzikos, and Susan M. Resnick. 2019. "Sex Differences in Brain Aging and Predictors of Neurodegeneration in Cognitively Healthy Older Adults." *Neurobiology of Aging* 81 (September): 146–56.
- Ashburner, J., C. Hutton, R. Frackowiak, I. Johnsrude, C. Price, and K. Friston. 1998. "Identifying Global Anatomical Differences: Deformation-Based Morphometry." *Human Brain Mapping* 6 (5-6): 348–57.
- Attar, Aida, Tingyu Liu, Wai-Ting Coco Chan, Jane Hayes, Mona Nejad, Kaichyuan Lei, and Gal Bitan. 2013. "A Shortened Barnes Maze Protocol Reveals Memory Deficits at 4-Months of Age in the Triple-Transgenic Mouse Model of Alzheimer's Disease." *PloS One* 8 (11): e80355.
- Azam, Shofiul, Md Ezazul Haque, Rengasamy Balakrishnan, In-Su Kim, and Dong-Kug Choi. 2021. "The Ageing Brain: Molecular and Cellular Basis of Neurodegeneration." *Frontiers in Cell and Developmental Biology* 9 (August): 683459.
- Bacchetti, Peter. 2010. "Current Sample Size Conventions: Flaws, Harms, and

- Alternatives.” *BMC Medicine* 8 (March): 17.
- Badhwar, Amanpreet, Jason P. Lerch, Edith Hamel, and John G. Sled. 2013. “Impaired Structural Correlates of Memory in Alzheimer’s Disease Mice.” *NeuroImage. Clinical* 3 (September): 290–300.
- Barbier, Pascale, Orgeta Zejneli, Marlène Martinho, Alessia Lasorsa, Valérie Belle, Caroline Smet-Nocca, Philipp O. Tsvetkov, François Devred, and Isabelle Landrieu. 2019. “Role of Tau as a Microtubule-Associated Protein: Structural and Functional Aspects.” *Frontiers in Aging Neuroscience* 11 (August): 204.
- Barnes, C. A. 1979. “Memory Deficits Associated with Senescence: A Neurophysiological and Behavioral Study in the Rat.” *Journal of Comparative and Physiological Psychology* 93 (1): 74–104.
- Barnes, Lisa L., Robert S. Wilson, Julia L. Bienias, Julie A. Schneider, Denis A. Evans, and David A. Bennett. 2005. “Sex Differences in the Clinical Manifestations of Alzheimer Disease Pathology.” *Archives of General Psychiatry* 62 (6): 685–91.
- Bartha, Robert. 2007. “Effect of Signal-to-Noise Ratio and Spectral Linewidth on Metabolite Quantification at 4 T.” *NMR in Biomedicine* 20 (5): 512–21.
- Bateman, Randall J., Chengjie Xiong, Tammie L. S. Benzinger, Anne M. Fagan, Alison Goate, Nick C. Fox, Daniel S. Marcus, et al. 2012. “Clinical and Biomarker Changes in Dominantly Inherited Alzheimer’s Disease.” *The New England Journal of Medicine* 367 (9): 795–804.
- Bates, Douglas, Martin Mächler, Ben Bolker, and Steve Walker. 2015. “Fitting Linear Mixed-Effects Models Using lme4.” *Journal of Statistical Software, Articles* 67 (1): 1–48.
- Bazzigaluppi, Paolo, Tina L. Beckett, Margaret M. Koletar, Aaron Y. Lai, Illsung L. Joo, Mary E. Brown, Peter L. Carlen, Joanne McLaurin, and Bojana Stefanovic. 2018. “Early-Stage Attenuation of Phase-Amplitude Coupling in the Hippocampus and Medial Prefrontal Cortex in a Transgenic Rat Model of Alzheimer’s Disease.” *Journal of Neurochemistry* 144 (5): 669–79.
- Béard, Elidie, and Olivier Braissant. 2010. “Synthesis and Transport of Creatine in the CNS: Importance for Cerebral Functions.” *Journal of Neurochemistry* 115 (2): 297–313.
- Behar, K. L., and T. Ogino. 1991. “Assignment of Resonance in the ¹H Spectrum of Rat Brain by Two-Dimensional Shift Correlated and J-Resolved NMR Spectroscopy.” *Magnetic Resonance in Medicine: Official Journal of the Society of Magnetic Resonance in Medicine / Society of Magnetic Resonance in Medicine* 17 (2): 285–303.
- . 1993. “Characterization of Macromolecule Resonances in the ¹H NMR Spectrum of Rat Brain.” *Magnetic Resonance in Medicine: Official Journal of the Society of Magnetic Resonance in Medicine / Society of Magnetic Resonance in Medicine* 30 (1): 38–44.
- Behar, K. L., D. L. Rothman, D. D. Spencer, and O. A. Petroff. 1994. “Analysis of Macromolecule Resonances in ¹H NMR Spectra of Human Brain.” *Magnetic Resonance in Medicine: Official Journal of the Society of Magnetic Resonance in Medicine / Society of Magnetic Resonance in Medicine* 32 (3): 294–302.
- Benarroch, E. E. 2008. “N-Acetylaspartate and N-Acetylaspartylglutamate: Neurobiology and Clinical Significance.” *Clinical Implications of Neuroscience Research* 70 (16): 1353–57.
- Benjamini, Yoav, and Yosef Hochberg. 1995. “Controlling the False Discovery Rate: A Practical and Powerful Approach to Multiple Testing.” *Journal of the Royal Statistical Society. Series B, Statistical Methodology* 57 (1): 289–300.

- Berent-Spillson, Alison, Amanda M. Robinson, David Golovoy, Barbara Slusher, Camilo Rojas, and James W. Russell. 2004. "Protection against Glucose-Induced Neuronal Death by NAAG and GCP II Inhibition Is Regulated by mGluR3." *Journal of Neurochemistry* 89 (1): 90–99.
- Berkowitz, Laura E., Ryan E. Harvey, Emma Drake, Shannon M. Thompson, and Benjamin J. Clark. 2018. "Progressive Impairment of Directional and Spatially Precise Trajectories by TgF344-Alzheimer's Disease Rats in the Morris Water Task." *Scientific Reports* 8 (1): 16153.
- Bernal-Rusiel, Jorge L., Douglas N. Greve, Martin Reuter, Bruce Fischl, Mert R. Sabuncu, and Alzheimer's Disease Neuroimaging Initiative. 2013. "Statistical Analysis of Longitudinal Neuroimage Data with Linear Mixed Effects Models." *NeuroImage* 66 (February): 249–60.
- Bernard, Jessica A., and Rachael D. Seidler. 2013. "Relationships between Regional Cerebellar Volume and Sensorimotor and Cognitive Function in Young and Older Adults." *Cerebellum* 12 (5): 721–37.
- Best, Jonathan G., Charlotte J. Stagg, and Andrea Dennis. 2014. "Chapter 2.5 - Other Significant Metabolites: Myo-Inositol, GABA, Glutamine, and Lactate." In *Magnetic Resonance Spectroscopy*, edited by Charlotte Stagg and Douglas Rothman, 122–38. San Diego: Academic Press.
- Bettio, Luis E. B., Luckshi Rajendran, and Joana Gil-Mohapel. 2017. "The Effects of Aging in the Hippocampus and Cognitive Decline." *Neuroscience and Biobehavioral Reviews* 79 (August): 66–86.
- Bevilacqua, Arturo, and Mariano Bizzarri. 2018. "Inositols in Insulin Signaling and Glucose Metabolism." *International Journal of Endocrinology* 2018 (November): 1968450.
- Bezprozvanny, Ilya, and Mark P. Mattson. 2008. "Neuronal Calcium Mishandling and the Pathogenesis of Alzheimer's Disease." *Trends in Neurosciences* 31 (9): 454–63.
- Bianchini, F., A. Di Vita, L. Palermo, L. Piccardi, C. Blundo, and C. Guariglia. 2014. "A Selective Egocentric Topographical Working Memory Deficit in the Early Stages of Alzheimer's Disease: A Preliminary Study." *American Journal of Alzheimer's Disease and Other Dementias* 29 (8): 749–54.
- Bobinski, M., M. J. de Leon, J. Wegiel, S. Desanti, A. Convit, L. A. Saint Louis, H. Rusinek, and H. M. Wisniewski. 2000. "The Histological Validation of Post Mortem Magnetic Resonance Imaging-Determined Hippocampal Volume in Alzheimer's Disease." *Neuroscience* 95 (3): 721–25.
- Bocancea, Diana I., Anna C. van Loenhoud, Colin Groot, Frederik Barkhof, Wiesje M. van der Flier, and Rik Ossenkoppele. 2021. "Measuring Resilience and Resistance in Aging and Alzheimer Disease Using Residual Methods: A Systematic Review and Meta-Analysis." *Neurology*.
- Boumezbeur, Fawzi, Kitt F. Petersen, Gary W. Cline, Graeme F. Mason, Kevin L. Behar, Gerald I. Shulman, and Douglas L. Rothman. 2010. "The Contribution of Blood Lactate to Brain Energy Metabolism in Humans Measured by Dynamic ¹³C Nuclear Magnetic Resonance Spectroscopy." *The Journal of Neuroscience: The Official Journal of the Society for Neuroscience* 30 (42): 13983–91.
- Boutajangout, Allal, Hanna Lindberg, Abdulaziz Awwad, Arun Paul, Rabaa Baitalmal, Ismail Almokyad, Ingmarie Höiden-Guthenberg, et al. 2019. "Affibody-Mediated Sequestration of Amyloid β Demonstrates Preventive Efficacy in a Transgenic Alzheimer's

- Disease Mouse Model.” *Frontiers in Aging Neuroscience* 11 (March): 64.
- Braak, H., and E. Braak. 1991a. “Alzheimer’s Disease Affects Limbic Nuclei of the Thalamus.” *Acta Neuropathologica* 81 (3): 261–68.
- . 1991b. “Neuropathological Staging of Alzheimer-Related Changes.” *Acta Neuropathologica* 82 (4): 239–59.
- . 1995. “Staging of Alzheimer’s Disease-Related Neurofibrillary Changes.” *Neurobiology of Aging* 16 (3): 271–78; discussion 278–84.
- . 1997. “Frequency of Stages of Alzheimer-Related Lesions in Different Age Categories.” *Neurobiology of Aging* 18 (4): 351–57.
- Braak, Heiko, Irina Alafuzoff, Thomas Arzberger, Hans Kretschmar, and Kelly Del Tredici. 2006. “Staging of Alzheimer Disease-Associated Neurofibrillary Pathology Using Paraffin Sections and Immunocytochemistry.” *Acta Neuropathologica* 112 (4): 389–404.
- Braak, Heiko, and Kelly Del Tredici. 2011. “The Pathological Process Underlying Alzheimer’s Disease in Individuals under Thirty.” *Acta Neuropathologica* 121 (2): 171–81.
- Brand, A., C. Richter-Landsberg, and D. Leibfritz. 1993. “Multinuclear NMR Studies on the Energy Metabolism of Glial and Neuronal Cells.” *Developmental Neuroscience* 15: 289–98.
- Breitner, John C., Laura D. Baker, Thomas J. Montine, Curtis L. Meinert, Constantine G. Lyketsos, Karen H. Ashe, Jason Brandt, et al. 2011. “Extended Results of the Alzheimer’s Disease Anti-Inflammatory Prevention Trial.” *Alzheimer’s & Dementia: The Journal of the Alzheimer’s Association* 7 (4): 402–11.
- Buckley, Rachel F., Elizabeth C. Mormino, Rebecca E. Amariglio, Michael J. Properzi, Jennifer S. Rabin, Yen Ying Lim, Kathryn V. Papp, et al. 2018. “Sex, Amyloid, and APOE ϵ 4 and Risk of Cognitive Decline in Preclinical Alzheimer’s Disease: Findings from Three Well-Characterized Cohorts.” *Alzheimer’s & Dementia: The Journal of the Alzheimer’s Association* 14 (9): 1193–1203.
- Buerger, Katharina, Michael Ewers, Tuula Pirtilä, Raymond Zinkowski, Irina Alafuzoff, Stefan J. Teipel, John DeBernardis, et al. 2006. “CSF Phosphorylated Tau Protein Correlates with Neocortical Neurofibrillary Pathology in Alzheimer’s Disease.” *Brain: A Journal of Neurology* 129 (Pt 11): 3035–41.
- Burnham, Kenneth P., and David R. Anderson. 2004. “Multimodel Inference: Understanding AIC and BIC in Model Selection.” *Sociological Methods & Research* 33 (2): 261–304.
- Bussy, Aurelie, Eric Plitman, Raihaan Patel, Stephanie Tullo, Alyssa Salaciak, Saashi A. Bedford, Sarah Farzin, et al. 2021. “Hippocampal Subfield Volumes across the Healthy Lifespan and the Effects of MR Sequence on Estimates.” *NeuroImage*, March, 117931.
- Cabello, C. R., J. J. Thune, H. Pakkenberg, and B. Pakkenberg. 2002. “Ageing of Substantia Nigra in Humans: Cell Loss May Be Compensated by Hypertrophy.” *Neuropathology and Applied Neurobiology* 28 (4): 283–91.
- Cabezas, Mariano, Arnau Oliver, Xavier Lladó, Jordi Freixenet, and Meritxell Bach Cuadra. 2011. “A Review of Atlas-Based Segmentation for Magnetic Resonance Brain Images.” *Computer Methods and Programs in Biomedicine* 104 (3): e158–77.
- Cahill, Larry. 2006. “Why Sex Matters for Neuroscience.” *Nature Reviews. Neuroscience* 7 (6): 477–84.
- Callen, D. J., S. E. Black, F. Gao, C. B. Caldwell, and J. P. Szalai. 2001. “Beyond the Hippocampus: MRI Volumetry Confirms Widespread Limbic Atrophy in AD.” *Neurology*

57 (9): 1669–74.

Camandola, Simonetta, and Mark P. Mattson. 2017. “Brain Metabolism in Health, Aging, and Neurodegeneration.” *The EMBO Journal* 36 (11): 1474–92.

Carroll, Jenna C., Emily R. Rosario, Sara Kreimer, Angela Villamagna, Elisabet Gentschein, Frank Z. Stanczyk, and Christian J. Pike. 2010. “Sex Differences in β -Amyloid Accumulation in 3xTg-AD Mice: Role of Neonatal Sex Steroid Hormone Exposure.” *Brain Research* 1366 (December): 233–45.

Casas, Rafael, Siva Muthusamy, Paul G. Wakim, Sanhita Sinharay, Margaret R. Lentz, William C. Reid, and Dima A. Hammoud. 2018. “MR Brain Volumetric Measurements Are Predictive of Neurobehavioral Impairment in the HIV-1 Transgenic Rat.” *NeuroImage. Clinical* 17: 659–66.

Castanho, Isabel, Tracey K. Murray, Eilis Hannon, Aaron Jeffries, Emma Walker, Emma Laing, Hedley Baulf, et al. 2020. “Transcriptional Signatures of Tau and Amyloid Neuropathology.” *Cell Reports* 30 (6): 2040–54.e5.

Cecil, Kim M. 2013. “Proton Magnetic Resonance Spectroscopy: Technique for the Neuroradiologist.” *Neuroimaging Clinics of North America* 23 (3): 381–92.

Chakravarty, M. Mallar, Patrick Steadman, Matthijs C. van Eede, Rebecca D. Calcott, Victoria Gu, Philip Shaw, Armin Raznahan, D. Louis Collins, and Jason P. Lerch. 2013. “Performing Label-Fusion-Based Segmentation Using Multiple Automatically Generated Templates.” *Human Brain Mapping* 34 (10): 2635–54.

Chan, Dennis, Laura Marie Gallaher, Kuven Moodley, Ludovico Minati, Neil Burgess, and Tom Hartley. 2016. “The 4 Mountains Test: A Short Test of Spatial Memory with High Sensitivity for the Diagnosis of Pre-Dementia Alzheimer’s Disease.” *Journal of Visualized Experiments: JoVE*, no. 116 (October). <https://doi.org/10.3791/54454>.

Chaney, Aisling, Martin Bauer, Daniela Bochicchio, Alison Smigova, Michael Kassiou, Karen E. Davies, Steve R. Williams, and Herve Boutin. 2018. “Longitudinal Investigation of Neuroinflammation and Metabolite Profiles in the APPswe \times PS1 Δ e9 Transgenic Mouse Model of Alzheimer’s Disease.” *Journal of Neurochemistry* 144 (3): 318–35.

Chaney, Aisling M., Francisco R. Lopez-Picon, Sophie Serrière, Rui Wang, Daniela Bochicchio, Samuel D. Webb, Matthias Vandesquille, et al. 2021. “Prodromal Neuroinflammatory, Cholinergic and Metabolite Dysfunction Detected by PET and MRS in the TgF344-AD Transgenic Rat Model of AD: A Collaborative Multi-Modal Study.” *Theranostics* 11 (14): 6644–67.

Chaney, A. M., F. R. Lopez-Picon, S. Serriere, R. Wang, D. Bochicchio, S. D. Webb, M. Vandesquille, et al. 2021. *Prodromal Neuroinflammatory, Cholinergic and Metabolite Dysfunction Detected by PET and MRS in the TgF344-AD Transgenic Rat Model of AD: A Collaborative Multi-Modal Study*. <https://zenodo.org/record/4710273>.

Chang, Linda, Thomas Ernst, Russell E. Poland, and Donald J. Jenden. 1996. “In Vivo Proton Magnetic Resonance Spectroscopy of the Normal Aging Human Brain.” *Life Sciences* 58 (22): 2049–56.

Chesky, J. A., and M. Rockstein. 1976. “Life Span Characteristics in the Male Fischer Rat.” *Experimental Aging Research* 2 (5): 399–407.

Chhetri, Dhani Raj. 2019. “Myo-Inositol and Its Derivatives: Their Emerging Role in the Treatment of Human Diseases.” *Frontiers in Pharmacology* 10 (October): 1172.

Choi, Ji-Kyung, Isabel Carreras, Nur Aytan, Eric Jenkins-Sahlin, Alpaslan Dedeoglu, and Bruce G. Jenkins. 2014. “The Effects of Aging, Housing and Ibuprofen Treatment on Brain

Neurochemistry in a Triple Transgene Alzheimer's Disease Mouse Model Using Magnetic Resonance Spectroscopy and Imaging." *Brain Research* 1590 (November): 85–96.

Choi, Yu Yong, Jang Jae Lee, Kyu Yeong Choi, Eun Hyun Seo, Il Han Choo, Hoowon Kim, Min-Kyung Song, et al. 2020. "The Aging Slopes of Brain Structures Vary by Ethnicity and Sex: Evidence From a Large Magnetic Resonance Imaging Dataset From a Single Scanner of Cognitively Healthy Elderly People in Korea." *Frontiers in Aging Neuroscience* 12 (August): 233.

Chung, M. K., K. J. Worsley, T. Paus, C. Cherif, D. L. Collins, J. N. Giedd, J. L. Rapoport, and A. C. Evans. 2001. "A Unified Statistical Approach to Deformation-Based Morphometry." *NeuroImage* 14 (3): 595–606.

Chung, Moo K., Keith J. Worsley, Steve Robbins, Tomás Paus, Jonathan Taylor, Jay N. Giedd, Judith L. Rapoport, and Alan C. Evans. 2003. "Deformation-Based Surface Morphometry Applied to Gray Matter Deformation." *NeuroImage* 18 (2): 198–213.

Clark, J. B. 1998. "N-Acetyl Aspartate: A Marker for Neuronal Loss or Mitochondrial Dysfunction." *Developmental Neuroscience* 20 (4-5): 271–76.

Cleeland, Carlee, Andrew Pipingas, Andrew Scholey, and David White. 2019. "Neurochemical Changes in the Aging Brain: A Systematic Review." *Neuroscience and Biobehavioral Reviews* 98 (March): 306–19.

Coffey, C. E., J. F. Lucke, J. A. Saxton, G. Ratcliff, L. J. Uritas, B. Billig, and R. N. Bryan. 1998. "Sex Differences in Brain Aging: A Quantitative Magnetic Resonance Imaging Study." *Archives of Neurology* 55 (2): 169–79.

Cohen, Robert M., Kavon Rezai-Zadeh, Tara M. Weitz, Altan Rentsendorj, David Gate, Inna Spivak, Yasmin Bholat, et al. 2013. "A Transgenic Alzheimer Rat with Plaques, Tau Pathology, Behavioral Impairment, Oligomeric A β , and Frank Neuronal Loss." *The Journal of Neuroscience: The Official Journal of the Society for Neuroscience* 33 (15): 6245–56.

Coiro, Pierluca, and Daniela D. Pollak. 2019. "Sex and Gender Bias in the Experimental Neurosciences: The Case of the Maternal Immune Activation Model." *Translational Psychiatry* 9 (1): 90.

Colla, Michael, Gabriele Ende, Markus Bohrer, Michael Deuschle, Golo Kronenberg, Fritz Henn, and Isabella Heuser. 2003. "MR Spectroscopy in Alzheimer's Disease: Gender Differences in Probabilistic Learning Capacity." *Neurobiology of Aging* 24 (4): 545–52.

Cooke, B., C. D. Hegstrom, L. S. Villeneuve, and S. M. Breedlove. 1998. "Sexual Differentiation of the Vertebrate Brain: Principles and Mechanisms." *Frontiers in Neuroendocrinology* 19 (4): 323–62.

Corre, Christina, Miriam Friedel, Dulcie A. Vousden, Ariane Metcalf, Shoshana Spring, Lily R. Qiu, Jason P. Lerch, and Mark R. Palmert. 2016. "Separate Effects of Sex Hormones and Sex Chromosomes on Brain Structure and Function Revealed by High-Resolution Magnetic Resonance Imaging and Spatial Navigation Assessment of the Four Core Genotype Mouse Model." *Brain Structure & Function* 221 (2): 997–1016.

Cosgrove, Kelly P., Carolyn M. Mazure, and Julie K. Staley. 2007. "Evolving Knowledge of Sex Differences in Brain Structure, Function, and Chemistry." *Biological Psychiatry* 62 (8): 847–55.

Cowell, P. E., B. I. Turetsky, R. C. Gur, R. I. Grossman, D. L. Shtasel, and R. E. Gur. 1994. "Sex Differences in Aging of the Human Frontal and Temporal Lobes." *The Journal of Neuroscience: The Official Journal of the Society for Neuroscience* 14 (8): 4748–55.

Craveiro, Mélanie, Virginie Clément-Schatlo, Denis Marino, Rolf Gruetter, and Cristina

- Cudalbu. 2014. "In Vivo Brain Macromolecule Signals in Healthy and Glioblastoma Mouse Models: 1H Magnetic Resonance Spectroscopy, Post-Processing and Metabolite Quantification at 14.1 T." *Journal of Neurochemistry* 129 (5): 806–15.
- Craveiro, Mélanie, Cristina Cudalbu, and Rolf Gruetter. 2012. "Regional Alterations of the Brain Macromolecule Resonances Investigated in the Mouse Brain Using an Improved Method for the Pre-Processing of the Macromolecular Signal." *Proc. Intl. Soc. Mag. Reson. Med.* 20: 1748.
- Cudalbu, Cristina, Vladimir Mlynárik, and Rolf Gruetter. 2012. "Handling Macromolecule Signals in the Quantification of the Neurochemical Profile." *Journal of Alzheimer's Disease: JAD* 31 Suppl 3: S101–15.
- Cui, Yilong, Tadayuki Takashima, Misato Takashima-Hirano, Yasuhiro Wada, Miho Shukuri, Yasuhisa Tamura, Hisashi Doi, Hirota Onoe, Yosky Kataoka, and Yasuyoshi Watanabe. 2009. "11C-PK11195 PET for the in Vivo Evaluation of Neuroinflammation in the Rat Brain after Cortical Spreading Depression." *Journal of Nuclear Medicine: Official Publication, Society of Nuclear Medicine* 50 (11): 1904–11.
- Currie, Stuart, Nigel Hoggard, Ian J. Craven, Marios Hadjivassiliou, and Iain D. Wilkinson. 2013. "Understanding MRI: Basic MR Physics for Physicians." *Postgraduate Medical Journal* 89 (1050): 209–23.
- Dage, Jeffrey L., Alexandra M. V. Wennberg, David C. Airey, Clinton E. Hagen, David S. Knopman, Mary M. Machulda, Rosebud O. Roberts, Clifford R. Jack Jr, Ronald C. Petersen, and Michelle M. Mielke. 2016. "Levels of Tau Protein in Plasma Are Associated with Neurodegeneration and Cognitive Function in a Population-Based Elderly Cohort." *Alzheimer's & Dementia: The Journal of the Alzheimer's Association* 12 (12): 1226–34.
- David, J. P., F. Ghozali, C. Fallet-Bianco, A. Watzet, S. Delaine, B. Boniface, C. Di Menza, and A. Delacourte. 1997. "Glial Reaction in the Hippocampal Formation Is Highly Correlated with Aging in Human Brain." *Neuroscience Letters* 235 (1-2): 53–56.
- Dedeoglu, Alpaslan, Ji-Kyung Choi, Kerry Cormier, Neil W. Kowall, and Bruce G. Jenkins. 2004. "Magnetic Resonance Spectroscopic Analysis of Alzheimer's Disease Mouse Brain That Express Mutant Human APP Shows Altered Neurochemical Profile." *Brain Research* 1012 (1-2): 60–65.
- Dehghani, Masoumeh, Kim Q. Do, Pierre Magistretti, and Lijing Xin. 2020. "Lactate Measurement by Neurochemical Profiling in the Dorsolateral Prefrontal Cortex at 7T: Accuracy, Precision, and Relaxation Times." *Magnetic Resonance in Medicine: Official Journal of the Society of Magnetic Resonance in Medicine / Society of Magnetic Resonance in Medicine* 83 (6): 1895–1908.
- De-Paula, Vanessa J., Marcia Radanovic, Breno S. Diniz, and Orestes V. Forlenza. 2012. "Alzheimer's Disease." In *Protein Aggregation and Fibrillogenesis in Cerebral and Systemic Amyloid Disease*, edited by J. Robin Harris, 329–52. Dordrecht: Springer Netherlands.
- Despotović, Ivana, Bart Goossens, and Wilfried Philips. 2015. "MRI Segmentation of the Human Brain: Challenges, Methods, and Applications." *Computational and Mathematical Methods in Medicine* 2015 (March): 450341.
- De Strooper, Bart, and Eric Karran. 2016. "The Cellular Phase of Alzheimer's Disease." *Cell* 164 (4): 603–15.
- DeTure, Michael A., and Dennis W. Dickson. 2019. "The Neuropathological Diagnosis of Alzheimer's Disease." *Molecular Neurodegeneration* 14 (1): 32.

Dhamala, Elvisha, Ines Abdelkefi, Mavesa Nguyen, T. Jay Hennessy, H el ene Nadeau, and Jamie Near. 2019. "Validation of in Vivo MRS Measures of Metabolite Concentrations in the Human Brain." *NMR in Biomedicine* 32 (3): e4058.

Dillon, Serena E., Demitra Tsivos, Michael Knight, Bryony McCann, Catherine Pennington, Anna I. Shiel, Myra E. Conway, Margaret A. Newson, Risto A. Kauppinen, and Elizabeth J. Coulthard. 2017. "The Impact of Ageing Reveals Distinct Roles for Human Dentate Gyrus and CA3 in Pattern Separation and Object Recognition Memory." *Scientific Reports* 7 (1): 14069.

Do Carmo, Sonia, and A. Claudio Cuello. 2013. "Modeling Alzheimer's Disease in Transgenic Rats." *Molecular Neurodegeneration* 8 (October): 37.

Doig, Andrew J., Maria P. Del Castillo-Frias, Olivia Berthoumieu, Bogdan Tarus, Jessica Nasica-Labouze, Fabio Sterpone, Phuong H. Nguyen, Nigel M. Hooper, Peter Faller, and Philippe Derreumaux. 2017. "Why Is Research on Amyloid-  Failing to Give New Drugs for Alzheimer's Disease?" *ACS Chemical Neuroscience* 8 (7): 1435–37.

Dona, Anthony C., Michael Kyriakides, Flora Scott, Elizabeth A. Shephard, Dorsa Varshavi, Kirill Veselkov, and Jeremy R. Everett. 2016. "A Guide to the Identification of Metabolites in NMR-Based Metabonomics/metabolomics Experiments." *Computational and Structural Biotechnology Journal* 14 (March): 135–53.

Dong, Yue, and Gregory J. Brewer. 2019. "Global Metabolic Shifts in Age and Alzheimer's Disease Mouse Brains Pivot at NAD⁺/NADH Redox Sites." *Journal of Alzheimer's Disease: JAD* 71 (1): 119–40.

Doody, Rachelle S., Ronald G. Thomas, Martin Farlow, Takeshi Iwatsubo, Bruno Vellas, Steven Joffe, Karl Kieburtz, et al. 2014. "Phase 3 Trials of Solanezumab for Mild-to-Moderate Alzheimer's Disease." *The New England Journal of Medicine* 370 (4): 311–21.

Dorr, A. E., J. P. Lerch, S. Spring, N. Kabani, and R. M. Henkelman. 2008. "High Resolution Three-Dimensional Brain Atlas Using an Average Magnetic Resonance Image of 40 Adult C57Bl/6J Mice." *NeuroImage* 42 (1): 60–69.

Driscoll, I., C. Davatzikos, Y. An, X. Wu, D. Shen, M. Kraut, and S. M. Resnick. 2009. "Longitudinal Pattern of Regional Brain Volume Change Differentiates Normal Aging from MCI." *Neurology* 72 (22): 1906–13.

Driscoll, I., S. R. Howard, J. C. Stone, M. H. Monfils, B. Tomanek, W. M. Brooks, and R. J. Sutherland. 2006. "The Aging Hippocampus: A Multi-Level Analysis in the Rat." *Neuroscience* 139 (4): 1173–85.

Drummond, Eleanor, and Thomas Wisniewski. 2017. "Alzheimer's Disease: Experimental Models and Reality." *Acta Neuropathologica* 133 (2): 155–75.

Duarte, Jo o M. N., Kim Q. Do, and Rolf Gruetter. 2014. "Longitudinal Neurochemical Modifications in the Aging Mouse Brain Measured in Vivo by 1H Magnetic Resonance Spectroscopy." *Neurobiology of Aging* 35 (7): 1660–68.

Duarte, Jo o M. N., Hongxia Lei, Vladim r Mlyn rik, and Rolf Gruetter. 2012. "The Neurochemical Profile Quantified by in Vivo 1H NMR Spectroscopy." *NeuroImage* 61 (2): 342–62.

Dubois, Bruno, Howard H. Feldman, Claudia Jacova, Jeffrey L. Cummings, Steven T. Dekosky, Pascale Barberger-Gateau, Andr e Delacourte, et al. 2010. "Revising the Definition of Alzheimer's Disease: A New Lexicon." *Lancet Neurology* 9 (11): 1118–27.

Dumitriu, Dani, Jiandong Hao, Yuko Hara, Jeffrey Kaufmann, William G. M. Janssen, Wendy Lou, Peter R. Rapp, and John H. Morrison. 2010. "Selective Changes in Thin Spine

- Density and Morphology in Monkey Prefrontal Cortex Correlate with Aging-Related Cognitive Impairment.” *The Journal of Neuroscience: The Official Journal of the Society for Neuroscience* 30 (22): 7507–15.
- Ellenbroek, Bart, and Jiun Youn. 2016. “Rodent Models in Neuroscience Research: Is It a Rat Race?” *Disease Models & Mechanisms* 9 (10): 1079–87.
- Elmaoğlu, Muhammed, and Azim Çelik. 2011. *MRI Handbook: MR Physics, Patient Positioning, and Protocols*. Springer New York.
- Emir, Uzay E., Susan Raatz, Susan McPherson, James S. Hodges, Carolyn Torkelson, Pierre Tawfik, Tonya White, and Melissa Terpstra. 2011. “Noninvasive Quantification of Ascorbate and Glutathione Concentration in the Elderly Human Brain.” *NMR in Biomedicine* 24 (7): 888–94.
- Ernst, T., R. Kreis, and B. D. Ross. 1993. “Absolute Quantitation of Water and Metabolites in the Human Brain. I. Compartments and Water.” *Journal of Magnetic Resonance. Series B* 102 (1): 1–8.
- Farooqui, Tahira, and Akhlaq A. Farooqui. 2009. “Aging: An Important Factor for the Pathogenesis of Neurodegenerative Diseases.” *Mechanisms of Ageing and Development* 130 (4): 203–15.
- Febo, Marcelo, and Thomas C. Foster. 2016. “Preclinical Magnetic Resonance Imaging and Spectroscopy Studies of Memory, Aging, and Cognitive Decline.” *Frontiers in Aging Neuroscience* 8 (June): 158.
- Ferreira, Sergio T., Julia R. Clarke, Theresa R. Bomfim, and Fernanda G. De Felice. 2014. “Inflammation, Defective Insulin Signaling, and Neuronal Dysfunction in Alzheimer’s Disease.” *Alzheimer’s & Dementia: The Journal of the Alzheimer’s Association* 10 (1 Suppl): S76–83.
- Filon, Jessica R., Anthony J. Intorcchia, Lucia I. Sue, Elsa Vazquez Arreola, Jeffrey Wilson, Kathryn J. Davis, Marwan N. Sabbagh, et al. 2016. “Gender Differences in Alzheimer Disease: Brain Atrophy, Histopathology Burden, and Cognition.” *Journal of Neuropathology and Experimental Neurology* 75 (8): 748–54.
- Fitzmaurice, Garrett M., and Caitlin Ravichandran. 2008. “A Primer in Longitudinal Data Analysis.” *Circulation* 118 (19): 2005–10.
- Fitz, Nicholas F., Emilie L. Castranio, Alexis Y. Carter, Ravindra Kodali, Iliya Lefterov, and Radosveta Koldamova. 2014. “Improvement of Memory Deficits and Amyloid- β Clearance in Aged APP23 Mice Treated with a Combination of Anti-Amyloid- β Antibody and LXR Agonist.” *Journal of Alzheimer’s Disease: JAD* 41 (2): 535–49.
- Fjell, Anders M., Linda McEvoy, Dominic Holland, Anders M. Dale, Kristine B. Walhovd, and Alzheimer’s Disease Neuroimaging Initiative. 2014. “What Is Normal in Normal Aging? Effects of Aging, Amyloid and Alzheimer’s Disease on the Cerebral Cortex and the Hippocampus.” *Progress in Neurobiology* 117 (June): 20–40.
- Fjell, Anders M., and Kristine B. Walhovd. 2010. “Structural Brain Changes in Aging: Courses, Causes and Cognitive Consequences.” *Reviews in the Neurosciences* 21 (3): 187–221.
- Fjell, Anders M., Kristine B. Walhovd, Christine Fennema-Notestine, Linda K. McEvoy, Donald J. Hagler, Dominic Holland, James B. Brewer, and Anders M. Dale. 2009. “One-Year Brain Atrophy Evident in Healthy Aging.” *The Journal of Neuroscience: The Official Journal of the Society for Neuroscience* 29 (48): 15223–31.
- Foidl, Bettina M., and Christian Humpel. 2020. “Can Mouse Models Mimic Sporadic

- Alzheimer's Disease?" *Neural Regeneration Research* 15 (3): 401–6.
- Forster, Duncan, Karen Davies, and Steve Williams. 2013. "Magnetic Resonance Spectroscopy in Vivo of Neurochemicals in a Transgenic Model of Alzheimer's Disease: A Longitudinal Study of Metabolites, Relaxation Time, and Behavioral Analysis in TASTPM and Wild-Type Mice." *Magnetic Resonance in Medicine: Official Journal of the Society of Magnetic Resonance in Medicine / Society of Magnetic Resonance in Medicine* 69 (4): 944–55.
- Fortea, Juan, Roser Sala-Llonch, David Bartrés-Faz, Beatriz Bosch, Albert Lladó, Nuria Bargalló, José Luis Molinuevo, and Raquel Sánchez-Valle. 2010. "Increased Cortical Thickness and Caudate Volume Precede Atrophy in PSEN1 Mutation Carriers." *Journal of Alzheimer's Disease: JAD* 22 (3): 909–22.
- Fowler, Caitlin F., Dan Madularu, Masoumeh Dehghani, Gabriel A. Devenyi, and Jamie Near. 2020. "Longitudinal Quantification of Metabolites and Macromolecules Reveals Age- and Sex-Related Changes in the Healthy Fischer 344 Rat Brain." *Neurobiology of Aging* 101 (December): 109–22.
- Fowler, Caitlin, Dana Goerzen, Dan Madularu, Gabriel A. Devenyi, M. Mallar Chakravarty, and Jamie Near. 2021. "LONGITUDINAL CHARACTERIZATION OF NEUROANATOMICAL CHANGES IN THE FISCHER 344 RAT BRAIN DURING NORMAL AGING AND BETWEEN SEXES." *Neurobiology of Aging*, October. <https://doi.org/10.1016/j.neurobiolaging.2021.10.003>.
- Fowler, Caitlin, Dana Goerzen, Dan Madularu, Gabriel A. Devenyi, M. Mallar Chakravarty, and Jamie Near. 2021. "Longitudinal Characterization of Neuroanatomical Changes in the Fischer 344 Rat Brain during Normal Aging and between Sexes." *bioRxiv*. <https://doi.org/10.1101/2021.04.12.439510>.
- Fox, John, and Sanford Weisberg. 2019. "An R Companion to Applied Regression." Thousand Oaks CA: Sage. <https://socialsciences.mcmaster.ca/jfox/Books/Companion/index.html>.
- Franceschi, Claudio, Paolo Garagnani, Cristina Morsiani, Maria Conte, Aurelia Santoro, Andrea Grignolio, Daniela Monti, Miriam Capri, and Stefano Salvioli. 2018. "The Continuum of Aging and Age-Related Diseases: Common Mechanisms but Different Rates." *Frontiers of Medicine* 5 (March): 61.
- Frazier, Hilaree N., Adam O. Ghoweri, Emily Sudkamp, Eleanor S. Johnson, Katie L. Anderson, Grant Fox, Keomany Vatthanaphone, et al. 2020. "Long-Term Intranasal Insulin Aspart: A Profile of Gene Expression, Memory, and Insulin Receptors in Aged F344 Rats." *The Journals of Gerontology. Series A, Biological Sciences and Medical Sciences* 75 (6): 1021–30.
- Friedel, Miriam, Matthijs C. van Eede, Jon Pipitone, M. Mallar Chakravarty, and Jason P. Lerch. 2014. "Pydpiper: A Flexible Toolkit for Constructing Novel Registration Pipelines." *Frontiers in Neuroinformatics* 8 (July): 67.
- Frisoni, Giovanni B., Nick C. Fox, Clifford R. Jack Jr, Philip Scheltens, and Paul M. Thompson. 2010. "The Clinical Use of Structural MRI in Alzheimer Disease." *Nature Reviews. Neurology* 6 (2): 67–77.
- Gallagher, Michela, Amy M. Stocker, and Ming Teng Koh. 2011. "Mindspan: Lessons from Rat Models of Neurocognitive Aging." *ILAR Journal / National Research Council, Institute of Laboratory Animal Resources* 52 (1): 32–40.
- Gao, F., and P. B. Barker. 2014. "Various MRS Application Tools for Alzheimer Disease

and Mild Cognitive Impairment.” *AJNR. American Journal of Neuroradiology* 35 (6 Suppl): S4–11.

Garcia, Tanya P., and Karen Marder. 2017. “Statistical Approaches to Longitudinal Data Analysis in Neurodegenerative Diseases: Huntington’s Disease as a Model.” *Current Neurology and Neuroscience Reports* 17 (2): 14.

Gaser, Christian, Silvio Schmidt, Martin Metzler, Karl-Heinz Herrmann, Ines Krumbein, Jürgen R. Reichenbach, and Otto W. Witte. 2012. “Deformation-Based Brain Morphometry in Rats.” *NeuroImage* 63 (1): 47–53.

Gaser, C., I. Nenadic, B. R. Buchsbaum, E. A. Hazlett, and M. S. Buchsbaum. 2001. “Deformation-Based Morphometry and Its Relation to Conventional Volumetry of Brain Lateral Ventricles in MRI.” *NeuroImage* 13 (6 Pt 1): 1140–45.

Gawel, Kinga, Ewa Gibula, Marta Marszalek-Grabska, Joanna Filarowska, and Jolanta H. Kotlinska. 2019. “Assessment of Spatial Learning and Memory in the Barnes Maze Task in Rodents-Methodological Consideration.” *Naunyn-Schmiedeberg’s Archives of Pharmacology* 392 (1): 1–18.

Geerts, Hugo. 2009. “Of Mice and Men: Bridging the Translational Disconnect in CNS Drug Discovery.” *CNS Drugs* 23 (11): 915–26.

Giedd, Jay N., Armin Raznahan, Kathryn L. Mills, and Rhoshel K. Lenroot. 2012. “Review: Magnetic Resonance Imaging of Male/female Differences in Human Adolescent Brain Anatomy.” *Biology of Sex Differences* 3 (1): 19.

Giedd, J. N., J. Blumenthal, N. O. Jeffries, F. X. Castellanos, H. Liu, A. Zijdenbos, T. Paus, A. C. Evans, and J. L. Rapoport. 1999. “Brain Development during Childhood and Adolescence: A Longitudinal MRI Study.” *Nature Neuroscience* 2 (10): 861–63.

Gillies, Glenda E., and Simon McArthur. 2010. “Estrogen Actions in the Brain and the Basis for Differential Action in Men and Women: A Case for Sex-Specific Medicines.” *Pharmacological Reviews* 62 (2): 155–98.

Giorgi, Filippo Sean, Luigi Francesco Saccaro, Alessandro Galgani, Carla Letizia Busceti, Francesca Biagioni, Alessandro Frati, and Francesco Fornai. 2019. “The Role of Locus Coeruleus in Neuroinflammation Occurring in Alzheimer’s Disease.” *Brain Research Bulletin* 153 (November): 47–58.

Giuffrida, Maria Laura, Filippo Caraci, Bruno Pignataro, Sebastiano Cataldo, Paolo De Bona, Valeria Bruno, Gemma Molinaro, et al. 2009. “Beta-Amyloid Monomers Are Neuroprotective.” *The Journal of Neuroscience: The Official Journal of the Society for Neuroscience* 29 (34): 10582–87.

Godbolt, A. K., A. D. Waldman, D. G. MacManus, J. M. Schott, C. Frost, L. Cipolotti, N. C. Fox, and M. N. Rossor. 2006. “MRS Shows Abnormalities before Symptoms in Familial Alzheimer Disease.” *Neurology* 66 (5): 718–22.

Godbout, Jonathan P., and Rodney W. Johnson. 2009. “Age and Neuroinflammation: A Lifetime of Psychoneuroimmune Consequences.” *Immunology and Allergy Clinics of North America* 29 (2): 321–37.

Goerzen, Dana, Caitlin Fowler, Gabriel A. Devenyi, Jurgen Germann, Dan Madularu, M. Mallar Chakravarty, and Jamie Near. 2020. “An MRI-Derived Neuroanatomical Atlas of the Fischer 344 Rat Brain.” *Scientific Reports* 10 (1): 6952.

Goldstein, J. M., L. J. Seidman, N. J. Horton, N. Makris, D. N. Kennedy, V. S. Caviness Jr, S. V. Faraone, and M. T. Tsuang. 2001. “Normal Sexual Dimorphism of the Adult Human Brain Assessed by in Vivo Magnetic Resonance Imaging.” *Cerebral Cortex* 11 (6): 490–

- Gonzalez-Uarquin, Fernando, Markus Rodehutschord, and Korinna Huber. 2020. "Myo-Inositol: Its Metabolism and Potential Implications for Poultry Nutrition-a Review." *Poultry Science* 99 (2): 893–905.
- Goodman, Y., and M. P. Mattson. 1994. "Secreted Forms of Beta-Amyloid Precursor Protein Protect Hippocampal Neurons against Amyloid Beta-Peptide-Induced Oxidative Injury." *Experimental Neurology* 128 (1): 1–12.
- Gordon, Brian A., Tyler M. Blazey, Yi Su, Amrita Hari-Raj, Aylin Dincer, Shaney Flores, Jon Christensen, et al. 2018. "Spatial Patterns of Neuroimaging Biomarker Change in Individuals from Families with Autosomal Dominant Alzheimer's Disease: A Longitudinal Study." *Lancet Neurology* 17 (3): 241–50.
- Govindaraju, V., K. Young, and A. A. Maudsley. 2000. "Proton NMR Chemical Shifts and Coupling Constants for Brain Metabolites." *NMR in Biomedicine* 13 (3): 129–53.
- Graaf, Robin A. de. 2007. *In Vivo NMR Spectroscopy – 2nd Edition: Principles and Techniques*. John Wiley & Sons Ltd.
- . 2018. "Basic Principles." In *In Vivo NMR Spectroscopy*, 1–42. In VivoNMR Spectroscopy. Chichester, UK: John Wiley & Sons, Ltd.
- Graaf, Robin A. de, Peter B. Brown, Scott McIntyre, Terence W. Nixon, Kevin L. Behar, and Douglas L. Rothman. 2006. "High Magnetic Field Water and Metabolite Proton T1 and T2 Relaxation in Rat Brain in Vivo." *Magnetic Resonance in Medicine: Official Journal of the Society of Magnetic Resonance in Medicine / Society of Magnetic Resonance in Medicine* 56 (2): 386–94.
- Graff-Radford, Jonathan, and Kejal Kantarci. 2013. "Magnetic Resonance Spectroscopy in Alzheimer's Disease." *Neuropsychiatric Disease and Treatment* 9 (May): 687–96.
- Green, Kim N., and Frank M. LaFerla. 2008. "Linking Calcium to Abeta and Alzheimer's Disease." *Neuron* 59 (2): 190–94.
- Green, Peter, and Catriona J. MacLeod. 2016. "SIMR : An R Package for Power Analysis of Generalized Linear Mixed Models by Simulation." Edited by Shinichi Nakagawa. *Methods in Ecology and Evolution / British Ecological Society* 7 (4): 493–98.
- Grothe, Michel J., Christina Schuster, Florian Bauer, Helmut Heinsen, Johannes Prudlo, and Stefan J. Teipel. 2014. "Atrophy of the Cholinergic Basal Forebrain in Dementia with Lewy Bodies and Alzheimer's Disease Dementia." *Journal of Neurology* 261 (10): 1939–48.
- Gruber, Bernhard, Martijn Froeling, Tim Leiner, and Dennis W. J. Klomp. 2018. "RF Coils: A Practical Guide for Nonphysicists." *Journal of Magnetic Resonance Imaging: JMRI*, June. <https://doi.org/10.1002/jmri.26187>.
- Gruber, S., K. Pinker, F. Riederer, M. Chmelik, A. Stadlbauer, M. Bittsanksy, V. Mlynarik, et al. 2008. "Metabolic Changes in the Normal Ageing Brain: Consistent Findings from Short and Long Echo Time Spectroscopy." *European Journal of Radiology* 68: 320–27.
- Gruetter, Rolf. 1993. "Automatic, Localized in Vivo Adjustment of All First- and Second-Order Shim Coils." *Journal of Magnetic Resonance in Medicine* 29: 804–11.
- Güell-Bosch, J., S. Lope-Piedrafita, G. Esquerda-Canals, L. Montoliu-Gaya, and S. Villegas. 2020. "Progression of Alzheimer's Disease and Effect of scFv-h3D6 Immunotherapy in the 3xTg-AD Mouse Model: An in Vivo Longitudinal Study Using Magnetic Resonance Imaging and Spectroscopy." *NMR in Biomedicine* 33 (5): e4263.
- Guidi, Michael, Ashok Kumar, Asha Rani, and Thomas C. Foster. 2014. "Assessing the Emergence and Reliability of Cognitive Decline over the Life Span in Fisher 344 Rats

Using the Spatial Water Maze.” *Frontiers in Aging Neuroscience* 6 (January): 2.

Gur, R. C., P. D. Mozley, S. M. Resnick, G. L. Gottlieb, M. Kohn, R. Zimmerman, G. Herman, S. Atlas, R. Grossman, and D. Berretta. 1991. “Gender Differences in Age Effect on Brain Atrophy Measured by Magnetic Resonance Imaging.” *Proceedings of the National Academy of Sciences of the United States of America* 88 (7): 2845–49.

Haass, Christian, and Dennis J. Selkoe. 2007. “Soluble Protein Oligomers in Neurodegeneration: Lessons from the Alzheimer’s Amyloid Beta-Peptide.” *Nature Reviews. Molecular Cell Biology* 8 (2): 101–12.

Hädel, Sven, Christoph Wirth, Michael Rapp, Jürgen Gallinat, and Florian Schubert. 2013. “Effects of Age and Sex on the Concentrations of Glutamate and Glutamine in the Human Brain: Brain Glutamate and Glutamine With Age and Sex.” *Journal of Magnetic Resonance Imaging: JMRI* 38 (6): 1480–87.

Haga, Kristin K., Yuet Peng Khor, Andrew Farrall, and Joanna M. Wardlaw. 2009. “A Systematic Review of Brain Metabolite Changes, Measured with ¹H Magnetic Resonance Spectroscopy, in Healthy Aging.” *Neurobiology of Aging* 30 (3): 353–63.

Hagiwara, Akifumi, Kotaro Fujimoto, Koji Kamagata, Syo Murata, Ryusuke Irie, Hideyoshi Kaga, Yuki Someya, et al. 2020. “Age-Related Changes in Relaxation Times, Proton Density, Myelin, and Tissue Volumes in Adult Brain Analyzed by 2-Dimensional Quantitative Synthetic Magnetic Resonance Imaging.” *Investigative Radiology*, August. <https://doi.org/10.1097/RLI.0000000000000720>.

Hamezah, Hamizah Shahirah, Lina Wati Durani, Nor Faeizah Ibrahim, Daijiro Yanagisawa, Tomoko Kato, Akihiko Shiino, Sachiko Tanaka, Hanafi Ahmad Damanhuri, Wan Zurinah Wan Ngah, and Ikuo Tooyama. 2017. “Volumetric Changes in the Aging Rat Brain and Its Impact on Cognitive and Locomotor Functions.” *Experimental Gerontology* 99 (December): 69–79.

Hammen, Thilo, and Ruben Kuzniecky. 2012. “Chapter 25 - Magnetic Resonance Spectroscopy in Epilepsy.” In *Handbook of Clinical Neurology*, edited by Hermann Stefan and William H. Theodore, 107:399–408. Elsevier.

Hampel, Harald, John Hardy, Kaj Blennow, Christopher Chen, George Perry, Seung Hyun Kim, Victor L. Villemagne, et al. 2021. “The Amyloid- β Pathway in Alzheimer’s Disease.” *Molecular Psychiatry*, August. <https://doi.org/10.1038/s41380-021-01249-0>.

Hanes, Jozef, Norbert Zilka, Miriam Bartkova, Miroslava Caletkova, Dusan Dobrota, and Michal Novak. 2009. “Rat Tau Proteome Consists of Six Tau Isoforms: Implication for Animal Models of Human Tauopathies.” *Journal of Neurochemistry* 108 (5): 1167–76.

Han, Shuo, Yang An, Aaron Carass, Jerry L. Prince, and Susan M. Resnick. 2020. “Longitudinal Analysis of Regional Cerebellum Volumes during Normal Aging.” *NeuroImage* 220 (October): 117062.

Hardy, J., and D. Allsop. 1991. “Amyloid Deposition as the Central Event in the Aetiology of Alzheimer’s Disease.” *Trends in Pharmacological Sciences* 12 (10): 383–88.

Harris, Janna L., In-Young Choi, and William M. Brooks. 2015. “Probing Astrocyte Metabolism in Vivo: Proton Magnetic Resonance Spectroscopy in the Injured and Aging Brain.” *Frontiers in Aging Neuroscience* 7 (October): 202.

Harris, Janna L., Hung-Wen Yeh, Russell H. Swerdlow, In-Young Choi, Phil Lee, and William M. Brooks. 2014. “High-Field Proton Magnetic Resonance Spectroscopy Reveals Metabolic Effects of Normal Brain Aging.” *Neurobiology of Aging* 35 (7): 1686–94.

Harrison, Xavier A., Lynda Donaldson, Maria Eugenia Correa-Cano, Julian Evans, David

- N. Fisher, Cecily E. D. Goodwin, Beth S. Robinson, David J. Hodgson, and Richard Inger. 2018. "A Brief Introduction to Mixed Effects Modelling and Multi-Model Inference in Ecology." *PeerJ* 6 (May): e4794.
- Hasan, Khader M., Indika S. Walimuni, Larry A. Kramer, and Richard E. Frye. 2010. "Human Brain Atlas-Based Volumetry and Relaxometry: Application to Healthy Development and Natural Aging." *Magnetic Resonance in Medicine: Official Journal of the Society of Magnetic Resonance in Medicine / Society of Magnetic Resonance in Medicine* 64 (5): 1382–89.
- Hayek, Dayana, Friederike Thams, Agnes Flöel, and Daria Antonenko. 2020. "Dentate Gyrus Volume Mediates the Effect of Fornix Microstructure on Memory Formation in Older Adults." *Frontiers in Aging Neuroscience* 12 (March): 79.
- Hedman, Anna M., Neeltje E. M. van Haren, Hugo G. Schnack, René S. Kahn, and Hilleke E. Hulshoff Pol. 2012. "Human Brain Changes across the Life Span: A Review of 56 Longitudinal Magnetic Resonance Imaging Studies." *Human Brain Mapping* 33 (8): 1987–2002.
- Heneka, Michael T., and M. Kerry O'Banion. 2007. "Inflammatory Processes in Alzheimer's Disease." *Journal of Neuroimmunology* 184 (1-2): 69–91.
- Henley, David B., Patrick C. May, Robert A. Dean, and Eric R. Siemers. 2009. "Development of Semagacestat (LY450139), a Functional Gamma-Secretase Inhibitor, for the Treatment of Alzheimer's Disease." *Expert Opinion on Pharmacotherapy* 10 (10): 1657–64.
- Herrup, Karl. 2010. "Reimagining Alzheimer's Disease--an Age-Based Hypothesis." *The Journal of Neuroscience: The Official Journal of the Society for Neuroscience* 30 (50): 16755–62.
- Hoenig, John M., and Dennis M. Heisey. n.d. "The Abuse of Power: The Pervasive Fallacy of Power Calculations for Data Analysis."
- Hoffman-Kuczynski, Beth, and Nicholas V. Reo. 2004. "Studies of Myo-Inositol and Plasmalogen Metabolism in Rat Brain." *Neurochemical Research* 29 (4): 843–55.
- Hofmann, L., J. Slotboom, C. Boesch, and R. Kreis. 2001. "Characterization of the Macromolecule Baseline in LocalizedH-MR Spectra of Human Brain." *Magnetic Resonance in Medicine: Official Journal of the Society of Magnetic Resonance in Medicine / Society of Magnetic Resonance in Medicine* 46: 855–63.
- Hofmann, L., J. Slotboom, B. Jung, P. Maloca, C. Boesch, and R. Kreis. 2002. "Quantitative 1H-Magnetic Resonance Spectroscopy of Human Brain: Influence of Composition and Parameterization of the Basis Set in Linear Combination Model-Fitting." *Magnetic Resonance in Medicine: Official Journal of the Society of Magnetic Resonance in Medicine / Society of Magnetic Resonance in Medicine* 48 (3): 440–53.
- Hou, Yujun, Xiuli Dan, Mansi Babbar, Yong Wei, Steen G. Hasselbalch, Deborah L. Croteau, and Vilhelm A. Bohr. 2019. "Ageing as a Risk Factor for Neurodegenerative Disease." *Nature Reviews. Neurology* 15 (10): 565–81.
- Iglewicz, B., and D. C. Hoaglin. 1997. *How to Detect and Handle Outliers*. Edited by E. F. Mykytka, S. Westergard, and A. Wall. Vol. 16. ASQC Basic References in Quality Control. ASQC Quality Press 611 East Wisconsin Avenue, Milwaukee, Wisconsin, 53202: ASQC/Quality Press.
- Ikonomovic, Milos D., William E. Klunk, Eric E. Abrahamson, Chester A. Mathis, Julie C. Price, Nicholas D. Tsopelas, Brian J. Lopresti, et al. 2008. "Post-Mortem Correlates of in

- Vivo PiB-PET Amyloid Imaging in a Typical Case of Alzheimer's Disease." *Brain: A Journal of Neurology* 131 (Pt 6): 1630–45.
- Iqbal, Khalid, Alejandra del C. Alonso, She Chen, M. Omar Chohan, Ezzat El-Akkad, Cheng-Xin Gong, Sabiha Khatoun, et al. 2005. "Tau Pathology in Alzheimer Disease and Other Tauopathies." *Biochimica et Biophysica Acta* 1739 (2-3): 198–210.
- Jack, Clifford R., Frederik Barkhof, Matt A. Bernstein, Marc Cantillon, Patricia E. Cole, Charles DeCarli, Bruno Dubois, et al. 2011. "Steps to Standardization and Validation of Hippocampal Volumetry as a Biomarker in Clinical Trials and Diagnostic Criterion for Alzheimer's Disease." *Alzheimer's & Dementia: The Journal of the Alzheimer's Association* 7 (4): 474–85.e4.
- Jack, Clifford R., Jr, David A. Bennett, Kaj Blennow, Maria C. Carrillo, Billy Dunn, Samantha Budd Haeberlein, David M. Holtzman, et al. 2018. "NIA-AA Research Framework: Toward a Biological Definition of Alzheimer's Disease." *Alzheimer's & Dementia: The Journal of the Alzheimer's Association* 14 (4): 535–62.
- Jack, Clifford R., Jr, David A. Bennett, Kaj Blennow, Maria C. Carrillo, Howard H. Feldman, Giovanni B. Frisoni, Harald Hampel, et al. 2016. "A/T/N: An Unbiased Descriptive Classification Scheme for Alzheimer Disease Biomarkers." *Neurology* 87 (5): 539–47.
- Jack, Clifford R., Jr, David S. Knopman, William J. Jagust, Ronald C. Petersen, Michael W. Weiner, Paul S. Aisen, Leslie M. Shaw, et al. 2013. "Tracking Pathophysiological Processes in Alzheimer's Disease: An Updated Hypothetical Model of Dynamic Biomarkers." *Lancet Neurology* 12 (2): 207–16.
- Jack, Clifford R., Jr, David S. Knopman, William J. Jagust, Leslie M. Shaw, Paul S. Aisen, Michael W. Weiner, Ronald C. Petersen, and John Q. Trojanowski. 2010. "Hypothetical Model of Dynamic Biomarkers of the Alzheimer's Pathological Cascade." *Lancet Neurology* 9 (1): 119–28.
- Jack, Clifford R., Jr, Malgorzata Marjanska, Thomas M. Wengenack, Denise A. Reyes, Geoffrey L. Curran, Joseph Lin, Gregory M. Preboske, Joseph F. Poduslo, and Michael Garwood. 2007. "Magnetic Resonance Imaging of Alzheimer's Pathology in the Brains of Living Transgenic Mice: A New Tool in Alzheimer's Disease Research." *The Neuroscientist: A Review Journal Bringing Neurobiology, Neurology and Psychiatry* 13 (1): 38–48.
- Jack, C. R., Jr, R. C. Petersen, Y. Xu, P. C. O'Brien, G. E. Smith, R. J. Ivnik, B. F. Boeve, E. G. Tangalos, and E. Kokmen. 2000. "Rates of Hippocampal Atrophy Correlate with Change in Clinical Status in Aging and AD." *Neurology* 55 (4): 484–89.
- Jack, C. R., Jr, M. M. Shiung, S. D. Weigand, P. C. O'Brien, J. L. Gunter, B. F. Boeve, D. S. Knopman, et al. 2005. "Brain Atrophy Rates Predict Subsequent Clinical Conversion in Normal Elderly and Amnesic MCI." *Neurology* 65 (8): 1227–31.
- Jankowsky, J. L., H. H. Slunt, T. Ratovitski, N. A. Jenkins, N. G. Copeland, and D. R. Borchelt. 2001. "Co-Expression of Multiple Transgenes in Mouse CNS: A Comparison of Strategies." *Biomolecular Engineering* 17 (6): 157–65.
- Jansen, Jacobus F. A., M. S. Walter H. Backes, Klaas Nicolay, and M. Eline Kooi. 2006. "1H MR Spectroscopy of the Brain: Absolute Quantification of Metabolites." *Radiology* 240 (2).
- Jenkinson, Mark, Christian F. Beckmann, Timothy E. J. Behrens, Mark W. Woolrich, and Stephen M. Smith. 2012. "FSL." *NeuroImage* 62 (2): 782–90.

- Jiang, Wei-Dan, Lin Feng, Yang Liu, Jun Jiang, and Xiao-Qiu Zhou. 2009. "Myo-Inositol Prevents Oxidative Damage, Inhibits Oxygen Radical Generation and Increases Antioxidant Enzyme Activities of Juvenile Jian Carp (Cyprinus Carpio var. Jian)." *Aquaculture Research* 40 (15): 1770–76.
- Jones, Lesley, Peter A. Holmans, Marian L. Hamshere, Denise Harold, Valentina Moskvina, Dobril Ivanov, Andrew Pocklington, et al. 2010. "Genetic Evidence Implicates the Immune System and Cholesterol Metabolism in the Aetiology of Alzheimer's Disease." *PloS One* 5 (11): e13950.
- Jong, L. W. de, K. van der Hiele, I. M. Veer, J. J. Houwing, R. G. J. Westendorp, E. L. E. M. Bollen, P. W. de Bruin, H. A. M. Middelkoop, M. A. van Buchem, and J. van der Grond. 2008. "Strongly Reduced Volumes of Putamen and Thalamus in Alzheimer's Disease: An MRI Study." *Brain: A Journal of Neurology* 131 (Pt 12): 3277–85.
- Joo, Illsung L., Aaron Y. Lai, Paolo Bazzigaluppi, Margaret M. Koletar, Adrienne Dorr, Mary E. Brown, Lysie A. M. Thomason, John G. Sled, Joanne McLaurin, and Bojana Stefanovic. 2017. "Early Neurovascular Dysfunction in a Transgenic Rat Model of Alzheimer's Disease." *Scientific Reports* 7 (1): 1–14.
- Juchem, Christoph, and Douglas L. Rothman. 2014. "Chapter 1.1 - Basis of Magnetic Resonance." In *Magnetic Resonance Spectroscopy*, edited by Charlotte Stagg and Douglas Rothman, 3–14. San Diego: Academic Press.
- Juraska, Janice M., and Nioka C. Lowry. 2012. "Neuroanatomical Changes Associated with Cognitive Aging." In *Behavioral Neurobiology of Aging*, edited by Marie-Christine Pardon and Mark W. Bondi, 137–62. Berlin, Heidelberg: Springer Berlin Heidelberg.
- Juraska, Janice M., Cheryl L. Sisk, and Lydia L. DonCarlos. 2013. "Sexual Differentiation of the Adolescent Rodent Brain: Hormonal Influences and Developmental Mechanisms." *Hormones and Behavior* 64 (2): 203–10.
- Kantarci, Kejal, and Terry E. Goldberg. 2016. "MR Spectroscopy, APOE Genotype, and Evolving β -Amyloid Pathology: What Is Being Detected and When." *Neurology*.
- Kantarci, Kejal, and Clifford R. Jack Jr. 2003. "Neuroimaging in Alzheimer Disease: An Evidence-Based Review." *Neuroimaging Clinics of North America* 13 (2): 197–209.
- Kantarci, Kejal, Glenn E. Smith, Robert J. Ivnik, Ronald C. Petersen, Bradley F. Boeve, David S. Knopman, Eric G. Tangalos, and Clifford R. Jack Jr. 2002. "1H Magnetic Resonance Spectroscopy, Cognitive Function, and Apolipoprotein E Genotype in Normal Aging, Mild Cognitive Impairment and Alzheimer's Disease." *Journal of the International Neuropsychological Society: JINS* 8 (7): 934–42.
- Kantarci, K., C. R. Jack Jr, Y. C. Xu, N. G. Campeau, P. C. O'Brien, G. E. Smith, R. J. Ivnik, et al. 2000. "Regional Metabolic Patterns in Mild Cognitive Impairment and Alzheimer's Disease: A 1H MRS Study." *Neurology* 55 (2): 210–17.
- Kantarci, K., R. C. Petersen, B. F. Boeve, D. S. Knopman, D. F. Tang-Wai, P. C. O'Brien, S. D. Weigand, et al. 2004. "1H MR Spectroscopy in Common Dementias." *Neurology* 63 (8): 1393–98.
- Kaur, G., M. Pawlik, S. E. Gandy, M. E. Ehrlich, J. F. Smiley, and E. Levy. 2017. "Lysosomal Dysfunction in the Brain of a Mouse Model with Intraneuronal Accumulation of Carboxyl Terminal Fragments of the Amyloid Precursor Protein." *Molecular Psychiatry* 22 (7): 981–89.
- Kawas, C., S. Gray, R. Brookmeyer, J. Fozard, and A. Zonderman. 2000. "Age-Specific Incidence Rates of Alzheimer's Disease: The Baltimore Longitudinal Study of Aging."

Neurology 54 (11): 2072–77.

Kienlin, Markus von, Basil Künnecke, Friedrich Metzger, Guido Steiner, J. Grayson Richards, Laurence Ozmen, Helmut Jacobsen, and Hansruedi Loetscher. 2005. “Altered Metabolic Profile in the Frontal Cortex of PS2APP Transgenic Mice, Monitored throughout Their Life Span.” *Neurobiology of Disease* 18 (1): 32–39.

Kilborn, Susan H., Guy Trudel, and Hans Uthoff. 2002. “Review of Growth Plate Closure Compared with Age at Sexual Maturity and Lifespan in Laboratory Animals.” *Contemporary Topics in Laboratory Animal Science / American Association for Laboratory Animal Science* 41 (5): 21–26.

Klein, J. 2000. “Membrane Breakdown in Acute and Chronic Neurodegeneration: Focus on Choline-Containing Phospholipids.” *Journal of Neural Transmission* 107 (8-9): 1027–63.

Kline, Adam. 2012. “Apolipoprotein E, Amyloid- β Clearance and Therapeutic Opportunities in Alzheimer’s Disease.” *Alzheimer’s Research & Therapy* 4 (4): 32.

Knopman, David S., David T. Jones, and Michael D. Greicius. 2021. “Failure to Demonstrate Efficacy of Aducanumab: An Analysis of the EMERGE and ENGAGE Trials as Reported by Biogen, December 2019.” *Alzheimer’s & Dementia: The Journal of the Alzheimer’s Association* 17 (4): 696–701.

Komoroski, R. A., C. Heimberg, D. Cardwell, and C. N. Karson. 1999. “Effects of Gender and Region on Proton MRS of Normal Human Brain.” *Magnetic Resonance Imaging* 17 (3): 427–33.

Kong, Vincent, Gabriel A. Devenyi, Daniel Gallino, Gülebru Ayranci, Jürgen Germann, Colleen Rollins, and M. Mallar Chakravarty. 2018. “Early-in-Life Neuroanatomical and Behavioural Trajectories in a Triple Transgenic Model of Alzheimer’s Disease.” *Brain Structure & Function* 223 (7): 3365–82.

Kong, Xiang, Song Luo, Jin Rong Wu, Shawn Wu, Carlo N. De Cecco, U. Joseph Schoepf, Adam J. Spandorfer, et al. 2016. “(18)F-DPA-714 PET Imaging for Detecting Neuroinflammation in Rats with Chronic Hepatic Encephalopathy.” *Theranostics* 6 (8): 1220–31.

Koran, Mary Ellen I., Madison Wagener, Timothy J. Hohman, and Alzheimer’s Neuroimaging Initiative. 2017. “Sex Differences in the Association between AD Biomarkers and Cognitive Decline.” *Brain Imaging and Behavior* 11 (1): 205–13.

Kostidis, Sarantos, Ruben D. Addie, Hans Morreau, Oleg A. Mayboroda, and Martin Giera. 2017. “Quantitative NMR Analysis of Intra- and Extracellular Metabolism of Mammalian Cells: A Tutorial.” *Analytica Chimica Acta* 980 (August): 1–24.

Kreis, Roland. 2016. “The Trouble with Quality Filtering Based on Relative Cramér-Rao Lower Bounds.” *Magnetic Resonance in Medicine: Official Journal of the Society of Magnetic Resonance in Medicine / Society of Magnetic Resonance in Medicine* 75 (1): 15–18.

Kreis, Roland, Vincent Boer, In-Young Choi, Cristina Cudalbu, Robin A. de Graaf, Charles Gasparovic, Arend Heerschap, et al. 2020. “Terminology and Concepts for the Characterization of in Vivo MR Spectroscopy Methods and MR Spectra: Background and Experts’ Consensus Recommendations.” *NMR in Biomedicine*, August, e4347.

Kreis, Roland, Johannes Slotboom, Lucie Hofmann, and Chris Boesch. 2005. “Integrated Data Acquisition and Processing to Determine Metabolite Contents, Relaxation Times, and Macromolecule Baseline in Single Examinations of Individual Subjects.” *Magnetic Resonance in Medicine: Official Journal of the Society of Magnetic Resonance in Medicine*

- / Society of Magnetic Resonance in Medicine* 54 (4): 761–68.
- Krstic, Dimitrije, and Irene Knuesel. 2013. “Deciphering the Mechanism Underlying Late-Onset Alzheimer Disease.” *Nature Reviews. Neurology* 9 (1): 25–34.
- Kruman, Inna I., Robert P. Wersto, Fernando Cardozo-Pelaez, Lubomir Smilenov, Sic L. Chan, Francis J. Chrest, Roland Emokpae Jr, Myriam Gorospe, and Mark P. Mattson. 2004. “Cell Cycle Activation Linked to Neuronal Cell Death Initiated by DNA Damage.” *Neuron* 41 (4): 549–61.
- Kuhla, Angela, Claire Rühlmann, Tobias Lindner, Stefan Polei, Stefan Hadlich, Bernd J. Krause, Brigitte Vollmar, and Stefan J. Teipel. 2017. “APPswe/PS1dE9 Mice with Cortical Amyloid Pathology Show a Reduced NAA/Cr Ratio without Apparent Brain Atrophy: A MRS and MRI Study.” *NeuroImage. Clinical* 15 (June): 581–86.
- Kulkarni, Praveen, Simone Grant, Thomas R. Morrison, Xuezhu Cai, Sade Iriah, Bruce S. Kristal, Jennifer Honeycutt, et al. 2020. “Characterizing the Human APOE Epsilon 4 Knock-in Transgene in Female and Male Rats with Multimodal Magnetic Resonance Imaging.” *Brain Research* 1747 (November): 147030.
- Kupeli, Ali, Mehmet Kocak, Mehmet Goktepel, Erdal Karavas, and Gurkan Danisan. 2020. “Role of T1 Mapping to Evaluate Brain Aging in a Healthy Population.” *Clinical Imaging* 59 (1): 56–60.
- Kuznetsova, Alexandra, Per B. Brockhoff, and Rune H. B. Christensen. 2017. “lmerTest Package: Tests in Linear Mixed Effects Models.” *Journal of Statistical Software, Articles* 82 (13): 1–26.
- Lambert, J. C., C. A. Ibrahim-Verbaas, D. Harold, A. C. Naj, R. Sims, C. Bellenguez, A. L. DeStafano, et al. 2013. “Meta-Analysis of 74,046 Individuals Identifies 11 New Susceptibility Loci for Alzheimer’s Disease.” *Nature Genetics* 45 (12): 1452–58.
- Lanz, Bernard, Alireza Abaei, Olivier Braissant, In-Young Choi, Cristina Cudalbu, Pierre-Gilles Henry, Rolf Gruetter, et al. 2020. “Magnetic Resonance Spectroscopy in the Rodent Brain: Experts’ Consensus Recommendations.” *NMR in Biomedicine*, August, e4325.
- Lau, Jonathan C., Jason P. Lerch, John G. Sled, R. Mark Henkelman, Alan C. Evans, and Barry J. Bedell. 2008. “Longitudinal Neuroanatomical Changes Determined by Deformation-Based Morphometry in a Mouse Model of Alzheimer’s Disease.” *NeuroImage* 42 (1): 19–27.
- Lee, Grace J., Po H. Lu, Luis D. Medina, Yaneth Rodriguez-Agudelo, Stephanie Melchor, Giovanni Coppola, Meredith N. Braskie, et al. 2013. “Regional Brain Volume Differences in Symptomatic and Presymptomatic Carriers of Familial Alzheimer’s Disease Mutations.” *Journal of Neurology, Neurosurgery, and Psychiatry* 84 (2): 154–62.
- Lee, Hyeong Hun, and Hyeonjin Kim. 2017. “Parameterization of Spectral Baseline Directly from Short Echo Time Full Spectra in 1 H-MRS.” *Magnetic Resonance in Medicine: Official Journal of the Society of Magnetic Resonance in Medicine / Society of Magnetic Resonance in Medicine* 78 (3): 836–47.
- Lee, J. H., E. Arcinue, and B. D. Ross. 1994. “Brief Report: Organic Osmolytes in the Brain of an Infant with Hypernatremia.” *The New England Journal of Medicine* 331 (7): 439–42.
- Leon, Wanda Carolina, Fabio Caneva, Vanessa Partridge, Simon Allard, Maria Teresa Ferretti, Arald DeWilde, Freya Vercauteren, et al. 2010. “A Novel Transgenic Rat Model with a Full Alzheimer’s-like Amyloid Pathology Displays Pre-Plaque Intracellular Amyloid-Beta-Associated Cognitive Impairment.” *Journal of Alzheimer’s Disease: JAD* 20 (1): 113–26.

- Lepus, Aurelie, Inger Lauritzen, Christophe Melon, Lydia Kerkerian-Le Goff, Denys Fontaine, and Frederic Checler. 2019. "Chronic Fornix Deep Brain Stimulation in a Transgenic Alzheimer's Rat Model Reduces Amyloid Burden, Inflammation, and Neuronal Loss." *Brain Structure & Function* 224 (1): 363–72.
- Lepore, Natasha, Caroline A. Brun, Ming-Chang Chiang, Yi-Yu Chou, Rebecca A. Dutton, Kiralee M. Hayashi, Oscar L. Lopez, et al. 2006. "Multivariate Statistics of the Jacobian Matrices in Tensor Based Morphometry and Their Application to HIV/AIDS." In *Medical Image Computing and Computer-Assisted Intervention – MICCAI 2006*, 191–98. Springer Berlin Heidelberg.
- Lerch, Jason P., Lisa Gazdzinski, Jürgen Germann, John G. Sled, R. Mark Henkelman, and Brian J. Nieman. 2012. "Wanted Dead or Alive? The Tradeoff between in-Vivo versus Ex-Vivo MR Brain Imaging in the Mouse." *Frontiers in Neuroinformatics* 6 (March): 6.
- Lerch, Jason P., André J. W. van der Kouwe, Armin Raznahan, Tomáš Paus, Heidi Johansen-Berg, Karla L. Miller, Stephen M. Smith, Bruce Fischl, and Stamatios N. Sotiropoulos. 2017. "Studying Neuroanatomy Using MRI." *Nature Neuroscience* 20 (3): 314–26.
- Lerch, Jason P., Adelaide P. Yiu, Alonso Martinez-Canabal, Tetyana Pekar, Veronique D. Bohbot, Paul W. Frankland, R. Mark Henkelman, Sheena A. Josselyn, and John G. Sled. 2011. "Maze Training in Mice Induces MRI-Detectable Brain Shape Changes Specific to the Type of Learning." *NeuroImage* 54 (3): 2086–95.
- Lerch, J., C. Hammill, M. van Eede, and D. Cassel. 2017. "Statistical Tools for Medical Imaging NetCDF (MINC) Files. R Package Version 1.5.2.3." 2017. <http://mouse-imaging-centre.github.io/RMINC/>.
- Leuzy, Antoine, Kerstin Heurling, Nicholas J. Ashton, Michael Schöll, and Eduardo R. Zimmer. 2018. "In Vivo Detection of Alzheimer's Disease." *The Yale Journal of Biology and Medicine* 91 (3): 291–300.
- Lewis, J., D. W. Dickson, W. L. Lin, L. Chisholm, A. Corral, G. Jones, S. H. Yen, et al. 2001. "Enhanced Neurofibrillary Degeneration in Transgenic Mice Expressing Mutant Tau and APP." *Science* 293 (5534): 1487–91.
- Leys, Christophe, Christophe Ley, Olivier Klein, Philippe Bernard, and Laurent Licata. 2013. "Detecting Outliers: Do Not Use Standard Deviation around the Mean, Use Absolute Deviation around the Median." *Journal of Experimental Social Psychology* 49 (4): 764–66.
- Ligneul, Clémence, Marco Palombo, Edwin Hernández-Garzón, María-Angeles Carrillo-de Sauvage, Julien Flament, Philippe Hantraye, Emmanuel Brouillet, Gilles Bonvento, Carole Escartin, and Julien Valette. 2019. "Diffusion-Weighted Magnetic Resonance Spectroscopy Enables Cell-Specific Monitoring of Astrocyte Reactivity in Vivo." *NeuroImage* 191 (May): 457–69.
- Lin, Alexander, Brian D. Ross, Kent Harris, and Willis Wong. 2005. "Efficacy of Proton Magnetic Resonance Spectroscopy in Neurological Diagnosis and Neurotherapeutic Decision Making." *NeuroRx: The Journal of the American Society for Experimental Neurotherapeutics* 2 (2): 197–214.
- Lin, Joanne C., and Nicholas Gant. 2014. "Chapter 2.3 - The Biochemistry of Choline." In *Magnetic Resonance Spectroscopy*, edited by Charlotte Staggs and Douglas Rothman, 104–10. San Diego: Academic Press.
- Lithfous, Ségolène, André Dufour, and Olivier Després. 2013. "Spatial Navigation in Normal Aging and the Prodromal Stage of Alzheimer's Disease: Insights from Imaging and

Behavioral Studies.” *Ageing Research Reviews* 12 (1): 201–13.

Liu, Chang, and Jürgen Götz. 2013. “Profiling Murine Tau with 0N, 1N and 2N Isoform-Specific Antibodies in Brain and Peripheral Organs Reveals Distinct Subcellular Localization, with the 1N Isoform Being Enriched in the Nucleus.” *PloS One* 8 (12): e84849.

Liu, Ying, Mi-Jeong Yoo, Alena Savonenko, Wanda Stirling, Donald L. Price, David R. Borchelt, Laura Mamounas, W. Ernest Lyons, Mary E. Blue, and Michael K. Lee. 2008. “Amyloid Pathology Is Associated with Progressive Monoaminergic Neurodegeneration in a Transgenic Mouse Model of Alzheimer’s Disease.” *The Journal of Neuroscience: The Official Journal of the Society for Neuroscience* 28 (51): 13805–14.

Long, Xiaojing, Weiqi Liao, Chunxiang Jiang, Dong Liang, Bensheng Qiu, and Lijuan Zhang. 2012. “Healthy Aging: An Automatic Analysis of Global and Regional Morphological Alterations of Human Brain.” *Academic Radiology* 19 (7): 785–93.

Lopez-Kolkovskiy, Alfredo L., Sebastien Mériaux, and Fawzi Boumezbeur. 2016. “Metabolite and Macromolecule T1 and T2 Relaxation Times in the Rat Brain in Vivo at 17.2T.” *Magnetic Resonance in Medicine: Official Journal of the Society of Magnetic Resonance in Medicine / Society of Magnetic Resonance in Medicine* 75 (2): 503–14.

Lutz, Michael W., Daniel Sprague, and Ornit Chiba-Falek. 2019. “Bioinformatics Strategy to Advance the Interpretation of Alzheimer’s Disease GWAS Discoveries: The Roads from Association to Causation.” *Alzheimer’s & Dementia: The Journal of the Alzheimer’s Association* 15 (8): 1048–58.

MacDonald, M. Ethan, and G. Bruce Pike. 2021. “MRI of Healthy Brain Aging: A Review.” *NMR in Biomedicine* 34 (9): e4564.

MacLusky, N. J., A. S. Clark, F. Naftolin, and P. S. Goldman-Rakic. 1987. “Estrogen Formation in the Mammalian Brain: Possible Role of Aromatase in Sexual Differentiation of the Hippocampus and Neocortex.” *Steroids* 50 (4-6): 459–74.

Maheswaran, Satheesh, Hervé Barjat, Daniel Rueckert, Simon T. Bate, David R. Howlett, Lorna Tilling, Sean C. Smart, et al. 2009. “Longitudinal Regional Brain Volume Changes Quantified in Normal Aging and Alzheimer’s APP X PS1 Mice Using MRI.” *Brain Research* 1270 (May): 19–32.

Maia, Miguel A., and Emília Sousa. 2019. “BACE-1 and γ -Secretase as Therapeutic Targets for Alzheimer’s Disease.” *Pharmaceuticals* 12 (1). <https://doi.org/10.3390/ph12010041>.

Malinowski, Mark N. 2019. “Anatomy of the Brain and Brain Stem.” In *Deer’s Treatment of Pain: An Illustrated Guide for Practitioners*, edited by Timothy R. Deer, Jason E. Pope, Tim J. Lamer, and David Provenzano, 49–59. Cham: Springer International Publishing.

Malykhin, Nikolai V., Yushan Huang, Stanislaw Hrybowski, and Fraser Olsen. 2017. “Differential Vulnerability of Hippocampal Subfields and Anteroposterior Hippocampal Subregions in Healthy Cognitive Aging.” *Neurobiology of Aging* 59 (November): 121–34.

Mao, Jintong, T. H. Mareci, and E. R. Andrew. 1988. “Experimental Study of Optimal Selective 180 Radiofrequency Pulses.” *Journal of Magnetic Resonance* 79 (1): 1–10.

Marjanska, Malgorzata, Geoffrey L. Curran, Thomas M. Wengenack, Pierre-Gilles Henry, Robin L. Bliss, Joseph F. Poduslo, Clifford R. Jack Jr, Kâmil Ugurbil, and Michael Garwood. 2005. “Monitoring Disease Progression in Transgenic Mouse Models of Alzheimer’s Disease with Proton Magnetic Resonance Spectroscopy.” *Proceedings of the National Academy of Sciences of the United States of America* 102 (33): 11906–10.

Marjańska, Małgorzata, Dinesh K. Deelchand, James S. Hodges, J. Riley McCarten, Laura

- S. Hemmy, Andrea Grant, and Melissa Terpstra. 2018. "Altered Macromolecular Pattern and Content in the Aging Human Brain." *NMR in Biomedicine* 31 (2).
<https://doi.org/10.1002/nbm.3865>.
- Marjańska, Małgorzata, J. Riley McCarten, James Hodges, Laura S. Hemmy, Andrea Grant, Dinesh K. Deelchand, and Melissa Terpstra. 2017. "Region-Specific Aging of the Human Brain as Evidenced by Neurochemical Profiles Measured Noninvasively in the Posterior Cingulate Cortex and the Occipital Lobe Using 1H Magnetic Resonance Spectroscopy at 7 T." *Neuroscience* 354 (June): 168–77.
- Marjańska, Małgorzata, J. Riley McCarten, James S. Hodges, Laura S. Hemmy, and Melissa Terpstra. 2019. "Distinctive Neurochemistry in Alzheimer's Disease via 7 T In Vivo Magnetic Resonance Spectroscopy." *Journal of Alzheimer's Disease: JAD* 68 (2): 559–69.
- Marjańska, M., S. D. Weigand, G. Preboske, T. M. Wengenack, R. Chamberlain, G. L. Curran, J. F. Poduslo, et al. 2014. "Treatment Effects in a Transgenic Mouse Model of Alzheimer's Disease: A Magnetic Resonance Spectroscopy Study after Passive Immunization." *Neuroscience* 259 (February): 94–100.
- Marrone, Diano F., Elham Satvat, and Anuj Patel. 2018. "Age-Related Deficits in Recognition Memory Are Protocol-Dependent." *Aging and Disease* 9 (5): 798–807.
- Martínez-Pinilla, Eva, Cristina Ordóñez, Eva Del Valle, Ana Navarro, and Jorge Tolivia. 2016. "Regional and Gender Study of Neuronal Density in Brain during Aging and in Alzheimer's Disease." *Frontiers in Aging Neuroscience* 8 (September): 213.
- Masoro, E. J. 1980. "Mortality and Growth Characteristics of Rat Strains Commonly Used in Aging Research." *Experimental Aging Research* 6 (3): 219–33.
- Masters, Colin L., Randall Bateman, Kaj Blennow, Christopher C. Rowe, Reisa A. Sperling, and Jeffrey L. Cummings. 2015. "Alzheimer's Disease." *Nature Reviews. Disease Primers* 1 (October): 15056.
- Mattson, Mark P. 2004. "Pathways towards and Away from Alzheimer's Disease." *Nature* 430 (7000): 631–39.
- Mattson, Mark P., and Thiruma V. Arumugam. 2018. "Hallmarks of Brain Aging: Adaptive and Pathological Modification by Metabolic States." *Cell Metabolism* 27 (6): 1176–99.
- Mattson, Mark P., and Tim Magnus. 2006. "Ageing and Neuronal Vulnerability." *Nature Reviews. Neuroscience* 7 (4): 278–94.
- Mattsson, Niklas, Ulf Andreasson, Henrik Zetterberg, Kaj Blennow, and Alzheimer's Disease Neuroimaging Initiative. 2017. "Association of Plasma Neurofilament Light With Neurodegeneration in Patients With Alzheimer Disease." *JAMA Neurology* 74 (5): 557–66.
- Mawhinney, Lana J., Juan Pablo de Rivero Vaccari, Gordon A. Dale, Robert W. Keane, and Helen M. Bramlett. 2011. "Heightened Inflammation Activation Is Linked to Age-Related Cognitive Impairment in Fischer 344 Rats." *BMC Neuroscience* 12 (December): 123.
- Mawuenyega, Kwasi G., Wendy Sigurdson, Vitaliy Ovod, Ling Munsell, Tom Kasten, John C. Morris, Kevin E. Yarasheski, and Randall J. Bateman. 2010. "Decreased Clearance of CNS Beta-Amyloid in Alzheimer's Disease." *Science* 330 (6012): 1774.
- Mazure, Carolyn M., and Joel Swendsen. 2016. "Sex Differences in Alzheimer's Disease and Other Dementias." *Lancet Neurology*.
- McKenna, Mary C., Gerald A. Dienel, Ursula Sonnewald, Helle S. Waagepetersen, and Arne Schousboe. 2012. "Chapter 11 - Energy Metabolism of the Brain." In *Basic Neurochemistry (Eighth Edition)*, edited by Scott T. Brady, George J. Siegel, R. Wayne

Albers, and Donald L. Price, 200–231. New York: Academic Press.

McKhann, G., D. Drachman, M. Folstein, R. Katzman, D. Price, and E. M. Stadlan. 1984. “Clinical Diagnosis of Alzheimer’s Disease: Report of the NINCDS-ADRDA Work Group under the Auspices of Department of Health and Human Services Task Force on Alzheimer’s Disease.” *Neurology* 34 (7): 939–44.

McKhann, Guy M., David S. Knopman, Howard Chertkow, Bradley T. Hyman, Clifford R. Jack Jr, Claudia H. Kawas, William E. Klunk, et al. 2011. “The Diagnosis of Dementia due to Alzheimer’s Disease: Recommendations from the National Institute on Aging-Alzheimer’s Association Workgroups on Diagnostic Guidelines for Alzheimer’s Disease.” *Alzheimer’s & Dementia: The Journal of the Alzheimer’s Association* 7 (3): 263–69.

Mehra, Divy, and Majid Moshirfar. 2020. “Neuroanatomy, Optic Tract.” In *StatPearls*. Treasure Island (FL): StatPearls Publishing.

Ménoret, Séverine, Sandra Fontanière, Derek Jantz, Laurent Tesson, Reynald Thinar, Séverine Rémy, Claire Usal, Laure-Hélène Ouisse, Alexandre Fraichard, and Ignacio Anegón. 2013. “Generation of Rag1-Knockout Immunodeficient Rats and Mice Using Engineered Meganucleases.” *FASEB Journal: Official Publication of the Federation of American Societies for Experimental Biology* 27 (2): 703–11.

Mersman, Brittany, Wali Zaidi, Naweed I. Syed, and Fenglian Xu. 2020. “Taurine Promotes Neurite Outgrowth and Synapse Development of Both Vertebrate and Invertebrate Central Neurons.” *Frontiers in Synaptic Neuroscience* 12 (July): 29.

Miccheli, Alfredo, Caterina Puccetti, Giorgio Capuani, Maria Enrica Di Cocco, Luciana Giardino, Laura Calzà, Angelo Battaglia, Leontino Battistin, and Filippo Conti. 2003. “[1-¹³C]Glucose Entry in Neuronal and Astrocytic Intermediary Metabolism of Aged Rats: A Study of the Effects of Nicergoline Treatment by ¹³C NMR Spectroscopy.” *Brain Research* 966 (1): 116–25.

Mietchen, Daniel, and Christian Gaser. 2009. “Computational Morphometry for Detecting Changes in Brain Structure due to Development, Aging, Learning, Disease and Evolution.” *Frontiers in Neuroinformatics* 3 (August): 25.

Mitchell, Sarah J., Morten Scheibye-Knudsen, Dan L. Longo, and Rafael de Cabo. 2015. “Animal Models of Aging Research: Implications for Human Aging and Age-Related Diseases.” *Annual Review of Animal Biosciences* 3: 283–303.

Mlynárik, Vladimír, Cristina Cudalbu, Lijing Xin, and Rolf Gruetter. 2008. “¹H NMR Spectroscopy of Rat Brain in Vivo at 14.1 Tesla: Improvements in Quantification of the Neurochemical Profile.” *Journal of Magnetic Resonance* 194 (2): 163–68.

Mlynárik, Vladimír, Giulio Gambarota, Hanne Frenkel, and Rolf Gruetter. 2006. “Localized Short-Echo-Time Proton MR Spectroscopy with Full Signal-Intensity Acquisition.” *Magnetic Resonance in Medicine: Official Journal of the Society of Magnetic Resonance in Medicine / Society of Magnetic Resonance in Medicine* 56 (5): 965–70.

Moffett, John R., Prasanth Ariyannur, Peethambaran Arun, and Aryan M. A. Namboodiri. 2014. “Chapter 2.1 - N-Acetylaspartate and N-Acetylaspartylglutamate in Central Nervous System Health and Disease.” In *Magnetic Resonance Spectroscopy*, edited by Charlotte Stagg and Douglas Rothman, 71–90. San Diego: Academic Press.

Moffett, John R., Brian Ross, Peethambaran Arun, Chikkathur N. Madhavarao, and Aryan M. A. Namboodiri. 2007. “N-Acetylaspartate in the CNS: From Neurodiagnostics to Neurobiology.” *Progress in Neurobiology* 81 (2): 89–131.

Morris, John C., Catherine M. Roe, Chengjie Xiong, Anne M. Fagan, Alison M. Goate,

- David M. Holtzman, and Mark A. Mintun. 2010. "APOE Predicts Amyloid-Beta but Not Tau Alzheimer Pathology in Cognitively Normal Aging." *Annals of Neurology* 67 (1): 122–31.
- Morrison, John H., Paul C. Stern, and Laura L. Carstensen. 2000. *Age-Related Shifts in Neural Circuit Characteristics and Their Impact on Age-Related Cognitive Impairments*. National Academies Press (US).
- Morrone, Christopher D., Paolo Bazzigaluppi, Tina L. Beckett, Mary E. Hill, Margaret M. Koletar, Bojana Stefanovic, and Joanne McLaurin. 2020. "Regional Differences in Alzheimer's Disease Pathology Confound Behavioural Rescue after Amyloid- β Attenuation." *Brain: A Journal of Neurology* 143 (1): 359–73.
- Mortera, Priscilla, and Suzana Herculano-Houzel. 2012. "Age-Related Neuronal Loss in the Rat Brain Starts at the End of Adolescence." *Frontiers in Neuroanatomy* 6 (October): 45.
- Mosconi, Lisa. 2013. "Glucose Metabolism in Normal Aging and Alzheimer's Disease: Methodological and Physiological Considerations for PET Studies." *Clinical and Translational Imaging* 1 (4). <https://doi.org/10.1007/s40336-013-0026-y>.
- Mosconi, Lisa, Valentina Berti, Crystal Quinn, Pauline McHugh, Gabriella Petrongolo, Isabella Varsavsky, Ricardo S. Osorio, et al. 2017. "Sex Differences in Alzheimer Risk: Brain Imaging of Endocrine vs Chronologic Aging." *Neurology* 89 (13): 1382–90.
- Mueller, S. G., N. Schuff, and M. W. Weiner. 2006. "Evaluation of Treatment Effects in Alzheimer's and Other Neurodegenerative Diseases by MRI and MRS." *NMR in Biomedicine* 19 (6): 655–68.
- Mullard, Asher. 2021. "Landmark Alzheimer's Drug Approval Confounds Research Community." *Nature* 594 (7863): 309–10.
- Muñoz-Moreno, Emma, Raúl Tudela, Xavier López-Gil, and Guadalupe Soria. 2018. "Early Brain Connectivity Alterations and Cognitive Impairment in a Rat Model of Alzheimer's Disease." *Alzheimer's Research & Therapy* 10 (1): 16.
- Murphy, D. G., C. DeCarli, A. R. McIntosh, E. Daly, M. J. Mentis, P. Pietrini, J. Szczepanik, et al. 1996. "Sex Differences in Human Brain Morphometry and Metabolism: An in Vivo Quantitative Magnetic Resonance Imaging and Positron Emission Tomography Study on the Effect of Aging." *Archives of General Psychiatry* 53 (7): 585–94.
- Murray, Melissa E., Scott A. Przybelski, Timothy G. Lesnick, Amanda M. Liesinger, Anthony Sychalla, Bing Zhang, Jeffrey L. Gunter, et al. 2014. "Early Alzheimer's Disease Neuropathology Detected by Proton MR Spectroscopy." *The Journal of Neuroscience: The Official Journal of the Society for Neuroscience* 34 (49): 16247–55.
- Nakai, Tsuyoshi, Kiyofumi Yamada, and Hiroyuki Mizoguchi. 2021. "Alzheimer's Disease Animal Models: Elucidation of Biomarkers and Therapeutic Approaches for Cognitive Impairment." *International Journal of Molecular Sciences* 22 (11). <https://doi.org/10.3390/ijms22115549>.
- Nakamura, Akinori, Naoki Kaneko, Victor L. Villemagne, Takashi Kato, James Doecke, Vincent Doré, Chris Fowler, et al. 2018. "High Performance Plasma Amyloid- β Biomarkers for Alzheimer's Disease." *Nature* 554 (7691): 249–54.
- Naressi, A., C. Couturier, J. M. Devos, M. Janssen, C. Mangeat, R. de Beer, and D. Graveron-Demilly. 2001. "Java-Based Graphical User Interface for the MRUI Quantitation Package." *Magma* 12 (2-3): 141–52.
- Narvacan, Karl, Sarah Treit, Richard Camicioli, Wayne Martin, and Christian Beaulieu. 2017. "Evolution of Deep Gray Matter Volume across the Human Lifespan." *Human Brain*

Mapping 38 (8): 3771–90.

Near, Jamie, Ashley D. Harris, Christoph Juchem, Roland Kreis, Małgorzata Marjańska, Gülin Öz, Johannes Slotboom, Martin Wilson, and Charles Gasparovic. 2020.

“Preprocessing, Analysis and Quantification in Single-Voxel Magnetic Resonance Spectroscopy: Experts’ Consensus Recommendations.” *NMR in Biomedicine*, February, e4257.

Nelson, Peter T., Heiko Braak, and William R. Markesbery. 2009. “Neuropathology and Cognitive Impairment in Alzheimer Disease: A Complex but Coherent Relationship.” *Journal of Neuropathology and Experimental Neurology* 68 (1): 1–14.

Neuwirth, Erich. 2014. “RColorBrewer: ColorBrewer Palettes.” <https://CRAN.R-project.org/package=RColorBrewer>.

Nilsen, L. H., T. M. Melø, M. P. Witter, and U. Sonnewald. 2014. “Early Differences in Dorsal Hippocampal Metabolite Levels in Males but Not Females in a Transgenic Rat Model of Alzheimer’s Disease.” *Neurochemical Research* 39 (2): 305–12.

Nilsen, Linn H., Torun M. Melø, Oddbjørn Saether, Menno P. Witter, and Ursula Sonnewald. 2012. “Altered Neurochemical Profile in the McGill-R-Thy1-APP Rat Model of Alzheimer’s Disease: A Longitudinal in Vivo 1 H MRS Study.” *Journal of Neurochemistry* 123 (4): 532–41.

Nixon, Ralph A., and Anne M. Cataldo. 2006. “Lysosomal System Pathways: Genes to Neurodegeneration in Alzheimer’s Disease.” *Journal of Alzheimer’s Disease: JAD* 9 (3 Suppl): 277–89.

Nixon, Ralph A., and Dun-Sheng Yang. 2011. “Autophagy Failure in Alzheimer’s Disease—Locating the Primary Defect.” *Neurobiology of Disease* 43 (1): 38–45.

Oberg, Johanna, Christian Spenger, Fu-Hua Wang, Anders Andersson, Eric Westman, Peter Skoglund, Dan Sunnemark, et al. 2008. “Age Related Changes in Brain Metabolites Observed by 1H MRS in APP/PS1 Mice.” *Neurobiology of Aging* 29 (9): 1423–33.

Oddo, Salvatore, Lauren Billings, J. Patrick Kesslak, David H. Cribbs, and Frank M. LaFerla. 2004. “Abeta Immunotherapy Leads to Clearance of Early, but Not Late, Hyperphosphorylated Tau Aggregates via the Proteasome.” *Neuron* 43 (3): 321–32.

Oddo, Salvatore, Antonella Caccamo, Jason D. Shepherd, M. Paul Murphy, Todd E. Golde, Rakez Kaye, Raju Metherate, Mark P. Mattson, Yama Akbari, and Frank M. LaFerla. 2003. “Triple-Transgenic Model of Alzheimer’s Disease with Plaques and Tangles: Intracellular Abeta and Synaptic Dysfunction.” *Neuron* 39 (3): 409–21.

Oh, Esther S., Alena V. Savonenko, Julie F. King, Stina M. Fangmark Tucker, Gay L. Rudow, Guilian Xu, David R. Borchelt, and Juan C. Troncoso. 2009. “Amyloid Precursor Protein Increases Cortical Neuron Size in Transgenic Mice.” *Neurobiology of Aging* 30 (8): 1238–44.

Okada Kana, and Okaichi Hiroshige. 2006. “[The functional cooperation of the hippocampus and anterior thalamus via the fimbria-fornix in spatial memory in rats].” *Shinrigaku kenkyu: The Japanese journal of psychology* 77 (3): 261–70.

Ossenkoppele, Rik, and Oskar Hansson. 2018. “Genetic Characterization of Amyloid- β and Tau Network Spread.” *Nature Medicine*.

Osterlund, M. K., and Y. L. Hurd. 2001. “Estrogen Receptors in the Human Forebrain and the Relation to Neuropsychiatric Disorders.” *Progress in Neurobiology* 64 (3): 251–67.

Otazo, Ricardo, Bryon Mueller, Kamil Ugurbil, Lawrence Wald, and Stefan Posse. 2006. “Signal-to-Noise Ratio and Spectral Linewidth Improvements between 1.5 and 7 Tesla in

Proton Echo-Planar Spectroscopic Imaging.” *Magnetic Resonance in Medicine: Official Journal of the Society of Magnetic Resonance in Medicine / Society of Magnetic Resonance in Medicine* 56 (6): 1200–1210.

Otsu, N. 1979. “A Threshold Selection Method from Gray-Level Histograms.” *IEEE Transactions on Systems, Man, and Cybernetics* 9 (1): 62–66.

Paban, Véronique, Florence Fauvelle, and Béatrice Alescio-Lautier. 2010. “Age-Related Changes in Metabolic Profiles of Rat Hippocampus and Cortices.” *The European Journal of Neuroscience* 31 (6): 1063–73.

Palmqvist, Sebastian, Shorena Janelidze, Yakeel T. Quiroz, Henrik Zetterberg, Francisco Lopera, Erik Stomrud, Yi Su, et al. 2020. “Discriminative Accuracy of Plasma Phospho-tau217 for Alzheimer Disease vs Other Neurodegenerative Disorders.” *JAMA: The Journal of the American Medical Association* 324 (8): 772–81.

Palombo, Marco, Clémence Ligneul, Chloé Najac, Juliette Le Douce, Julien Flament, Carole Escartin, Philippe Hantraye, Emmanuel Brouillet, Gilles Bonvento, and Julien Valette. 2016. “New Paradigm to Assess Brain Cell Morphology by Diffusion-Weighted MR Spectroscopy in Vivo.” *Proceedings of the National Academy of Sciences of the United States of America* 113 (24): 6671–76.

Pang, Keliang, Richeng Jiang, Wei Zhang, Zhengyi Yang, Lin-Lin Li, Makoto Shimozawa, Simone Tambaro, et al. 2021. “An App Knock-in Rat Model for Alzheimer’s Disease Exhibiting A β and Tau Pathologies, Neuronal Death and Cognitive Impairments.” *Cell Research*, November. <https://doi.org/10.1038/s41422-021-00582-x>.

Pardon, Marie-Christine, Maria Yanez Lopez, Ding Yuchun, Małgorzata Marjańska, Malcolm Prior, Christopher Brignell, Samira Parhizkar, et al. 2016. “Magnetic Resonance Spectroscopy Discriminates the Response to Microglial Stimulation of Wild Type and Alzheimer’s Disease Models.” *Scientific Reports* 6 (1): 19880.

Parent, Maxime J., Eduardo R. Zimmer, Monica Shin, Min Su Kang, Vladimir S. Fonov, Axel Mathieu, Antonio Aliaga, et al. 2017. “Multimodal Imaging in Rat Model Recapitulates Alzheimer’s Disease Biomarkers Abnormalities.” *The Journal of Neuroscience: The Official Journal of the Society for Neuroscience* 37 (50): 12263–71.

Patterson, Christina. 2018. “World Alzheimer Report 2018. The State of the Art of Dementia Research: New Frontiers.” *Alzheimer’s Disease International*. <https://apo.org.au/sites/default/files/resource-files/2018-09/apo-nid260056.pdf>.

Pfefferbaum, A., E. Adalsteinsson, D. Spielman, E. V. Sullivan, and K. O. Lim. 1999. “In Vivo Brain Concentrations of N-Acetyl Compounds, Creatine, and Choline in Alzheimer Disease.” *Archives of General Psychiatry* 56 (2): 185–92.

Pfefferbaum, Adolf, Elfar Adalsteinsson, Daniel Spielman, Edith V. Sullivan, and Kelvin O. Lim. n.d. “Of Brain Gray and White Matter: Effects of Normal Aging.”

Pfefferbaum, Adolf, Torsten Rohlfing, Margaret J. Rosenbloom, Weiwei Chu, Ian M. Colrain, and Edith V. Sullivan. 2013. “Variation in Longitudinal Trajectories of Regional Brain Volumes of Healthy Men and Women (ages 10 to 85 Years) Measured with Atlas-Based Parcellation of MRI.” *NeuroImage* 65 (January): 176–93.

Pfeuffer, Josef, Ivan Tkáč, Stephen W. Provencher, and Rolf Gruetter. 1999. “Toward an in Vivo Neurochemical Profile: Quantification of 18 Metabolites in Short-Echo-TimeH NMR Spectra of the Rat Brain.” *Journal of Magnetic Resonance* 141: 104–20.

Pijnappel, W. W. F., A. van den Boogaart, R. de Beer, and D. van Ormondt. 1992. “SVD-Based Quantification of Magnetic Resonance Signals.” *Journal of Magnetic Resonance*

- (1969). [https://doi.org/10.1016/0022-2364\(92\)90241-x](https://doi.org/10.1016/0022-2364(92)90241-x).
- Pinheiro, José C., and Douglas M. Bates. 2000. *Mixed-Effects Models in S and S-PLUS*. Springer, New York, NY.
- Pini, Lorenzo, Michela Pievani, Martina Bocchetta, Daniele Altomare, Paolo Bosco, Enrica Cavedo, Samantha Galluzzi, Moira Marizzoni, and Giovanni B. Frisoni. 2016. "Brain Atrophy in Alzheimer's Disease and Aging." *Ageing Research Reviews* 30 (September): 25–48.
- Pitts, Matthew W. 2018. "Barnes Maze Procedure for Spatial Learning and Memory in Mice." *Bio-Protocol* 8 (5). <https://doi.org/10.21769/bioprotoc.2744>.
- Plewes, Donald B., and Walter Kucharczyk. 2012. "Physics of MRI: A Primer." *Journal of Magnetic Resonance Imaging: JMRI* 35 (5): 1038–54.
- Podcasy, Jessica L., and C. Neill Epperson. 2016. "Considering Sex and Gender in Alzheimer Disease and Other Dementias." *Dialogues in Clinical Neuroscience* 18 (4): 437–46.
- Pol, L. A. van de, W. M. van der Flier, E. S. C. Korf, N. C. Fox, F. Barkhof, and P. Scheltens. 2007. "Baseline Predictors of Rates of Hippocampal Atrophy in Mild Cognitive Impairment." *Neurology* 69 (15): 1491–97.
- Považan, Michal, Bernhard Strasser, Gilbert Hangel, Eva Heckova, Stephan Gruber, Siegfried Trattnig, and Wolfgang Bogner. 2018. "Simultaneous Mapping of Metabolites and Individual Macromolecular Components via Ultra-Short Acquisition Delay 1 H MRSI in the Brain at 7T : Simultaneous Mapping of Metabolites and Macromolecules." *Magnetic Resonance in Medicine: Official Journal of the Society of Magnetic Resonance in Medicine / Society of Magnetic Resonance in Medicine* 79 (3): 1231–40.
- Provencher, Stephen. 2019. "LCModel & LCMgui User's Manual."
- Provencher, S. W. 1993. "Estimation of Metabolite Concentrations from Localized in Vivo Proton NMR Spectra." *Magnetic Resonance in Medicine: Official Journal of the Society of Magnetic Resonance in Medicine / Society of Magnetic Resonance in Medicine* 30 (6): 672–79.
- . 2001. "Automatic Quantitation of Localized in Vivo 1H Spectra with LCModel." *NMR in Biomedicine* 14 (4): 260–64.
- Qiu, Lily R., Darren J. Fernandes, Kamila U. Szulc-Lerch, Jun Dazai, Brian J. Nieman, Daniel H. Turnbull, Jane A. Foster, Mark R. Palmert, and Jason P. Lerch. 2018. "Mouse MRI Shows Brain Areas Relatively Larger in Males Emerge before Those Larger in Females." *Nature Communications* 9 (1): 2615.
- Qiu, Lily R., Jürgen Germann, Shoshana Spring, Christina Alm, Dulcie A. Vousden, Mark R. Palmert, and Jason P. Lerch. 2013. "Hippocampal Volumes Differ across the Mouse Estrous Cycle, Can Change within 24 Hours, and Associate with Cognitive Strategies." *NeuroImage* 83 (December): 593–98.
- Rahman, Aneela, Hande Jackson, Hollie Hristov, Richard S. Isaacson, Nabeel Saif, Teena Shetty, Orli Etingin, Claire Henchcliffe, Roberta Diaz Brinton, and Lisa Mosconi. 2019. "Sex and Gender Driven Modifiers of Alzheimer's: The Role for Estrogenic Control Across Age, Race, Medical, and Lifestyle Risks." *Frontiers in Aging Neuroscience* 11 (November): 315.
- Rajamohamedsait, Hameetha B., and Einar M. Sigurdsson. 2012. "Histological Staining of Amyloid and Pre-Amyloid Peptides and Proteins in Mouse Tissue." *Methods in Molecular Biology* 849: 411–24.

- Rasgon, N. L., G. W. Small, P. Siddarth, K. Miller, L. M. Ercoli, S. Y. Bookheimer, H. Lavretsky, S. C. Huang, J. R. Barrio, and M. E. Phelps. 2001. "Estrogen Use and Brain Metabolic Change in Older Adults. A Preliminary Report." *Psychiatry Research* 107 (1): 11–18.
- Ravera, Silvia, Marina Podestà, Federica Sabatini, Monica Dagnino, Daniela Cilloni, Samuele Fiorini, Annalisa Barla, and Francesco Frassoni. 2019. "Discrete Changes in Glucose Metabolism Define Aging." *Scientific Reports* 9 (1): 10347.
- Raz, Naftali, Paolo Ghisletta, Karen M. Rodrigue, Kristen M. Kennedy, and Ulman Lindenberger. 2010. "Trajectories of Brain Aging in Middle-Aged and Older Adults: Regional and Individual Differences." *NeuroImage* 51 (2): 501–11.
- Raz, Naftali, Ulman Lindenberger, Karen M. Rodrigue, Kristen M. Kennedy, Denise Head, Adrienne Williamson, Cheryl Dahle, Denis Gerstorff, and James D. Acker. 2005. "Regional Brain Changes in Aging Healthy Adults: General Trends, Individual Differences and Modifiers." *Cerebral Cortex* 15 (11): 1676–89.
- Raz, Naftali, and Karen M. Rodrigue. 2006. "Differential Aging of the Brain: Patterns, Cognitive Correlates and Modifiers." *Neuroscience and Biobehavioral Reviews* 30 (6): 730–48.
- R Core Team. 2020. "R: A Language and Environment for Statistical Computing." Vienna, Austria: R Foundation for Statistical Computing. <https://www.R-project.org/>.
- Reichel, J. M., B. T. Bedenk, M. Czisch, and C. T. Wotjak. 2017. "Age-Related Cognitive Decline Coincides with Accelerated Volume Loss of the Dorsal but Not Ventral Hippocampus in Mice." *Hippocampus* 27 (1): 28–35.
- Rettberg, Jamaica R., Jia Yao, and Roberta Diaz Brinton. 2014. "Estrogen: A Master Regulator of Bioenergetic Systems in the Brain and Body." *Frontiers in Neuroendocrinology* 35 (1): 8–30.
- Riudavets, Miguel Angel, Diego Iacono, Susan M. Resnick, Richard O'Brien, Alan B. Zonderman, Lee J. Martin, Gay Rudow, Olga Pletnikova, and Juan C. Troncoso. 2007. "Resistance to Alzheimer's Pathology Is Associated with Nuclear Hypertrophy in Neurons." *Neurobiology of Aging* 28 (10): 1484–92.
- Rollins, Colleen P. E., Daniel Gallino, Vincent Kong, Gülebru Ayranci, Gabriel A. Devenyi, Jürgen Germann, and M. Mallar Chakravarty. 2019. "Contributions of a High-Fat Diet to Alzheimer's Disease-Related Decline: A Longitudinal Behavioural and Structural Neuroimaging Study in Mouse Models." *NeuroImage. Clinical* 21: 101606.
- Rolls, Edmund T. 2015. "Limbic Systems for Emotion and for Memory, but No Single Limbic System." *Cortex; a Journal Devoted to the Study of the Nervous System and Behavior* 62 (January): 119–57.
- Rorabaugh, Jacki M., Termpanit Chalermphanupap, Christian A. Botz-Zapp, Vanessa M. Fu, Natalie A. Lembeck, Robert M. Cohen, and David Weinschenker. 2017. "Chemogenetic Locus Coeruleus Activation Restores Reversal Learning in a Rat Model of Alzheimer's Disease." *Brain: A Journal of Neurology* 140 (11): 3023–38.
- Ross, Amy J., and Perminder S. Sachdev. 2004. "Magnetic Resonance Spectroscopy in Cognitive Research." *Brain Research. Brain Research Reviews* 44 (2-3): 83–102.
- Ross, Amy J., Perminder S. Sachdev, Wei Wen, and Henry Brodaty. 2006. "Longitudinal Changes during Aging Using Proton Magnetic Resonance Spectroscopy." *The Journals of Gerontology. Series A, Biological Sciences and Medical Sciences* 61 (3): 291–98.
- Roy, Upasana, Lara Stute, Corinna Höfling, Maike Hartlage-Rübsamen, Jörg Matysik,

- Steffen Roßner, and A. Alia. 2018. “Sex- and Age-Specific Modulation of Brain GABA Levels in a Mouse Model of Alzheimer’s Disease.” *Neurobiology of Aging* 62 (February): 168–79.
- Rudow, Gay, Richard O’Brien, Alena V. Savonenko, Susan M. Resnick, Alan B. Zonderman, Olga Pletnikova, Laura Marsh, et al. 2008. “Morphometry of the Human Substantia Nigra in Ageing and Parkinson’s Disease.” *Acta Neuropathologica* 115 (4): 461–70.
- Ruigrok, Amber N. V., Gholamreza Salimi-Khorshidi, Meng-Chuan Lai, Simon Baron-Cohen, Michael V. Lombardo, Roger J. Tait, and John Suckling. 2014. “A Meta-Analysis of Sex Differences in Human Brain Structure.” *Neuroscience and Biobehavioral Reviews* 39 (February): 34–50.
- Saint-Aubert, Laure, Laetitia Lemoine, Konstantinos Chiotis, Antoine Leuzy, Elena Rodriguez-Vieitez, and Agneta Nordberg. 2017. “Tau PET Imaging: Present and Future Directions.” *Molecular Neurodegeneration* 12 (1): 19.
- Saito, Takashi, Yukio Matsuba, Naomi Mihira, Jiro Takano, Per Nilsson, Shigeyoshi Itohara, Nobuhisa Iwata, and Takaomi C. Saido. 2014. “Single App Knock-in Mouse Models of Alzheimer’s Disease.” *Nature Neuroscience* 17 (5): 661–63.
- Sandner, Guy, Marie-Josée Angst, Thierry Guiberteau, Blandine Guignard, and David Brasse. 2010. “MRI and X-Ray Scanning Images of the Brain of 3-, 6- and 9-Month-Old Rats with Bilateral Neonatal Ventral Hippocampus Lesions.” *NeuroImage* 53 (1): 44–50.
- Santiago, Jose A., Virginie Bottero, and Judith A. Potashkin. 2017. “Dissecting the Molecular Mechanisms of Neurodegenerative Diseases through Network Biology.” *Frontiers in Aging Neuroscience* 9 (May): 166.
- Saré, Rachel Michelle, Spencer K. Cooke, Leland Krych, Patricia M. Zerfas, Robert M. Cohen, and Carolyn Beebe Smith. 2020. “Behavioral Phenotype in the TgF344-AD Rat Model of Alzheimer’s Disease.” *Frontiers in Neuroscience* 14 (June): 601.
- Sasaguri, Hiroki, Per Nilsson, Shoko Hashimoto, Kenichi Nagata, Takashi Saito, Bart De Strooper, John Hardy, Robert Vassar, Bengt Winblad, and Takaomi C. Saido. 2017. “APP Mouse Models for Alzheimer’s Disease Preclinical Studies.” *The EMBO Journal* 36 (17): 2473–87.
- Saunders, D. E., F. A. Howe, A. van den Boogaart, J. R. Griffiths, and M. M. Brown. 1997. “Discrimination of Metabolite from Lipid and Macromolecule Resonances in Cerebral Infarction in Humans Using Short Echo Proton Spectroscopy.” *Journal of Magnetic Resonance Imaging: JMRI* 7 (6): 1116–21.
- Scahill, Rachael I., Chris Frost, Rhian Jenkins, Jennifer L. Whitwell, Martin N. Rossor, and Nick C. Fox. 2003. “A Longitudinal Study of Brain Volume Changes in Normal Aging Using Serial Registered Magnetic Resonance Imaging.” *Archives of Neurology* 60 (7): 989–94.
- Scarce-Levie, Kimberly, Pascal E. Sanchez, and Joseph W. Lewcock. 2020. “Leveraging Preclinical Models for the Development of Alzheimer Disease Therapeutics.” *Nature Reviews. Drug Discovery* 19 (7): 447–62.
- Scheltens, Philip, Bart De Strooper, Miia Kivipelto, Henne Holstege, Gael Chételat, Charlotte E. Teunissen, Jeffrey Cummings, and Wiesje M. van der Flier. 2021. “Alzheimer’s Disease.” *The Lancet* 397 (10284): 1577–90.
- Schöll, Michael, Samuel N. Lockhart, Daniel R. Schonhaut, James P. O’Neil, Mustafa Janabi, Rik Ossenkoppele, Suzanne L. Baker, et al. 2016. “PET Imaging of Tau Deposition

- in the Aging Human Brain.” *Neuron* 89 (5): 971–82.
- Schuff, Norbert, Diane L. Amend, Robert Knowlton, David Norman, George Fein, and Michael W. Weiner. 1999. “Age-Related Metabolite Changes and Volume Loss in the Hippocampus by Magnetic Resonance Spectroscopy and Imaging.” *Neurobiology of Aging* 20: 279–85.
- Seeger, Uwe, Uwe Klose, Irina Mader, Wolfgang Grodd, and Thomas Nägele. 2003. “Parameterized Evaluation of Macromolecules and Lipids in Proton MR Spectroscopy of Brain Diseases.” *Magnetic Resonance in Medicine: Official Journal of the Society of Magnetic Resonance in Medicine / Society of Magnetic Resonance in Medicine* 49 (1): 19–28.
- Selkoe, Dennis J. 2011. “Alzheimer’s Disease.” *Cold Spring Harbor Perspectives in Biology* 3 (7). <https://doi.org/10.1101/cshperspect.a004457>.
- Selkoe, Dennis J., and John Hardy. 2016. “The Amyloid Hypothesis of Alzheimer’s Disease at 25 Years.” *EMBO Molecular Medicine* 8 (6): 595–608.
- Selkoe, D. J. 1991. “The Molecular Pathology of Alzheimer’s Disease.” *Neuron* 6 (4): 487–98.
- . 2001. “Alzheimer’s Disease: Genes, Proteins, and Therapy.” *Physiological Reviews* 81 (2): 741–66.
- Seyfried, Nicholas T., Eric B. Dammer, Vivek Swarup, Divya Nandakumar, Duc M. Duong, Luming Yin, Qiudong Deng, et al. 2017. “A Multi-Network Approach Identifies Protein-Specific Co-Expression in Asymptomatic and Symptomatic Alzheimer’s Disease.” *Cell Systems* 4 (1): 60–72.e4.
- Shetty, A. K., and D. A. Turner. 1999. “Vulnerability of the Dentate Gyrus to Aging and Intracerebroventricular Administration of Kainic Acid.” *Experimental Neurology* 158 (2): 491–503.
- Shetty, Geetha A., Bharathi Hattiangady, and Ashok K. Shetty. 2013. “Neural Stem Cell- and Neurogenesis-Related Gene Expression Profiles in the Young and Aged Dentate Gyrus.” *Age* 35 (6): 2165–76.
- Shineman, Diana W., Guriqbal S. Basi, Jennifer L. Bizon, Carol A. Colton, Barry D. Greenberg, Beth A. Hollister, John Lincecum, et al. 2011. “Accelerating Drug Discovery for Alzheimer’s Disease: Best Practices for Preclinical Animal Studies.” *Alzheimer’s Research & Therapy* 3 (5): 28.
- Sholl, S. A., and K. L. Kim. 1990. “Aromatase, 5-Alpha-Reductase, and Androgen Receptor Levels in the Fetal Monkey Brain during Early Development.” *Neuroendocrinology* 52 (1): 94–98.
- Shonk, T. K., R. A. Moats, P. Gifford, T. Michaelis, J. C. Mandigo, J. Izumi, and B. D. Ross. 1995. “Probable Alzheimer Disease: Diagnosis with Proton MR Spectroscopy.” *Radiology* 195 (1): 65–72.
- Sibson, N. R., A. Dhankhar, G. F. Mason, K. L. Behar, D. L. Rothman, and R. G. Shulman. n.d. “In Vivo ¹³C NMR Measurements of Cerebral Glutamine Synthesis as Evidence for Glutamate–glutamine Cycling.”
- Simpson, Robin, Gabriel A. Devenyi, Peter Jezzard, T. Jay Hennessy, and Jamie Near. 2017. “Advanced Processing and Simulation of MRS Data Using the FID Appliance (FID-A)—An Open Source, MATLAB-Based Toolkit.” *Magnetic Resonance in Medicine: Official Journal of the Society of Magnetic Resonance in Medicine / Society of Magnetic Resonance in Medicine* 77 (1): 23–33.

Sled, J. G., and G. B. Pike. 1998. "Standing-Wave and RF Penetration Artifacts Caused by Elliptic Geometry: An Electrodynamics Analysis of MRI." *IEEE Transactions on Medical Imaging* 17 (4): 653–62.

Sleepers, Kristel, Jean-Charles Lambert, Lars Bertram, Marc Cruts, Philippe Amouyel, and Christine Van Broeckhoven. 2010. "The Pursuit of Susceptibility Genes for Alzheimer's Disease: Progress and Prospects." *Trends in Genetics: TIG* 26 (2): 84–93.

Small, Scott A., Monica K. Chawla, Michael Buonocore, Peter R. Rapp, and Carol A. Barnes. 2004. "Imaging Correlates of Brain Function in Monkeys and Rats Isolates a Hippocampal Subregion Differentially Vulnerable to Aging." *Proceedings of the National Academy of Sciences of the United States of America* 101 (18): 7181–86.

Smith, Lindsey A., and Lori L. McMahon. 2018. "Deficits in Synaptic Function Occur at Medial Perforant Path-Dentate Granule Cell Synapses prior to Schaffer Collateral-CA1 Pyramidal Cell Synapses in the Novel TgF344-Alzheimer's Disease Rat Model." *Neurobiology of Disease* 110 (February): 166–79.

Snoussi, Karim, Joseph S. Gillen, Alena Horska, Nicolaas A. J. Puts, Subechhya Pradhan, Richard A. E. Edden, and Peter B. Barker. 2015. "Comparison of Brain Gray and White Matter Macromolecule Resonances at 3 and 7 Tesla." *Magnetic Resonance in Medicine: Official Journal of the Society of Magnetic Resonance in Medicine / Society of Magnetic Resonance in Medicine* 74 (3): 607–13.

Sowell, Elizabeth R., Paul M. Thompson, and Arthur W. Toga. 2004. "Mapping Changes in the Human Cortex throughout the Span of Life." *The Neuroscientist: A Review Journal Bringing Neurobiology, Neurology and Psychiatry* 10 (4): 372–92.

Spencer, N. G., L. R. Bridges, K. Elderfield, K. Amir, B. Austen, and F. A. Howe. 2013. "Quantitative Evaluation of MRI and Histological Characteristics of the 5xFAD Alzheimer Mouse Brain." *NeuroImage* 76 (August): 108–15.

Sperling, Reisa A., Paul S. Aisen, Laurel A. Beckett, David A. Bennett, Suzanne Craft, Anne M. Fagan, Takeshi Iwatsubo, et al. 2011. "Toward Defining the Preclinical Stages of Alzheimer's Disease: Recommendations from the National Institute on Aging-Alzheimer's Association Workgroups on Diagnostic Guidelines for Alzheimer's Disease." *Alzheimer's & Dementia: The Journal of the Alzheimer's Association* 7 (3): 280–92.

Sperling, Reisa A., Clifford R. Jack Jr, and Paul S. Aisen. 2011. "Testing the Right Target and Right Drug at the Right Stage." *Science Translational Medicine* 3 (111): 111cm33.

Sperling, Reisa A., Dorene M. Rentz, Keith A. Johnson, Jason Karlawish, Michael Donohue, David P. Salmon, and Paul Aisen. 2014. "The A4 Study: Stopping AD before Symptoms Begin?" *Science Translational Medicine* 6 (228): 228fs13.

Spring, Shoshana, Jason P. Lerch, and R. Mark Henkelman. 2007. "Sexual Dimorphism Revealed in the Structure of the Mouse Brain Using Three-Dimensional Magnetic Resonance Imaging." *NeuroImage* 35 (4): 1424–33.

Spring, Shoshana, Jason P. Lerch, Monica K. Wetzel, Alan C. Evans, and R. Mark Henkelman. 2010. "Cerebral Asymmetries in 12-Week-Old C57Bl/6J Mice Measured by Magnetic Resonance Imaging." *NeuroImage* 50 (2): 409–15.

Stefan, D., F. Di Cesare, A. Andrasescu, E. Popa, A. Lazariev, E. Vescovo, O. Strbak, et al. 2009. "Quantitation of Magnetic Resonance Spectroscopy Signals: The jMRUI Software Package." *Measurement Science & Technology* 20 (10): 104035.

Stephan, Marius, Paul Volkman, and Moritz J. Rossner. 2019. "Assessing Behavior and Cognition in Rodents, Nonhuman Primates, and Humans: Where Are the Limits of

Translation?" *Dialogues in Clinical Neuroscience* 21 (3): 249–59.

Stoiljkovic, Milan, Craig Kelley, Bernardo Stutz, Tamas L. Horvath, and Mihály Hajós. 2019. "Altered Cortical and Hippocampal Excitability in TgF344-AD Rats Modeling Alzheimer's Disease Pathology." *Cerebral Cortex* 29 (6): 2716–27.

Sullivan, Edith V., Margaret Rosenbloom, Kathleen L. Serventi, and Adolf Pfefferbaum. 2004. "Effects of Age and Sex on Volumes of the Thalamus, Pons, and Cortex." *Neurobiology of Aging* 25 (2): 185–92.

Sultana, Rukhsana, and D. Allan Butterfield. 2011. "Identification of the Oxidative Stress Proteome in the Brain." *Free Radical Biology & Medicine* 50 (4): 487–94.

Sumiyoshi, Akira, Hiroi Nonaka, and Ryuta Kawashima. 2017. "Sexual Differentiation of the Adolescent Rat Brain: A Longitudinal Voxel-Based Morphometry Study." *Neuroscience Letters* 642 (March): 168–73.

Swordlow, Russell H., Jeffrey M. Burns, and Shaharyar M. Khan. 2014. "The Alzheimer's Disease Mitochondrial Cascade Hypothesis: Progress and Perspectives." *Biochimica et Biophysica Acta* 1842 (8): 1219–31.

Tampi, Rajesh R., Brent P. Forester, and Marc Agronin. 2021. "Aducanumab: Evidence from Clinical Trial Data and Controversies." *Drugs in Context* 10 (October). <https://doi.org/10.7573/dic.2021-7-3>.

Tapiola, Tero, Irina Alafuzoff, Sanna-Kaisa Herukka, Laura Parkkinen, Päivi Hartikainen, Hilikka Soininen, and Tuula Pirttilä. 2009. "Cerebrospinal Fluid {beta}-Amyloid 42 and Tau Proteins as Biomarkers of Alzheimer-Type Pathologic Changes in the Brain." *Archives of Neurology* 66 (3): 382–89.

Tarawneh, Rawan. 2020. "Biomarkers: Our Path Towards a Cure for Alzheimer Disease." *Biomarker Insights* 15 (November): 1177271920976367.

Teipel, Stefan, Alexander Drzezga, Michel J. Grothe, Henryk Barthel, Gaël Chételat, Norbert Schuff, Pawel Skudlarski, et al. 2015. "Multimodal Imaging in Alzheimer's Disease: Validity and Usefulness for Early Detection." *Lancet Neurology* 14 (10): 1037–53.

Teipel, Stefan J., Michel Grothe, Simone Lista, Nicola Toschi, Francesco G. Garaci, and Harald Hampel. 2013. "Relevance of Magnetic Resonance Imaging for Early Detection and Diagnosis of Alzheimer Disease." *The Medical Clinics of North America* 97 (3): 399–424.

Thompson, Wesley K., Joachim Hallmayer, Ruth O'Hara, and Alzheimer's Disease Neuroimaging Initiative. 2011. "Design Considerations for Characterizing Psychiatric Trajectories across the Lifespan: Application to Effects of APOE-ε4 on Cerebral Cortical Thickness in Alzheimer's Disease." *The American Journal of Psychiatry* 168 (9): 894–903.

Tkac̣, I., Z. Starc̣uk, I. -Y. Choi, and R. Gruetter. 1999. "In Vivo H NMR Spectroscopy of Rat Brain at 1 Ms Echo Time." *Magnetic Resonance in Medicine: Official Journal of the Society of Magnetic Resonance in Medicine / Society of Magnetic Resonance in Medicine* 41: 649–56.

Tong, Tong, Katherine Gray, Qinquan Gao, Liang Chen, and Daniel Rueckert. 2017. "Multi-Modal Classification of Alzheimer's Disease Using Nonlinear Graph Fusion." *Pattern Recognition* 63 (March): 171–81.

Tullo, Stephanie, Raihaan Patel, Gabriel A. Devenyi, Alyssa Salaciak, Saashi A. Bedford, Sarah Farzin, Nancy Wlodarski, et al. 2019. "MR-Based Age-Related Effects on the Striatum, Globus Pallidus, and Thalamus in Healthy Individuals across the Adult Lifespan." *Human Brain Mapping* 40 (18): 5269–88.

Tustison, Nicholas J., Brian B. Avants, Philip A. Cook, Yuanjie Zheng, Alexander Egan,

Paul A. Yushkevich, and James C. Gee. 2010. "N4ITK: Improved N3 Bias Correction." *IEEE Transactions on Medical Imaging* 29 (6): 1310–20.

Tustison, Nicholas J., Philip A. Cook, Arno Klein, Gang Song, Sandhitsu R. Das, Jeffrey T. Duda, Benjamin M. Kandel, et al. 2014. "Large-Scale Evaluation of ANTs and FreeSurfer Cortical Thickness Measurements." *NeuroImage* 99 (October): 166–79.

Valdés-Hernández, Pedro Antonio, Akira Sumiyoshi, Hiroi Nonaka, Risa Haga, Eduardo Aubert-Vásquez, Takeshi Ogawa, Yasser Iturria-Medina, Jorge J. Riera, and Ryuta Kawashima. 2011. "An in Vivo MRI Template Set for Morphometry, Tissue Segmentation, and fMRI Localization in Rats." *Frontiers in Neuroinformatics* 5 (November): 26.

Vanhamme, L., van den Boogaart A, and Van Huffel S. 1997. "Improved Method for Accurate and Efficient Quantification of MRS Data with Use of Prior Knowledge." *Journal of Magnetic Resonance* 129 (1): 35–43.

Van Hoesen, G. W., B. T. Hyman, and A. R. Damasio. 1991. "Entorhinal Cortex Pathology in Alzheimer's Disease." *Hippocampus* 1 (1): 1–8.

Varvel, Nicholas H., Kiran Bhaskar, Maria Z. Kounnas, Steven L. Wagner, Yan Yang, Bruce T. Lamb, and Karl Herrup. 2009. "NSAIDs Prevent, but Do Not Reverse, Neuronal Cell Cycle Reentry in a Mouse Model of Alzheimer Disease." *The Journal of Clinical Investigation* 119 (12): 3692–3702.

Vigorito, Michael, Kaitlyn P. Connaghan, and Sulie L. Chang. 2015. "The HIV-1 Transgenic Rat Model of neuroHIV." *Brain, Behavior, and Immunity* 48 (August): 336–49.

Villeneuve, Sylvia, Miranka Wirth, and Renaud La Joie. 2015. "Are AD-Typical Regions the Convergence Point of Multiple Pathologies?" *Frontiers in Aging Neuroscience* 7 (March): 42.

Vincent, Robert D., Peter Neelin, Najmeh Khalili-Mahani, Andrew L. Janke, Vladimir S. Fonov, Steven M. Robbins, Leila Baghdadi, et al. 2016. "MINC 2.0: A Flexible Format for Multi-Modal Images." *Frontiers in Neuroinformatics* 10 (August): 35.

Vitek, Michael P., Joseph A. Araujo, Michael Fossel, Barry D. Greenberg, Gareth R. Howell, Stacey J. Sukoff Rizzo, Nicholas T. Seyfried, et al. 2020. "Translational Animal Models for Alzheimer's Disease: An Alzheimer's Association Business Consortium Think Tank." *Alzheimer's & Dementia: The Journal of the Alzheimer's Association* 6 (1): e12114.

Voevodskaya, Olga, Konstantinos Poulakis, Pia Sundgren, Danielle van Westen, Sebastian Palmqvist, Lars-Olof Wahlund, Erik Stomrud, Oskar Hansson, Eric Westman, and for the Swedish BioFINDER Study Group. 2019. "Brain Myoinositol as a Potential Marker of Amyloid-Related Pathology." *Neurology* 92 (5): e395–405.

Volloch, Vladimir, and Sophia Rits. 2018. "Results of Beta Secretase-Inhibitor Clinical Trials Support Amyloid Precursor Protein-Independent Generation of Beta Amyloid in Sporadic Alzheimer's Disease." *Medical Sciences (Basel, Switzerland)* 6 (2). <https://doi.org/10.3390/medsci6020045>.

Voorhees, Jaymie R., Matthew T. Remy, Coral J. Cintrón-Pérez, Eli El Rassi, Michael Z. Khan, Laura M. Dutca, Terry C. Yin, et al. 2018. "(-)-P7C3-S243 Protects a Rat Model of Alzheimer's Disease From Neuropsychiatric Deficits and Neurodegeneration Without Altering Amyloid Deposition or Reactive Glia." *Biological Psychiatry* 84 (7): 488–98.

Walhovd, Kristine B., Anders M. Fjell, Ivar Reinvang, Arvid Lundervold, Anders M. Dale, Dag E. Eilertsen, Brian T. Quinn, David Salat, Nikos Makris, and Bruce Fischl. 2005. "Effects of Age on Volumes of Cortex, White Matter and Subcortical Structures." *Neurobiology of Aging* 26 (9): 1261–70; discussion 1275–78.

Wang, Hui, Lan Tan, Hui-Fu Wang, Ying Liu, Rui-Hua Yin, Wen-Ying Wang, Xiao-Long Chang, Teng Jiang, and Jin-Tai Yu. 2015. "Magnetic Resonance Spectroscopy in Alzheimer's Disease: Systematic Review and Meta-Analysis." *Journal of Alzheimer's Disease: JAD* 46 (4): 1049–70.

Waragai, Masaaki, Masaru Moriya, and Takeshi Nojo. 2017. "Decreased N-Acetyl Aspartate/Myo-Inositol Ratio in the Posterior Cingulate Cortex Shown by Magnetic Resonance Spectroscopy May Be One of the Risk Markers of Preclinical Alzheimer's Disease: A 7-Year Follow-Up Study." *Journal of Alzheimer's Disease: JAD* 60 (4): 1411–27.

Watanabe, Memi, Joseph H. Liao, Hernán Jara, and Osamu Sakai. 2013. "Multispectral Quantitative MR Imaging of the Human Brain: Lifetime Age-Related Effects." *Radiographics: A Review Publication of the Radiological Society of North America, Inc* 33 (5): 1305–19.

Watanabe, Toshiyuki, Akihiko Shiino, and Ichiro Akiguchi. 2010. "Absolute Quantification in Proton Magnetic Resonance Spectroscopy Is Useful to Differentiate Amnesic Mild Cognitive Impairment from Alzheimer's Disease and Healthy Aging." *Dementia and Geriatric Cognitive Disorders* 30 (1): 71–77.

Weiner, Michael W., Dallas P. Veitch, Paul S. Aisen, Laurel A. Beckett, Nigel J. Cairns, Robert C. Green, Danielle Harvey, et al. 2017. "Recent Publications from the Alzheimer's Disease Neuroimaging Initiative: Reviewing Progress toward Improved AD Clinical Trials." *Alzheimer's & Dementia: The Journal of the Alzheimer's Association* 13 (4): e1–85.

Welniak-Kaminska, Marlena, Michal Fiedorowicz, Jaroslaw Orzel, Piotr Bogorodzki, Klaudia Modlinska, Rafal Stryjek, Anna Chrzanowska, Wojciech Pisula, and Pawel Grieb. 2019. "Volumes of Brain Structures in Captive Wild-Type and Laboratory Rats: 7T Magnetic Resonance in Vivo Automatic Atlas-Based Study." *PloS One* 14 (4): e0215348.

Wen, Tong-Chun, Anil Sindhurakar, Violeta Contreras Ramirez, Honggeun Park, Disha Gupta, and Jason B. Carmel. 2019. "Targeted Infarction of the Internal Capsule in the Rat Using Microstimulation Guidance." *Stroke; a Journal of Cerebral Circulation* 50 (9): 2531–38.

West, Mark J., Georg Bach, Andreas Söderman, and Jens Ledet Jensen. 2009. "Synaptic Contact Number and Size in Stratum Radiatum CA1 of APP/PS1DeltaE9 Transgenic Mice." *Neurobiology of Aging* 30 (11): 1756–76.

Wickens, Megan M., Debra A. Bangasser, and Lisa A. Briand. 2018. "Sex Differences in Psychiatric Disease: A Focus on the Glutamate System." *Frontiers in Molecular Neuroscience* 11 (June): 197.

Wickham, Hadley, Mara Averick, Jennifer Bryan, Winston Chang, Lucy McGowan, Romain François, Garrett Grolemond, et al. 2019. "Welcome to the Tidyverse." *Journal of Open Source Software* 4 (43): 1686.

Wickham, Hadley, and Jennifer Bryan. 2019. "Readxl: Read Excel Files." <https://CRAN.R-project.org/package=readxl>.

Wisse, Laura E. M., Geert Jan Biessels, Sophie M. Heringa, Hugo J. Kuijf, Dineke H. L. Koek, Peter R. Luijten, Mirjam I. Geerlings, and Utrecht Vascular Cognitive Impairment (VCI) Study Group. 2014. "Hippocampal Subfield Volumes at 7T in Early Alzheimer's Disease and Normal Aging." *Neurobiology of Aging* 35 (9): 2039–45.

Wu, Chongyun, Luodan Yang, Yong Li, Yan Dong, Baocheng Yang, Lorelei Donovan Tucker, Xuemei Zong, and Quanguang Zhang. 2020. "Effects of Exercise Training on

- Anxious-Depressive-like Behavior in Alzheimer Rat.” *Medicine and Science in Sports and Exercise* 52 (7): 1456–69.
- Yang, Yan, Elliott J. Mufson, and Karl Herrup. 2003. “Neuronal Cell Death Is Preceded by Cell Cycle Events at All Stages of Alzheimer’s Disease.” *The Journal of Neuroscience: The Official Journal of the Society for Neuroscience* 23 (7): 2557–63.
- Yin, Fei, Harsh Sancheti, Ishan Patil, and Enrique Cadenas. 2016. “Energy Metabolism and Inflammation in Brain Aging and Alzheimer’s Disease.” *Free Radical Biology & Medicine* 100 (November): 108–22.
- Yin, Fei, Jia Yao, Harsh Sancheti, Tao Feng, Roberto C. Melcangi, Todd E. Morgan, Caleb E. Finch, et al. 2015. “The Perimenopausal Aging Transition in the Female Rat Brain: Decline in Bioenergetic Systems and Synaptic Plasticity.” *Neurobiology of Aging* 36 (7): 2282–95.
- Yin, Wencheng, Navei Cerda-Hernández, Atahualpa Castillo-Morales, Mayra L. Ruiz-Tejada-Segura, Jimena Monzón-Sandoval, Perla Moreno-Castilla, Rodrigo Pérez-Ortega, Federico Bermudez-Rattoni, Araxi O. Urrutia, and Humberto Gutiérrez. 2020. “Transcriptional, Behavioral and Biochemical Profiling in the 3xTg-AD Mouse Model Reveals a Specific Signature of Amyloid Deposition and Functional Decline in Alzheimer’s Disease.” *Frontiers in Neuroscience* 14 (December): 602642.
- Zahr, Natalie M., Dirk Mayer, Torsten Rohlfing, Sandra Chanraud, Meng Gu, Edith V. Sullivan, and Adolf Pfefferbaum. 2013. “In Vivo Glutamate Measured with Magnetic Resonance Spectroscopy: Behavioral Correlates in Aging.” *Neurobiology of Aging* 34 (4): 1265–76.
- Zhang, Xianrong, Huilang Liu, Junfang Wu, Xu Zhang, Maili Liu, and Yong Wang. 2009. “Metabonomic Alterations in Hippocampus, Temporal and Prefrontal Cortex with Age in Rats.” *Neurochemistry International* 54 (8): 481–87.
- Zhu, Xiongwei, George Perry, Paula I. Moreira, Gjumrakch Aliev, Adam D. Cash, Keisuke Hirai, and Mark A. Smith. 2006. “Mitochondrial Abnormalities and Oxidative Imbalance in Alzheimer Disease.” *Journal of Alzheimer’s Disease: JAD* 9 (2): 147–53.